Title
Neuromechanical Control Architectures of Arthropod Locomotion

Author
REVZEN, Shai

Publication Date
2009

Peer reviewed|Thesis/dissertation

Neuromechanical Control Architectures of Arthropod Locomotion

by

Shai Revzen

A dissertation submitted in partial satisfaction of the
requirements for the degree of
Doctor of Philosophy

in

Integrative Biology

in the

Graduate Division
of the
University of California, Berkeley

Committee in charge:
Professor Robert J. Full, Chair
Professor Robert Dudley
Professor Andrew Packard

Fall 2009

Neuromechanical Control Architectures of Arthropod Locomotion

Abstract

Neuromechanical Control Architectures of Arthropod Locomotion

by

Shai Revzen

Doctor of Philosophy in Integrative Biology

University of California, Berkeley

Professor Robert J. Full, Chair

We define a theoretical framework for the experimental study of neuromechanical control in animals, based on mathematical concepts from dynamical systems theory. This approach allows experiments, results and theoretical models to be shared among biologists, engineers and mathematicians, and is applicable to the study of control in any system, biological, artificial or simulated, provided the system exhibits stable rhythmic solutions. The basis of this framework is the notion that rhythmic systems are best expressed as periodic functions of their phase. Using phase as a predictor, an extrapolated prediction of future animal motions can be compared with the motions that occur when a perturbation is applied. Phase also serves as a succinct summary of the kinematic state, allowing the difference between the expected state as summarized by phase and the phase found in the perturbed animal – a "residual phase". In the first chapter we introduce the key concepts and describe how the residual phase may be used to identify the neuromechanical control architecture of an animal. In the following two chapters we use residual phase to analyze running arthropods subjected to perturbations. In the final chapter, we extend the kinematic phase based models to the construction of a linearized approximation of animal dynamics based on Floquet theory. The Floquet model allows us to directly test the "Templates and Anchors Hypothesis" of motor control and to characterize a "template" – a low dimensional model of the dynamics of the animal.

In chapter 2, our residual phase results from running cockroaches over a hurdle show that kinematic phase was reset, while running frequency was closely maintained to within $\pm 5\%$. Kinematic phase changes were distributed bi-modally with modes one step (half a cycle) apart, which corresponds to a left-right reflection of the kinematic state of the body. The results decrease the plausibility of feedforward control and support the use of neural feedback for this task. Based on the results, we propose a controller that expresses the timing of the two leg tripods of the animals as two coupled phase oscillators, which in turn, may also be coupled to a master clock.

In chapter 3, we analyze cockroaches which ran onto a movable cart that translated laterally. The specific impulse imposed on animals was $50 \pm 4\ cm/s$ (mean,SD), nearly twice their forward speed $25 \pm 6\ cm/s$. Animals corrected for these perturbations by decreasing stride frequency, thereby demonstrating neural feedback. Trials fell into two classes, one class slowing down after a step ($50\ ms$), the other after nearly three steps ($130\ ms$). Classes were predicted by the kinematic phase of the animal at onset of perturbation. We hypothesize that the differences in response time is a consequence of the mechanical posture of the animal during perturbation, as expressed by the phase, and the coupling of neural and mechanical control.

In chapter 4 we attempted to use kinematic phase methods to reconstruct the linearized (Floquet) structure of running cockroaches when viewed as nonlinear oscillators.

The development of this approach required several innovations in applied mathematics and statistics. We analyzed foot and body positions of 34 animals running on a treadmill. Results showed that cockroaches running at preferred speed possess a six dimensional template with each dimension recovering by less than 50% in a stride ($P < 0.05$, 11 animals, 24 trials, 532 strides).

To the goddess, by her many names:
Danu, Shakti, Gaia, Kali,
Hecate trimorpha

Contents

List of Figures

List of Tables

Acknowledgments

It is a most rare and unusual project that is both a significant accomplishment and the work of just one person. This thesis is not that rare or unusual. There are many people who contributed, directly and indirectly. Without their efforts this work would have been difficult or impossible to carry out.

I would like to acknowledge the intellectual contributions of Michael Revzen, my father, and Dan Eytan, my childhood friend. Without the conversations I had with them both when I started graduate school, the ideas that form the basis of my thesis might not have appeared at all.

Similarly critical to the scientific contents are the many talented and dedicated undergraduates whose work forms the basis for what you will read in the following pages, and foremost among them Joshua Bishop-Moser, Pei-ran Gao and Talia Moore. My thanks go to my collaborators – my lab-mates Ardian Jusufi and Daniel Dudek, my fellow graduate student Sam Burden and the post-doctoral lab members Dr. Andrew Spence and Dr. Justin Seipel. My thanks to the Berkeley Biomechanics group, headed by Professors Mimi Koehl, Robert Dudley and Robert Full and my qualifying committee members who taught me their respective fields and approaches to science, Professors Steve Lehman, Robert Dudley, Shankar Sastry and Sheila Patek. My adviser, Professor Robert Full, deserves my thanks for his sincere efforts on my behalf; I was not an easy student to supervise, and I thank him for his forbearance. Last, but far from least, I most deeply thank Professors John Guckenheimer and Daniel Koditschek for their patient mentoring, without which most of this body of work would have never come into being.

Academia, despite its pretensions to that effect, is not isolated from life. The focus and dedication required for this work would have been impossible without my dear wife Shlomit, who has undergone great hardship in supporting me in my work, and the enduring patience of my children Eli and Gabriella. I am deeply thankful for the emotional and financial support of my parents Chava and Michael Revzen. For his friendship and guidance above and beyond the call of academic duty I thank Robert Dudley. Daniel Dudek, Yonatan Munk, Tamara Blain, Sam Burden, Megan Luecke and Pauline Jennings I thank for their friendship and companionship through both hard and happy times. Margaret Kenaga I thank for her support in the most stressful final phase of typesetting.

Subtracting the sum of all these generous contributions to my work, it seems I have added precious little.

Part I

Thesis

Chapter 1

Neuromechanical Architectures

1.1 Introduction

Our objective is to provide experimentalists with neuromechanical control hypotheses that can be tested with kinematic data sets. To illustrate the approach, we select legged animals responding to perturbations during running. In the following sections, we briefly outline our dynamical systems approach, state our over-arching hypotheses, define four neuromechanical control architectures (NCAs) and conclude by proposing a series of perturbation experiments that can begin to identify the simplest architecture that best represents an animal's controller.

1.1.1 From description to prescription of motor control

Descriptive neuromechanical studies of the last decade have achieved a broad consensus that Bernstein's (Bernstein, 1967) "degrees of freedom" problem finds its resolution in a hierarchy of coordinated synergies. There is widespread biomechanical evidence of kinematic reduction in a diversity of mammalian motor patterns such as reaching (Lacquaniti et al., 1983), body segment coordination (Balasubramaniam and Turvey, 2004), and walking (Ivanenko et al., 2002; Grasso et al., 2000). Similarly, dynamical motor behaviors offer longstanding (Blickhan and Full, 1993) and accumulating (Full and Farley, 2000) evidence for collapse of dimension in vertebrate and invertebrate running and, more recently, climbing (Goldman et al., 2006). Discoveries from vertebrate (Burke, 1999; Saltiel et al., 2001; Burke, 2002) and invertebrate (Pearson, 1993) neuroscience suggest that neural activation results in precise, kinematically selective synergies of muscle activation. A consensus view has emerged for a hierarchical description of animal motion control architecture in which a modular (Mussa-Ivaldi, 1999) complex of motor functions combines distributed (Burke, 1999) feedforward pattern generating units (Grillner, 1985) mediated by local feedback (Pearson, 1995) with influence from, rather than domination by conventionally posited "higher" centers of function (Bizzi et al., 2000).

The next challenge in motor science is to move from this broad consensus regarding description to the point of prescription. This latter term denotes computational models that might tie the widely accepted accounts of biological structure to their function in the production of empirical motor behavior, thereby producing testable predictions of motor control architecture. Our use of the term "architecture" underscores our larger interest in how the components of motor control are put together under various circumstances. The descriptive consensus supporting a modular hierarchy encourages the expectation that this should now be possible. Namely, prescriptive computational models capable of accounting for a diverse variety of animal activity

ought to incorporate some hierarchical decomposition into motor primitives (Schaal and Schweighofer, 2005).

In the contemporary literature such models take divergent form and seem to vary widely even concerning their scope. For example, several decades of advances in the primate reaching and grasping literature have achieved the textbook (Shadmehr and Wise, 2005) consensus that a kinematic task-oriented reference trajectory "leads" the compliant musculoskeletal system through a representative motion around which the necessary stabilizing torques and forces are generated at the joint level. However, elements of controversy (Jaric and Latash, 2000) still surround the extent to which such feedforward signals (Domen et al., 1999) are "pre-processed" by the nervous system using learned internal models to compute the inverse dynamics (Kawato, 1999) as would be required to insure asymptotically exact tracking in the equivalent rigid body mechanism and as observed in humans (Hinder and Milner, 2003). Moreover, the very question of how such a library of feedforward signals is constructed, deployed, and potentially mediated by the animal's immediate or longer term mechanical experience remains uncertain.

In reaching tasks, the endpoints of the reference trajectory are presumably driven by perception. Various optimality criteria have been proposed to explain how the resulting interpolating curve is constructed (Todorov and Jordan, 1998; Nakano et al., 1999; Biess et al., 2006). Within this framework, the tradeoffs between feedforward and feedback influences can be determined by stochastic optimal control theory (Kuo, 2002; Kording and Wolpert, 2006). Recent evidence (Schaal et al., 2004) suggests that such discrete motor acts may be initiated and organized differently from rhythmic behaviors such as steady running.

It is worth noting that notions of optimality do not always offer broad prescriptive power. For example, the composition of optimal trajectories is typically not optimal. The appeal to optimality may confound the development of more fundamental compositional principles. For example, arguments for the "power law" (Todorov and Jordan, 1998; Richardson and Flash, 2002), and, more particularly, that the observed episodic power law trajectories constitute the alphabet of a "motor language" have been shown to be equally well explained as artifacts of nonlinear kinematics (Sternad and Schaal, 1999; Schaal and Sternad, 2001).

In contrast, we find the framework of dynamical systems particularly attractive because it permits a malleable but precise means of exploring the composition of modules respecting both their spatial arrangement and temporal sequencing. Dynamical representations of mechanical modules are familiar, and the utility of "collapsed" abstractions of such models has a growing tradition in biomechanics (Full and Koditschek, 1999; Blickhan, 1989) and robotics (Raibert, 1986; Koditschek and

Bühler, 1991) – a bouncing spring mass system being one such model or template. Physiologically meaningful dynamical models of neurons (Hodgkin and Huxley, 1952) can be reduced to two (Morris and Lecar, 1981; Fitzhugh, 1961) or three (Ghigliazza and Holmes, 2004b) dimensional dynamical systems in principled ways that retain the salient physiological dependencies with very few lumped parameters. In turn, these can be assembled as physiologically representative (Pearson, 1976) modules, in a network of coupled oscillators that admits further mathematically principled reduction in dimension via phase variables (Ghigliazza and Holmes, 2004a).

1.1.2 Dynamical systems approach to neuromechanics

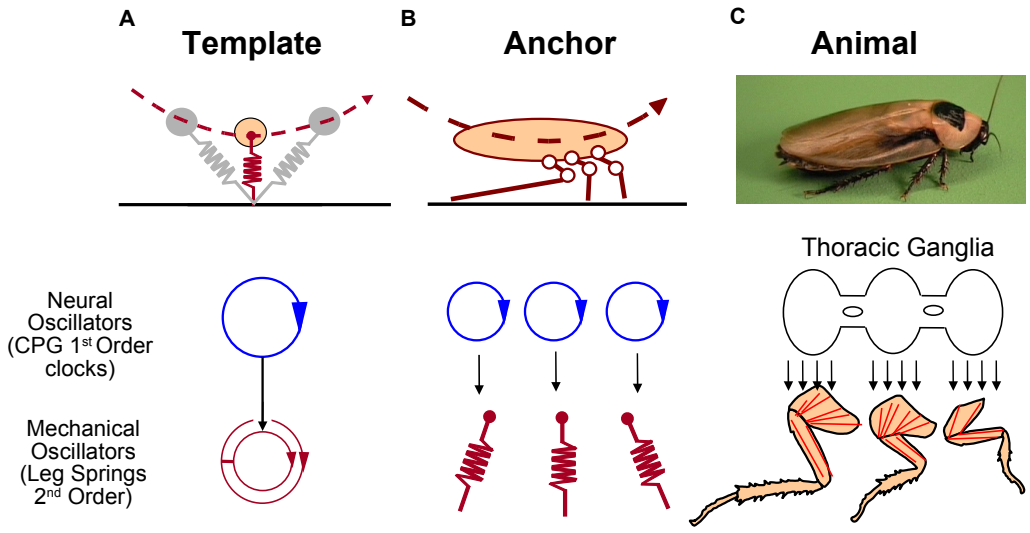

Figure 1.1: Representation of animal locomotion as coupled oscillators. Systems are modeled by using two different types of oscillators. The hypothesized thoracic ganglion central pattern generators in arthropods are represented by first order clocks or oscillators (single circles). The musculo-skeletal system is represented by mass-spring systems or second order oscillators. We represent this second order property of a mechanical degree of freedom by means of the double circle icon. **A Template**. The model with fewest parameters is termed the template. **B Anchor**. A model more representative of the animal, the anchor, shows the coupling of three neural and mechanical oscillators. **C Animal**. A modified form of this figure appeared in Koditschek et al. (2004)

Adopting a dynamical systems approach to the study of steady state rhythmic activities such as running has led to several general hypotheses regarding the structure of neuromechanical control (Koditschek et al., 2004). For ease of exposition we state these hypotheses within the framework of deterministic dynamical systems theory, although it is clear that a far more subtle treatment of the inevitable variability in real data, for example along the lines presented in Riley and Turvey (2002), would be required to handle the results of physical experimentation.

Hypothesis H_1 - Dynamic stability We have proposed that the primary requirement of an animal's neuromechanical control strategy is to stabilize its motion around orbits or limit cycles – periodic solutions to the equations of motion describing the animal coupled to its environment in whose neighborhood there are no other periodic solutions (Full et al., 2002). In a dynamical systems sense, stability can be defined as the tendency of a system to return to a steady state even when perturbed. Perturbations shift the state onto nearby trajectories that are either stable (lead back toward the limit cycle) or unstable (lead away from it). For a locomotor behavior to be effective, the limit cycle must be stable and the motion must return to the limit cycle after all sufficiently small perturbations. Typically, dynamical systems models predict that perturbations to mechanical state variables (positions and velocities) will differ in rate of recovery, be coupled, and will reveal systematic shifts in the relative timing of limb coordination.

Hypothesis H_2 - Collapse of dimensions We have proposed that multiple legs, joints and muscles operate synergistically to reduce the number of dimensions permitting the limit cycle to be represented by a simple, low dimensional template (Full and Koditschek, 1999) dynamical system (see fig. 1.1). The relationship between the low dimensional template and the higher dimensional anchor models that are more closely tied to the animal's morphology is via a posture principle. The posture principle states that each behavior has a characteristic family of body postures associated with it, and that through maintaining the body in these postures the animal forces the high dimensional anchor dynamics to closely follow those of a lower dimensional template. For example, many animals with diverse morphologies and varying number of legs run in a way that moves the center of mass as though it is bouncing on a single elastic pogo-stick (Blickhan and Full, 1993) (fig. 1.1).

Hypothesis H_3 - Tunable coordination control architecture We have hypothesized the presence of a tunable coordination control architecture that couples together

an "internal" clock or central pattern generator (CPG), whose period is directly controllable, and the rhythmically oscillating mechanical system of the animal's body, whose period is only controllable indirectly by adding or removing energy. Following the example of Cohen et al. (1982), we represent the CPGs in animal's nerve cord as first order oscillators in phase coordinates on the circle. A first order system cannot oscillate without some switching controller unless its state lies on a circle (Winfree, 1980). Because frequency is the control input to the system, we denote a first order oscillator by a single circle (blue circles with an arrow; fig. 1.1). We represent an animal's musculoskeletal system as a body mass atop a leg spring. These mechanical systems function as second order oscillators that have a phase velocity (frequency) altered generally through the intermediary of a power input changing its energy. We represent this second order property of a mechanical degree of freedom by means of the double circle icon (double red circles with arrows; fig. 1.1).

The coupling of a neuro-oscillator with a mechanical oscillator substantially reduces the number of feedforward signals required for motion. Paradigms such as Equilibrium Point Trajectory and adaptive inverse dynamics internal models, are yet to explain the construction and organization of the library of feedforward signals necessary for each movement. In a coupled oscillator model, feedforward reference signals arise as the output of a dynamical system – a neural pattern generator equivalent to an explicitly parametrized "library" of trajectories – whose "entries" are parametrized by the dynamical system's state space or initial condition. Each different initial condition gives rise to a different reference trajectory. Yet, *no independent library of particular trajectories* is stored.

Even more importantly for our present purposes, a dynamical representation of the driving signal or neural clock is not only amenable to hypotheses related to motor "learning" but to the possibility of more immediate influences back from the musculoskeletal system up to the internal clock. Whether modified more or less by feedback a purely feedforward signal generator cannot readily change the timing of events. In contrast, expressing our internal command generator as a clock allows the possibility that the mechanical subsystem might retard or advance its phase. By embracing a dynamical representation of the internal reference signal generator, we will explore in this chapter the extent to which relatively simple physical mechanical perturbations of an animal's gait can be used to probe the presence and nature of such feedback influences upon an internal pattern generator by the physical experience of the musculoskeletal system.

1.1.3 The neuromechanical "operating point"

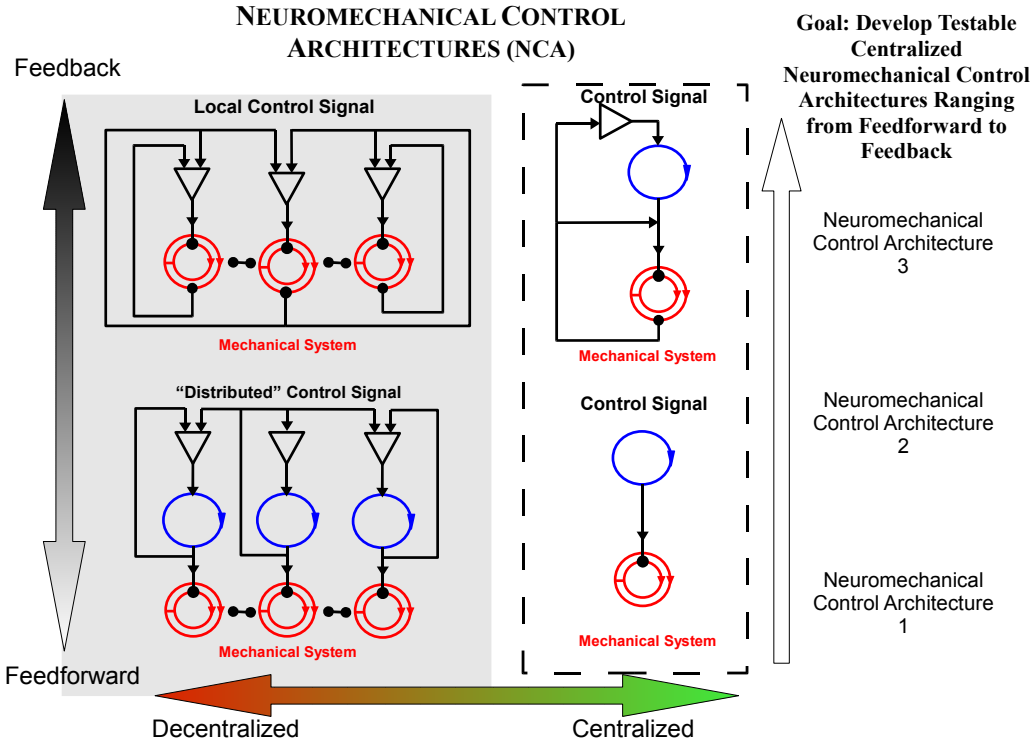

Figure 1.2: Neuromechanical control architectures (NCAs) can be classified by broad properties that include the degree of centralization and the extent feedback information can affect the feed-forward signals the controller produces. In this chapter we describe three control architectures with a central pattern generator that utilize increasing levels of feedback processing (as indicated by the white arrow) and compare them with an architecture NCA0 that has no CPG

Within a coupled oscillator framework, we adopt the classification of Klavins et al. (2002); Koditschek et al. (2004), organizing the range of variation of neuromechanical control models into a plane of designs (fig. 1.2) available for selection by the animal's nervous system. We posit that the choice of operating point in this plane selects the coordination coupling the dynamics of internal neural oscillator and musculoskeletal force production. The axes of this plane can be characterized by the balance between

feed-forward and feedback control, and the degree of centralization of the information flow.

No single operating point in the plane seems to characterize exclusively the behavior of any animal model. For example, at the more extreme "feedback, decentralized quadrant" of the two axis design plane (fig. 1.2) lie decades of careful empirical study on invertebrate walking (Cruse, 1990) that have yielded algorithmic prescriptions less familiar to optimal control theory, but readily studied using the tools of dynamical systems theory (Calvitti and Beer, 2000; Klavins et al., 2002) and demonstrably capable of coordinating complex multi-limbed locomotion in physical (Chiel et al., 1992) models operating in the quasi-static regime. Yet recent experiments have identified (Büschges and El-Manira, 1998) and simulation studies confirmed the important role of feedforward pattern generators in the walking behavior of this animal model (Ekeberg et al., 2004). In contrast, early models of rhythmic vertebrate behavior suggested the prominence of a strongly centralized feedforward CPG signal (Grillner, 1985), whereas recent studies (Guan et al., 2001) have revealed a more nuanced balance between feedforward and feedback influences. It seems increasingly clear that animal locomotion strategies span the entire neuromechanical architecture plane (fig. 1.2).

Surely, one contributing factor to the difficulty of prescribing motor behavior is that the theoretical underpinnings of different regions in this design plane manifest different levels of maturity. Whereas the theory and practice of adaptive inverse dynamics reference tracking controllers for rigid body manipulators, was worked out two decades ago (Whitcomb et al., 1993; Slotine and Weiping, 1986; Sadegh and Witz, 1987), the dynamics of coupled nonlinear oscillators underlying the complete architectural design space of interest remains an active area of mathematical research. Similarly, while there is a three hundred year old literature on Lagrangian mechanics, neural models admit no appeal to physical first principles at the comparable level of universality and methods of abstraction. Nevertheless, the last two decade's intense effort put into both the mathematical formalism and the modeling applications of CPG theory (Holmes et al., 2006) supply us with a two important concepts: the notions of phase and phase response curves.

A large literature on locomotion oriented coupled-oscillators, following on the seminal Cohen-Holmes-Rand Lamprey CPG model (Cohen et al., 1982), enjoys a ubiquity guaranteed by *isochron theory* (Winfree, 1980; Guckenheimer, 1975). This model of coupled first order oscillators has been successfully applied to numerous rhythmic applications ranging from human hand manipulations (Sternad et al., 1992) to robotic juggling (Klavins and Koditschek, 2002) and running (Weingarten et al., 2004a). One subsequent effort toward integrated neuromechanical (in the sense of a second order dynamical generator) modeling of the coupling between internal pattern generators and

the mechanical body working in its environment, the Haken-Kelso-Bunz model (Haken et al., 1985) has stimulated rhythmic studies in humans (Kelso et al., 2001) that support the predicted appearance of certain bifurcations. Moreover, recent efforts (Peper et al., 2004) to ground this model in more detail seem to give the promise of further insight into the mechanisms of human coordination. But the model hypothesizes a fundamentally fixed architecture, occupying a particular point in the feed-forward/feedback and centralized/decentralized plane of motor coordination.

Still missing are broadly applicable behavioral assays such as perturbation experiments that might help pin down at what operating point in this "design space" (Koditschek et al., 2004; Klavins et al., 2002) any specific motor activity is maintained, much less a *prescriptive* view of how some specific environmental condition or particular task might dictate (or at least constrain) that selection. This chapter places particular emphasis on the feedforward/feedback axis of the design space for more centralized controllers (right side of fig. 1.2). We do so within the framework of coupled oscillators where we couple a single neural pattern generator to a single mechanical oscillator rather than focusing on the decentralized coupling of individual neural pattern generators to each other (Golubitsky et al., 1999) or mechanical oscillators to one another (Haken et al., 1985).

1.2 Neuromechanical control architectures

Here we compare four classes of neuromechanical control architectures (NCA0 through NCA3, illustrated in fig. 1.2). NCA1 through NCA3 embody increasing levels of feedback influence on pattern generated by the nervous system, and NCA0 offers an alternative with no CPG. These explore the operating points in the neuromechanical control architectural space that go from more feedforward to greater feedback within a centralized architecture (fig. 1.2). Our choice of architectures is strongly influenced by the biological literature and by analogies to controllers of legged robots built by one of the authors (Koditschek, Saranli et al. 2001) and robots built by other collaborators.

Our architectural classes sample a range of possible couplings between the subsystems of fig. 1.1. The simplest instance is one where only the mechanical state of the animal is of importance and processing is minimal, whereas the most complex is one where a neural controller uses feedback to stabilize the mechanics and internally represents the phase of the mechanical system with bidirectional coupling to a CPG. Two more architectures of intermediate complexity and processing ability are described.

In proposing these architectures we do not suggest that any one of them describes the structure of the neuromechanical control system in any given animal, or corresponds

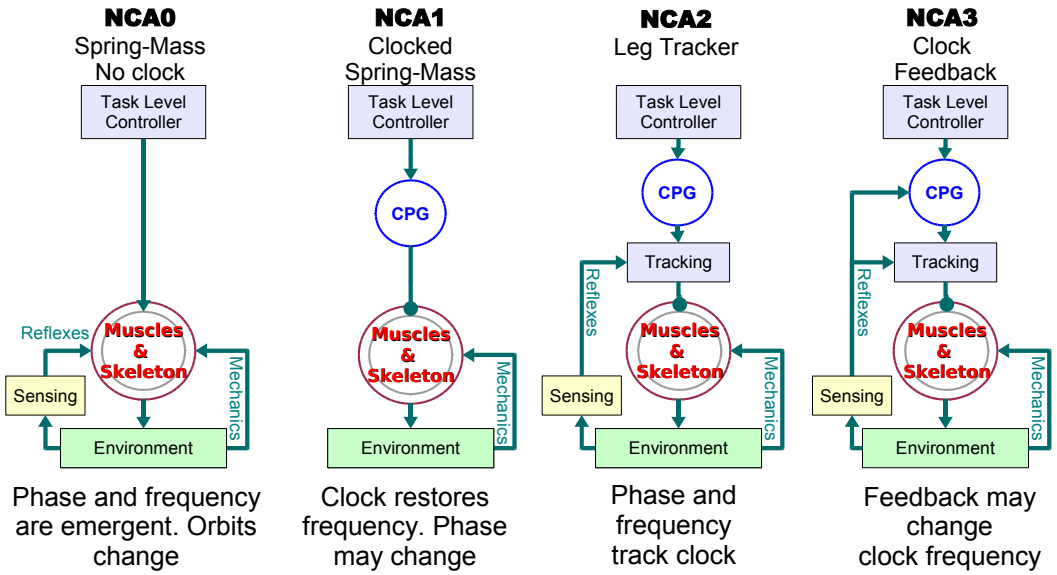

Figure 1.3: Columns represent the control architectures NCA0 through NCA3. The "Task Level Control" block generates a constant setting of parameters for the behavior (e.g. "use tripod gait at 15 cm/sec"). "CPG" plays out a scheduled periodic signal at the frequency selected by the task level control and possibly modulated by feedback. "Tracking" compares actual and reference trajectories in a time–invariant way to generate a force activation. "Muscles and Skeleton" interact mechanically with the "Environment" and also modify the representation of the environment returned by "Sensing"

in a direct way to morphology. Rather, we propose these as parsimonious and testable models for control used in specific behaviors. A conclusive experimental outcome – one that rejects simpler feedback architectures in favor of more elaborate ones – enables us to say that during a specific task or behavior a control architecture as simple as the one we find is sufficient for explaining the outcome, and is functionally equivalent to the animal's controller within this restricted context. An animal may use controllers from all of these classes in different behavioral contexts, or when dealing with extreme perturbations in the same behavioral context.

The exact outcomes possible with models belonging to each architecture class are sensitive to the details of the equations of motion. Nevertheless, some conclusions can be drawn if we assume two properties: asymptotic stability of the periodic motion,

and structural stability of the dynamical system. The former property implies that any initial state sufficiently close to the periodic orbit governing the locomotor behavior moves onto the orbit. The latter property implies that the dynamics remain unchanged (in a topological sense) if the equations of motion are modified by small changes.

While both these assumptions may not hold for some models of locomotion, we feel they are justified for practical reasons. Persistent locomotive behaviors seem to have a periodic structure that animals revert to even when perturbed by the environment. Asymptotic stability expresses this reversion in mathematical language. Structural stability expresses the fact that properties of the animal's body and environment are variable, and to maintain a behavior, the equations of motion must be effectively insensitive to this variability.

1.2.1 NCA0 – Spring Mass with no Clock

The simplest class of architectures we propose is outside the feedforward – feedback axis of fig. 1.2, in that it contains no CPG at all and thus the extent of feedback to CPG is immaterial. The behavior of NCA0 systems is governed almost entirely by mechanical dynamics. As the block diagram in fig. 1.2 illustrates, once the task level goals are set all dynamics are mediated by the mechanical interaction alone. The defining property of NCA0 systems is this lack of "internal" non-mechanical state, allowing equations of motion to be written solely in terms of instantaneous mechanical state variables. By observing the mechanical state of a NCA0 system one may predict its future course, and so mechanically identical "snapshots" of a behavior should reliably lead to similar motions over multiple cycles of motion. What little control there is occurs at the transition between mechanical regimes. Like the lateral leg spring model (LLS) (Schmitt and Holmes, 2000a,b) and the spring loaded inverted pendulum model (SLIP) (Blickhan, 1989), running NCA0 systems stabilize by virtue of how the posture of the body evolves from ground contact to ground contact [1]. For example, in the simplest model presented in Schmitt and Holmes (2000a) it is shown that after a perturbation by a lateral impulse, the angle between the body heading and the direction of motion becomes smaller from step to step by virtue of the leg force acting on the body. The instantaneous mechanical state of the model is sufficient to make such an argument, and predict future cycles of motion.

[1] The LLS and SLIP models would fall into the NCA0 category – except for the technicality that they are not fully asymptotically stable and thus do not satisfy our H_1 hypothesis

1.2.2 NCA1 – Clock Driven Spring Mass

The second class of architectures is a family of driven mechanisms with variable stiffness. These and all subsequent architecture classes we consider differ from the previous class by the introduction of a clock that "keeps internal time" via its phase θ. In this second architectural class, the clock is uncontrolled. It runs at a constant frequency ω and sets the mechanism's stiffness using a periodic function (a "schedule") $\psi(\theta)$. No reciprocal influence from the mechanical state modifies either the clock frequency or the stiffness imposed at any particular phase (see second column of fig. 1.2 for a block diagram).

It is convenient to imagine NCA1 systems as compliant-legged clockwork toys. A snapshot of the kinematic state of a clockwork toy does not tell us whether the internal spring is wound-up or not, but after observing its motions for a few cycles – they are completely predictable, and they do not vary except in so far as external forces directly hinder or aid them. The motions themselves cannot be predicted directly from the mechanical state, but they are predictable periodic functions of time, and changes to these motions are accomplished only by mechanical means.

Many actual toys are built with NCA1 architectures, as are the fastest running legged robots – the Sprawl robots (Bailey et al., 2001).

1.2.3 NCA2 – Tracking Leg Controller

The third class of architectures also contains a feed-forward (dynamically uncoupled) driving clock. The clock schedule interacts with the body mechanics by inducing the generation of forces. These forces are not a scheduled pattern of activations – instead they are infinitesimally generated [2] by comparing the actual trajectory of a leg and a reference schedule driven by the clock. The comparison is carried out by a filter [3] which in robotics applications would be referred to as a "tracking controller" because it would cause a leg to track any reference signal. In that sense, the filter realizes an internal representation of the mechanical dynamics of a leg.

Reflecting this view, our depiction of the "Tracking" block in fig. 1.2 incorporates a feedback channel that reaches "up" to a level mediating the clock output but not as "high up" as to affect the internal dynamics of the clock itself.

We constrain the filter to be time invariant, so that the feedback it generates can

[2] We use the phrase "infinitesimally generated" to represent the fact the trajectories are defined in terms of an ordinary differential equation, which is an equation relating infinitesimal quantities.

[3] The term "filter" refers to the feedback laws being specified by a function of the tracking error *and its derivatives* rather than merely a function of instantaneous tracking error

depend on the form of the reference trajectory and of the actual trajectory – but cannot depend directly on time. The filter encodes the mechanical dynamics in the sense of being able to anticipate what force is necessary as a function of tracking error and state to drive this error to zero, thereby making the mechanical trajectory converge to the reference.

Unlike NCA1 systems, NCA2 systems react to mechanical perturbations using non-mechanical means that require some form of neural sensing. As forces are exerted by the musceloskeletal system of the animal, the kinematic changes induced by these forces are compared with the reference provided by the clock and forces are adjusted according to discrepancy detected with the sensory information. The adjustment is time-invariant – it does not depend on "when" in the cycle of motion a particular kinematic discrepancy occurs, only on the difference between the actual and reference trajectories. Like the stiffness of the clockwork NCA1 systems, the "desired" reference trajectory is a predictable, periodic function of time, and by knowing this function, the reaction to an external perturbation is predictable – but unlike NCA1 systems, this prediction is not purely a mechanical outcome.

Examples of NCA2 systems include most commercially available robots, and the first generation of controllers for the RHex robots (Saranli et al., 2001). In the RHex robots, each leg has a "proportional-derivative (PD) controller" attached to its driveshaft motor. These PD controllers read the state of the driveshaft, compare it to the desired reference angle for that leg and cause the motor to exert a force proportional to the size of the error ("Proportional" gain) and the rate of change of that error ("Derivative gain"). In the sense of fig. 1.2, each leg has its own "Tracking" block that knows nothing about the state of other legs, and brings that individual leg into conformance with the clock signal.

The filter as set out here bears some correspondence to the classical notion of an "Equilibrium Point Hypothesis" controller. The major distinction to be drawn here is the origin and meaning of the reference signal itself. Proponents of the Equilibrium Point Hypothesis (Jaric and Latash, 2000) and of the more detailed internal model architecture (Kawato, 1999) and its associated optimization literature posit a kinematically (and, possibly, dynamically) particular reference signal that encodes in detail space-time information sufficient for the specific motor act being indexed, presuming the mediating feedback will correct the minor imperfections of the internal model as well as the potentially major perturbations of the un-modeled external world.

In contrast, the reference signal issued by NCA2 works primarily as an infinitesimally generated "clock" arising as the output of a (typically simple) dynamical system. It may well have space-time detail grafted on — for example, as in Saranli et al. (2001); Weingarten et al. (2004a,b), where the piecewise constant vector field is not simply a

constant — but its primary purpose is to time the onset of the different repeated phases of the rhythmic locomotion cycle.

1.2.4 NCA3 – Clock Feedback Controller

The fourth and final class of architectures extends the previous class by allowing the clock dynamics to be affected by the mechanical state, rather than merely having the clock output filtered. We restrict the NCA3 architecture to systems where the clock feedback is "small" in the sense that the clock never stops or reverses direction. We also require that the signal generated by the clock remains the same except for changes in frequency, and that changes to the clock are slow with respect to the gait cycle time and thus take a step or longer to become noticeable.

It is convenient to think of a NCA3 system as assessing overall "difficulty" and adjusting its desired frequency accordingly. Depending on the task and the perturbation, the system might speed up or slow down, always "trying" to accomplish the goals set by the task level control. NCA3 systems are similar to those with simpler architectures in that they express a one-dimensional loop of "desired" states – the reference trajectory – in a predictable cyclic order. The forces exerted are a time invariant function of the difference between the reference and actual trajectories. Yet, unlike simpler architectures, the rate at which this sequence of "desires" is expressed depends on sensory information.

An example of a NCA3 device is the RHex robot with the new generation controllers described in Weingarten et al. (2004b).

The succession of architecture classes just introduced may reveal to the reader that we do not posit the clock as the source of kinematic or dynamic "space-time" detail (although it might be used for that purpose as well by appropriately detailing the vector field or the feedforward component as exemplified by Weingarten et al. (2004b)) as much as viewing it as a time-keeper. Our point of view is so agnostic about the "true function" of the internal reference signal that we may just as readily embrace the interpretation that it is the body's internal state estimator for the mechanical phase and beyond, as suggested for example in Kuo (2002).

1.3 Kinematic phase – a window into a dynamical system

The challenge of testing neuromechanical control architectures (fig. 1.2) and determining the operating point of an animal in an architectural design space (fig. 1.2) is

considerable. Perturbations to a system and its subsequent response are necessary to reject architectures. Recovery responses must be measurable. Ideally, the approach taken should allow a window into the dynamical system. Both the global responses at the level of the template or system as well as more local responses at the level of the anchor (the detailed joint and appendage motions that result in a characteristic posture) should be identifiable. Recovery of the center of mass to its original limit cycle or to a new one should be detectible. It should be apparent whether and how perturbations of joints collapse back to a representative posture.

Measuring the recovery of the center of mass from perturbations during running has proved difficult. Support for the lateral leg spring model (most similar to NCA0) has come from perturbations using a jetpack on running cockroaches (Jindrich and Full, 2002). Cockroaches recover within a step using the intrinsic properties of their tuned musculo-skeletal system. Evidence for spring-loaded, inverted pendulum behavior has been found when helmeted guinea fowl recover from a step perturbation when running along a track with a false top (Daley and Biewener, 2006) and when humans run on surfaces of various compliance (Ferris and Farley, 1998). More common are detailed kinematics responses to perturbations that add to our intuition about a control hypothesis, but do not reject a neuromechanical control architecture (Kohlsdorf and Biewener, 2006).

Here, we propose a kinematic approach based on phase analysis that can be used by experimentalists to test neuromechanical control architectures. Biomechanists have long employed gait diagrams and phase response curves for the study of rhythmic locomotor tasks. In the study of terrestrial locomotor gaits, the repetitive motions of the limbs are partitioned into cycles based on foot landing and liftoff events. Phase within a step is typically defined in terms of the fraction of time elapsed since the last footfall relative to the interval ending with the next footfall. These techniques have been used effectively in many studies, such as those characterizing inter-leg influences in stick insect walking using phase response curves (Cruse and Epstein, 1982; Cruse, 1985a,b).

This standard approach is dependent on a distinguished footfall "event". It is often difficult, if not impossible, to define phase when perturbations significantly change or even destroy the event altogether, such as when locomoting on a rough terrain where footfalls can be missed entirely. Low time resolution makes it difficult to differentiate both perturbations and recoveries. For example, a delay in the motion of a limb induced in early swing may not be resolved from one induced in late swing. More generally, in such classical methods, frequency is defined by the time elapsed between footfalls – meaning that frequency is only "measured" once a step, and it is difficult to deduce at what point in time frequency actually started changing.

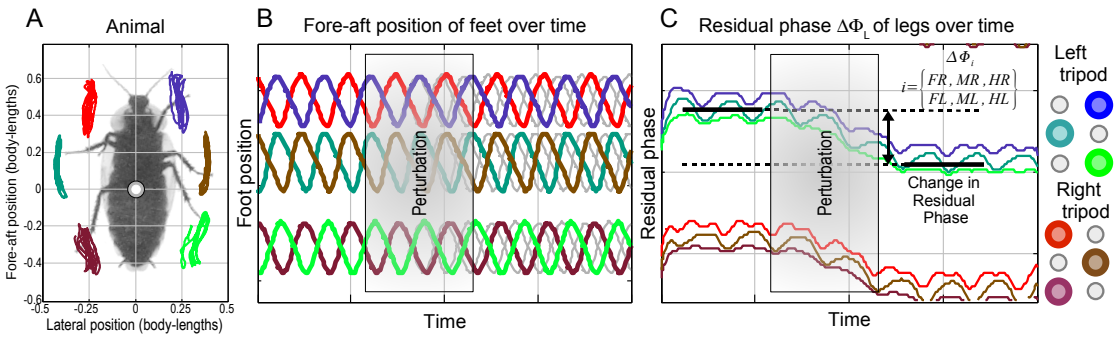

Figure 1.4: Relationship between foot or tarsal paths, their periodic coordinates and phases for a running cockroach. **A** Paths of feet relative to the body in constant speed running (experimental data); **B** Periodic fore-aft positions x_i $i = \mathsf{FL}, \mathsf{ML}, \ldots$ of feet in the body frame (model). The grey lines indicate extrapolated positions of the feet consistent with motions before the perturbation; **C** Residual phase of the feet in **B** ($\Delta\Phi_i$) relative to a putative constant frequency model ($\hat{\Phi}_{\mathsf{ext}}$). The π phase difference between the two tripods and the constant frequency are clearly apparent. Each tripod comprises the front and hind legs on one side of the body together with the middle leg of the other side, as illustrated by the color-coded circles on the right of the figure

Our kinematic phase method enables phase and frequency to be resolved "instantaneously". In high-speed video-based kinematic measurements, a phase and frequency can be reliably computed for each pair of consecutive video frames. For example, movements of the feet of a running cockroach relative to its body (fig. 1.4-**A**) can be plotted as near sinusoidal oscillations as a function of time (fig. 1.4-**B**). If a cockroach was perturbed by an obstacle that altered the phase of all its legs, then a phase change should be apparent in the sinusoidal oscillations when the oscillations before the perturbation are compared with those after (fig. 1.4-**B**). This can be seen by extrapolating the oscillations before the perturbation into the time after the perturbation (fig. 1.4-**B**, grey lines). Our method determines the change in relative phase at every instant in the cycle (fig. 1.4-**C**). Cockroaches use an alternating tripod when running fast. The front left, middle right and left hind leg are in phase, but move in anti-phase to the front right, middle left and right hind leg. In our example (fig. 1.4-**C**), the relative phase of legs within a tripod is the same. Before the perturbation, there is no change in the phase of the legs. After the perturbation, a phase change has occurred in all legs and both tripods. The phase change can be detected for any leg at any time, even within a step, with readily available kinematic data.

From a theoretical standpoint, our method to calculate instantaneous phase change relies on a dynamical systems view. We assume that a locomoting animal is best represented by a high dimensional dynamical system. Its high dimensional state consists of mechanical quantities such as positions, velocities, strains, etc., as well as myriad non-mechanical quantities representing the state of the nervous system and the animal's physiology. In steady state, our hypothesis H_1 asserts that its deterministic periodic behavior is manifest as an isolated cycle embedded in this high dimensional state-space and thus defining a global phase Φ_{G}. The projection of global phase Φ_{G} on any subset of coordinates associated with some sub-system specifies a phase consistent with global phase but expressed only in terms of that sub-system. As a consequence we can speak of a "mechanical phase" Φ_{M} defined in terms of the mechanical state variables alone; "kinematic phase" Φ_{K} defined in terms of the kinematic state variables alone and "leg phases" $\Phi_{\mathsf{FR}}, \Phi_{\mathsf{MR}}, \Phi_{\mathsf{HR}}, \Phi_{\mathsf{FL}}, \Phi_{\mathsf{ML}}, \Phi_{\mathsf{HL}}$ for the individual legs (front-right, middle-right, etc.) of a hexapedal animal.

A priori, the global phase Φ_{G} is difficult to estimate, whereas the "kinematic phase" Φ_{L} of a sub-system such as a leg L can be estimated more easily by some phase estimation function $\hat{\Phi}_{\mathsf{L}}$ (we use the hat $\hat{\cdot}$ to denote estimates of quantities) of its directly observable kinematics. Such an estimate function is a smooth function of kinematic observations of leg L and corresponds to the actual leg phase Φ_{L} on the cycle itself. For all states sufficiently near the limit cycle, the global phase Φ_{G} is well defined. The projected phase Φ_{L} for a sub-system L may be multi-valued because it depends on the state of other sub-systems outside of L. As a consequence, the phase estimate $\hat{\Phi}_{\mathsf{L}}$ for states off the limit cycle will be different from the actual phase of the sub-system Φ_{L} by a (linearly) small term. Nevertheless, we argue that by using a combination of these estimates that includes all of the sub-systems that may move independently in the behavior (e.g. all legs), we can obtain an estimate $\hat{\Phi}_{\mathsf{K}}$ of the whole kinematic phase Φ_{K}. In a repetitive and persistent locomotor behavior such as constant velocity forward running, the complete state of the animal is in correspondence with its kinematic state – otherwise the behavior would not persist in a repetitive form – and so the kinematic phase estimate $\hat{\Phi}_{\mathsf{K}}$ is (a posteriori) a reasonable proxy for estimating global phase Φ_{G}.

fig. 1.5 illustrates the relationship between a global kinematic phase estimate $\hat{\Phi}_{\mathsf{K}}$ and the kinematic phases of the legs $\hat{\Phi}_{\mathsf{FR}}, \hat{\Phi}_{\mathsf{MR}}, \hat{\Phi}_{\mathsf{HR}}, \hat{\Phi}_{\mathsf{FL}}, \hat{\Phi}_{\mathsf{ML}}, \hat{\Phi}_{\mathsf{HL}}$ from the running cockroach in fig. 1.4-**A,B**. We assume that our kinematic phase estimate $\hat{\Phi}_{\mathsf{K}}$ (fig. 1.5-**A**) represents the global phase Φ_{G}. In this example, the kinematic phase estimate $\hat{\Phi}_{\mathsf{K}}$ is constructed from the positions and velocities of the animal's six feet by treating the centroids of the two tripods as "virtual legs". We used the relative position of the tripod centroids and its derivative (velocity) to generate a phase estimate by normalizing them to mean 0 and variance 1, and taking them as the X and Y coordinates of a point. The

phase estimate is the angle of the point, as plotted in fig. 1.5-**A**, relative to the X axis. The cycles of individual feet can be viewed as projections into different sub-systems (fig. 1.5-**B**) of our kinematic phase estimate $\hat{\Phi}_{\mathsf{K}}$.

We derived our estimate of the future motions of the animal (fig. 1.4-**B,C**) from our kinematic phase estimate $\hat{\Phi}_{\mathsf{K}}$ (fig. 1.5-**A**) which we also consider to be a reasonable estimate for global phase $\hat{\Phi}_{\mathsf{G}}$. We used the fact that by construction, global phase Φ_{G} evolves linearly in time. We "unwrapped" the cycles in our phase estimates so that phase is increasing rather than wrapping around from π to $-\pi$. These instantaneous unwrapped phases as a function of time – global and per-leg – are plotted in fig. 1.5-**C**. Once we were confident that our global phase estimate $\hat{\Phi}_{\mathsf{G}}$ evolved linearly over extended periods of time when validated with unperturbed motion data, we took pre-perturbation experimental data from a trial and extrapolated a model of the "unwrapped" data with some constant frequency ω and phase intercept ϕ_0 using linear regression:

$$\begin{aligned} \hat{\Phi}_{\mathsf{ext}}(t) \triangleq \omega t + \phi_0 \quad &= \quad \hat{\Phi}_{\mathsf{G}}(t) + \rho(t) \\ &\qquad \rho(t) \;\; \text{regression} \;\; \text{residual} \end{aligned} \tag{1.1}$$

The model predicts the future behavior that should have occurred without the perturbation. Because of the high temporal resolution of the phase estimate $\hat{\Phi}_{\mathsf{G}}$, a short pre-perturbation interval – potentially an interval as short as a step or two – may be sufficient for extrapolating several strides into the future with $\hat{\Phi}_{\mathsf{ext}}$.

The "(global prediction) residual phase", in the form of

$$\Delta\hat{\Phi}_{\mathsf{G}}(t) \quad \triangleq \quad \hat{\Phi}_{\mathsf{G}}(t) - \hat{\Phi}_{\mathsf{ext}}(t) \tag{1.2}$$

and its sub-system analogs for any sub-system S

$$\Delta\hat{\Phi}_{\mathsf{S}}(t) \quad \triangleq \quad \hat{\Phi}_{\mathsf{S}}(t) - \hat{\Phi}_{\mathsf{ext}}(t) \tag{1.3}$$

can be used to observe how the whole animal is perturbed in timing, and how different sub-systems reestablish their relative phasing. In the present example, fig. 1.5-**C** shows that the sub-systems in question – individual legs – exhibit characteristic phase relationships, and that the three legs with similar relative phases are those functioning as a tripod. Moreover, it illustrates that our estimate of global phase – the kinematic phase estimate $\hat{\Phi}_{\mathsf{K}}$ (fig. 1.5-**A** and grey line in fig. 1.5-**C**) also represents the phase and frequency (i.e. slope of the line in fig. 1.5-**C**) of the leg sub-systems when no perturbations are present. The lack of a change in instantaneous phase in fig. 1.4-**C** before the perturbation is simply a consequence of a constant difference in phase between the leg

phase and our global phase estimate (fig. 1.5-**C**). As shown in fig. 1.4-**C**, a perturbation may alter the residual phase, i.e. the phase relationship between the extrapolated phase estimate $\hat{\Phi}_{\mathsf{ext}}$ and the actual phase.

The utility of a global phase estimate in the study of non-linear oscillators cannot be over-emphasized. We expect that a global phase estimate will become an invaluable tool for the experimentalist studying biological systems that are, in mathematical essence, non-linear oscillators comprising a neural pattern generator, a musculoskeletal system and their interactions with the environment. The most obvious use of a global phase estimate is to allow the future motions of the animal to be predicted by linear regression of the global phase using its recent motions. This prediction may be compared with the outcome of the animal's response to perturbations – forming an assay that can be used to test neuromechanical control architectures (fig. 1.2).

1.4 Perturbation experiments

We examine several types of perturbations that can assist in revealing which control architecture best represents periodic locomotor behaviors like running. It is important to impress upon the reader that nonlinear hybrid systems, such as those governing animal locomotion, are unlike linear systems used in engineering in that their behavior cannot be fully characterized by their reactions to a standard set of stimuli. While linear time-invariant systems can be fully described by their response to impulses, chirps, and other textbook stimuli, our choices here are not governed by any such hope.

Instead, we chose perturbations that modify some aspects of the dynamical system while keeping other aspects fixed. We have tried to select perturbations that are "biological" in that one may expect such deviations from steady state horizontal running in a natural environment. We have also tried to pick perturbations that are tractable experimentally. These choices should not be seen by the reader as an exact recipe for experiments in all studies of running. Rather, these are exemplars from different classes of perturbations, applied to the study of running to provide the reader with concrete instances. The exact choice of perturbation should be made in light of a specific locomotor behavior, the animal system and its experimental feasibility – but we are confident that these broad classes of perturbations are generally useful.

1.4.1 Types of outcomes

Many outcomes are possible as a result of a perturbation. The outcome may depends on both the magnitude of the perturbation and that phase in which is was applied. In the remainder of this section, we describe types of outcomes that can readily be observed and quantified in kinematic phase measurements using an insect as our animal runner. In the next section we go on to relate these outcomes to perturbation type and control architecture class.

First, an insect may recover back to its original phase and frequency (fig. 1.6-**A**). Second, the perturbation may cause all the legs of a tripod to change phase from the original phase to settle back down to a phase different from the original phase (control compared to phase shifted; fig. 1.6-**B**). Third, the perturbation may cause all the legs of a tripod to change frequency (shown by a slope change in the phase plot; fig. 1.6-**C**). Finally, the perturbation may cause an orbit shift changing both phase and frequency from the original the shape of the trajectories in time and making phase comparisons more challenging to interpret (fig. 1.6-**D**).

Phase changes

Table 1.1: Expected outcome by perturbation and NCA class. The table summarizes the changes we would expect to see in phase, frequency and orbit shape if running animals using a controller architecture from a given class (column) are perturbed with the given perturbation (row). By performing multiple experimental perturbations we can obtain independent lines of evidence about the controller's architectural class

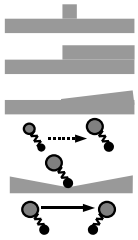

	NCA0 *Spring Mass No Clock*	**NCA1** *Clocked Spring-Mass*	**NCA2** *Leg Tracker*	**NCA3** *Clock Feedback*
Bump	P	D	=	P
Step	P	D	=	P
Incline	O(F)→N	D,P→N	P→N	P,F
Mass	P	P	P	P,F
Substrate	O(F)	O	=	P,F
Impulse	P	D	=	P

=	no asymptotic changes	F	frequency change
P	continuous phase resetting	O	change of orbit
D	discrete phase resetting	N	no stable solutions

By definition, the phase of undisturbed locomotion is a linear function of time, with a constant frequency as its slope. Phase change outcomes (P and D in Table 1.1) are changes in which the animal remains near the same periodic orbit, and thus moving with the same frequency, but at a constant offset relative to the phase's expected value at that time according to the motion prior to perturbation.

We separate two classes of phase change outcomes: discrete phase changes (D) and continuous phase changes (P). Discrete phase changes have characteristic values that depend only weakly on the magnitude of the applied perturbation such as the height of a bump or the grade of an incline. Typically, the discrete phase change (D) appears when the perturbation magnitude exceeds a threshold, and remains constant beyond that threshold. Continuous phase changes (P) depend in a continuous way on the magnitude of the perturbation and appear gradually as the perturbation magnitude grows.

Frequency changes

Frequency change outcomes (F in Table 1.1) are experimental outcomes where the period of the motion changes. Frequency expresses itself as the slope of the trend-line of phase as a function of time, and therefore frequency change outcomes correspond to significant changes in this slope. In practice, it is convenient to examine the residual phase, and statistically reject a slope of zero.

Mathematically speaking, a frequency change always requires a change of orbit – but changes in orbit shape may be too small to detect directly even when the associated frequency is different. Whenever frequency changes, the phases before and after the perturbation are no longer directly comparable because the linear equations predicting them have different slopes, causing the phase difference to be a function of time.

Orbit changes

Orbit change outcomes (O in Table 1.1) are outcomes where the limit cycle (the closed curve in the high dimensional state space along which the oscillations repeat) is sufficiently deformed that significant changes may be readily observable in the animal's kinematics. In such cases the coordinate transformation defining the phase of the original orbit must break down, and phases can no longer be compared in a trivial way before and after the perturbation. The breakdown of the old phase coordinate implies a large increase in magnitude of the fitting error when fitting a linear model to phase estimates applied to post-perturbation kinematic data. The large errors signify that the old phase estimate is no longer as useful because it assumes different orbit kinematics than those observed. A statistical hypothesis test of what constitutes a breakdown of the phase estimate, and thus an O outcome, is the converse of establishing that a phase estimate is useful: finding that the goodness of fit of a linear regression of the phase estimate is below what the investigator considers to be the minimal acceptable quality.

While relating phases across orbit changes is challenging, frequencies remain comparable in as much as they tell us whether the period of the new pattern of motions is different from the period of the old pattern. For some architecture and perturbation combinations the new orbit is almost certainly expected to have a different frequency (O(F) in Table 1.1).

Destabilization failures

Sometimes a given controller cannot handle a certain class of perturbation, leading to a situation where no steady state periodic solution is possible (N in Table 1.1). In such a case the kinematic patterns either do not approach any specific orbit and

undergo continuous changes, or the motions lead to some failure like crashing into the ground.

1.4.2 Perturbation types and their expected outcomes

Table 1.1 illustrates several perturbation types that are sufficient when considered collectively for identifying the controller architecture class. Here we describe the perturbation types, the reasoning behind their selection, and the expected outcomes they generate.

In repeated experiments with a given perturbation type, it is important to note that outcome may well depend on both the magnitude and the phase at which the perturbation was applied. Given the large variability in most biological data, proper experimental design and a large number of replicates are paramount. A more detailed treatment of these important topics is outside the scope of this chapter.

Bump perturbation

The simplest perturbation we consider is running over a bump. The bump provides a transient change in terrain followed by an environment that is in all ways identical to that preceding perturbation. We imagine that for each of the NCAs, a bump would be manifest as a change in ground height restricted to a single stance period.

The NCA0 controllers are governed entirely by their mechanical state. A bump modifies this state to a degree that depends continuously on the size of the bump. The NCA0 system has no "memory" of its prior phase and frequency, but the similarity between terrain before and after perturbation suggests that a return to the old limit cycle would provide a stable solution – incurring a phase lag or lead related to the size of the bump. Hence the expect outcome is P.

NCA1 controllers are governed by the inexorable nature of their driving clock. If the clock is oblivious to the mechanical state, a well defined phase relationship between the internal driving signal and the physical response can only occur if the mechanical interactions with the environment bring the body into phase with the clock. In turn, this implies that the mechanical orbit is partitioned into basins converging to different phase offsets relative to the driving clock. Bump perturbations are thus likely to generate discrete phase changes (D) when crossing basin boundaries and no changes if these boundaries are not crossed.

Systems with effective tracking will tend to function the same way regardless of external perturbation. Such is the case for the NCA2 class whose controller brings the tracking error to zero for all transient perturbations in the mechanical state. This

implies that the mechanical phase before and after a bump must follow the same linear schedule (=), exactly as dictated by the CPG.

The NCA3 controllers allow feedback to affect the clock by changing its frequency. The effect of these countervailing influences on clock rate by transient perturbations, such as bumps, is to generate a phase change (P) – the integral of the induced frequency change during the recovery period. The phase change is continuously dependent on perturbation magnitude because the recovery time and frequency change also depend on perturbation magnitude.

The reader may now already observe in Table 1.1 a general difficulty in distinguishing regulatory outcomes affected by algorithmic "internal" controllers from those due to comparably tuned mechanical feedback systems. For example, the Table 1.1 summarizes our prediction of identical outcomes (no change) for NCA0 and NCA3 architectures (continuous phase shift) when perturbed by bumps. The difficulty separating NCA0 and NCA3 is due in no small part to the fact that purely mechanical nonlinear systems can exhibit very complicated behaviors – as complicated as those exhibited by systems with sophisticated feedback mechanisms. Nevertheless, some general properties can separate NCA0 and NCA3 architectures with bump perturbations. First, NCA0s have no hidden state variables so their mechanically observable state should completely predict their behavior whereas one may imagine that different "internal" conditions will yield different kinematically observable dynamics for the NCA3 class. Second, because mechanical feedback can operate very quickly compared to algorithmic or neuromuscular feedback, it is reasonable to assume that very fast responses are purely mechanical as in NCA0. For responses to span times on the order of a stride period with no obvious mechanical conservation law maintaining them, a neural representation that persists over time is required, and thus implicates a NCA3 controller.

Step perturbation

Idealized mechanical models are often posited as manifesting conserved quantities, such as total energy and components of linear and angular momenta. While true physical systems cannot be entirely lossless, it is frequently the case that strongly underdamped mechanical components can yield behavior manifesting a reasonable facsimile of the idealized conservation properties. For these types of systems, a slightly more obtrusive terrain perturbation for running would be a step – a sudden and enduring change in ground height. The kinematic and dynamic changes are still localized in space and time, but the regime after the perturbation differs in one of the key integrals of motion – the potential energy. In such a case the controller is required to compensate

for the energy imbalance, which is never necessary in level running.

Because it is encountered by the legs as a transient, a step perturbation has similar outcomes to those of a bump perturbation for controllers of the NCA1, NCA2 and NCA3 classes. All these classes of controllers can and do stabilize the total energy of the system. Several purely mechanical NCA0 controller models have been proposed whose elements are tuned to closely approximate an energy conserving system – for example, the "passively stabilized" SLIP models in Ghigliazza et al. (2005). A step forces such a simple system to shift orbits, thereby likely changing the frequency. A sufficiently large step would cause the runner to halt by not being able to transition into flight, or to crash into the ground by having too much kinetic energy for the leg spring to absorb and return. Accordingly, for this kind of NCA0 variant the step recovery would be summarized by the symbol F or N.

However, some systems in the NCA0 class may regulate energy without neural feedback, for example by having positive force feedback (Geyer et al., 2003). In such cases the hybrid system's limit cycle is regulated with respect to energy. Since the floor remains level after its initial shift, any initial excess or deficit of energy will be bled out after a number of strides. The same limit cycle will reappear on a new isochron, so there will be a permanent change in the recovered phase relative to the old one. Magnitude of the phase changes is expected to be continuous in the magnitude and direction of perturbation. We have entered this outcome in the summary Table 1.1 as P, rather than the F or N consequences of the simpler "passively" stabilized mechanical variants described in the previous paragraph.

As the step perturbation to these architectures illustrates, roughly conserved mechanical quantities can readily reveal architectural differences, because they preclude full asymptotic stability in the absence of concerted neuromuscular feedback. They offer apt targets of the experiments we propose, because results reveal a specific non-mechanical regulatory mechanism. For example, the outcomes plotted along the corresponding row of Table 1.1 show the difference between NCA1, NCA2 and NCA3 controllers when encountering a step. The first would typically have kinematic phase lagging the clock, whereas in the second the tracking controller would correct the kinematic phase offset back to zero. In contrast, in the third, the transient errors would have temporarily altered the internal clock frequency to allow the kinematics time to "catch up" with the result of an overall phase resetting.

Finally, the reader should observe that the same difficulties as in the case of the bump perturbation are encountered here in distinguishing purely mechanical from neurally generated implementations of the same style of control. Similar outcomes of NCA0 with NCA3 suggest the desirability of adding some internal perturbations, such as disrupting neural feedback, to the complement of purely mechanical perturbations we

consider in this chapter.

Incline perturbation

In both bumps and steps the post-perturbation regime is geometrically similar to the pre-perturbation regime, with respect to the animal's body. The same body kinematics could, in principle, work equally well before and after the perturbation event. However, if an animal were to use the exact same kinematics (relative to gravity) running up an incline as it does running horizontally, it would introduce a systematic error in all foot placements and center of mass forces. Thus, an incline would challenge the controller to adjust to a new, slightly modified kinematic regime. For our posited physical models, an"incline" should be construed as a regular, linear change in ground height as a function of distance traveled.

Our NCA0 system will alter its frequency (F) or fail entirely when confronted by inclines. If feedback only at the transitions allows energy to be injected in this predominately mechanical architecture, then touchdown events will repeatedly occur "too early". Each time the controller will compensate for a wrong "neutral point." For small slopes there will be a net change in steady state cycle period resulting in a permanent frequency shift relative to the original. As the slope increases, the qualitative kinematic features of the steady state behavior will begin to depart significantly from the level ground periodic orbit. The combination of orbit and frequency change we denote symbolically by O(F). For larger slopes, no stabilization may be possible and critical failure may result. Thus in the end, the NCA0 system manifests disrupted orbits and gait instability that we mark with the symbol N in Table 1.1. This is illustrated in fig. 1.6-**D** by showing a phase plot of a system whose orbit is losing its similarity to the initial steady state orbit.

The oblivious clock of NCA1 systems would also encounter difficulties with inclines, although the approach to instability with increasing incline would likely take a different course. An incline perturbation would change the frequency of steady state solutions. For small inclines, this may well be within the basin of convergence for correctable phase differences and would express itself as a consistent phase error proportional to the incline. Namely, these intermediate inclines (significant but prior to failure) might induce significant enough postural changes in the body (in consequence of the passive compliant response to shifted gravitational loading) as to be dynamically viable and measureable as phase changes (P, D). At inclines sufficient to exceed the phase convergence basin of zero phase change, no steady state solutions are likely to exist (N).

NCA2 controllers deal with persistent kinematic challenges such as inclines by ap-

plying a constant correction each cycle. This leads initially to a phase change that is continuously dependent on the incline magnitude (P), and the existence of steady state solutions over a small range of incline gradients. The persistently corrective controller effort could be viewed a "penalty" for the mismatch between the CPG driving frequency tuned to flat ground and the changed frequency necessary for "optimal" incline running. Eventually, the frequency mismatch and inappropriate kinematic posture would disrupt the attracting cycle entirely (N).

Both NCA1 and NCA2 architectures have a driving clock that runs oblivious to the environment. With sufficiently large slopes, we might expect such a mismatch between stride frequency and ground contact mechanics to incur sub-harmonic oscillations. If these occur, systematic differences will appear between the kinematics of even and odd steps, causing the phase estimation function to degrade. The gradual deterioration of the orbit (O) will have a systematic structure, where the linear phase model residuals in even cycles have one characteristic form and the residuals in odd cycles have another form. In both NCA1 and NCA2 the clock frequency cannot change, almost entirely precluding the possibility of frequency change outcomes.

The NCA3 controllers have the capability to avoid the frequency mismatch penalty by changing their CPG frequency to accommodate the incline. The nominal gait will be retuned for the slope just as in the case of NCA2. However, now there is a chance if the feedback to the clock has sufficient influence at time constants well within the stride period, then the "early" (or "late") touchdowns may be corrected by advancing (retarding) the clock phase and then retarding (advancing) it to correct for wrongly anticipated stance phase duration. In this case, we would expect a distorted version of the original limit cycle. The cycle may have the same frequency albeit shifted phase, since the system would settle down on a new isochron (P). The system also may operate at a different frequency, since the internal clock advance and retard effects might not necessarily balance. The change in frequency means that the phase evolution controller governing the system before the incline is no longer meaningful. In the new limit cycle's phase coordinate, corresponding orbit events such as touchdown will be phase shifted relative to their positions in the previous orbit by a magnitude that is continuously dependent on the grade of the incline. fig. 1.6-**C** illustrates a NCA3 system compensating for an incline by changing frequency (F).

Dynamical perturbation

The last three rows of the table in Table 1.1 address perturbations that have already appeared in the empirical animal motor literature and we include their consideration in this chapter for the sake of continuity. Adding mass and changing the moment

of inertia of human runners has been studied for its own sake and as a model for dinosaurs (Lee et al., 2001; Carrier et al., 2001). Humans (Ferris and Farley, 1998) have been run on substrates of variable compliance. Jindrich and Full have reported the response of intact cockroach runners to sudden impulse perturbations (Jindrich and Full, 2002). In none of these previous studies has the relative kinematic phase explicitly been measured. We now briefly review what the expected phase responses would be to each of these distinct dynamical perturbations and include the outcomes in Table 1.

For NCA0 systems, a center of mass shift (either magnitude or position) or change in moments will again change the steady state posture, incurring a small but likely measurable offset (in proportion to leg compliance) in phase (P) that varies continuously with the shift. A small change in substrate mechanics (e.g. damping or compliance) may likely incur changes in individual leg transients at touchdown and liftoff and thus alter the kinematic phase (P) by shifting the ground-contact-feedback-triggered schedule for application of energy during leg stance. More dramatic substrate changes might lead to a sever deformation in the steady state kinematics, causing the original phase estimation function to have little power (O). A transient impulse applied to the center of mass carries kinetic energy and momentum that need to be bled off, entailing a change in phase that depends continuously on the magnitude of the impulse (P).

For the NCA1 system, a center of mass shift or change in moments will once again change the steady state posture, incurring a small but likely measurable offset in phase (P) that varies continuously with the shift. A change in substrate mechanics may once again incur changes in individual leg transients at touchdown and liftoff, but should not have a measurable effect on steady state phase (=) until the ground becomes so much more compliant that the kinematic shape of the limit cycle is altered (O). A transient impulse applied to the center of mass should yield no change for small impulses, but may switch the system to a new stable CPG-body phase relationship when larger. The phase change is thus a discrete function of impulse magnitude (D).

For the leg tracking controller of NCA2, a COM shift (either magnitude or position) or change in moments will once again change the steady state posture, incurring a small but likely measurable offset (in proportion to leg compliance) in phase that varies continuously with the shift. A change in substrate mechanics (e.g. damping or compliance) may once again incur changes in individual leg transients at touchdown and liftoff but should not have a measurable effect on steady state phase. A transient impulse applied to the mass center should yield no change in phase.

Finally, for the NCA3 systems, center of mass shifts, changes in moments and changes in substrate compliance may all be compensated for by the controller in two ways. One form of feedback stabilization would be for forces to change so as to maintain

a close semblance of the original kinematics, by way of the tracking controller. This type of stabilization would tend to induce a continuous phase change (P). The other form of stabilization would change the frequency of the motion, also leaving the kinematics essentially the same, and adapting the rate of motion to the change in environment. Due to the dependency of this interplay on the specific feedback gains, it is difficult to predict a general outcome. One may reasonably assume that NCA3 controllers are exceptionally good at maintaining the shape of kinematic trajectories, suggesting that changes in orbit shape (O) are very unlikely.

A transient impulse applied to the mass center might well introduce a lagging change in frequency (transient) and thus a likely phase shift (P) in rough proportion to the magnitude of perturbation.

1.5 Conclusions

In an effort to create testable hypotheses for the control of running, we introduce a progression of neuromechanical control architectures. Within a dynamical systems framework, we explore the coupling of an internal "neural" pattern generator with an "external" mechanical body and legs. We progress from strongly feedforward controllers dominated by the mechanical system viewed as a hybrid oscillator to a controller with feedback signals driven by mechanical perturbations that influence the feedforward command signal emanating from the neural pattern generator (fig. 1.2 and fig. 1.2).

To begin to define these architectures, we use a series of legged physical models (robots) that offer the most direct exposition of our central argument that "external' body-limb kinematics can offer a window into "internal" architecture. Specifically, we propose that kinematically derived measurements of mechanical phase manifest the internal neural clock phase and hence can be used to capture aspects of the coupled motor system's phase response curve during rhythmic behavior.

By reasoning about the likely properties of the phase response curve for each architecture in the progression, we conclude that an appropriately diverse battery of distinct mechanical perturbations must elicit an observable pattern of phase and frequencies changes that distinguish each individual architecture. Thus, we hypothesize that applying such a battery of perturbations to an intact runner – robot or animal – may shed significant light on the nature of its seemingly inaccessible feedforward/feedback internal architecture. Mathematically succinct exemplars of this architectural plane are straightforward to design and their analysis should be of considerable interest.

In particular, it is interesting to speculate on the extent to which our informal rea-

soning about the likely empirical phase response of complicated mechanisms to perturbations might be shown to be mathematically necessary. Because we take advantage of the ubiquity of isochrons (Guckenheimer and Holmes, 1983; Winfree, 1980) in coupled oscillators (Cohen et al., 1982), such mathematical prescriptions might likely extend to the far more elaborate kinematics of runners. If so, such perturbation batteries attain the character of an empirical assay with the power to characterize important aspects of an intact runner's motor control operating point.

1.6 Overview of the sequel

The following two chapters describe experiments conducted within the framework of perturbation assays suggested here.

The first experiment studies the response of running *Blaberus discoidalis* cockroaches to traversing a hurdle. The results are developed into a mathematical control model that suggests that bilaterally symmetric perturbations such as a hurdle excite fundamentally different aspects of the controller from bilaterally asymmetric perturbations.

The second experiment introduces such an asymmetric perturbation in the form of a large lateral impulse. Lateral impulses have been studied with respect to stability of the lateral leg spring (LLS) model. It is particularly interesting to study LLS dynamics on an animal whose non-dimensional moment of inertia was manipulated, as quantative predictions of the ensuing instablity can be tested.

The fourth and final chapter introduces tools for the study of stability using kinematic data, and specifically address the question of finding a structural signature of a Template. The analyses used in the first three chapters examine phase, whereas the fourth chapter extends the quantitative analysis of dynamics off the limit cycle, showing how the Floquet multipliers that govern stability can be recovered. Such an analysis forms the first step of recovering the Floquet structure of the dynamics directly from data. This coordinate-invariant structure expresses the intrinsic properties of the neuromechanical controller in mathematical form.

1.7 Bibliography

S A Bailey, J G Cham, M R Cutkosky, and R J Full. *Experimental Robotics VII*, volume 271 of *Lecture Notes in Control and Information Sciences*, chapter Comparing the Locomotion Dynamics of the Cockroach and a Shape Deposition Manufactured

Biomimetic Hexapod, pages 239 – 248. Springer Berlin / Heidelberg, Jan 2001. ISSN: 0170-8643.

R Balasubramaniam and M T Turvey. Coordination modes in the multisegmental dynamics of hula hooping. *Biol Cybern*, 90:176–190, 2004. doi: 10.1007/s00422-003-0460-4.

N Bernstein. *The Co-ordination and Regulation of Movements*. Pergamon Press, Oxford, 1967.

A Biess, M Nagurka, and T Flash. Simulating discrete and rhythmic multi-joint human arm movements by optimization of nonlinear performance indices. *Biol Cybern*, 95 (1):31–53, 2006.

E Bizzi, M C Tresch, P Saltiel, and A d'Avella. New perspectives on spinal motor systems. *Nat Rev Neurosci*, 1:101–108, 2000.

R Blickhan. The spring mass model for running and hopping. *J Biomech*, 22(11-12): 1217–1227, 1989.

R Blickhan and R J Full. Similarity in multilegged locomotion - bouncing like a monopode. *J Comp Physiol , A*, 173(5):509–517, 1993. ISSN 0340-7594.

R E Burke. Some unresolved issues in motor unit research. *Adv Exp Med Biol*, 508: 171–178, 2002. PMID: 12171107.

R E Burke. Revisiting the notion of 'motor unit types'. *Prog Brain Res*, 123:167–75, 1999.

A Büschges and A El-Manira. Sensory pathways and their modulation in the control of locomotion. *Curr Opin Neurobiol*, 8:733–739, 1998.

A Calvitti and R D Beer. Analysis of a distributed model of leg coordination, i. individual coordination mechanisms. *Biol Cybern*, 82(3):197–206, February 2000. doi: 10.1007/s004220050019.

D R Carrier, R M Walter, and D V Lee. Influence of rotational inertia on turning performance of theropod dinosaurs: clues from humans with increased rotational inertia. *J Exp Biol*, 204(22):3917–3926, November 2001.

H J Chiel, R D Beer, R D Quinn, and K S Espenschied. Robustness of a distributed neural network controller for locomotion in a hexapod robot. *IEEE Trans Robot Autom*, 8(3):293–303, 1992.

A Cohen, P J Holmes, and R H Rand. The nature of coupling between segmental oscillators of the lamprey spinal generator for locomotion: a model. *J Math Biol*, 13:345–369, 1982.

H Cruse. Coactivating influences between neighbouring legs in walking insects. *J Exp Biol*, 114:513–519, 1985a.

H Cruse. Which parameters control the leg movement of a walking insect? ii. the start of the swing phase. *J Exp Biol*, 116:357–362, 1985b.

H Cruse. What mechanisms coordinate leg movement in walking arthropods? *Trends Neurosci*, 13:15–21, 1990.

H Cruse and S Epstein. Peripheral influences on the movement of the legs in a walking insect carausius morosus. *J Exp Biol*, 101:161–170, 1982.

M A Daley and A A Biewener. Running over rough terrain reveals limb control for intrinsic stability. *PNAS*, 103(42):15681–15686, October 2006.

K Domen, M L Latash, and V M Zatsiorsky. Reconstruction of equilibrium trajectories during whole-body movements. *Biol Cybern*, 80(3):195–204, 1999.

O Ekeberg, M Blümel, and A Büschges. Dynamic simluation of insect walking. *Arthropod Struct Dev*, 33:287 – 300, 2004. doi: 10.1016/j.asd.2004.05.002.

D P Ferris and M Louieand C T Farley. Running in the real world: adjusting leg stiffness for different surfaces. *Proc R Soc Lond , Ser B: Biol Sci*, 265(1400):989–994, June 1998.

R Fitzhugh. Impulses and physiological states in theoretical models of nerve membrane. *Biophysics Journal*, 1:445–466., 1961.

R J Full and C T Farley. Musculoskeletal dynamics in rhythmic systems - a comparative approach to legged locomotion. In J M Winters and P E Crago, editors, *Biomechanics and Neural Control of Movement*, pages 192–202. Springer-Verlag, New York, 2000. ISBN-10: 0-387-94974-7, ISBN-13: 978-0-387-94974-1.

R J Full and D E Koditschek. Templates and anchors: Neuromechanical hypotheses of legged locomotion on land. *J Exp Biol*, 202(23):3325–3332, 1999.

R J Full, T Kubow, J Schmitt, P Holmes, and D Koditschek. Quantifying dynamic stability and maneuverability in legged locomotion. *Integr Comp Biol*, 42(1):149–157, FEB 2002. ISSN 1540-7063.

H. Geyer, A. Seyfarth, and R. Blickhan. Positive force feedback in bouncing gaits? *Proc R Soc Lond , Ser B: Biol Sci*, 270(1529):2173–2183, October 2003.

R M Ghigliazza and P Holmes. A minimal model of a central pattern generator and motoneurons for insect locomotion. *SIAM journal of applied dynamical systems*, 3 (4):671–700, 2004a.

R M Ghigliazza and P Holmes. Minimal models of bursting neurons: How multiple currents, conductances, and timescales affect bifurcation diagrams*. *SIAM journal of applied dynamical systems*, 3(4):636–670, 2004b.

R M Ghigliazza, R Altendorfer, P Holmes, and D E Koditschek. A simply stabilized running model. *Siam Review*, 47(3):519–549, sep 2005.

D I Goldman, T S Chen, D M Dudek, and R J Full. Dynamics of rapid vertical climbing in cockroaches reveals a template. *J Exp Biol*, 209:2990–3000, 2006.

M Golubitsky, I Stewart, P L Buono, and J J Collins. Symmetry in locomotor central pattern generators and animal gaits. *Nature*, 401(6754):693–695, 1999.

R Grasso, M Zago, and F Lacquaniti. Interactions between posture and locomotion: motor patterns in humans walking with bent posture versus erect posture. *J Neurophysiol*, 83(1):288–300, 2000. PMID: 10634872.

S Grillner. Neurobiological bases of rhythmic motor acts in vertebrates. *Science*, 228: 143–149, 1985.

L Guan, T Kiemel, and A H Cohen. Impact of movement and movement-related feedback on the lamprey central pattern generator for locomotion. *J Exp Biol*, 204 (Pt 13):2361–2370, 2001.

J Guckenheimer. Isochrons and phaseless sets. *J Math Biol*, 1:259–273, 1975.

J Guckenheimer and P Holmes. *Nonlinear Oscillations, Dynamical Systems, and Bifurcations of Vector Fields*. Springer-Verlag, 1983.

H Haken, J A Kelso, and H Bunz. A theoretical model of phase transitions in human hand movements. *Biol Cybern*, 51(5):347–356, 1985.

M R Hinder and T E Milner. The case for an internal dynamics model versus equilibrium point control in human movement. *J Physiol (Lond)*, 549(3):953–963, 2003. doi: 10.1113/jphysiol.2002.033845.

A L Hodgkin and A F Huxley. A quantitative description of membrane current and its application to conduction and excitation in nerves. *J Physiol*, 117:500–544, 1952.

P Holmes, R J Full, D E Koditschek, and J Guckenheimer. The dynamics of legged locomotion: Models, analyses, and challenges. *SIAM Reviews*, 48(2):207–304, 2006.

Y P Ivanenko, R Grasso, V Macellari, and F Lacquaniti. Control of foot trajectory in human locomotion: Role of ground contact forces in simulated reduced gravity. *J Neurophysiol*, 87(6):3070–3089, 2002.

S Jaric and M L Latash. The equilibrium-point hypothesis is still doing fine. *Hum Movement Sci*, 19(6):933–938, 2000.

D L Jindrich and R J Full. Dynamic stabilization of rapid hexapedal locomotion. *J Exp Biol*, 205(18):2803–2823, Sep 2002. ISSN 0022-0949.

M Kawato. Internal models for motor control and trajectory planning. *Curr Opin Neurobiol*, 9:718–727, 1999.

J A Kelso, P W Fink, C R DeLaplain, and R G Carson. Haptic information stabilizes and destabilizes coordination dynamics. *Proc R Soc Lond , Ser B: Biol Sci*, 268 (1472):1207–1213, 2001.

E Klavins and D E Koditschek. Phase regulation of decentralized cyclic robotic systems. *The International Journal of Robotics Research*, 21(3):257–275, 2002.

E Klavins, H Komsuoglu, R J Full, and D E Koditschek. The role of reflexes versus central pattern generators in dynamical legged locomotion. In J Ayers, J Davis, and A Rudolph, editors, *Neurotechnology for Biomimetic Robots*, pages 351–382. MIT Press, Boston, MA, 2002.

D E Koditschek and M Bühler. Analysis of a simplified hopping robot. *Int J Rob Res*, 10(6):587–605, 1991.

D E Koditschek, R J Full, and M Bühler. Mechanical aspects of legged locomotion control. *Arthropod Struct Dev*, 33(3):251–272, July 2004.

T Kohlsdorf and A A Biewener. Negotiating obstacles: running kinematics of the lizard sceloporus malachiticus. *J Zool*, 270(2):359–371, oct 2006.

K P Kording and D M Wolpert. Bayesian decision theory in sensorimotor control. *Trends Cognitive Sciences*, 10(7):319–326, 2006.

A D Kuo. The relative roles of feedforward and feedback in the control of rhythmic movements. *Motor Control*, 6(2):129–145, 2002.

F Lacquaniti, C Terzuolo, and P Viviani. The law relating the kinematic and figural aspects of drawing movements. *Acta psychologica (Amst)*, 54(1-3):115–130, 1983. PMID: 6666647.

D V Lee, R M Walter, S M Deban, and D R Carrier. Influence of increased rotational inertia on the turning performance of humans. *J Exp Biol*, 204(22):3927–3934, November 2001.

C Morris and H Lecar. Voltage oscillations in the barnacle giant muscle. *Biophysics Journal*, 35:193–213, 1981.

F A Mussa-Ivaldi. Modular features of motor control and learning. *Curr Opin Neurobiol*, 9:713–717, 1999.

E Nakano, H Imamizu, R Osu, Y Uno, H Gomi, T Yoshioka, and M Kawato. Quantitative examinations of internal representations for arm trajectory planning: minimum commanded torque change model. *J Neurophysiol*, 81:2140–2155, 1999.

K G Pearson. Common principles of motor control in vertebrates and invertebrates. *Annual Reviews Neuroscience*, 16:265–297, 1993.

K G Pearson. Proprioceptive regulation of locomotion. *Curr Opin Neurobiol*, 5:786–791, 1995.

K G Pearson. The control of walking,. *Sci Am*, 464:72–86, 1976.

C Peper, E Liekeand A Ridderikhoff, A Dafferthör, and P J Beek. Explanatory limitations of the hkb model: Incentives for a two-tiered model of rhythmic interlimb coordination. *Hum Movement Sci*, 23:673–697, 2004.

M H Raibert. Legged robots. *Commun ACM*, 29(6):499–514, 1986.

M J E Richardson and T Flash. Comparing smooth arm movements with the two-thirds power law and the related segmented-control hypothesis. *J Neurosci*, 22(18): 8201–8211, 2002.

M A Riley and M T Turvey. Variability and determinism in motor behavior. *Journal of Motor Behavior*, 34:99–125, 2002.

N Sadegh and R Witz. Stability analysis of an adaptive controller for robotic manipulators. In *Proceedings IEEE International Conference on Robotics and Automation*, Raleigh, NC, Apr 1987.

P Saltiel, K Wyler-Duda, A d'Avella, M C Tresch, and E Bizzi. Muscle synergies encoded within the spinal cord: evidence from focal intraspinal nmda iontophoresis in the frog. *J Neurophysiol*, 85(2):605–619, 2001.

U Saranli, M Buehler, and D E Koditschek. Rhex: a simple and highly mobile hexapedal robot. *Int J Rob Res*, 20(7):616–631, 2001.

S Schaal and N Schweighofer. computational motor control in humans and robots. *Current Opinions Neurobiology*, 6:675–682, 2005. URL http://www-clmc.usc.edu/publications/S/schaal-CON2005.pdf.

S Schaal and D Sternad. Origins and violations of the 2/3 power law in rhythmic three-dimensional arm movements. *Exp Brain Res*, 136(1):60–72, 2001.

S Schaal, D Sternad, R Osu, and M Kawato. Rhythmic arm movement is not discrete. *Nat Neurosci*, 7(10):1136–1143, 2004.

J Schmitt and P Holmes. Mechanical models for insect locomotion: dynamics and stability in the horizontal plane - i. theory. *Biol Cybern*, 83(6):501–515, December 2000a.

J Schmitt and P Holmes. Mechanical models for insect locomotion: dynamics and stability in the horizontal plane - ii. application. *Biol Cybern*, 83(6):517–527, 2000b.

R Shadmehr and S P Wise. *Computational Neurobiology of Reaching and Pointing: A Foundation for Motor Learning*. MIT Press, 2005.

J J E Slotine and L Weiping. On the adaptive control of robot manipulators. In *Proceedings of the ASME Winter Annual Meeting*, Anaheim, CA., Dec 1986.

D Sternad and S Schaal. Segmentation of endpoint trajectories does not imply segmented control. *Exp Brain Res*, 124(1):118–136, 1999.

D Sternad, M T Turvey, and R C Schmidt. Average phase difference theory and 1:1 phase entrainment in interlimb coordination. *Biol Cybern*, 67(3):223–231, 1992. doi: 10.1007/BF00204395.

E Todorov and M I Jordan. Smoothness maximization along a predefined path accurately predicts the speed profiles of complex arm movements. *J Neurophysiol*, 80(2): 696–714, 1998.

J D Weingarten, R E Groff, and D E Koditschek. Coordination for legged robots. In *IEEE Conference on Robotics, Automation and Mechatronics*, page (to appear), Singapore, 2004a.

J D Weingarten, G A D Lopes, M Buehler, R E Groff, and D E Koditschek. Automated gait adaptation for legged robots. In *IEEE International Conference on Robotics and Automation*, page (to appear), 2004b.

L L Whitcomb, A A Rizzi, and D E Koditschek. Comparative experiments with a new adaptive contoller for robot arms. *IEEE Trans Robot Autom*, 9(1):59–70, Feb 1993.

A T Winfree. *The Geometry of Biological Time*. Springer-Verlag, New York, 1980.

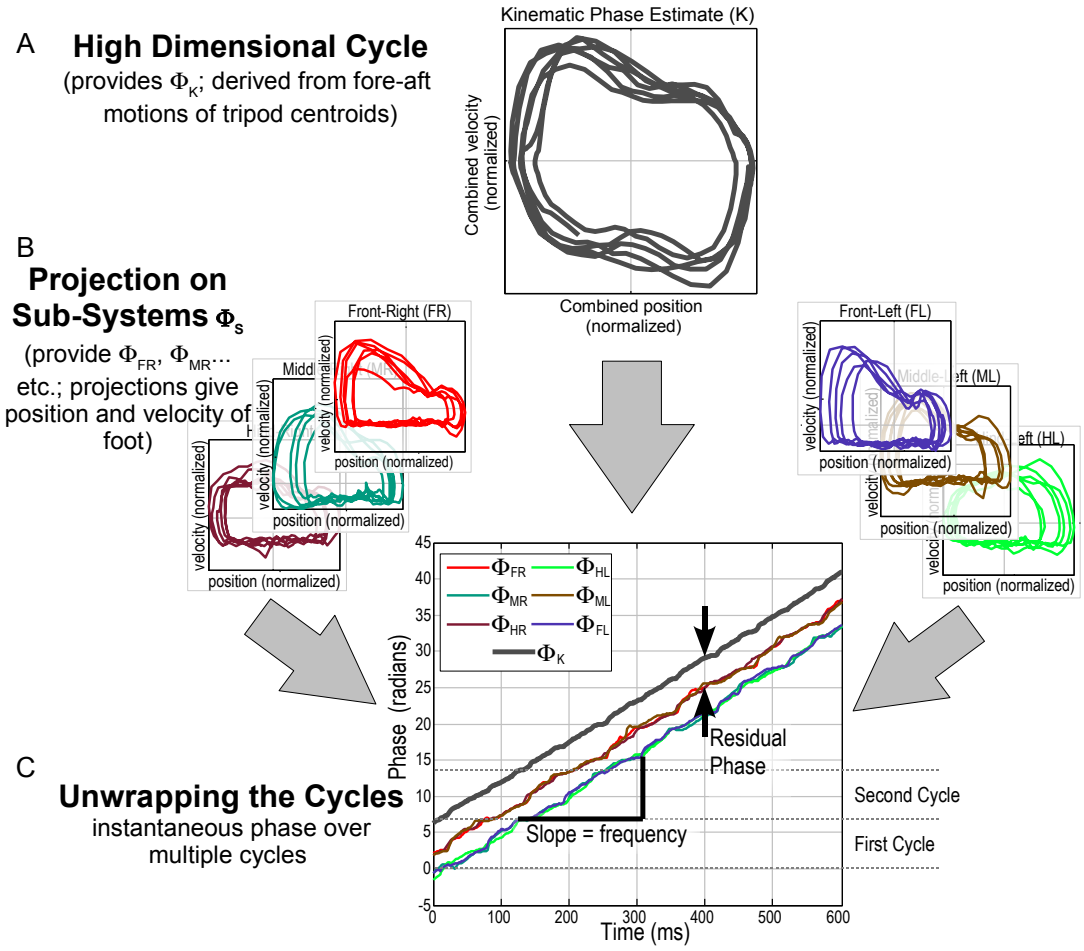

Figure 1.5: Determining instantaneous phase change in a running insect using a dynamical systems approach. **A** Plot of kinematic phase estimate $\hat{\Phi}_K$. Kinematic phase estimate represents the global high dimensional dynamical system of a locomoting animal. Kinematic phase estimate $\hat{\Phi}_K$ is constructed from the positions and velocities of the animal's six feet by treating each tripod as a viritual leg at its centroid. By taking the difference in fore-aft position of the centroids and its derivative we obtain plot of **A**. **B** Plots of sub-system phase estimates $\hat{\Phi}_S$ for individual feet $S = FL, ML, HL, FR, MR, HR$, which may be viewed as projections of our overall kinematic phase estimate $\hat{\Phi}_K$. **C** Instantaneous phase as a function of time for both (global) kinematic phase and leg phases of individual legs. Leg phases fall into two groups, each set representing a tripod of support. The slope of the lines represents cycle frequency. The instantaneous difference of a phase from the trend-line of the kinematic phase estimate $\hat{\Phi}_K$ is used to calculate any phase changes that result from a perturbation as in fig. 1.4

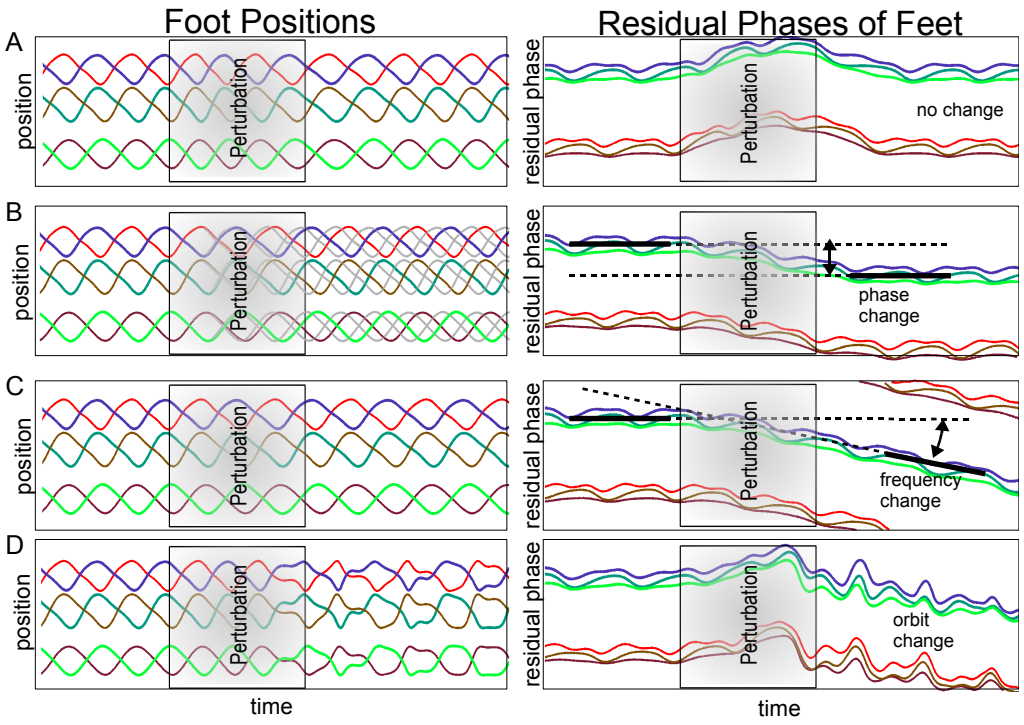

Figure 1.6: Types of outcomes from a transient perturbation, such as a bump, expressed in terms of fore-aft foot position and residual phases as a function of time. The left column shows the fore-aft position of each foot as in fig. 1.4, and the right column shows the residual kinematic phase based on an extrapolation of the phase before perturbation. Each cycle in the left column represents a single stride. **A** phase and frequency recovery (no change).**B** a phase change outcome, where frequency is recovered but phase is not. The gray lines extrapolate foot motions prior to perturbation to illustrate how phase shifted movements differ from un-shifted movements. **C** a frequency change outcome. **D** a gradual breakdown of the periodic orbit's shape

Chapter 2

Hurdle Traversal

2.1 Summary

Using hypotheses derived from a dynamical system approach, we tested whether the control of running uses neural feedback to recover from a perturbation. If feedforward neural signals are unmodified by the perturbation, then the timing (phase) of tarsal (foot) kinematics should remain phase-locked to the pre-perturbation rhythm. We video recorded *Blaberus discoidalis* cockroaches traversing a hurdle and processed the kinematic data from the fore-aft excursions of all tarsi to produce a single kinematic phase variable. Kinematic phase may be used to reliably predict future leg motions based on the preceding strides. The time derivative of kinematic phase provides a frequency which must remain unchanged if neural patterns are unaffected by sensory feedback. Results of forty trials showed that the kinematic phase was reset, while running frequency was closely maintained to within ±5%. Kinematic phase changes were distributed bi-modally with modes 180° or half a stride apart (in an axial distribution)- a difference of one step, which corresponds to a left-right reflection of the kinematic state of the body. Neither mode had significant weight at zero phase change, decreasing the likelihood of feedforward control and supporting the use of neural feedback for this task. Phase changes did not depend on visual or antennal sensory ability. We propose a controller that expresses the timing of the two tripods as two coupled phase oscillators, which in turn, may also be coupled to a master clock. Our controller informs and is informed by controllers operating in legged robots.

2.2 Introduction

Both mechanical and neural feedback play a role in the control of animal locomotion (Dickinson et al., 2000). We propose an approach grounded in dynamical systems theory that allows questions of control to be studied using readily obtained kinematic data. We test hypotheses developed by Revzen et al. (2008) that consider what parts of the neuromechanical control architecture for a given locomotor behavior are modulated by feedback when locomotion is perturbed.

The most developed neural control architecture for legged locomotion comes from the study of slow quasi-static locomotion in stick insects has emphasized the importance of neural reflexes. This controller, known as WalkNet, is expressed as a distributed artificial neural net (Cruse et al., 1998, 2007) that effectively models the kinematics of leg movements in general and the inter-leg influences during slow walking in particular. WalkNet was extended (Schilling et al., 2007) to ensure that it correctly models how stick insects walk with amputated legs and under more dynamic conditions. WalkNet

is a kinematic controller in the sense that it governs the positions of leg joints over time, rather than the torques that drive them. It provides first order differential equations for joints, wherein momentum plays no role (Schilling et al., 2007). Recent experimental results from stick insects (Akay et al., 2004; Bueschges, 2005; Bueschges and Gruhn, 2007) suggest that the function of neural circuitry is critically dependent on mechano-sensory feedback, without which the central pattern generators (CPGs) that control different joints would not synchronize properly.

By contrast, there is ample evidence that the control of rapid running in cockroaches has a significant feedforward component that is governed primarily by what Pearson et al. (2006) called the "phase dependent part" of motor control. Kubow and Full (1999) simulated a mechanical model of a running cockroach with leg forces played out from recordings of force plate data, and noted its surprising stability when perturbed. Jindrich and Full (2002) showed that running cockroaches begin to recover from an impulse within 14 milliseconds – a response time that challenges the fastest of reflexes. Sponberg and Full (2008) ran cockroaches over a rough terrain while recording muscle action potentials from a set of putative control muscles, and found no differences with running on flat ground. Ridgel and Ritzmann (2005) showed that cockroaches with a circumoesophageal lesion tend to run continuously with a stereotyped gait. Taken together with Noah et al. (2004) demonstrating that distal leg denervation does not interfere with rapid running although it disrupts walking gait, one may conclude that mechanical feedback appears to play a greater role in rapidly running cockroaches. These discoveries support the development of mass-spring models emphasizing the mechanical system's role in control (Holmes et al., 2006). The virtual springs of both the Spring Loaded Inverted Pendulum (SLIP) and the Lateral Leg Spring model (LLS) represent the summed mechanical behavior of legs. Both models show self-stabilization to perturbations primarily through mechanical feedback.

In the present manuscript, we examine the coupling of both neural and mechanical feedback by testing neuromechanical control architectures at intermediate speeds.

2.2.1 Dynamical Systems are the natural choice of language

Because neural feedback, mechanical properties of the body and the dynamics of the task all play a role in legged locomotion, it is only by treating the moving animal in its environment as a single combined system that we can begin to obtain insight into control. To allow us to study animal-in-environment systems such as these, we must adopt an appropriate mathematical language that allows us to generate quantitative hypotheses.

A natural choice of language for expressing the dynamics of legged locomotion is

that of hybrid dynamical systems (Back et al., 1993; Holmes et al., 2006). Within this mathematical framework, an animal running in its environment with a regular gait is represented with respect to body-centered coordinates as a non-linear oscillator. The hybrid transitions provide a representation for the discontinuities that occur in the equations of motion when the number of legs contacting the ground changes.

One of the insights offered by Dynamical Systems Theory and its sister discipline Control Theory is the fundamentally different nature of control in slow, quasi-static locomotion versus highly dynamic locomotion. By definition, quasi-static mechanical systems are referred to by control theorists as *driftless* – the state of the system does not change if the controller does nothing. In contrast, in rapidly moving animals far from static equilibrium, inaction would result in significant changes in state corresponding to motions continuing with the momentum of the animal. The importance of momentum implies that the state-space descriptions of fast-moving animals require both configuration variables (positions) and their conjugate momenta – effectively doubling the dimension of the state space of slow-moving animals of similar morphology. It is thus expected that control of rapid, dynamic locomotion may be fundamentally different from control of slow locomotion (Holmes et al., 2006). Here, we test control architectures where both are likely to play a role.

Approaches using stochastic optimal control (Todorov and Jordan, 2002) can lead to predictions similar to those of dynamical systems. In the optimal control framework, much attention is given to the goal function (or functional) with respect to which optimality of the control strategy is sought. We believe that the behavior itself, expressed as a low-dimensional attracting sub-manifold of the state space, should be the object of primary interest. A putative goal functional for which this behavioral sub-manifold may be optimal can be difficult to ascertain, and is only of secondary concern. Instead, we focus on testing competing hypotheses about the architecture of the neuromechanical controller (see section 2.2.3), irrespective of whether or not those architectures are compatible with any particular notion of optimality.

We approached the classification of controller architectures acting in a given behavior from first principles, by proposing a framework for partitioning the dynamical system into clearly identifiable sub-system blocks based on the form information they store and the self-excitation properties they possess. This partition into blocks gives rise to a set of nested feedback loops that could contribute to control of the behavior we wish to study. We formulate hypotheses of control architecture to represent the choice of feedback loops that do in fact play a role, and test these against their expected kinematic consequences as expressed in phase (timing) of leg motions.

By focusing on fundamental structures such as phase, whose existence is guaranteed by dynamical systems theory for all stable oscillators, we may design experimental tests

for control hypotheses representing alternative feedback regimes. These tests can be broadly applied to many organisms and even robots.

2.2.2 Oscillators examined using Kinematic Phase

The theory of dynamical systems often describes stable nonlinear oscillators in terms of their phase variables and the entrainment effects that tie their phases together (Guckenheimer and Holmes, 1983; Abraham and Marsden, 1978). Every state in the stability basin of a stable periodic orbit is associated with a phase defined by the dynamics of convergence back to that stable orbit. The response of this *global phase* (Revzen et al., 2008) to various experimental manipulations can reveal important properties (Guckenheimer, 1975; Glass and Winfree, 1984; Winfree, 1980) of the underlying system.

Modeling and controlling motions with coupled phase oscillators has met with some success in the robotics community (Schaal, 2006). Thus both mathematical theory and engineering practice allow that the entire animal in its environment can be represented as a non-linear phase oscillator. This choice can be effective because we avoid the pitfalls of "piecemeal analysis of the different system components" (Pearson et al., 2006) by offering a simple model with few parameters. We are carrying the reduction of complexity to the point of leaving only the phase response dynamics[1]. We contend that these dynamics are often sufficient for deciding among the alternative structural hypotheses for the animal's control architecture (Revzen et al., 2008).

When a system oscillates periodically, all the subsystems involved in producing the behavior and all observable quantities s describing those subsystems must also oscillate periodically. The implication for experimental biomechanics is that the kinematics of the body and its subsystems must reflect the underlying periodic dynamics. As described in Revzen et al. (2008), kinematic measurements may be combined to provide an estimate of the phase of the underlying nonlinear oscillator. We refer to such an estimate as a *kinematic phase* of the system, and argue for its utility in the investigation of neuromechanical control of rhythmic behaviors.

Dynamical systems theory supports the contention that once phase is estimated reliably, the average state of the system (animal) as a function of phase is a representative model of its dynamics in the future. Because it is a linear function of time, extrapolating phase into the future is a simple task, and after doing so we obtain an extrapolated phase prediction of the state of the animal. In Revzen et al. (2008) we

[1]By phase response dynamics we mean the entire nonlinear gamut of phase responses – not merely the phase response curve (PRC) which is their linearization on the stable cycle.

suggested the use of the difference between the predicted and the actual phase of an animal's motion after experiencing a perturbation, referring to this difference as *residual phase*. We offered an assay of perturbation tests that can be used as a means of characterizing controller architecture based on the asymptotic (long-term) changes in residual phase. Here, we will also describe some use for features of the transient residual phase response in this classification.

Animals that conveniently expose their phase through kinematics would be most amenable to study by using the residual phase approach. The best candidates would be animals using rhythmic motions with many appendages and a simple nervous system. These animals would expose a great deal of phase information through the kinematics of their appendages, while maintaining a relatively simple neural state. For such animals, kinematic phase would provide a reliable estimate of their global phase.

To test neuromechanical control hypotheses using kinematic phase, we chose a six-legged arthropod, the cockroach, *Blaberus discoidalis*, running on a treadmill. We measured the change in leg phase (i.e. the residual phase) by comparing phase before and after a perturbation caused a small hurdle. We selected cockroaches because of the well developed characterization of their neuromechanical control architectures (fig. 2.1). Their kinematics and dynamics have been measured at a range of speeds on both tracks and treadmills (Kram et al., 1997; Full et al., 1991; Full and Tu, 1991; Watson and Ritzmann, 1998a,b; Kubow and Full, 1999; Jindrich and Full, 1999). Both simple and more representative neuromechanical models have been proposed and tested (Schmitt et al., 2002; Schmitt and Holmes, 2000a,b; Seipel et al., 2004; Ghigliazza et al., 2005; Kubow and Full, 1999; Jindrich and Full, 1999). Knowledge of the musculoskeletal mechanics (Ahn and Full, 2002; Ahn et al., 2006) and the sensory mechanisms (Zill et al., 1981, 2004; Ridgel et al., 2000) defines the components of the architectures. More specifically, our choice of hurdle height (3 mm) was informed by previous studies of obstacle traversal (Watson et al., 2002a,b), showing that 5.5 mm obstacles did not induce cockroaches to pitch upward and shift to a climbing behavior.

2.2.3 Neuromechanical Control Architectures provide testable control hypotheses

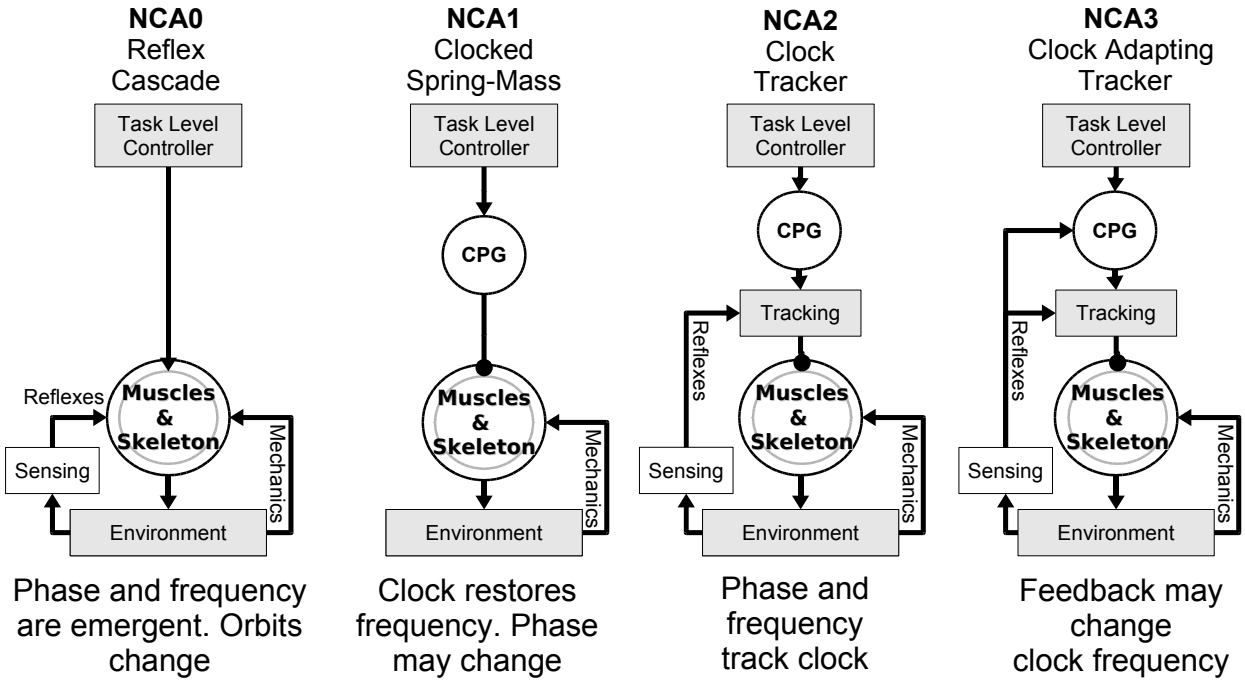

Figure 2.1: Neuromechanical control architectures (NCAs)

Description of fig. 2.1

Neuromechanical control architectures (NCAs): Reflex Cascade (NCA0), Clocked Spring Mass (NCA1), Clock Tracker (NCA2) and Clock Adapting Tracker (NCA3). We partitioned an animal's neuromechancal system into blocks based on the kind of state they contain and the information processing that they perform.

The "Task Level Control" block encapsulated settings of parameters for the behavior (e.g. desired stride frequency) as expressed in descending neural signals and physiological state. We assumed the outputs of Task Level Control are held constant throughout a behavior. A "Central Pattern Generator" (CPG) circle contains neural circuitry that endogenously produced the rhythmic pattern of the behavior (Delcomyn, 1980; Grillner, 1985; MacKay-Lyons, 2002). We relegated all reflex based neural modulation of the CPG signal (Ijspeert, 2008; Ritzmann and Bueschges, 2007) to the "Tracking" block. Mathematically, we assumed Tracking was time-invariant, stateless and functioned by comparing the state of the limbs (relative to the body) and the reference provided by the CPG to generate force activation in muscles. Tracking contained no persistent state and was not self-exciting. The "Muscles and Skeleton" double circles contain the mechanical state of the body, which is subject to manipulation by forces from the environment. The body interacted mechanically with the "Environment" and also modified the representation of the environment returned by "Sensing".

The control architectures include progressively more internal state that is influenced by feedback. Reflex Cascade (NCA0) has no internal state, and environmentally induced events trigger reflexive responses that generate the cyclical behavior. Clocked Spring Mass (NCA1) has a CPG, but neither the CPG nor the muscle activations are influenced by feedback. Clock Tracker (NCA2) uses Tracking reflexes to modulate the muscle activations, but the CPG remains oblivious to the environment. Clock Adapting Tracker (NCA3) expresses the most general case: all blocks other than Task Level Control (which is assumed constant) can be influenced by feedback. After Revzen et al. (2008) where a detailed discussion of the outcomes to perturbations we list below each NCA is found.

In Revzen et al. (2008), we proposed several plausible Neuromechanical Control Architectures (NCA) shown in fig. 2.1. When subjected to a collection of perturbation experiments, the predicted phase and frequency responses of systems belonging to each NCA provide related, testable hypotheses that may be verified or refuted experimentally - allowing us to reject some NCAs in favor of others.

Our experimental approach separates the architectures based on instantaneous phase and its slope, the instantaneous frequency, before versus after the perturbation. For constant frequency rhythmic behaviors, phase is a linear function of time. When frequencies pre- and post-perturbation are equal, the differences in intercepts of the pre- and post-perturbation linear models of phase becomes well defined[2] and we

[2]The intercepts are not well defined when frequencies are not equal because phases are cyclic

refer to this value as the *phase outcome* of the perturbation experiment. A zero phase outcome defined by no change in the residual phase before versus after the perturbation indicates that the pre-perturbation rhythm continues without modification.

A permanent change in frequency implies that the animal system is no longer following the pre-perturbation rhythm. Frequency changes reject the possibility of Clocked Spring Mass (NCA1) and the Clock Tracker (NCA2) because feed-forward neural control requires that the CPG output maintain a constant frequency unaffected by perturbation.

Changes in phase can occur in feedforward architectures such as Clocked Spring Mass (NCA1) and the Clock Tracker (NCA2), where they express the possibility that the musculoskeletal system oscillation may have different relative phases to the neural CPG. For example, the difference between a front leading trot (front legs landing first) and a back leading trot (hind legs landing first) in a quadruped need not require any changes in the outgoing signals from the nervous system. These two trots, when viewed through the lens of kinematic phase, are phase-shifted relative to each other. Changes in phase in a Clock Adapting Tracker (NCA3) can also be the result of a feedback induced frequency change integrated over the duration of the perturbation. The key difference between the feedforward phase change mechanism and the feedback phase change mechanism is that in the feedback phase change mechanism integrated frequency change depends smoothly on the perturbation history, whereas the available phase changes in feedforward architectures are a property of the gait itself and independent of the perturbation.

Very abrupt phase changes immediately following a perturbation imply that there is effectively no internal sense of time that the animal maintains, rejecting the Clock Adapting Tracker (NCA3) in favor a Reflex Cascade (NCA0). Phase changes are rapid (possibly discontinuous) for Reflex Cascades whereas they are gradual and require multiple strides in Clock Adapting Trackers.

History dependence in the phase outcome for perturbations ending in similar kinematic states, such as dependence on the duration of perturbation, is impossible for a Reflex Cascade (NCA0) architecture. Reflex Cascade states are entirely described by their kinematic variables implying that phase, which is a function of state, cannot depend on the path taken to reach that kinematic state. Clock Adapting Trackers (NCA3) change frequencies gradually as they are being perturbed and it is the time integrated frequency change that gives their phase outcomes. With end-of-perturbation conditions similar, a strong correlation between perturbation duration and the phase

(defined modulo 2π). When frequencies differ, any choice of intercept is equally valid, depending only on our arbitrary choice of initial time for the model.

or frequency change it induces rejects Reflex Cascades in favor of Clock Adapting Trackers.

2.3 Materials and Methods

We ran cockroaches across a three mm high hurdle at the animal's preferred running speed. We video recorded the animals from below with a high-speed camera and digitized their body and tarsal (foot) motions in the image (horizontal) plane. We used motions of the tarsi in the body frame of reference to produce a phase estimate based on an animal's kinematics. We used linear regression to fit and then extrapolate from our kinematic phase estimates, providing projections of an animal's expected motions were they not perturbed by hurdle traversal. Using the difference between observed and extrapolated phase, the *residual phase* in Revzen et al. (2008), we examined the changes in timing of leg motions induced by hurdle traversal to discover the structure of the neuromechanical architecture.

We used thirty three adult *Blaberus discoidalis* (Serville 1839) cockroaches (mass 3.3 ± 0.34 *gram* (mean,SD)). Animals were raised in a cage with unlimited food and water and tested at room temperature $25 \pm 3\ ^{\circ}C$.

2.3.1 Treadmill and hurdle

We ran the animals in a Plexiglas cage suspended on top of a treadmill with a transparent belt. Treadmill speeds ranged uniformly (failed to reject Kolmogorov-Smirnov test against a uniform distribution with $\alpha = 0.05$) between 17 cm/s and 29 cm/s. In each trial, we manually adjusted the belt speed to match the animal's preferred running speed.

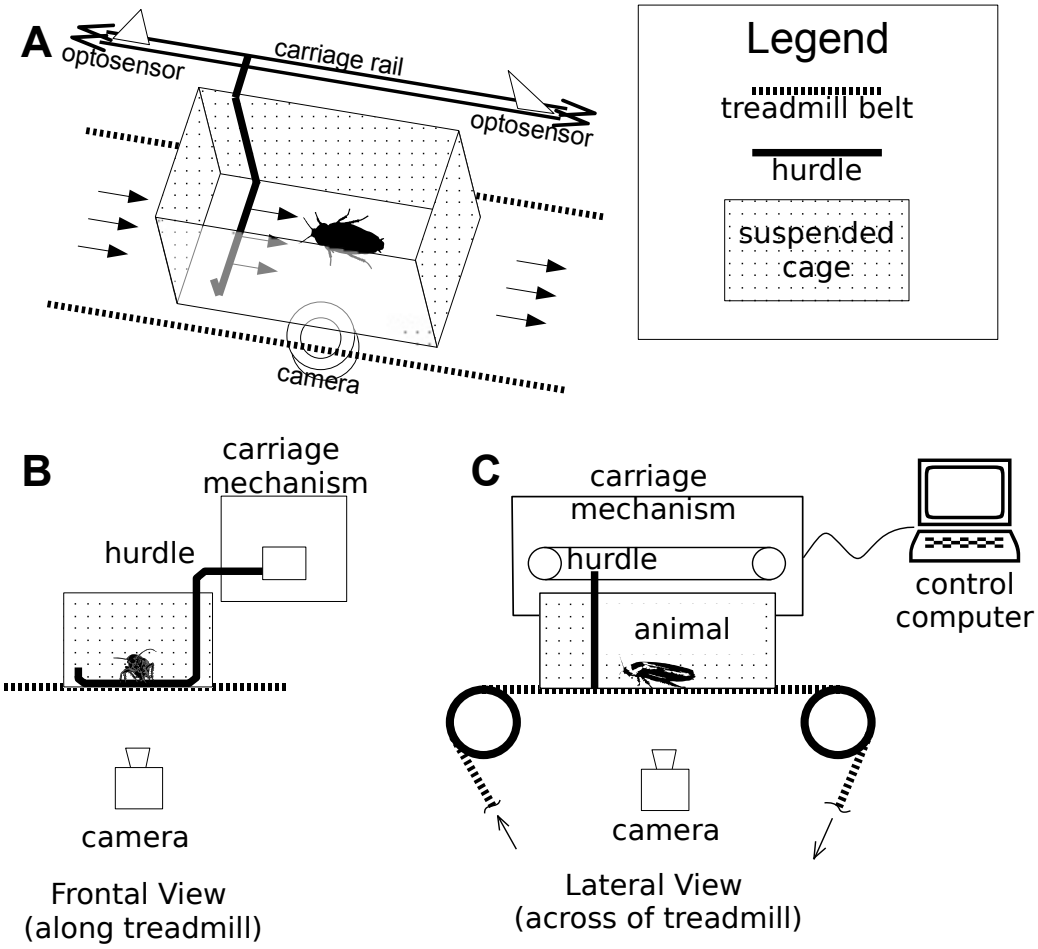

Figure 2.2: Treadmill hurdle. Illustration of our experimental apparatus from **A** diagonal, **B** frontal and **B** lateral views. We suspended a box shaped Plexiglas cage (dotted surface) above a transparent treadmill (thick dotted lines) whose direction of motion is indicated by arrows. Using a computer, we triggered the motion of a carriage (carriage mechanism as thin-lined box) that ran on a rail parallel to the treadmill (rail marked by thick arrows) and carried a hurdle constructed from a square bronze tube (thick black line). The hurdle moved across the cage at the speed of the belt allowing the animal to run over it. The hurdle then stopped, and returned slowly to its starting position. The computer detected start and stop positions using optosensors whose beam was interrupted by the carriage. The software that controlled the hurdle also triggered a high-speed camera that video recorded the animal through the treadmill belt from below (camera indicated schematically in frontal and lateral view; cylinder in diagonal view). (Note: for clarity, animals drawn larger than scale.).

We attached the cage (fig. 2.2) to a rail we salvaged from a dot-matrix printer (Epson 9pin dot matrix, Epson America, Inc., Long Beach, CA 90806, USA). We used the printer's stepper motor to move the print-head carriage on which we attached a bronze hurdle of 3 $mm \times 3$ mm square cross-section, shaped so that it would extend down to the bottom of the cage. We used four screws underneath the corners of the frame carrying both cage and rail to allow us to adjust the hurdle motion until it was parallel to the treadmill belt and in contact with it throughout the range of motion.

Previous work on obstacle traversal in *Blaberus discoidalis* shows little change in running kinematics for hurdles of 5.5 mm height, as front legs typically rise 6 mm during swing (Watson et al., 2002b). The height of 3 mm proved sufficient to elicit changes in timing, while reliably allowing animals to continue running.

We controlled the stepper motor from a PC (Pentium II generic) running Linux (Knoppix 3.2 booting from CD) using a commercial micro-stepping controller (R208, RMS Technologies, Carson City, NV 89706, USA). We set the speed via the frequency of a square wave emitted from the audio output of the computer, and controlled stepper direction via the computer's parallel port outputs. We used parallel port inputs to read optical sensors that detected the carriage end-of-travel positions. We used additional parallel port outputs to trigger the high-speed camera (Kodak Ektapro 1000; Eastman Kodak Company, Rochester, NY, USA) recording the trials. At higher speeds, it became impossible to bring the carriage to full speed from a standing start as it would cause the motor to stall. To circumvent the stall conditions, we provided an acceleration profile to bring the carriage up to the desired speed. We wrote the control software in Python (Python Software Foundation, Hampton, NH 03843, USA) using extension libraries **pyParallel** and **ossaudiodev**). The control software allowed the operator to specify a desired carriage speed and acceleration.

The carriage moved the hurdle at a speed that was stationary in the belt frame of reference. We calibrated the carriage speed commands by fitting a third order polynomial to multiple frequency and speed pairs measured with an oscilloscope and the high-speed camera.

We computed the treadmill belt velocities by tracking particles carried with the belt over 100 frames. In each trial, we manually digitized the positions of a particle at 10 points in 10 frame intervals to provide an estimate of both velocity and its precision. Velocities were known to within 0.5 cm/s, consistent with particle positions being resolved to within 2 pixels.

2.3.2 Protocol

We prodded the animals with a probe to guide them to run in the centre of the cage. We manually adjusted the treadmill speed before each trial to match the running speed preferred by the cockroach.

We selected trials so as to ensure that the animal ran for at least three strides before and after contact with the hurdle; that the animal did not contact the walls of the cage or vertical parts of the hurdle with body, legs or antennae; that the animal did not obviously get snagged in the crack between the hurdle and the treadmill belt; that animal ran straight ahead, in the sense that the maximal absolute difference between instantaneous body orientation and median body orientation was less than 0.7 *radian*. We only kept trials where the animal's gait appeared to be regular before contact with the hurdle. The criteria we used for regularity was that the root-mean-square of the residual for the linear regression 0 is less than 0.5 *radian*.

2.3.3 Video processing

We recorded high-speed video at 500 $frame/s$ using a color camera (Kodak Ektapro 1000; Eastman Kodak Company, Rochester, NY, USA). We placed the camera to record the animals through the belt (see fig. 2.2) with a diffuse reflector panel providing uniform background lighting from above the cage. We configured the camera to record two seconds of video before and after the hurdle movement, allowing for a maximum of 2048 frames per trial. We downloaded the captured videos to a host computer as a sequence of TIFF frames with resolution of 512×384 pixels.

We tracked an animals' position and heading using an automated body tracking algorithm written in **MatLab** (The MathWorks, Inc., Natick, MA, USA). After it corrected for lighting gradients and converted the images to gray-scale, the tracker located and removed the image of the hurdle, if present. It then located the axis of symmetry of the cockroach's silhouette. It used the posterior most pixel on the axis as its base position, and the angle of the silhouette axis as its orientation. We then rotated, scaled and clipped animals' images to generate a registered video sequence that contains the animal in a standard position, orientation and size. We verified the quality of body tracking in two control experiments, one tracking a cockroach carcass attached to a positioning stage with ground truth positions taken from the stage, another tracking an animal with markers on its abdomen and comparing with traditional marker tracking position data. Our auto-tracker code produced results comparable in accuracy and noise distribution to those obtained by more traditional marker based tracking methods without the requirement for prior marking of the animals.

Using a second tracking tool (also developed in **MatLab** for this purpose) we tracked the positions of all six tarsi in the registered animal videos. The tarsus tracking tool tracked the most distal point in the silhouette of each leg, which is typically a point between the tarsal claws of that leg. The operator could interactively correct tracking errors caused by occlusions, motion blurring and other sources by clicking on the desired points.

In each trial, we computed a length scale for converting pixel coordinates to lengths using the dimensions of a fixed length piece of Plexiglas that was next to the cage in all frames. We treated pixels as if they were square and of equal size. We found such a simplistic camera model to be justified because animals move within a small region near the camera's optical centre, and cannot move in and out along the viewing axis.

Additionally, we noted the first and last frames of each video sequence in which the animals were in contact with the hurdle. Contact was defined as having any part of the body other than antennae having a pixel adjacent to the hurdle in the image.

The output of this process was a dataset containing: absolute position and heading of the body, tarsal positions in the body frame, relative to centre of mass $(x_k(t), y_k(t)),\ k \in \{1 \dots 6\}$, absolute position and angle of the hurdle in each frame where it is present and times of first physical contact (start) t_0, and last physical contact (end) t_1 between the animal and the hurdle.

2.3.4 Statistics

Our dataset consists of forty trials conducted with thirty three animals. Of these animals, three were used for three trials each, and one was used for two trials. The phase outcomes of animals used for multiple trials were not significantly different from the statistical model fitted to the remaining animals (two way Kolmogorov-Smirnov test $\alpha = 0.05$). We therefore treat all trials as independent and identical for statistical purposes.

To control for the possibility that tactile or visual sensing was affecting the outcomes, we tested ten of the thrity three animals with clipped antennae and eyes blinded with white-out. The distributions of phase and frequency change were indistinguishable from those of the remaining wild type animal tests (two way Kolmogorov-Smirnov test $\alpha = 0.05$), and thus all results we report are pooled from both groups.

2.3.5 Signal processing

We began the data processing of the tarsus (foot) positions $(x_k(t), y_k(t)),\ k \in 1 \dots 6$ by linearly interpolating any missing measurements. We chose linear interpolation after

comparing with alternative interpolation schemes. We found this technique to predict missing measurements at comparable residual error rates to other methods we tested. A total of 1.0×10^4 samples out of the 1.8×10^5 that comprise our data were missing (5.7%), mostly due to tarsi being occluded by the body, by other legs or by the hurdle itself.

The tarsus tracking code provided position in units of a pixel. Tarsi move nearly parallel to the body axis for significant periods of time, causing the lateral coordinates $x_k(t)$ to take one of only a few possible values for many consecutive frames each cycle. The $y_k(t)$ were also obtained as integer pixel numbers. The noise introduced by expressing these continuous positions as integer pixel values is a form of quantization noise, which is a spectrally white broadband noise. Much of this noise was removed with an order 1 Butterworth smoother filter at a 0.25 cycle cut-off (**MatLab butter**, and **filtfilt**).

We extended the resulting twelve dimensional positional dataset (x_k, y_k) of six legs to twenty four dimensions by adding the velocities $(\dot{x}_k, \dot{y}_k)$ as computed by sample differencing of the Butterworth filtered positions. We tried several other filtering and differencing methods on synthesized data with known phase and additive noise comparable in magnitude to that in our raw measurements. Methods tested included Kalman filters and windowed FIR derivatives. For purposes of phase computation, these methods offered no advantages compared with the naive sample differencing method. Velocities were included in the state as a representation of momentum, which is a required part of the state for mechanical systems that are not quasi-static.

Finally, we rescaled all twenty four dimensions and translated them to obtain a mean of zero and a standard deviation of one. We subjected the renormalized dataset to principal component analysis and represented it in the coordinate system thus obtained. The projection of the data on the first and second principal components was distributed in an annulus around the origin and moved around the origin as the animal ran. We chose the sign of the second principal component so that the state moved counterclockwise around the origin.

We took the angle of the polar representation of the state's projection onto the plane defined by the first two principal components as our kinematic phase estimate Φ_K. We split each phase time series into three time segments: before (indicated by the subscript $_0$), during $(_D)$ and after $(_1)$ contact with the hurdle. We fitted a linear model to each time segment by applying iteratively re-weighted least squares linear regression (**MatLab** function **robustfit**) to Φ_K.

The three models are represented by the equations of table 2.1, with times comprising each segment given in milliseconds relative to first contact time (t_0) and last contact time (t_1) of the animal with the hurdle. From here forward, we make reference

to the "on" and "off" transitions – the transition "on" occurring between the segment pre-contact and the segment during contact with the hurdle, and the transition "off" occurring between the segment during contact and the segment post-contact. We offset the before and after segments from the "during contact" segments by a gap of 50 ms. We did this to ensure that the high leverage endpoints of those time segments in which the animals are not touching the hurdle. We required the before and after segments to contain at least three strides, which are approximately 300 ms long, and allowed them to be no more than 350 ms. Thus we used similar amounts of data in all trials for the 0 and 1 regressions.

Table 2.1: Regression models representing time segment before, during and after hurdle contact.

	Times (ms)	
Regression	Start	End
$\hat{\Phi}_0(t) = f_0 t + \phi_0$	$t_0 - 400$	$t_0 - 50$
$\hat{\Phi}_D(t) = f_D t + \phi_D$	t_0	t_1
$\hat{\Phi}_1(t) = f_1 t + \phi_1$	$t_1 + 50$	$t_1 + 400$

2.3.6 Kinematic Phase estimation

Following the seminal Cohen-Holmes-Rand Lamprey CPG model (Cohen et al., 1982), many investigators have treated questions of neural control of locomotion from the perspective of oscillator coupling. The approach enjoys a coherent theoretical framework for reduction of the modeled neural activation patterns to a mathematically simpler form (Winfree, 1980; Guckenheimer, 1975). While somewhat more difficult to analyze, the same ideas have been applied to coupling mechanical (second order) oscillators representing the body mechanics in the environment to internal pattern generators. The controller model we propose here is somewhat similar to the Haken-Kelso-Bunz model (Haken et al., 1985) for motor coordination, in that it too is formulated in terms of phase oscillators rather than physically explicit models of oscillators, and it too exhibits multiple stable solutions.

The theory of nonlinear oscillators guarantees that under appropriate generic conditions an asymptotically stable oscillator possesses a phase coordinate that is well-defined not only on the orbit itself, but in the entirety of its stability basin. The phase partitions the stability basin into isochrons, each of which is a surface consisting

of states with equal phase (Guckenheimer and Holmes, 1983; Abraham and Marsden, 1978; Winfree, 1980; Glass and Winfree, 1984).

We proposed (Revzen et al., 2008) that kinematic measurements may provide an effective way of estimating an animal's phase along the purported asymptotically stable locomotor orbit, and that such an estimate would extend to a neighborhood of the orbit. We refer to the phase as expressed by purely kinematic variables as kinematic phase (Φ_K). Kinematic phase corresponds to the global phase (Φ_G) guaranteed by theory on the periodic orbit itself. Thus an estimated[3] global kinematic phase ($\hat{\Phi_K}$) may also be used as an estimated global phase ($\hat{\Phi_G}$), provided the global phase is not too sensitive to non-kinematic changes of state near the orbit.

By definition, the canonical phase of an oscillator evolves linearly in time. Thus, given the phase estimates from a few cycles of kinematic data, the investigator may use linear regression to construct a model providing an extrapolated phase – an expected phase projected into past and future. We may now define the global residual phase as the difference between the extrapolated phase $\Phi_e xt$ and the actual phase Φ_G:

$$\Delta\Phi_{\mathsf{G}}(t) \triangleq \Phi_{\mathsf{G}}(t) - \Phi_{\mathsf{ext}}(t) \tag{2.1}$$

[3]We follow the convention of denoting the estimate of a quantity x with a "hat" $\hat{x}$.

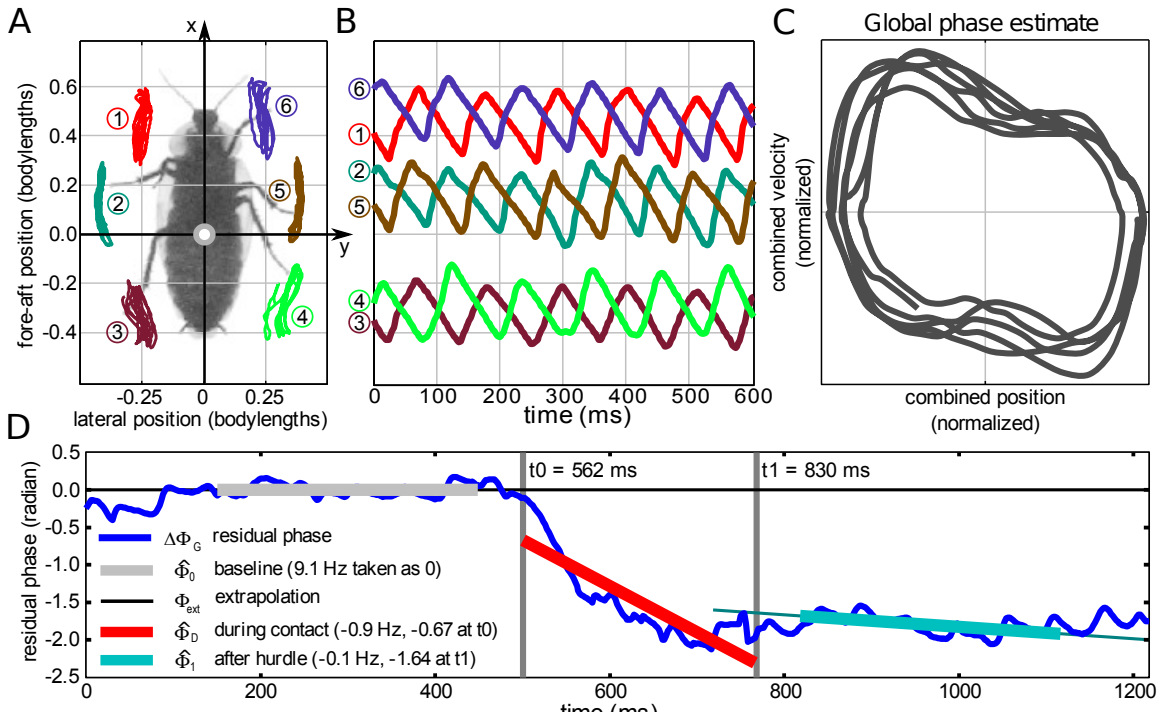

Figure 2.3: Example of estimating kinematic phase in a perturbation experiment. We tracked the tarsi in a registered video (colored tracks in **A**, numbered 1 through 6 counter-clockwise from the head) providing time series of positions. We used the fore-aft positions (**B**, plotted against time) to compute the difference in tripod fore-aft centroids $c(t)$. We plotted this combined position against its derivative $\dot{c}(t)$, the combined velocity in C. The annular shape showed that this 2D time series provided a useful global kinematic phase estimate by taking the angular part of its polar decomposition. We used this estimate and computed global residual phase after a perturbation (in **D**). The result exhibited a phase change outcome following the perturbation. (Note: data in **D** comes from a different trial than data in **A**, **B** and **C**). We showed the equations for regression lines of ϕ_D and ϕ_1 (see table 2.1) in the legend, and demonstrated that frequency changed by 0.1 Hz, together with a phase change of $-1.67 radian$. The thick lines represent the time segments for which we performed the linear regressions.

fig. 2.3 illustrates how we applied these ideas to running cockroaches. After con-

verting the videos to the animals' frame of reference by rotation and translation (the registered videos), we tracked the tips of the animals' tarsi (fig. 2.3-**A** $(x_k(t), y_k(t)),\ k \in \{1 \ldots 6\}$). We took the fore-aft coordinate (fig. 2.3-**B** plotting $y_k(t)$ versus t), and computed the difference between the centroids of the two tripods in the fore-aft direction:

$$c(t) \triangleq \frac{y_1(t) + y_3(t) + y_5(t)}{3} - \frac{y_6(t) + y_2(t) + y_4(t)}{3} \tag{2.2}$$

Our choice of formula for the tripod-centroid coordinate c(t) arose from observation of the gait being studied. In the alternating tripod running gait, legs 1, 3 and 5 move approximately in phase with each other and anti-phase to legs 2, 4 and 6. All legs move primarily in the fore-aft direction; thus the linear combination chosen provided an averaged coordinate the reliably reflected the state of the animal within the gait cycle. We plotted the tripod centroid coordinate $c(t)$ and its time derivative $\dot{c}(t)$ against each other in fig. 2.3-**C**, after subtracting the mean and rescaling to standard deviation of 1. We estimated phase by expressing the resulting 2D time series in polar coordinates and taking the polar angle to be our kinematically derived global phase estimate G:

$$\hat{\Phi}_{\mathsf{G}} \triangleq \text{atan2}\left(\frac{c - \langle c \rangle}{\text{std}(c)}, \frac{\dot{c} - \langle \dot{c} \rangle}{\text{std}(\dot{c})}\right) \tag{2.3}$$

The Φ_G estimate can be used to model the pre-perturbation behaviour, extrapolate it into the future and compare with the outcome of the perturbation experiment (see fig. 2.3-**D**). Using linear regression, we fitted the Φ_0 model to the time segment preceding contact with the hurdle. This regression line was extrapolated to future and past to give $\Phi_e xt$, which was used as a baseline model. The offset from this baseline is $\Delta\Phi_G$, the residual phase. We used similar regressions to provide the Φ_D and Φ_1 models during and after interaction with the hurdle. The plot in fig. 2.3-**D** shows these regression lines in a typical trial.

The constant frequency model of phase evolution (which corresponds to nearly linear segments on the $\Delta\Phi_G$ plot) is a reasonable one for periods of time far in excess of the duration of physical contact with the hurdle (region between two vertical lines in plot). We may therefore use the deviations from the extrapolated linear trends as a means for estimating changes from behaviour that would have occurred but for the perturbation. The plot in fig. 2.3-**D** also demonstrates that when linear regression was applied to consecutive segments in time, the regression lines need not match on the boundaries connecting the segments. At each boundary, the regression model changed to a new slope, indicating a frequency change, and an intercept that was

potentially incompatible with the current segment's predicted value, indicating a phase discontinuity.

Stated more precisely, one observes that the phase outcomes is a sum of several contributions, most obvious among them the difference in frequency $f_D - f_0$ multiplied by the duration of contact $t_1 - t_0$. Additionally, the phase regression models $\Phi_0(t)$ and $\Phi_D(t)$ may not agree in their predictions for phase at time t_0. We refer to this as the *On discontinuity*. Similarly $\Phi_D(t)$ and $\Phi_1(t)$ may not agree regarding time t_1, giving an *Off discontinuity*. The plot in fig. 2.3-**D** illustrates how the three linear models of table 2.1 related to each other in one trial. In this case $\Phi_D(t_0)$ and $\Phi_0(t_0)$ differed by more than $0.5 radian$.

2.4 Results

Animals ran at a stride frequency of $9.84 \pm 2.81\ Hz$ (mean,SD) and speed of $23.0 \pm 4.6\ cm/s$ (N = 40). Trial durations were $1.26 \pm 0.41\ s$ with the duration of hurdle contact equal to $0.27 \pm 0.051\ s$.

2.4.1 Instantaneous frequency

A strength of using kinematic phase is an enhanced ability to detect frequency changes. By definition, frequency is the time derivative of phase. From the frame-by-frame phase estimate, we obtained a frequency estimate for every frame, in contrast to a single frequency estimate for each stride – as is typically the case when stride durations are used to define frequency. For example, if some event were to make the animal stop for four milliseconds (two frames) and start moving again at the same speed as before, the kinematic phase method would detect the full frequency change down to 0 Hz and back toward the initial value, whereas methods based on stride duration would detect almost no change at all.

The distribution of frequency changes which occurred when animals began contact and ended contact with the hurdle is shown in fig. 2.4 using a Tukey box-plot. These changes are differences between the frequencies (phase regression line slopes) f_0, f_D and f_1 specified in table table 2.1. The total change in frequency $f_1 - f_0$ was normally distributed (Lilliefors $\alpha = 0.05$) with a value of $0.034 \pm 0.43\ Hz$. This mean change in frequency was small when compared with the $10 \pm 0.7\ Hz$ stride frequency, implying that frequency of the animals was unchanged.

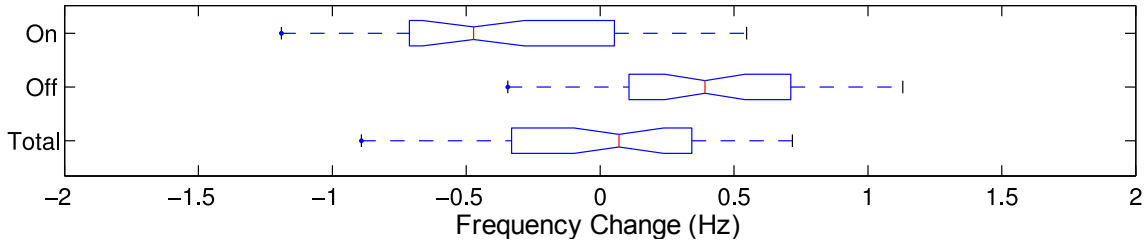

Figure 2.4: Frequency derived from kinematic phase on and off hurdle. "On" represents the frequency change distribution when animals contact with the hurdle, $f_D - f_0 = -0.35 \pm 0.49\ Hz$, represented by the difference in slope of the gray line and red line in fig. 2.3-**D**. ; "Off" represents the distribution when animals lose contact with the hurdle, $f_1 - f_D = 0.38 \pm 0.40\ Hz$, represented by the difference in slope of the light blue line and red line in fig. 2.3-**D**; "Total" represents the frequency distribution of total frequency change, $f_1 - f_0 = 0.034 \pm 0.43\ Hz$, represented by the difference in slope of the gray line and the light blue line in fig. 2.3-**D**. Boxes show median with surrounding notch indicating its 95% confidence interval, and extend from the 25th percentile to the 75th. Whiskers extend to full range of data. The notch in Total includes 0, showing that the total frequency change is not statistically different from 0.

The frequency changes we observed when contact with the hurdle begins and ends (fig. 2.4-**D** "On", "Off") were both normally distributed (Lilliefors alpha=0.05).

We explored our data for correlations between the following quantities: pre-perturbation frequency f_0, the frequency changes in the "On" transition $f_D - f_0$ and "Off" transition $f_1 - f_D$, duration of contact $t_1 - t_0$, total phase change $\Phi_0(t_1) - \Phi_1(t_1)$ and the phase changes in the transitions "On" $\Phi_D(t_0) - \Phi_0(t_0)$, and "Off" $\Phi_1(t_1) - \Phi_D(t_1)$ the hurdle. Correlations of angular quantities (phases) were computed by taking correlation with sine and cosine (Fisher, 1993).

The "On" transition $f_D - f_0$ and "Off" transition $f_1 - f_D$ frequency changes were negatively correlated ($R = -0.563$, $p < 2 \times 10^{-}4$), expressing the fact that not only does frequency remain unchanged on average, but individual animals return close to their original frequency after being perturbed. This correlation accounts for the variance of the "Total" frequency change fig. 2.4 being similar to that of "On" and "Off", while at the same time being their sum. No significant correlation was found among any of the phase differences "On", "Off" and "Total", suggesting that transient phase changes in the "On" and "Off" transitions were not linearly related. Taken together these results suggested that when animals were on the hurdle they attempted

to regulate frequency – how fast the gait cycle must advance – rather than regulating phase – where in the gait cycle their limbs must now be.

The frequency decrease during contact with the hurdle was not a constant offset below the pre-contact frequency. Instead, this frequency change $f_D - f_0$ was correlated to the duration of contact with the hurdle $t_1 - t_0$ ($R = -0.479$, $p < 2 \times\ 10^{-}3$). This suggested a history dependence in the frequency change. The longer the animal was in contact with the hurdle, the more its frequency was decreased.

The "Off" phase discontinuity $\Phi_1(t_1) - \Phi_D(t_1)$ was correlated to the duration of contact $t_1 - t_0$ ($R = 0.461$, $p < 3 \times 10^{-}3$), and was the only correlate we found for any of the phase differences examined. Taken together with frequency dependence on duration of contact which implied larger phase changes for longer contact times, this correlation suggests some tendency on the part of the animals to recover phase, and not only frequency, when contact with the hurdle ends.

2.4.2 Phase

Total phase change

Total phase change $\Phi_1(t_1) - \Phi_0(t_1)$ is the difference in phase between the predicted phase based on pre-perturbation motions $\Phi_0(t$ and the observed post-perturbation motions given by the model $\Phi_1(t)$. Were it the case that frequency was exactly maintained throughout the perturbation, then this difference would be the same at any all time (t). However, because in any given trial frequency was not the same before and after the hurdle, we had to select a time at which to compare the phases. We chose t_1 – the time at which the animal last touched the hurdle (i.e. in fig. 2.3 comparing the residual phase at t_0 between the gray and red lines with the residual phase at t_1 between the red and light blues lines). The distribution of Total phase change is plotted in fig. 2.5.

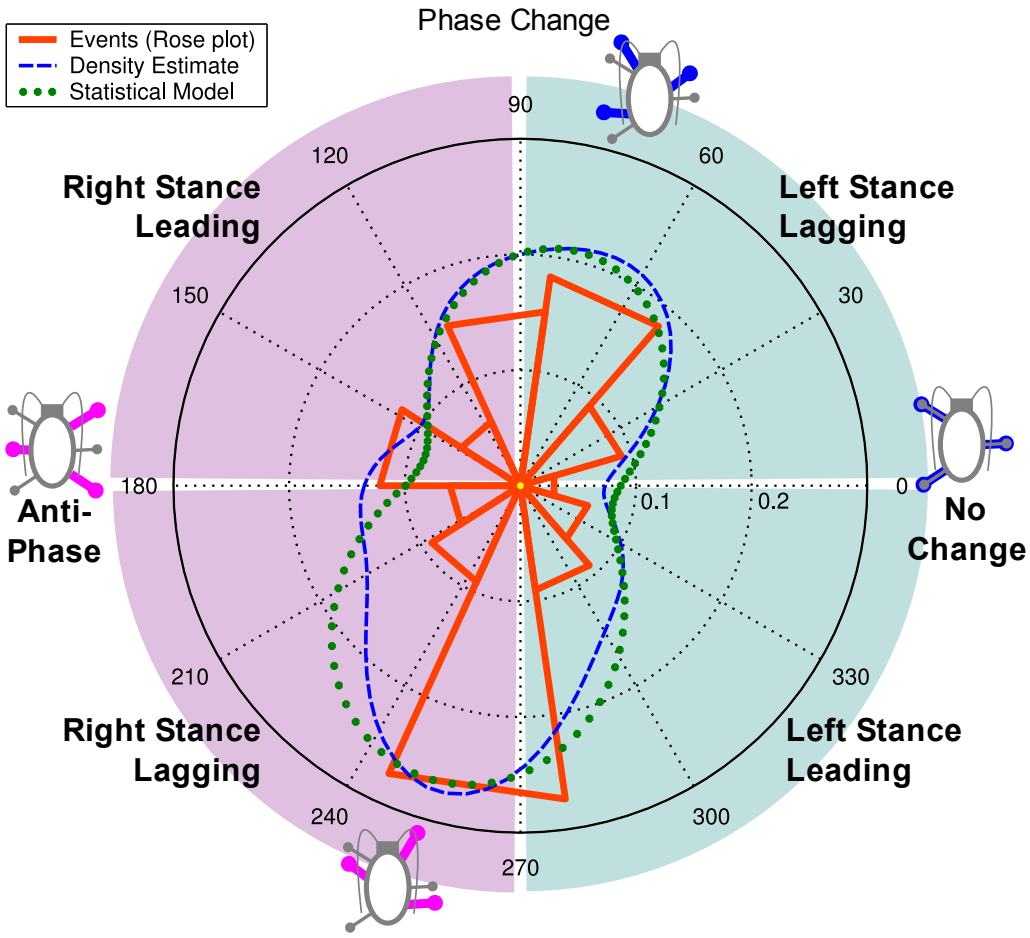

Figure 2.5: Rose plot of total phase change

Description of fig. 2.5

Rose plot of total phase change. Phase change is indicated as an angle, with illustrations of cockroach at various angles showing left mid-stance as phase zero (gray), and the phase shifted state (blue). Quadrants show whether a phase-shifted animal at that phase would be leading or lagging the unperturbed animal at left mid-stance at phase zero (blue for left stances; magenta for right stances). Total phase change results are presented in a rose plot (circular histogram; thick red lines.) For clarity, we plotted an alternative non-parametric representation of the same data. It represents the kernel smoothed density estimate (dashed blue line). The smoothing kernel we used was a Gaussian kernel with width equal to the rose plot bin size. We also plotted the parametric statistical model we fitted to the data (axial wrapped Gaussian distribution; dotted green line).

The bi-modal distribution of phase outcomes seen in fig. 2.5 showed an unexpected result. Given the pre-hurdle motions of the animal used for extrapolating a prediction from unperturbed motions, animals traversing the hurdle differ from the prediction by lagging by either 1.33 *radian* or by $1.33+\pi$ *radian*. Rather than having a single typical phase outcome, perturbed animals exhibited an *axial* phase outcome distribution. This implies that animals lagged by fraction of a cycle equal to 1.33 *radian*, or 1.33 *radian* which represents an extra step.

Following Fisher (1993), we described the circular statistics of the phase outcome distribution. The first moment of the distribution was $\rho = 0.135$, $\mu = -1.92$ *radian* and was not a statistically significant first moment (as is typical of axial distributions). Testing the distribution for axiality, we doubled the phase angles, computed the mean, and converted back to obtain $\rho_2 = 0.291$, $\mu = 1.33$ *radian*, a statistically significant result at $p < 0.05$. Parametrically, the results can be described by an axial wrapped Gaussian distribution with variance $\sigma = 0.812$ *radian*, mean $\mu = 1.33$ *radian* and mass of 0.56 on the lobe at the mean.

Discontinuities in phase changes

The discontinuity in phase between the "before" and "during" segment regression models was $\Phi_D(t_0) - \Phi_0(t_0) = 0.19(0.48)$ *radian*; between the "during" and "after" models $\Phi_1(t_1) - \Phi_D(t_1) = 0.15(0.60)$ *radian*. These phase change distributions were both normally distributed (Lilliefors test with $\alpha = 0.05$). The variances of these distributions were not small in comparison with the maximal possible variance of pi radians. However, the model fitting residuals themselves have a typical root-mean-square magnitude on the order of 0.2 *radian*, and it is typical for fitting residuals to be larger at the ends of the segment when using a robust linear fitting algorithm.

2.5 Discussion

The use of kinematic phase with an instantaneous estimation of frequency (fig. 2.3) revealed structure of the neuromechanical control architectures (fig. 2.1) previously unknown. The frequency (fig. 2.4) and phase (fig. 2.5) response to our perturbation led us to propose a novel biological controller sufficiently general that it can be applied to legged robots.

2.5.1 Axial phase outcomes – a new coupled oscillator model

The axial phase distribution shown in fig. 2.5 suggests that the dynamical system governing cockroach running possesses an internal symmetry related to delays of half a stride cycle. A delay of half a stride corresponds to a step, and the pose of the animal after a step is on average a mirror image of its pose before the step. Thus, these preferred phase shift modes are related in a natural way to the bilateral symmetry of the animal. Phasing of motion after perturbation maintains a preferred relationship to the phase before perturbation, but this preference seems nearly indifferent to reflection across the left-right axis of the animal.

Regardless of whether we interpret our results with the assumption of a feedforward architecture such as the Clocked Spring Mass (NCA1) or Clock Tracker (NCA2) or within the broader class of Clock Adaptive Trackers (NCA3), the analysis of residual phase responses provides insight into the controller. For feedforward architectures the CPG governs the long-term properties of the kinematics, causing the mechanical system – the animal's body – to entrain to its signal. The long term trends of the kinematic phase thus provide a model for the neural CPG, and the excursions from these trends, as expressed in the residual phase, indicate the various ways the mechanical system can stably entrain to the CPG signal. Seen in this light, the axial phase response distribution indicates that the mechanical system has at least three stable phase relationships to the CPG phase – the two modes seen in the results, and the additional stable solution of zero phase change. For the results we observed to have been generated by a Clocked Spring Mass or Clock Tracker, the initial population of pre-hurdle animals must have all been in an identical phase-locked state relative to their CPG. Interaction with the hurdle moved these animals into one of the two other stable phases relative to the CPG, but the perturbation had to have been regular enough to consistently depopulate that stability basin of zero phase change. Such a scenario seems rather unlikely, although technically possible.

History dependence in the phase outcome for perturbations ending in similar kinematic states, such as dependence on the duration of perturbation, is impossible for

a Reflex Cascade (NCA0) architecture. Reflex Cascade states are entirely described by their kinematic variables implying that phase, which is a function of state, cannot depend on the path taken to reach that kinematic state. We found a significant correlation between perturbation duration and the frequency change it induces, and therefore rejected the Reflex Cascade architectures.

Given that the three other proposed neuromechanical control architectures (fig. 2.1) are less likely to represent the present results, we consider the Clock Adaptive Tracker (NCA3) because it can also generate phase changes without a change in frequency. Because this class of architectures is extremely broad, we used the residual phase results to generate new hypotheses of control architecture that are compatible with our results and may be refuted by future experiments. The key insight we used to generate these new controllers is that the axial symmetry of phase outcomes can be the outcome of a master clock which maintains a "step clock" by generating a signal every step. The tripods vie with each other as to which entrains to the "even" tics and which to the "odd" tics of this central clock. The encounter with the hurdle may perturb posture sufficiently to knock the animal from one of these states to the other, causing a phase change of half a stride. Such dynamics are similar to that of the Haken-Kelso-Bunz (Haken et al., 1985) model. We can use their notion of a coupling potential to relate three clocks: a master clock coupled to two other clocks each representing a tripod of legs (fig. 2.6-**A**).

2.5.2 Phase responses in simulated Clock Adapting Trackers

Although they can account for the axial phase responses, the models we propose do not fully account for the frequency changes we observed.

Clock Adapting Trackers (NCA3) with and without a master clock

To investigate whether our experimental results support the notion of a Clock Adapting Tracker with a master clock (fig. 2.6-**A**) versus an alternative Clock Adapting Tracker design without one (fig. 2.6-**B**), we simulated the dynamics of two models – a Entrained Coordination controller with a master clock facilitating coordination, and a Decentralized Coordination controller where coordination emerges through a distributed interaction.

Both the Decentralized Coordination and the Entrained Coordination controller drive all three legs of each of the two tripods of cockroach legs from a single phase oscillator (circles with labels "Left" and "Right" in fig. 2.6) by emitting a single phase variable: ϕ_L for the left tripod, and ϕ_R for the right (labeled arrows in fig. 2.6). The

construction was similar to that of an adaptive controller developed for the RHex robots (Weingarten et al., 2004), and reduced the animal to a virtual biped. The dynamics of this bipedal model were governed by a differential equation that admitted kinematically identical, stable left-right antisymmetric periodic solutions representing the animals' alternating tripod running gait.

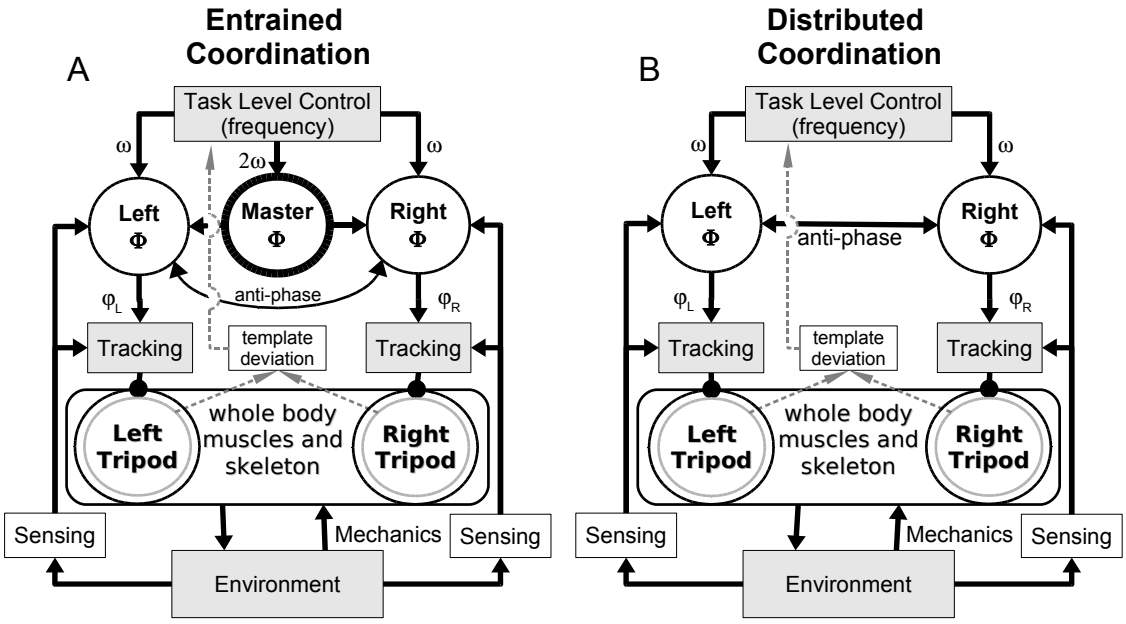

Figure 2.6: Structure of two Clock Adapting Tracker (NCA3) models. Both models have left and right tripod phase oscillators (circles with labels "Left" and "Right") coupled to independent "Tracking" blocks (gray boxes) representing the proprioceptive reflexes that make each tripod of legs track its designated phases (thick arrows labelled ϕ_L and ϕ_R). Perturbation of each tripod is assumed to feed back up to that tripod's oscillator (thick arrows in opposite direction from ϕ_L and ϕ_R). All oscillators are exposed to the global "template deviation" (thin arrow). In the Decentralized Coordination model, the anti-phase coupling of the tripod oscillators is strong (bidirectional thick arrow). In the Entrained Coordination model an additional master oscillator (circle with label "Master") facilitates coordination of left and right oscillators through a descending signal (thick arrows to "Left" and "Right" oscillators) that interacts with the distributed influence of anti-phase coupling (thin bidirectional arrow labeled anti-phase).

In Decentralized Coordination, the phases of the two tripods were pushed symmetrically into an anti-phase relationship, through dynamics that can be reduced to a simplified form of the Haken-Kelso-Bunz model (Haken et al., 1985). In Entrained Coordination, the same coordinating interaction between the tripods still exists, but it

vies with an entrainment effect introduced via a descending master clock signal. This descending coordination influence is symmetric with respect to the bilateral symmetry of the animal, allowing either tripod to phase lock at phase zero, provided the other tripod locks in anti-phase.

Template deviation feedback aside, despite possessing an autonomous clock oblivious to environmental influences the Entrained Coordination model does not fall in the simpler Clock Tracker architecture class. The distinction between Entrained Coordination and a Clock Tracker lies in the fact that we postulated the Tracking blocks to have no internal state. Requiring such a postulate of the tracking reflexes is not unreasonable. Such context-independent tracking was found in the intra-leg coordination of stick insects, where local avoidance reflexes are composed of context-independent joint actions (Duerr and Ebeling, 2005). The addition of an internal state corresponding the phase of the tripod implies that the influence of the master clock on the actual kinematics may become indirect, and incongruence between the pose and clock can by mediated through dynamics of that internal state. We conceive of the Entrained Coordination architecture as one where the descending clock provides a "hint" to the decentralized coordination mechanisms in how they should coordinate with each other.

Decentralized Coordination model

The simpler of the two models we examined is reproduced directly from Weingarten et al. (2004), where it governs the "model clocks". The system equations are defined in terms of a potential function U_2:

$$U_2 = a\,(1 + \cos(\phi_{\mathrm{L}} - \phi_{\mathrm{R}})) \tag{2.4}$$

$$\frac{d}{dt}\begin{bmatrix}\phi_{\mathrm{L}}\\ \phi_{\mathrm{R}}\end{bmatrix} = \omega(1 - bU_2)\begin{bmatrix}1\\ 1\end{bmatrix} - \nabla U_2 \tag{2.5}$$

The equations have one stable solution, given by the minimum of U_2:

$$\phi_{\mathrm{L}} = \phi_{\mathrm{R}} + \pi = \omega t + \phi_{\mathrm{L}}(0) \tag{2.6}$$

The stability is governed by the two parameters a and b. a sets the recovery rate from small disturbances. b sets the degree to which the animal speeds up or slows down when recovering from large perturbations – the coefficient governing the magnitude of confusion induced slow-down. Through b we model our observation that animals slow down when challenged with a small hurdle.

From a dynamical perspective, scaling a and b together scales the right hand side of the differential equation, and is therefore equivalent to rescaling time. For this reason, we restricted our parameter studies to $a = 1$.

Entrained Coordination model

The Entrained Coordination model adds a term extending the potential function of the Decentralized Coordination to couples the average phase of the two tripods to a master clock ϕ_C. By coupling to a symmetric combination of the tripod phases we express the indifference of the coupling to which of the two possible mirror image poses the animal adopts at a particular phase. It should be noted that this symmetry is inherent in the dynamics, as the sagittal plane dynamics of running in many animals seem to follow the Spring Loaded Inverted Pendulum model (Ghigliazza et al., 2005; Blickhan, 1989; Dickinson et al., 2000) whose cycles are one step long. For a bilaterally symmetric animal, either of two mirror image poses is equivalent with respect to the influence exerted by spring loaded inverted pendulum dynamics.

$$U_3 = a\,(1 + \cos(\phi_\mathrm{L} - \phi_\mathrm{R})) + c\,(1 + \cos(2\phi_\mathrm{C} - \phi_\mathrm{L} - \phi_\mathrm{R})) \tag{2.7}$$

$$\frac{d}{dt}\begin{bmatrix}\phi_\mathrm{L}\\ \phi_\mathrm{R}\\ \phi_\mathrm{C}\end{bmatrix} = \omega(1 - bU_3)\begin{bmatrix}1\\ 1\\ 1\end{bmatrix} - \nabla U_3 \tag{2.8}$$

The relative magnitude of the new parameter c to a and b of U_2 governs the trade-off between the entrainment to the master clock and inter-tripod influence. These equations have two stable solutions that are mirror images of each other:

$$\phi_\mathrm{C} = \phi_\mathrm{L} = \phi_\mathrm{R} + \pi = \omega t + \phi_\mathrm{C}(0) \tag{2.9}$$

$$\phi_\mathrm{C} = \phi_\mathrm{L} + \pi = \phi_\mathrm{R} = \omega t + \phi_\mathrm{C}(0) \tag{2.10}$$

Both these solutions overlap in their projections on the $\phi_L \times \phi_R$ plane, meaning that they produce kinematically identical gaits, which are also identical to the gait produced by the Decentralized Coordination model.

General properties of the Coordination models

Both tripod coordination models we present exhibit the same stable cycles of leg motions. The period of these cycles is identical and equal to $2\pi/\omega$.

Our models are particularly simple in that dynamics have a phase invariance symmetry: given any solution $[\phi_L(t), \phi_R(t), \phi_C(t)]$ of Entrained Coordination (and similarly for Distributed Coordination), the phase shifted version $[\theta + \phi_L(t), \theta + \phi_R(t), \theta + \phi_C(t)]$ is also a solution, for any choice of θ. Although this may seem like an extremely strong assumption to make about an animal's dynamics, the converse is true. The phase invariance symmetry always exists when dynamics are written with respect to the Floquet coordinates of the system, and thus requires us to make no additional assumptions about the animal. To derive direct computational benefit from this symmetry one requires an opportune choice of coordinates (Guckenheimer and Holmes, 1983; Floquet, 1883) which as designers of the simulation we have indeed made.

Thanks to phase invariance, we could model perturbations at only one phase, and draw conclusions valid for all phases. Our perturbations were generated by taking an initial point on a periodic solution and adding a randomly generated offset to the first two coordinates, as if physical leg feedback were to perturb the putative clock variable of the left or right phase reference (ϕ_L or ϕ_R). The phase offsets were taken from a 2D Gaussian which was elongated in the direction corresponding to fore-aft motions of the body with respect to the legs.

Starting with the perturbed initial condition, we integrated the system using an ODE integrator (dopri5 integrator code Hairer et al. (1993) ported by the authors to **Python SciPy**; **SciPy** is an open source platform supported by Enthought, Inc. Austin, TX 78701, USA) and determined the phase change in the outcome when compared with the initial, unperturbed state.

Phase shift outcomes of both models are similar

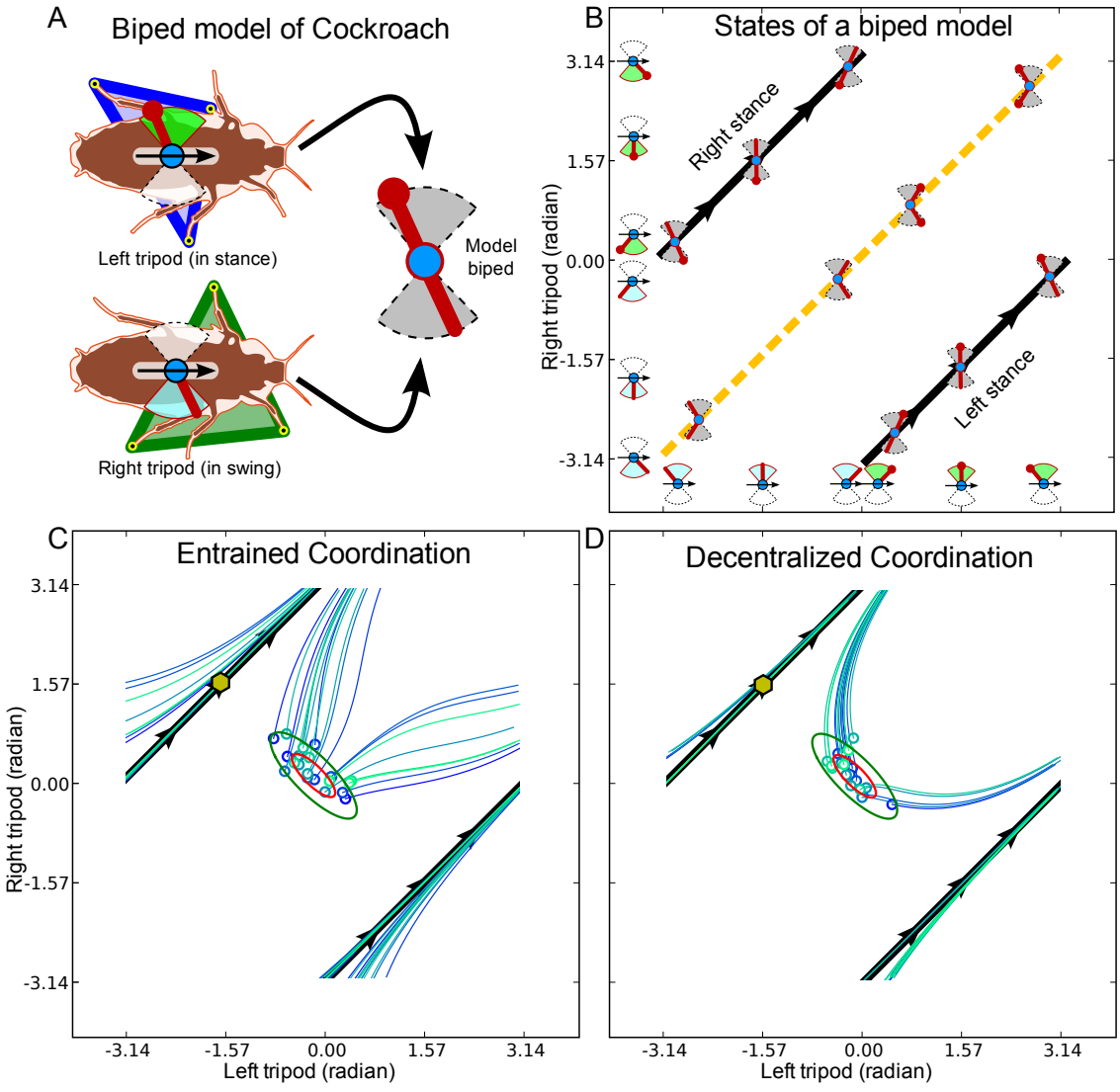

Figure 2.7: Simulated perturbation recovery trajectories for an Entrained versus Decentralized Coordination controller

Description of fig. 2.7

Simulated perturbation recovery trajectories for an Entrained versus Decentralized Coordination controller.

Simulations of both controllers lead to similar results. In our models we represented each tripod of the cockroach by a single angular phase variable. We illustrate each such tripod phase as the pose of a single (virtual) leg of a biped sweeping back and forth. **A** shows a cockroach with tripods and corresponding virtual legs highlighted; superposed on the cockroach are schematic representations of the equivalent virtual biped. The body of the schematic biped is shown as a blue circle with thick red lines which represent legs. All bipeds are moving left to right. Legs which are in stance end in a circular marker. The legs sweep through a quarter-circle, as indicated above and below the body. The left tripod (**A** top) is marked by a blue triangle and was nearing the end of stance. Its biped equivalent has its left leg (thick red line) near the rear of its sweep area, with circular end marker to indicate stance. The right tripod (**A** bottom) is marked by a green triangle and is nearing the end of swing. The superposed biped right leg is near the front of its range. The two tripod-equivalent legs are combined to give a complete biped (**A** right, following arrows).

B shows the limit cycle in terms of biped poses, and maps out the two-dimensional space of biped states. Bipeds with both legs and quarter-circles gray and dotted represent the pose at that point of the space. Bipeds with one leg omitted and an arrow intersecting the body correspond to the axis label they are adjacent to and graphically represent the pose of the leg which is shown (left leg on horizontal axis, right leg on vertical axis). The limit cycle, indicated by a thick dark line with arrowheads, is a single loop wrapping around right-to-left and top-to-bottom as the axes are angles. On the limit cycle lie bipeds whose legs are in anti-phase. We have also indicated the diagonal (dashed yellow line) upon which lie bipeds whose legs are in phase.

In **C** and **D** we show simulation results for our two proposed controllers. We simulated perturbation recovery trajectories by first choosing a base-point (indicated by the yellow hexagon) on the limit cycle (indicated by the dark lines with arrowheads, which lie behind the colored lines representing simulated trajectories). We then generated random perturbations as offsets from the base point. The perturbations represent a mechanical disturbance that moves the legs to a new position, and correspondingly changes the phases via the proprioceptive sensing in the Tracking blocks fig. 2.6.

An animal hitting a hurdle had its body pushed back, which caused the swing legs to move ahead of their expected points in the cycle (relative to body), and the stance legs to be retarded. Hitting a hurdle is expected to move the animal from the limit cycle in the $[1, -1]$ direction towards the diagonal. We used the perturbed state giving initial conditions (small circles) for integration of the controller dynamics, showing how animals would move their legs while at the same time recovering their coordination according to the two models (thin lines in **C** and **D**; each simulated run in a different shade of blue-green). Integration was terminated when state returned close to the limit cycle, indicating that coordinated movement was recovered.

In **C** we show the Entrained Coordination simulation and in **D** the Decentralized Coordination simulation. Animals encountered the hurdle head-on, guiding us to use a distribution of perturbations elongated in the direction corresponding to fore-aft motion of the body, which is represented by anti-symmetric changes in the phases (ellipsoids in **C** and **D**; 1 SD surface red line; 2 SD surface green line). We computed both simulations with $b = 0.45$. We selected the mean value of perturbations (center of ellipsoid) to lie over the diagonal of the torus, ensuring that all phase change outcome distributions were bi-modal.

The phase outcomes of the Decentralized Coordination model are presented in fig. 2.8 with an example of some simulated trajectories in fig. 2.7-**B**. Changes to the b parameter introduce phase shifts and broaden the outcome distribution.

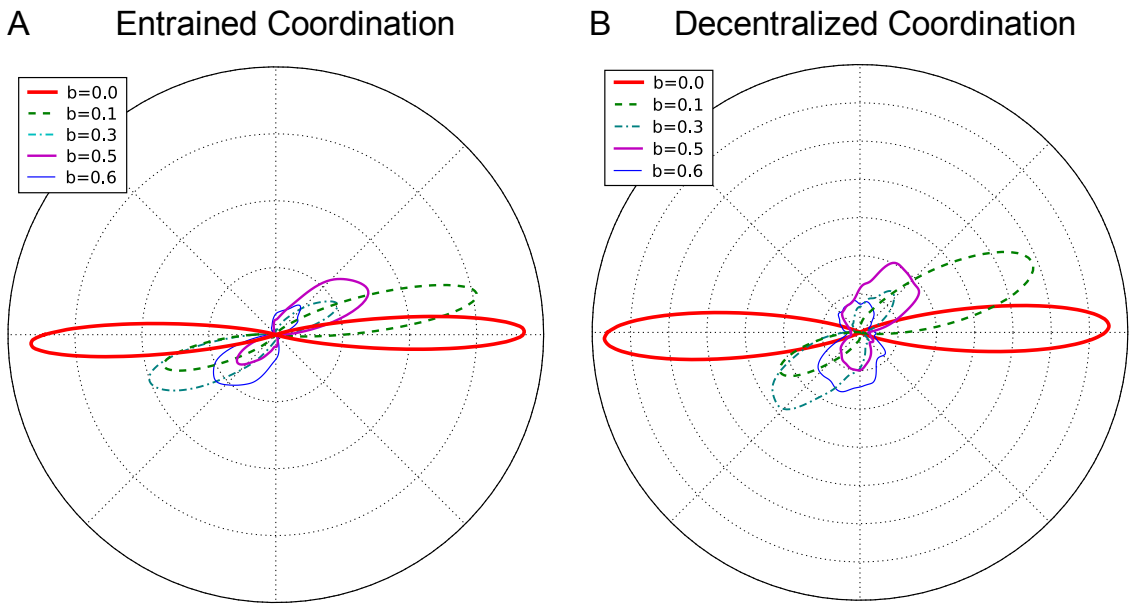

Figure 2.8: Phase responses of the **A** Entrained Coordination and **B** Decentralized Coordination models to the perturbation distribution shown in fig. 2.7-**A** and fig. 2.7-**B** respectively for various values of b – the coefficient of template deviation feedback (eqn. 2.5, eqn. 2.8) – each represented in the legend by a different color line. We simulated each perturbation distribution 1000 times. The lines in the plot were smoothed with a 0.1 *radian* Gaussian kernel.

The Entrained Coordination results of fig. 2.8-**A** are quite similar to the Decentralized Coordination results presented in fig. 2.8-**B**. Axial outcomes appear in both models in direct relation to having the perturbation distribution cross over the $\phi_L = \phi_R$ diagonal, with the mass of the two modes proportional to the fraction of the perturbations on either side.

The two models differed under correlated perturbations: perturbations that change both phases by the same amount (the $[1, 1]$ direction on the $\phi_L \times \phi_R$ torus). Such perturbations correspond to motions that mimic the limit cycle poses, but make them

appear either too early or too late with respect to pre-perturbation motions. Decentralized Coordination, having no internal sense of phase other than ϕ_L and ϕ_R, incurred a permanent phase change under such a perturbation regime. Entrained Coordination incurred a small phase change associated with the template deviation introduced by the perturbation and otherwise recovered its old phase. It may also switch over to a mirror-image gait for sufficiently large perturbations.

Decentralized Coordination is arguably the more parsimonious of the two models, and we therefore conclude that cockroaches running over a hurdle exhibit phase changes consistent with the controller proposed in Weingarten et al. (2004). Most practicing robotics engineers design robots with Clock Tracking architectures, or, at best, Entrained Coordination. The observation that the cockroach, an animal in use by several groups as a model organism for bio-inspired robots (Bachmann et al., 2009; Kim et al., 2006; Altendorfer et al., 2001; Yumaryanto et al., 2006; Spenko et al., 2008), exhibits a controller different from these initial designs may serve to stimulate further investigation into the trade-offs inherent in such control architectures.

Future investigation may present experimental treatments that can further differentiate the Decentralized Coordination from the Entrained Coordination (fig. 2.6). If the sensitivity of Decentralized Coordination to correlated perturbations proves to limit performance of robots under realistic conditions, the extension of such a controller toward the Entrained Coordination model by tuning the c parameter may provide a natural avenue for improvement. One may interpret the c parameter as expressing the trade-off between centralized and decentralized coordination of legs, and the importance of this trade-off was previously pointed out in hypothesis H3 of Koditschek et al. (2004).

2.5.3 Rejecting alternative interpretations of phase change distribution

Multimodal outcomes beg representation as mixtures of simpler uni-modal outcomes, and despite the appeal of the controllers introduced in the previous sub-section, we must consider the alternative interpretation of our axial phase distribution results as a mixture of two outcome modes. A mixture of two wrapped normal distributions is specified by five parameters (two means, two variances and a relative weight), whereas an axial distribution as obtained in our results requires only three (a mean, a variance and a relative weight). If additional knowledge of the system at hand suggests, as in our case, a plausible model for generating the axial outcome distribution, it is certainly the simpler explanation for the results.

Multimodal outcomes can also be the result of a mixed population consisting of animals each of which contributes to only one of the two modes. All three animals for which we had three trials exhibited total phase change outcomes in both modes of the axial distribution, allowing us to obtain an upper bound on the bias of animals towards a preferred mode. If we assume that each animal has a preferred mode occurring independently with probability p, the probability of the outcomes we observed is given by:

$$\left(1 - p^3 - (1-p)^3\right)^3 = 27(1-p)^3 p^3 \tag{2.11}$$

For our axial distribution, this probability is 0.41, showing that mode outcomes we observed are compatible with the model we chose. Setting the probability of our observation to 0.05 and solving for p we find that if $p > 0.86$ our results would constitute statistically significant evidence ($0.14 < p < 0.86$). We can therefore refute the hypothesis of a mixed population whose members have an individually preferred mode occurring more than 86% of the time.

If we wish to directly test the possibility that our axial distribution results were a consequence of what happened to be a $\pi radian$ phase difference between phase response modes in a mixture that could have had other phase differences between the modes, we would subject cockroaches to an alternative bilaterally symmetric perturbation. One such possibility could be applying an impulse in the direction of motion, using a system like that used in Jindrich and Full (2002), or Revzen et al. (2007).

A mixture model would be unlikely to predict an identical $\pi radian$ phase difference for the outcomes in vastly different perturbation regimes, whereas a symmetry-breaking argument of the sort we suggest inevitably requires an axial outcome.

If bi-modality appears, but the modes are closer together or significantly different in width, the model we propose may be rejected in favour of a mixture model. If an axial distribution appears, the results would provide further support for our model.

2.6 Summary and future work

Our analysis of the phase changes in leg motions of running cockroaches traversing a hurdle has shown us that these motions are most likely controlled using a control architecture along the lines of the fig. 2.2 Clock Adapting Tracker (NCA3).

Our results and the analytical approach that underlies them were developed for the study of sufficiently rapid behaviors in which dynamics of the body play a role. As Cruse et al. (2007) point out, in rapid behaviors such as running in cockroaches an estimate of state derived from phase of an internal oscillator may well be more reliable

than any that can be obtained from proprioceptive senses within the available time. If that were so, one would expect a shift towards Clock Tracker (NCA2) architectures and finally Clocked Spring Mass (NCA1) architectures as speed increases. The architecture we identified, which consists of a Clock Adapting Tracker (NCA3) with template deviation feedback to the clock may be a point on such a continuum. We predict that *Blaberus discoidalis* cockroaches will exhibit less feedback when running at maximal speeds, and that such simplification will be even more pronounced in faster species whose stride frequencies challenge sensory capabilities even more, such as Periplaneta americana.

The WalkNet model provides accurate predictions for the walking motions of stick insects under a variety of circumstances (Cruse et al., 2007). Early work leading to WalkNet (Cruse, 1985; Cruse and Epstein, 1982) relied heavily on phase response curves as a means of teasing apart inter-leg influences. Our analysis of residual phase allows phase responses to be tested against predictive models adapted to recent strides rather than expressing concurrent interactions between legs. The behavior of stick insects subjected to our residual phase analysis may expose additional details worthy of inclusion in WalkNet.

In its structure, WalkNet seems to be a Reflex Cascade architecture (NCA0). Our predictions for Reflex Cascade architecture residual phase outcomes (Revzen et al., 2008) should hold for simulated perturbations to WalkNet. A WalkNet driving a mechanical simulation of a stick insect is by far the most elaborate arthropod walking model available, and as such would provide excellent evidence of the generality of the methods we proposed. In the current publication we argue that axial outcomes are unlikely for Reflex Cascade (NCA0) systems. With its complexity and sophistication, WalkNet would be an excellent candidate for refuting our claim by generating bi-modal phase outcomes when presented with a bilaterally symmetric ensemble of perturbations similar to the hurdle experiment described herein.

Daley et al. (2006) conducted a study of how guinea fowl recover from a large and unexpected change in substrate height. Like cockroaches, guinea fowl are rapid and capable runners that use running primarily to escape predators. Unlike cockroaches, guinea fowl are bipedal, possess excellent vision, and run at stride durations far less likely to be pushing the limits of sensory input or motor output in terms of temporal resolution. Although Daley et al. (2006) report on the timing of various recovery strategies they observed, their analysis was not conducted from a perspective that considered the animals as oscillators, and they do not present the effects of perturbation on phase. A parsimonious approach would predict that even guinea fowl, who might have more time for computation and sensing due to their slower strides, would use a simple Clock Adapting Tracker (NCA3) architecture like the one we propose for the

cockroach. Their sagittal pose and the intrinsic muscle properties of their spring-like legs (Biewener and Daley, 2007) may even allow them to benefit more fully of the dynamic stability offered by Spring Loaded Inverted Pendulum running, placing them in a simpler architectural class such as Clocked Tracker (NCA2) or Clocked Spring Mass (NCA1). A refutation of these hypotheses would require evidence for a more complicated architecture than the ones we have described; such evidence may provide insight into the potential benefits of improved sensing and computation available to vertebrates.

Given the possible of our control models, we suspect that they can provide biological inspiration for the design of new controllers in legged robots. Several groups have investigated coupling clock-like stimulation to a legged robot, thereby exploring the same space of control architectures we have proposed for animals. Komsuoglu (2004) considered formal analysis of open-loop control of a hopping robot, which has more recently been treated from the hybrid control perspective by (Howley and Cutkosky, 2009). Although both consider feedback architectures that tie together the mechanical body and the driving oscillator, neither publication considers phase responses to different classes of perturbation, nor what they may provide for identification of the controller architecture.

The coupling of clocks to underactuated elastic robots has met with some success, as can be deduced from the numerous devices of this nature being developed. Most directly related to controller architectures we have considered for the cockroach are the Tekken2 robot (Kimura et al., 2007) and the control of the PUPPY II robot with frequency adaptive hopf oscillators (Buchli and Ijspeert, 2008). In both cases the investigators were able to obtain efficient and robust locomotor behaviors using Clock Adapting Tracker architectures similar to the Entrained Coordination controller we proposed here.

A far more elaborate adaptive clock, yet one which may well be amenable to formal reduction to a simple phase oscillator, was used in the "salamandra robotica" robot (Ijspeert et al., 2007), which aimed to simulate spinal feedback architectures controlling the transition between swimming and walking in Caudata. Ijspeert (2008) reviews the pros and cons of using CPG with robots. We believe that the experimental methodology used in our publication is a useful addition to the engineers' tool-chest. Rather than relying on the controller design to achieve the expected close-loop behaviors, the investigation of residual phase provides the means to experimentally verify which closed-loop architecture is governing the robot in practice when the robot is operating in its actual environment. As robots and the environments in which they function become more complex, the emerging field of experimental robotics will grow closer and closer to comparative biomechanics, and similar methodologies may be effective in

both.

An intriguing alternative hypothesis for the appearance of the axial distribution of phase outcomes is that these arise through symmetry properties of weakly unstable intermediate gaits of a hexpedal mathematical model similar to Kukillaya and Holmes (2007). If that proves to be the case, then symmetry (Golubitsky et al., 1999) and dynamical noise could provide a bridge between morphologically detailed neural network models and the reduced phase oscillator approach we have used here.

Empirical investigations based on kinematic phase can tie in phase oscillator models, animal locomotion and robot controller design. This combined approach allows us to generalize biomechanical control principles in a class of models that is both testable in animal experiments and feasible to implement in human-made physical devices.

2.7 Acknowledgements

This research was funded by the NSF Frontiers for Integrative Biological Research (FIBR). The authors are thankful to J. M. Guckenheimer for providing the key observation that axiality of phase outcomes is indicative of an additional bi-lateral symmetry of kinematic outcomes, and to P. Holmes for drawing their attention to the possibility that transitions through weakly unstable gaits could also generate multi-modal phase outcomes.

2.8 Bibliography

R Abraham and J E Marsden. *Foundations of Mechanics: Nonlinear Oscillations, Dynamical Systems, and Bifurcations of Vector Fields*. Addison-Wesley, 1978.

A N Ahn and R J Full. A motor and a brake: two leg extensor muscles acting at the same joint manage energy differently in a running insect. *J Exp Biol*, 205(3): 379–389, 2002.

A N Ahn, K Meijer, and R J Full. In situ muscle power differs without varying in vitro mechanical properties in two insect leg muscles innervated by the same motor neuron. *J Exp Biol*, 209(17):3370–3382, SEP 1 2006. ISSN 0022-0949. doi: 10.1242/jeb.02392.

T Akay, S Haehn, J Schmitz, and A Bueschges. Signals from load sensors underlie interjoint coordination during stepping movements of the stick insect leg. *J Neurophysiol*, 92(1):42–51, July 2004. ISSN 0022-3077. doi: 10.1152/jn.01271.2003.

R Altendorfer, N Moore, H Komsuolu, M Buehler, H B Brown, D McMordie, U Saranli, R J Full, and D E Koditschek. Rhex: A biologically inspired hexapod runner. *Autonomous Robots*, 11(3):207–213, Nov 2001. ISSN 1573-7527. doi: 10.1023/A:1012426720699.

R J Bachmann, F J Boria, R Vaidyanathan, P G Ifju, and R D Quinn. A biologically inspired micro-vehicle capable of aerial and terrestrial locomotion. *Mechanism and Machine Theory*, 44(3):513–526, MAR 2009. ISSN 0094-114X. doi: 10.1016/j.mechmachtheory.2008.08.008.

A Back, J G Guckenheimer, and M Myers. *Hybrid Systems*, volume 736/1993 of *Lecture Notes in Computer Science*, chapter A dynamical simulation facility for hybrid systems, pages 255–267. Springer, 1993. ISBN 978-3-540-57318-0. doi: 10.1007/3-540-57318-6_32.

A A Biewener and M A Daley. Unsteady locomotion: integrating muscle function with whole body dynamics and neuromuscular control. *J Exp Biol*, 210(17):2949, 2007. doi: 10.1242/jeb.005801.

R Blickhan. The spring mass model for running and hopping. *J Biomech*, 22(11-12):1217–1227, 1989.

J Buchli and A J Ijspeert. Self-organized adaptive legged locomotion in a compliant quadruped robot. *Autonomous Robotics*, 25:331–347, 2008. doi: 10.1007/s10514-008-9099-2.

A Bueschges. Sensory control and organization of neural networks mediating coordination of multisegmental organs for locomotion. *J Neurophysiol*, 93(3):1127–1135, 2005.

A Bueschges and M Gruhn. Mechanosensory feedback in walking: From joint control to locomotor patterns. In *Advances in Insect Physiology: Insect Mechanics and Control*, volume 34 of *Advances in Insect Physiology*, pages 193–230. 2007. doi: 10.1016/S0065-2806(07)34004-6.

A Cohen, P J Holmes, and R H Rand. The nature of coupling between segmental oscillators of the lamprey spinal generator for locomotion: a model. *J Math Biol*, 13:345–369, 1982. doi: 10.1007/BF00276069.

H Cruse. Coactivating influences between neighbouring legs in walking insects. *J Exp Biol*, 114:513–519, 1985.

H Cruse and S Epstein. Peripheral influences on the movement of the legs in a walking insect carausius morosus. *J Exp Biol*, 101:161–170, 1982.

H Cruse, T Kindermann, M Schumm, J Dean, and J Schmitz. Walknet - a biologically inspired network to control six-legged walking. *Neural Networks*, 11(7-8):1435–1447, 1998.

H. Cruse, V. Durr, and J. Schmitz. Insect walking is based on a decentralized architecture revealing a simple and robust controller. *Philos Trans R Soc Lond , Ser A: Math , Phys Eng Sci*, 365(1850):221–250, January 2007.

M A Daley, J R Usherwood, G Felix, and A A Biewener. Running over rough terrain: guinea fowl maintain dynamic stability despite a large unexpected change in substrate height. *J Exp Biol*, 209(1):171–187, January 2006. ISSN 0022-0949. doi: 10.1242/jeb.01986.

F Delcomyn. Neural basis of rhythmic behavior in animals. *Science*, 210(4469):492–498, 1980. doi: 10.1126/science.7423199.

M H Dickinson, C T Farley, R J Full, M A R Koehl, R Kram, and S Lehman. How animals move: an integrative view. *Science*, 288:100–106, 2000.

V Duerr and W Ebeling. The behavioural transition from straight to curve walking: kinetics of leg movement parameters and the initiation of turning. *J Exp Biol*, 208: 2237–2252, 2005. doi: 10.1242/jeb.01637.

N I Fisher. *Statistical Analysis of Circular Data*. Cambridge University Press, 1993. ISBN 0-521-35018-2.

G Floquet. Sur les équations différentielles linéaires à coefficients périodiques. *Annales Scientifiques de lÉcole Normale Supérieure, Sér*, 2:12, 1883.

R J Full and M S Tu. Mechanics of a rapid running insect - 2-legged, 4-legged and 6-legged locomotion. *J Exp Biol*, 156:215–231, MAR 1991. ISSN 0022-0949.

R J Full, R Blickhan, and L H Ting. Leg design in hexapedal runners. *J Exp Biol*, 158:369–390, 1991. ISSN 0022-0949.

R M Ghigliazza, R Altendorfer, P Holmes, and D E Koditschek. A simply stabilized running model. *SIAM Review*, 47(3):519–549, September 2005.

L Glass and A T Winfree. Discontinuities in phase-resetting experiments. *Am J Physiol Regul Integr Comp Physiol*, 246:R251–R258, 1984. PMID: 6696148.

M Golubitsky, I Stewart, P L Buono, and J J Collins. Symmetry in locomotor central pattern generators and animal gaits. *Nature*, 401(6754):693–695, 1999.

S Grillner. Neurobiological bases of rhythmic motor acts in vertebrates. *Science*, 228: 143–149, 1985.

J Guckenheimer. Isochrons and phaseless sets. *J Math Biol*, 1:259–273, 1975.

J Guckenheimer and P Holmes. *Nonlinear Oscillations, Dynamical Systems, and Bifurcations of Vector Fields*. Springer-Verlag, 1983.

E Hairer, S P Nørsett, and G Wanner. *Solving ordinary differential equations I: nonstiff problems*, volume 8 of *Springer Series in Computational Mathematics*. Springer-Verlag, Berlin, 2 edition, 1993. doi: 10.1007/978-3-540-78862-1.

H Haken, J A Kelso, and H Bunz. A theoretical model of phase transitions in human hand movements. *Biol Cybern*, 51(5):347–356, 1985.

P Holmes, R J Full, D E Koditschek, and J M Guckenheimer. The dynamics of legged locomotion: Models, analyses, and challenges. *SIAM Review*, 48(2):207–304, June 2006. ISSN 0036-1445. doi: 10.1137/S003614450445133.

B Howley and M R Cutkosky. Safe control of hopping in uneven terrain. *J Dyn Syst Meas Control, Trans ASME*, 131(1), JAN 2009. ISSN 0022-0434. doi: 10.1115/1.3023133.

A J Ijspeert. Central pattern generators for locomotion control in animals and robots: A review. *Neural Networks*, 21(4):642–653, MAY 2008. ISSN 0893-6080. doi: 10.1016/j.neunet.2008.03.014.

A J Ijspeert, A Crespi, D Ryczko, and J M Cabelguen. From swimming to walking with a salamander robot driven by a spinal cord model. *Science*, 315(5817):1416, 2007.

D L Jindrich and R J Full. Many-legged maneuverability: Dynamics of turning in hexapods. *J Exp Biol*, 202(12):1603–1623, 1999.

D L Jindrich and R J Full. Dynamic stabilization of rapid hexapedal locomotion. *J Exp Biol*, 205(18):2803–2823, Sep 2002. ISSN 0022-0949.

S Kim, J E Clark, and M R Cutkosky. isprawl: Design and tuning for high-speed autonomous open-loop running. *Int J Robotics Research*, 25(9):903–912, SEP 2006. ISSN 0278-3649. doi: 10.1177/0278364906069150.

H Kimura, Y Fukuoka, and A H Cohen. Adaptive dynamic walking of a quadruped robot on natural ground based on biological concepts. *Int J Rob Res*, 26(5):475–490, May 2007. ISSN 0278-3649. doi: 10.1177/0278364907078089.

D E Koditschek, R J Full, and M Buehler. Mechanical aspects of legged locomotion control. *Arthropod Struct Dev*, 33(3):251–272, 2004. doi: 10.1016/j.asd.2004.06.003.

H Komsuoglu. *Toward a Formal Framework for Open-Loop Stabilization of Rhythmic Tasks*. Ph.d., University of Michigan, Ann Arbor, October 2004.

R Kram, B Wong, and R J Full. Three-dimensional kinematics and limb kinetic energy of running cockroaches. *J Exp Biol*, 200(13):1919–1929, JUL 1997. ISSN 0022-0949.

T M Kubow and R J Full. The role of the mechanical system in control: a hypothesis of self-stabilization in hexapedal runners. *Philos Trans R Soc Lond , Ser B: Biol Sci*, 354(1385):849–861, MAY 29 1999. ISSN 0962-8436.

R P Kukillaya and P J Holmes. A hexapedal jointed-leg model for insect locomotion in the horizontal plane. *Biol Cybern*, 97(5-6):379–395, DEC 2007. ISSN 0340-1200. doi: 10.1007/s00422-007-0180-2.

M MacKay-Lyons. Central pattern generation of locomotion: A review of the evidence. *Physical Therapy*, 82(1):69–83, January 2002. ISSN 0031-9023. URL http://www.ptjournal.org/cgi/content/abstract/82/1/69.

J A Noah, L Quimby, S F Frazier, and S N Zill. Walking on a peg leg: extensor muscle activities and sensory feedback after distal leg denervation in cockroaches. *J Comp Physiol , A*, 190:217–231, 2004. ISSN 0340-7594. doi: 10.1007/s00359-003-0488-x.

K Pearson, O Ekeberg, and A Bueschges. Assessing sensory function in locomotor systems using neuro-mechanical simulations. *Trends Neurosci*, 29 (11):625 – 631, 2006. ISSN 0166-2236. doi: 10.1016/j.tins.2006.08.007. URL http://www.sciencedirect.com/science/article/B6T0V-4KV2R94-2/2/c4c9beac78cfbf6198fe128176a49b77.

S Revzen, J Bishop-Moser, A J Spence, and R J Full. Testing control models in rapid running insects using lateral ground translation (abstract only). *Integr Comp Biol*, 47(suppl 1):e1–152, 2007. doi: 10.1093/icb/icm104.

S Revzen, D E Koditschek, and R J Full. *Progress in Motor Control - A Multidisciplinary Perspective*, chapter Towards Testable Neuromechanical Control Architectures for Running, pages 25–56. Springer Science+Business Media, LLC - NY, 2008. doi: 10.1007/978-0-387-77064-2_3.

A L Ridgel and R E Ritzmann. Effects of neck and circumoesophageal connective lesions on posture and locomotion in the cockroach. *J Comp Physiol , A*, 191(6):559 – 573, June 2005.

A L Ridgel, S F Frazier, R A DiCaprio, and S N Zill. Encoding of forces by cockroach tibial campaniform sensilla: implications in dynamic control of posture and locomotion. *J Comp Physiol , A*, 186(4):359–374, Apr 2000. ISSN 0340-7594.

R E Ritzmann and A Bueschges. Adaptive motor behavior in insects. *Curr Opin Neurobiol*, 17(6):629–636, DEC 2007. ISSN 0959-4388. doi: 10.1016/j.conb.2008.01.001.

S Schaal. Dynamic movement primitives - a framework for motor control in humans and humanoid robotics. In H Kimura, K Tsuchiya, A Ishiguro, and H Witte, editors, *Adaptive Motion of Animals and Machines*, pages 261 – 280. Springer Tokyo, Tokyo, 2006.

M Schilling, H Cruse, and P Arena. Hexapod walking: an expansion to walknet dealing with leg amputations and force oscillations. *Biol Cybern*, 96(3):323–340, MAR 2007. ISSN 0340-1200. doi: 10.1007/s00422-006-0117-1.

J Schmitt and P Holmes. Mechanical models for insect locomotion: dynamics and stability in the horizontal plane - i. theory. *Biol Cybern*, 83(6):501–515, December 2000a.

J Schmitt and P Holmes. Mechanical models for insect locomotion: dynamics and stability in the horizontal plane - ii. application. *Biol Cybern*, 83(6):517–527, 2000b.

J Schmitt, M Garcia, R C Razo, P Holmes, and R J Full. Dynamics and stability of legged locomotion in the horizontal plane: a test case using insects. *Biol Cybern*, 86 (5):343–353, 2002.

J E Seipel, P J Holmes, and R J Full. Dynamics and stability of insect locomotion: a hexapedal model for horizontal plane motions. *Biol Cybern*, 91(2):76–90, AUG 2004. ISSN 0340-1200. doi: 10.1007/s00422-004-0498-y.

M J Spenko, G C Haynes, J A Saunders, M R Cutkosky, A A Rizzi, R J Full, and D E Koditschek. Biologically inspired climbing with a hexapedal robot. *J Field Robot*, 25(4-5):223–242, APR-MAY 2008. ISSN 1556-4959. doi: 10.1002/rob.20238.

S Sponberg and R J Full. Neuromechanical response of musculo-skeletal structures in cockroaches during rapid running on rough terrain. *J Exp Biol*, 211(3):433–446, FEB 1 2008. ISSN 0022-0949. doi: 10.1242/jeb.012385.

E Todorov and M I Jordan. Optimal feedback control as a theory of motor coordination. *Nat Neurosci*, 5(11):1226–1235, 2002. doi: 10.1038/nn963.

J T Watson and R E Ritzmann. Leg kinematics and muscle activity during treadmill running in the cockroach, blaberus discoidalis: I. slow running. *J Comp Physiol , A*, 182(1):11–22, JAN 1998a. ISSN 0340-7594. doi: 10.1007/s003590050153.

J T Watson and R E Ritzmann. Leg kinematics and muscle activity during treadmill running in the cockroach, blaberus discoidalis: Ii. fast running. *J Comp Physiol , A*, 182(1):23–33, JAN 1998b. ISSN 0340-7594. doi: 10.1007/s003590050154.

J T Watson, R E Ritzmann, and A J Pollack. Control of climbing behavior in the cockroach, blaberus discoidalis. ii. motor activities associated with joint movement. *J Comp Physiol , A*, 188(1):55–69, FEB 2002a. ISSN 0340-7594. doi: 10.1007/s00359-002-0278-x.

J T Watson, R E Ritzmann, S N Zill, and A J Pollack. Control of obstacle climbing in the cockroach, blaberus discoidalis. i. kinematics. *J Comp Physiol , A*, 188(1):39–53, FEB 2002b. ISSN 0340-7594. doi: 10.1007/s00359-002-0277-y.

J D Weingarten, R E Groff, and D E Koditschek. A framework for the coordination of legged robot gaits. In *Robotics, Automation and Mechatronics, 2004 IEEE Conference on*, volume 2, pages 679–686, 2004.

A T Winfree. *The Geometry of Biological Time*. Springer-Verlag, New York, 1980.

A A Yumaryanto, J An, and S Lee. Development of a biologically-inspired mesoscale robot. In Q Yang and G Webb, editors, *Pricai 2006: trends in artificial intelligence, proceedings*, volume 4099 of *Lecture notes in artificial intelligence*, pages 875–879. Springer-verlag, Berlin, 2006. ISBN 3-540-36667-9.

S N Zill, D T Moran, and F G Varela. The exoskeleton and insect proprioception .2. reflex effects of tibial campaniform sensilla in the american cockroach, periplaneta-americana. *J Exp Biol*, 94(Oct):43–55, 1981. ISSN 0022-0949.

S N Zill, J Schmitz, and A Bueschges. Load sensing and control of posture and locomotion. *Arthropod Struct Dev*, 33(3):273 – 286, 2004. ISSN 1467-8039. doi: 10.1016/j.asd.2004.05.005. Arthropod Locomotion Systems: from Biological Materials and Systems to Robotics.

Chapter 3

Lateral Perturbation

3.1 Summary

Animals running at intermediate speeds likely depend on both neural and mechanical feedback to maintain stability. When perturbed, changes in the kinematic phase and frequency of rhythmic appendage movements can provide evidence for neural feedback. To induce a perturbation, we ran cockroaches (*Blaberus discoidalis*) at their preferred speed onto a movable cart that was accelerated laterally with respect to the animals' motion. The specific impulse imposed on animals was $50 \pm 4\ cm/s$ (mean,SD), nearly twice the forward speed $25 \pm 6\ cm/s$ of the animals. Animals corrected for these perturbations by decreasing stride frequency, thereby demonstrating neural feedback to their central pattern generator. Trials fell into two classes in terms of response time, one class responding after a step (50 ms), whereas the other after nearly three steps 130 ms. The class of a trial could be predicted based on the pose of the body at onset of perturbation. Trials where the animals had front and hind feet in stance on the side from which the animals were pulled away by the impulse were in a more stable pose and fell in the class that showed the delay in frequency change. Trials where the animals had only a middle foot in stance on the side from which the animals were pulled were in a less stable pose and changed frequency more rapidly. These results are consistent with previous research on fast running showing that the recovery begins with rapid mechanical feedback promoting self-stabilization. Here, at intermediate speeds, we found that mechanical stabilization is followed by neural feedback modulation of a central pattern generator at delays comparable to the duration of a step. We hypothesize that the increased delay in trials where the animals were more stably positioned is due to recovery being initiated by event based feedback with a threshold. We suggest these hypotheses have ties to perceptual choice processes and the recently developed theory of self-triggered control.

3.2 Introduction

Using the rhythmic motion of diverse body structures and appendages, animals adopt a wide variety of locomotion behaviours to move through every variety of natural environment. As they move, animals must respond to unexpected perturbations such as changes in terrain, injury to limbs, and the behaviour of predators, prey and conspecifics. We propose that within the kinematic responses to these perturbations reside patterns revealing the interplay between the neural and mechanical systems producing stabilization. To test hypotheses regarding the interplay of neural feedback and mechanical self-stabilization that govern the recovery from perturbation in cou-

pled neuromechanical systems, we must find experimental means to distinguish neural from mechanical feedback. Using the instantaneous phase and frequency of rhythmic limb movements, Revzen et al. (2008) offer a general framework for identifying which candidate feedback pathways within neuromechanical control architectures play the dominant role in coordinating neuro-mechanical oscillations (see fig. 3.1).

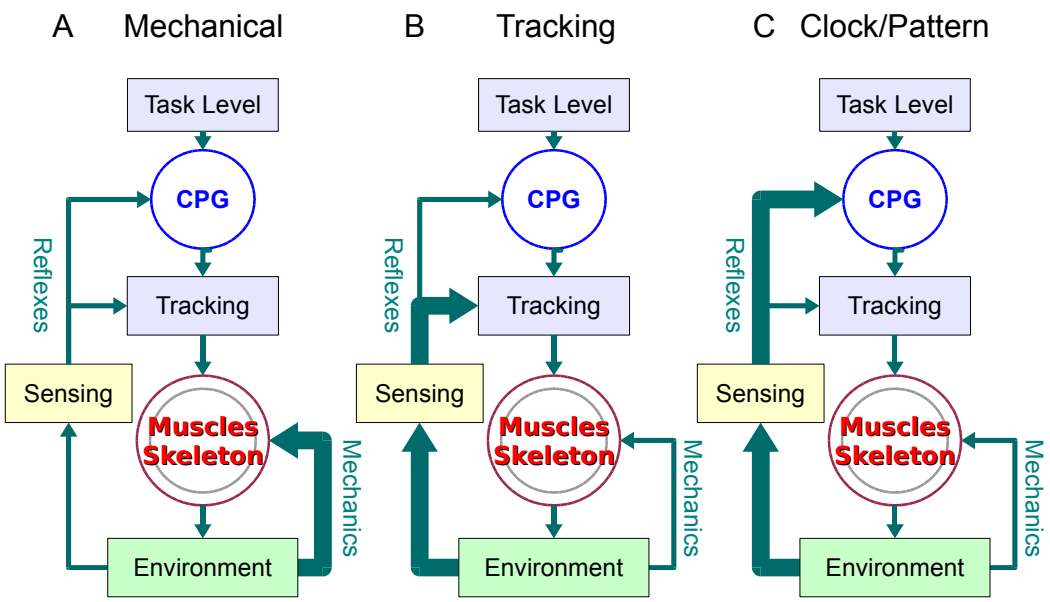

Figure 3.1: The "Task Level" control block represented descending neural signals and physiological state. We assumed its outputs to held constant throughout a behaviour. A Central Pattern Generator ("CPG"; blue circle) contained the self-exciting neural circuitry that generated the rhythmic pattern for the behaviour. All reflex based neural modulation of the CPG signal lay in the "Tracking" blocks. Tracking contained no persistent state and was not self-exciting. The "Muscles and Skeleton" (nested circles) contained the mechanical state of the body, which is subject to manipulation by forces from the environment. The body interacted mechanically with the "Environment" block and also modified the representation of the environment returned by "Sensing" block. Information flow is indicated by arrows. We considered three forms of feedback (thick arrows): **A** mechanical feedback, wherein muscle activation remains unchanged and recovery from perturbation is mediated by properties of the mechanical interaction with the environment; **B** tracking feedback, wherein recovery is the result of reflexes bringing the motions of the body into line with the reference motions indicated by the pattern produced from the CPG; **C** clock or pattern feedback, wherein feedback changes the pattern of activation produced by the CPG.

Using the simplest neuromechanical control architectures possible, at least three types of feedback pathways contribute to stabilization. fig. 3.1-**A** corresponds to a

hypothesis based primarily on mechanical stabilization, fig. 3.1-**B** on time-invariant (classical) reflex feedback and fig. 3.1-**C** on feedback modulation of the entire gait pattern. The overall framework of neuromechanical control in which we ground these hypotheses assumes that motions are driven by endogenously produced rhythmic pattern oscillations emitted from a central pattern generator (Delcomyn, 1980; Grillner, 1985; MacKay-Lyons, 2002). The CPG is coupled to an oscillating mechanical system composed of appendages, skeletons and the muscles that connect them. In turn, this mechanical system is coupled to the environment.

At the most rapid speeds, mechanical systems dominate control because they provide an immediate response to perturbations (fig. 3.1-**A**), while neural feedback may be limited by bandwidth and computation ability. When a mechanical system is tuned to its environment, mechanical feedback can be remarkably effective. Kubow and Full (1999) showed that when biologically realistic ground reaction forces are simulated, a hexapedal morphology could mechanically self-stabilize. This discovery was corroborated by finding that running cockroaches begin to recover from a lateral impulse within 14 milliseconds – a response time that challenges the fastest of reflexes (Jindrich and Full, 2002), and would barely provide sufficient time for neural feedback from their tibial campaniform sensilla (Ridgel et al., 2001). When running on rough terrain, muscle action potentials of a set of putative control muscles show no differences with running on flat ground (Sponberg and Full, 2008). Neither circumoesophageal lesion (disconnecting the brain from the thoracic nerve cord) nor distal leg denervation prevent rapid running in cockroaches (Ridgel and Ritzmann, 2005; Noah et al., 2004), demonstrating that large portions of the nervous system are not necessary for effective running. Spiders and cockroaches show no change in the limb kinematics when running rapidly over a mesh that removes ninety percent of the ground contact area (Spagna et al., 2007). Instead of relying on precise stepping informed by neural feedback, these arthropods use mechanical feedback distributed along their legs and enhanced by the passive mechanics of leg hairs.

There is a sound theoretical basis supporting mechanical self-stabilization in running. Mathematical analysis of models of running show self stabilization in both the Spring Loaded Inverted Pendulum (SLIP) model (Altendorfer et al., 2004; Ghigliazza et al., 2005; Seyfarth et al., 2003) that governs sagittal plane running dynamics and the Lateral Leg Spring (LLS) model (Schmitt and Holmes, 2000a,b) that describes horizontal running in sprawl postured animals. The simple LLS model of the cockroach and more morphologically grounded models exhibit robust stability to lateral impulse perturbations, despite using little or no sensory feedback (Schmitt et al., 2002; Schmitt and Holmes, 2003, 2001; Kukillaya et al., 2009; Proctor and Holmes, 2008). Taken together, the combination of theoretical plausibility and empirical evidence provides a

strong case for self stabilization in high speed running.

At slower speeds and for more precise movements, neural feedback from sensors dominates fig. 3.1-**B**. The important role of neural reflexes in locomotion is particularly well defined in insects. For the slow, quasi-static locomotion of stick insects, an artificial neural net model termed WalkNet provides an effective representation of control (Cruse et al., 1998, 2007; Schilling et al., 2007). The model is largely kinematic in nature because inertia and momentum play no role in slow walking. Even during slow running, sensors associated with neural reflexes respond to environmental perturbations by feeding back on the patterns emitted by a CPG (Ijspeert, 2008; Ritzmann and Bueschges, 2007) fig. 3.1-**B** symbolized by the "Tracking" block). A large body of research has shown that the neural reflexes controlling locomotion are far richer in behavior than our typical view of a stereotyped, negative feedback loop. For example, load compensating reactions in land mammals and arthropods depend on the type of sensor (sensing self versus environment), the preparation studied (intact versus isolated), the task (immobile, walking versus running), the intensity of muscle contraction, the phase in the gait (swing versus stance) and the relative importance of passive versus reflexive stiffness (Duysens et al., 2000; Zehr and Stein, 1999). Reflexes in mammal that provide negative force feedback under most circumstances, provide positive feedback during locomotion resulting in a greater and greater force production during stance (Prochazka et al., 1997b,a; Pearson and Collins, 1993).

Here, we place locomotor neural reflexes into two broad categories – one that affects the output of the CPG (Tracking; fig. 3.1-**B**) and the other that alters the rhythm of the CPG itself (fig. 3.1-**C**). One may envision tracking feedback to be a means of matching a limb's motion to a reference motion generated by the CPG and can be characterized as following an equilibrium point trajectory (Jaric and Latash, 2000). Mathematically, tracking is time-invariant, stateless and functions by comparing the actual state of the body and the reference provided by the CPG to generate force activation in muscles. Tracking contains no persistent state and is not self-exciting. Feedback via such tracking reflexes does not modulate the actual rhythm emitted by the CPG. In a second category, we define neural feedback that does alter the rhythm from the CPG (fig. 3.1-**C**). Neural feedback in this category could result in change in the frequency sent by the CPG.

3.2.1 Kinematic Phase exposes feedback to the CPG

In Revzen et al. (2008) we proposed methods for identifying the interplay of neural and mechanical feedback by probing rhythmic behaviours through computing phase estimates derived from kinematic observations – a *kinematic phase*. Examination of

kinematic phase can illuminate the coupling between the mechanical oscillator – the body, muscle and skeleton – and the neural oscillator (CPG) that drives it (fig. 3.1). When an animal is engaged in a periodic behaviour all the subsystems involved in producing that behaviour and all observable quantities describing those subsystems will oscillate periodically. The implication for experimental biomechanics is that the kinematics of the body and its subsystems must reflect the underlying periodic dynamics.

The advantage of the kinematic phase methods lies in that for animal locomotion with a stable oscillator template, phase provides a quantitative and predictive model of movement. When given the readily measured kinematic state of the animal in as little as two consecutive frames of video, one can compute the phase and frequency, extrapolate the linear relationship of phase to time, and predict the kinematic states at all future times. In practice, because animals are continuously perturbed from the idealized dynamics of the template, the accuracy of prediction diminishes over time and requires frequency estimates over more than just a pair of frames. Nevertheless, the ability to take a dataset only fraction of a step long and project anticipated kinematics several strides into the future provides a powerful means for testing perturbation recovery.

For constant frequency locomotion such as running, the animal's motions will over time settle to a constant phase relative to the timing of the signal emitted by the CPG. This phenomenon is known as *phase locking* or *entrainment*. We may thus assume that the pre-perturbation animal is an entrained neural-and-mechanical oscillator. Relative to time, the kinematic phase of such an animal would follow a linear model with running frequency being the slope of a phase versus time plot. Due to phase locking, the kinematic phase is at a constant phase offset relative to the phase of the CPG.

When the animal is perturbed, some transient response appears and decays, and the animal resumes running at a constant, but possibly different, frequency. We propose to detect changes in phase by fitting a linear regression model to pre-perturbation phase data and extrapolating an expected phase past the perturbation and into the recovery phase. Subtracting that estimate from the post-perturbation kinematic phase, we will provide a *residual phase* expressing in succinct form any changes in the animal's rhythm and timing of movement.

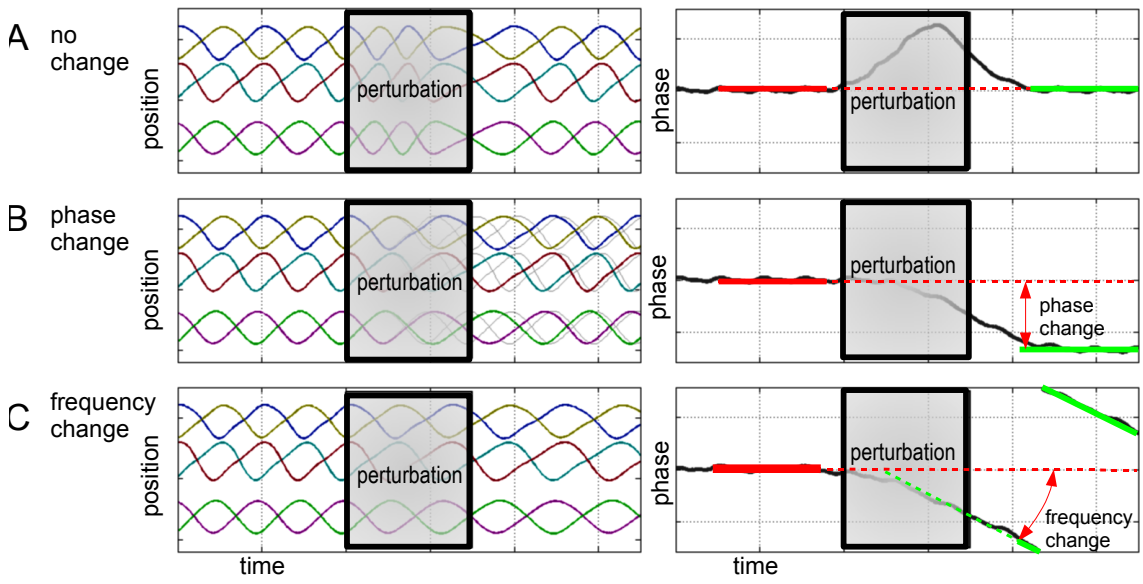

Figure 3.2: On the left we plot (simulated) fore-aft leg positions over time, next to the corresponding residual phase plot on the right. In **A** we show an animal that slowed down during perturbation, but fully recovered to motions matching the motions extrapolated from pre-perturbation motion (fitting region for regression model solid red; extrapolated model dashed red line; post perturbation regression solid green); this can be interpreted as the perturbation having broken the entrainment of body to neural CPG, and that entrainment re-establishing itself post-perturbation. It is compatible with both fig. 3.1-**A** and fig. 3.1-**B** feedback alternatives. In **B** we show an animal that recovers the same frequency at a phase offset; this can be interpreted as the re-entrainment locking on to a different stable relationship between the neural and mechanical oscillations, and is similarly compatible with fig. 3.1-**A** and fig. 3.1-**B**. In **C** we show an animal whose frequency changes, as expressed by the non-zero slope of the residual phase trend-line; such a change requires the CPG to change frequency, and is therefore only compatible with the fig. 3.1-**C** feedback to the CPG.

fig. 3.2 shows possible outcomes of a perturbation experiment applied to hexapedal running expressed as simulated kinematic data (left) and residual phase (right). The position data represent the fore-aft leg motions relative to the body as a function of time. We show the linear model extrapolations for position and residual phase

after perturbation (fig. 3.2 gray lines). Differences in the slope of the linear models express changes in running frequency, and can only persist if the neural signal driving the muscles changes frequency as well. Thus, if we see no residual phase change after a perturbation (fig. 3.2-**A**), we hypothesize that the most parsimonious neural control architecture characterizing the response is one that involves mechanical feedback (fig. 3.1-**A**). If the perturbation causes a change in the CPG frequency, as seen in fig. 3.2-**C**, we reject the possibility of mechanical feedback fig. 3.1-**A** and tracking neural feedback fig. 3.1-**B** pathways in favour of the control architecture sending neural feedback to the CPG fig. 3.1-**C**.

The best candidates to test neurmechanical control hypotheses using kinemaitc phase are animals whose anchored morphology expresses the rhythmic motions of the simple architecture or template with many easy to measure appendages. These animals would expose a great deal of phase information through their kinematics, making kinematic phase a reliable estimate of their overall phase. Here, we test these hypotheses using a hexapedal runner, the cockroach, *Blaberus discoidalis*, not only because of the phase data offered by six oscillating legs, but because few species have as extensive a biomechanical (Kram et al., 1997; Full et al., 1991; Full and Tu, 1990; Ting et al., 1994; Jindrich and Full, 1999; Ahn and Full, 2002; Ahn et al., 2006) and neurophysiological (Watson and Ritzmann, 1998a,b; Watson et al., 2002a,b; Zill et al., 1981, 2004, 2009) characterization.

In the present study, we used kinematic phase to investigate the time-course of cockroach recovery from a lateral impulse perturbation when the animal was running at intermediate speeds where the likelihood of viewing the interplay between neural and mechanical feedback was the greatest. By comparing instantaneous residual phase before and after the perturbation (fig. 3.2), we could begin to characterize when mechanical feedback was sufficient, neural feedback used or a sensory signal sent to modulate the CPG (fig. 3.1). Because we measured leg kinematics, we could explore the relationship of an animal's posture and its mechanical response to its control strategy.

3.3 Materials and Methods

We ran cockroaches onto a perturbation device consisting of a rail-mounted cart that was accelerated horizontally by a manually keyed mechanism. In the reference frame of the cart, the cockroach centre-of-mass received a large lateral impulse perpendicular to its heading. We recorded the trials using an overhead high-speed video camera and digitized the motions of the cockroach feet (tarsi). By applying methods developed in Revzen et al. (2008) and used in chapter 2, we used the tarsal trajectories in the

body frame of reference to estimate the kinematic phase of the animals, then fitted a constant frequency model to the pre-perturbation phase data using linear regression. We used these the residual phases derived from these regression models to test our neuromechanical hypotheses.

3.3.1 Experimental setup

Animals

We obtained the 15 *Blaberus discoidalis* cockroaches used in this study from a commercial supplier (Carolina Biological Supply Co.,Gladstone, OR, USA) and kept them in large, open containers in a room with elevated moisture and temperature. They had access to dried dog food, fruit, vegetables, and water. We conducted trials at an ambient temperature of $27 \pm 2°C$ (mean,SD). Before each trial, we examined the cockroach for damage to its tarsi and carapace. Each animal was used in multiple trials. While downloading the videos between one trial and the next (typically 2 minutes in duration), we allowed the animals to rest by covering them with a dark cup.

Moving cart as a perturbation device

We induced lateral perturbations by having the animals run onto a cart that we then accelerated at right angles to the direction of motion using a pre-loaded elastic pulley held fast by a magnetic lock (fig. 3.3). When released, the cart translated with acceleration of up to 1.5 ± 0.2 g over a duration of 100 ms and continued with a constant velocity until it hit breaking pads at the end of its track. The acceleration generated a specific impulse of 50 ± 4 cm/s in the lateral direction. Cart travel distance was nearly 1 m – sufficiently long so that no trial included the final breaking deceleration.

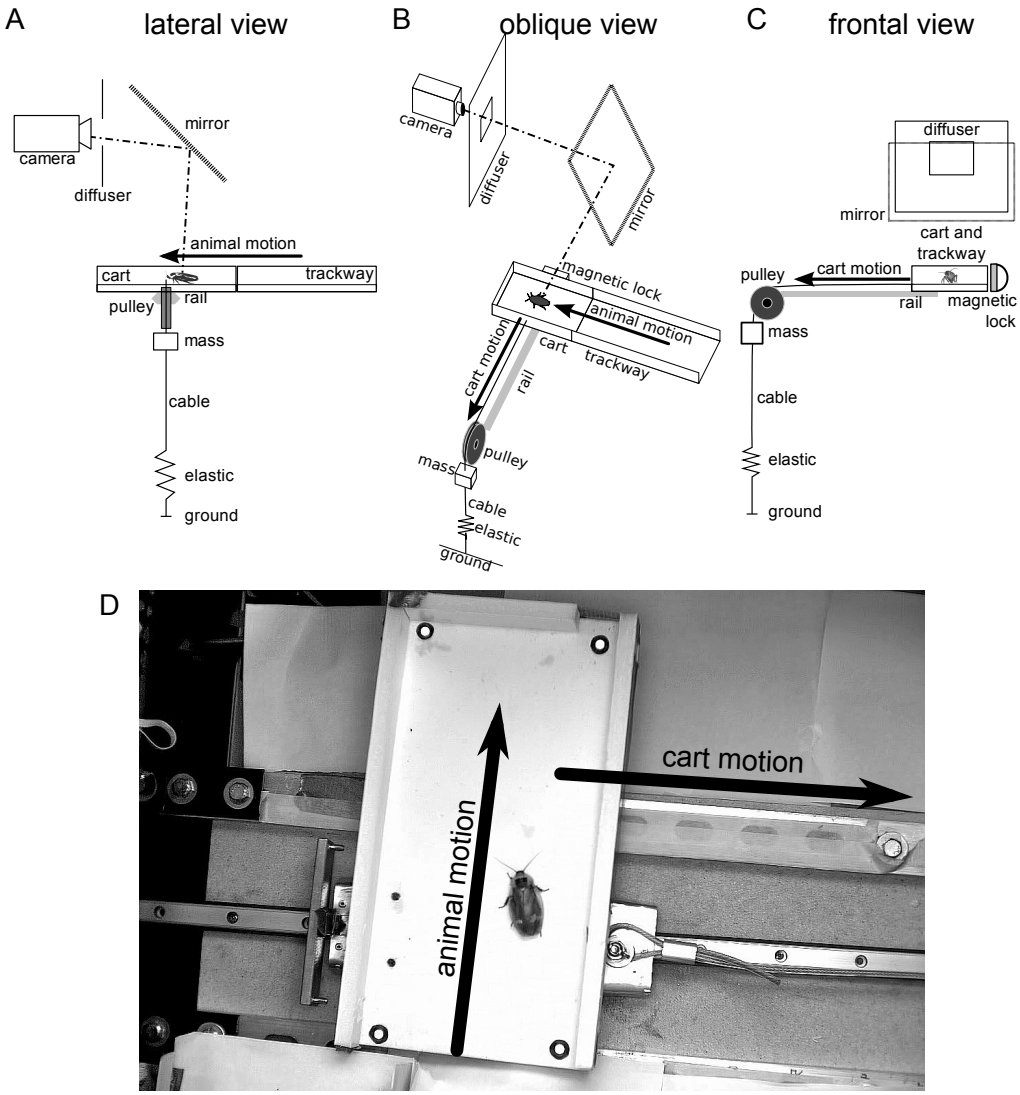

Figure 3.3: Schematic of moving cart apparatus

Description of fig. 3.3

Schematic of moving cart apparatus from lateral **A**, oblique **B** and frontal **C** viewing directions (not drawn to scale). We placed the cart as the final section of a trackway (white rectangles). It ran on a rail orthogonal to the trackway direction (light gray strip). On one side, we held the cart fast with a magnetic lock (shown in **B**,**C** next to cart). On the other side of the cart, we tied it to a steel cable (black line running from cart to ground) that we ran through a pulley (dark gray oval in **B**,**C**, rectangle in **A**) and pulled taught using an adjustable elastic (collection of rubber bands, indicated schematically by zigzag on cable) and a mass (white box on cable below pulley). When the operator released the magnetic lock, the elastic accelerated the cart until it fully contracted to rest length. The cart continued to move at uniform speed, as we chose the mass to compensate for friction between rail and cart. The direction of motion of the animals was along the trackway (thick arrow labelled "animal motion" in **A**, **B**) and orthogonal to cart motion (thick arrow labelled "cart motion" in **B**, **C**).

We filmed the motion with a high-speed video camera (camera seen in **A**,**B**; viewing animal along dot-dashed lines) that we mounted at a fixed position looking down on the trackway through a mirror (rectangle with thick dashed lines). We illuminated the trackway by bouncing a spotlight off a diffuser plate surrounding the camera lens (thin-lined rectangle with rectangular hole shown in all views), so that scene was illuminated from direction of camera, preventing shadows from appearing under the animal. **D** Photograph of an animal running on the moving cart. The cart had high contrast markers near the corners on its surface. We constructed the cart from foam-core plates attached on top of a metal plate. The vertical metal plate on the left of the cart locked on to the magnetic lock, whereas the cart itself ran on a rail (metal strip running across the photograph and under the animal with dark top and bottom edges). A steel cable pulled the cart, providing the lateral accelerations. In the position shown, the cart has nearly moved an entire trackway-width to the right from its starting position. The edge of the trackway is visible at the bottom left of the image.

We marked the top of the cart with high-contrast circular markers (see fig. 3.3-**D**; circles of black paper with retro-reflective stickers in their centres) at known locations bracketing the area occupied by the running animals, and level with the surface on which they ran. We used these markers for tracking the cart, computing its acceleration using a Kalman smoother with a constant acceleration model (also known as a Rauch-Tung-Striebel smoother; Kalman (1960); Rauch et al. (1965)). We also used the markers to compute a projective transformation which corrected for the changes in animal image due to changes in viewing angle and distance as the cart moves, giving what was effectively the view from a camera translating in parallel with the cart.

3.3.2 Protocol

We prodded the animals to run along the trackway shown in fig. 3.3 and onto the cart. Careful adjustment insured that the gap between the top of the cart and the trackway was only a few millimeters wide. We spanned this gap with a paper flap that was pushed aside when the cart moved, so the animals experienced neither any noticeable step nor break in the ground. We examined the animals' running for speed changes when crossing the trackway-cart gap, but found none.

The operator released the cart by breaking the circuit powering the magnetic lock holding it in place as soon as the animal was perceived to be on the cart. Taking into account human reaction times, animals were at least a body length from the cart edge by the time the cart started moving laterally.

We ended trials when the cockroach touched any wall of the cart, or the cart moved out of view. We rejected trials if the cockroach did not adopt a tripod gait for at least three strides prior to perturbation and three strides post perturbation, or if the cockroach contacted the side walls with antennae or feet at any point within these requisite six strides. If the platform acceleration showed signs of vibration or non-zero post perturbation acceleration, we discarded the trial. We defined non-zero acceleration post perturbation as being outside $\pm 0.3\ g$ 200 ms after onset of cart motion. We defined vibration to be a secondary acceleration peak greater than 33% of the primary peak.

3.3.3 Processing video data into residual phases

After we tracked the cart markers in each video frame, we projectively transformed the frames to a standard reference position, thereby cancelling any warping and size changes due to changes in viewing angle. We then analyzed the corrected videos using a custom built MatLab video processing tool described more fully in section 2 and briefly described below.

First, we auto-tracked the bodies of the animals by finding the axis of symmetry of their body silhouettes, thereby obtaining their position and orientation over time. We rotated the translated images to a registered position and orientation. We tracked the positions of the animals' tarsal claws (tips of the feet) on the registered videos using an additional custom tool (written in **MatLab 6.5**, The MathWorks, Inc., Natick, MA, USA).

We converted these 12 dimensional positions (two dimensions of six feet) into 24 dimensional positions and velocities using a Kalman smoother (Kalman, 1960; Rauch et al., 1965). We rescaled the unit of time measurement so that the variance of position values (taken for all coordinates together) equalled the variance of velocity

values. We subjected this rescaled collection of 24 dimensional vectors to principal components analysis to obtain the first two principal components. We used the angle of the projection of the 24D state on these first two principal components as an estimate of phase, with zero phase taken to be the surface where the mean fore-aft positions of the left and right tripods are equal ("midstance") and the right tripod is moving forward. This method produced phase estimates of slightly better quality in terms of fitting residuals than the Hilbert transform based method used in section 2.

We marked the start and end of the perturbation manually by clicking on graphs of the acceleration. We used a window starting 250 ms and ending 100 ms prior to start of perturbation to regress a trend-line for kinematic phase. This operation corresponds to fitting a constant frequency model to the animal based on a window of close to three strides. We used the residual phase given by subtracting this model from the kinematic phase test our neuromechanical control hypotheses. If the residual phase was a horizontal line (slope of zero) with an intercept of zero (fig. 3.2-**A**), it represented animals that continued running at the same frequency and phase as they did prior to perturbation. A horizontal line with non-zero intercept (fig. 3.2-**B**) implied a phase change, and any non-zero slope (fig. 3.2-**C**) represented a frequency change.

3.3.4 Classifying phase histories

Residual phases responses to lateral perturbation fell into two classes. Animals perturbed in one half-cycle of the stride responded differently from animals perturbed in the other half-cycle. From a physical standpoint, this is reasonable, because the same lateral force applied to an animal with two legs of a tripod down on one side may not necessarily respond in the same manner as an animal with one middle leg down.

A statistical test for significance of outcomes classes

We constructed a statistical test for dependence of outcome on a predictor phase ϕ_0 taken before onset of perturbation. The prediction classified trials into one of two classes based on $\text{sign}(\sin(\phi_0 - \Phi))$ for some Φ, thereby partitioning the circle of possible phase values into halves with the transition between classes occurring at phases Φ and $\Phi + \pi$.

We assessed the quality of a classification of trials into $\mathsf{C_0}$ and $\mathsf{C_1}$ using the average *relative margin* clustering quality measure (Ackerman, 2007). The relative margin associated with a given data point (time series in our case) is its distance to the nearest cluster centroid divided by its distance to the second nearest cluster centroid. The best classification has relative margin zero: each data point is exactly at the cluster centroid.

The worst classification has relative margin one: each data point is no nearer to its nearest cluster centroid than it is to the second nearest. To compute a relative margin, we needed to choose a means for measuring distance between phases, and by extension, phase time series. We took the distance of two phases ϕ and θ to be $1 - cos(\phi - \theta)$, and the distance of two time series of phase to be the total distance between the corresponding phases (also known as the L1 norm). We computed centroids of the C_0 and C_1 classes by point-wise circular averaging of the residual phase time series (Fisher, 1993).

Our algorithm selected the Φ producing the best classification with respect to our chosen quality measure. We wished to test this classification for statistical significance. We formulated such a test by comparing the classification quality measure of the real data with the classification quality measure of surrogate (randomized) data[1] for which the relationship between the predictor (phase at perturbation) and the outcome (residual phase time series) destroyed by adding uniformly distributed random phase offsets. We calculated the fraction of surrogate datasets that produced a classification of comparable quality to that of the animal data; this fraction is the probability of a false positive under the null hypothesis of no predictive ability. The approach is also known as using "percentile confidence intervals generated from a bootstrap" (Politis, 1998b,a).

We examined the distribution of relative margins obtainable by choosing Φ where this selection was applied to ensembles of trials generated from the following processes:

H_1 **animal data** : N^2 times Bootstrap samples of the actual experimental trials.

$\mathsf{H}_{0(a)}$ **simple surrogates** : N^2 times, generate bootstrap samples that also add a (uniformly distributed) random offset to the phases in each trial. This randomizes ϕ_0 in each sample, while maintaining all internal correlations within each trial.

$\mathsf{H}_{0(b)}$ **bootstrapped surrogates** : N times, randomize trials as per $\mathsf{H}_{0(a)}$, but instead of using each collection of trials once, compute best relative margins for N bootstraps of the surrogate data.

Whenever the best relative margin results generated by the H_1 process fall well outside the distributions generated in the two H_0 processes, we concluded that the relationship of the predictor phases ϕ_0 of the trials to our selected Φ did find a statistically significant partition into classes C_0 and C_1.

[1] In formal terms, we used a bootstrap computation to establish the probability distribution of our quality measure under the null hypothesis of uniformly random relationship between perturbation phase and residual outcome.

3.3.5 Controlling for individual variation in the predictor phases

One potential cause for the appearance of classes in the residual phase time-series could be individual variation in predictor phases. We tested the hypothesis that the classes $\mathsf{C_0}$ and $\mathsf{C_1}$ were an outcome of inter-individual variation: having some individuals biased toward being in $\mathsf{C_0}$ and other individuals biased toward being in $\mathsf{C_1}$.

If an individual falls preferentially in any one class, this implies that the ϕ_0 values for this individual's trials are biased toward appearing in this class. We developed a test for comparing the hypotheses: $\mathrm{H}_{0(\phi)}$ - the ϕ_0 angles of individual animals are drawn from uniform distributions; $\mathrm{H}_{1(\phi)}$ - each animal has a (possibly different) preferred phase angle θ such that ϕ_0 values for trials of this animal are more likely close to θ than far from θ.

For each collection of phase angles from an animal we used the $\bar{\mathrm{C}}$ statistic – the mean of the cosine of differences of angles, taken for some random pairing of those angle. This statistic is invariant to the unknown value of preferred phase angle θ[2], and will always take on a larger expected value when animals have a preferred class ($\mathrm{H}_{1(\phi)}$) than when their classes are uniformly random ($\mathrm{H}_{0(\phi)}$).

For each number of trials n that an individual provided, we computed the distribution $\bar{\mathrm{C}}[n]$ of $\bar{\mathrm{C}}$ for n trials under $\mathrm{H}_{0(\mathsf{phi})}$. If an animal truly had uniformly distributed ϕ_0 values over n trials (follows $\mathrm{H}_{0(\mathsf{phi})}$), the inverse cumulative distribution function of $\bar{\mathrm{C}}[n]$ applied to the $\bar{\mathrm{C}}$ of this individual's trials would have given a uniformly distributed variable in the range 0 to 1. We used the Kolmogorov-Smirnov statistic comparing the transformed values to a uniform distribution as our test for $\mathrm{H}_{1(\phi)}$.

3.4 Results

We used a total of 15 animals and collected 47 trials. The animals ran at $25 \pm 6\ cm/s$ (mean,SD) at a frequency of $11.1 \pm 0.2\ Hz$. This implies that the lateral perturbations of $50 \pm 4\ cm/s$ were typically of a magnitude double that of the forward velocity.

3.4.1 Residual phase change reflects frequency change

Starting with onset of perturbation (time = 0), animals showed no noticeable responses in kinematic phase for 50 ms – the duration of an entire step. After that time, frequency decreased (see fig. 3.4-**A** mean). Forward velocity remained unchanged for

[2]If we assume for $\mathrm{H}_{0(\mathsf{c})}$ that the distributions for different animals differ only in theta, $\bar{\mathrm{C}}$ is a "pivotal statistic".

50 ms, then slightly increased for a step and then decreased for a step, settling to a new, lower value (fig. 3.4-**C**). The linear decrease in residual phase reflected a decrease in the frequency of the animal's leg movements ($P < 0.05$).

3.4.2 Two classes of residual phase outcomes

The residual phases differed at 80 ms after onset of perturbation (see fig. 3.4-**A**). The across-trial inter-quartile ranges of residual phases increased more than 5-fold when compared with pre-perturbation spread. This increased variability was not due to random outcomes. We found that the population of trials can be partitioned into two classes based on the animals' phase at onset of perturbation ϕ_0. We computed ϕ_0 as the (circular) average of the phases in a 54 ms (step long) window centred on the onset time of perturbation. We chose our reference phase of 0 so that the trials with $0 < \phi_0 < \pi$ form class $\mathsf{C_0}$, and the trials with $-\pi < \phi_0 < 0$ form class $\mathsf{C_1}$ (red and blue colours in fig. 3.4). $\mathsf{C_0}$ represented a stance of what we designated as a *left tripod* (left front, right middle, left hind), whereas class $\mathsf{C_1}$ represented a stance of a *right tripod* (right front, left middle, right hind),

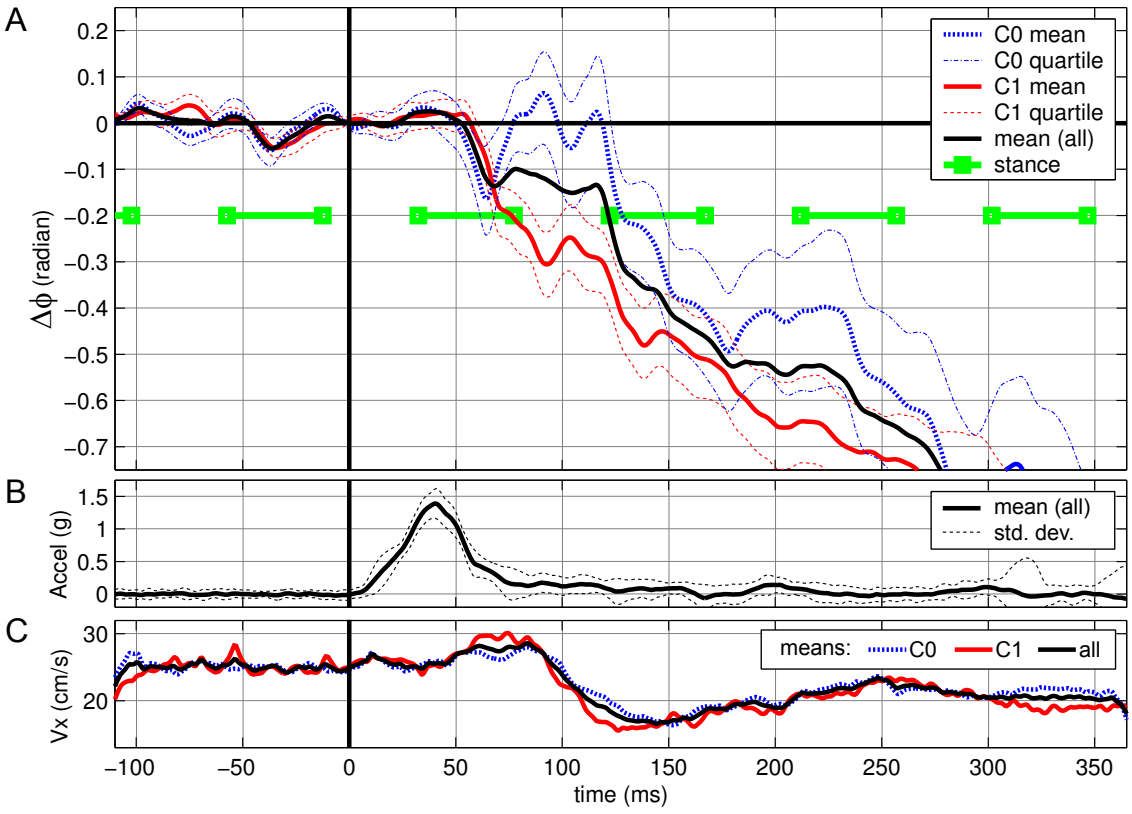

Figure 3.4: Response of residual phase and forward velocity to a lateral perturbation

Description of fig. 3.4

Response of residual phase and forward velocity to a lateral perturbation.

We plotted (**A**) residual phases obtained by subtracting from the phase estimate a linear regression model fitted to the phase at times $-250\ ms$ to $-100\ ms$. Time 0 (thick vertical line) indicates onset of perturbation, as can be seen from the cart acceleration plot (**B**, thick line is mean; thin dashed lines one standard deviation above and below). We found that trials fall into two classes of residual phase outcome: C_0 (**A**, thick densely dashed blue line showing mean; dot-dashed thin blue line showing quartiles) and C_1 (**A**, thick red line show showing mean; dashed thin line showing quartiles) that fall on either side of the population mean (**A**, thick black line).

Trials were classified into C_0 or C_1 based on their mean absolute phase in the window $|t| < 27\ ms$ (window was one step long). We indicated pose schematically using horizontal bars (**A**, green) that demarcate stance of left tripod (left front, right middle, left hind) in the class C_0 and stance of right tripod in the class C_1. We plotted the mean velocity along the trackway axis for classes C_0 (**C**, thick densely dashed blue line), C_1 (**C**, thick red line) and all trials (**C** thick black line). The standard deviation of velocity was $\pm 6\ cm/s$, therefore these velocity means were not significantly different.

We tested the statistical significance of the classification based on phi_0 values by examining the distribution of the mean, relative margin clustering quality measure it induced. We compared this quality to quality distributions generated by randomized (surrogate) null models. We estimated the quality distributions by executing 2500 bootstrap replications each of surrogate and unmodified data. The distributions of the results are in fig. 3.5. The P-values we found were 8×10^{-3} for bootstrapped surrogates $H_{0(b)}$ and 6×10^{-3} for simple surrogates $H_{0(a)}$, clearly rejecting both null hypotheses. These results show that the separation computed for our dataset was typical of the bootstraps of the data (i.e. it is a robust outcome), and highly atypical ($p < 0.01$) of both $H_{0(a)}$ and $H_{0(b)}$ null hypotheses.

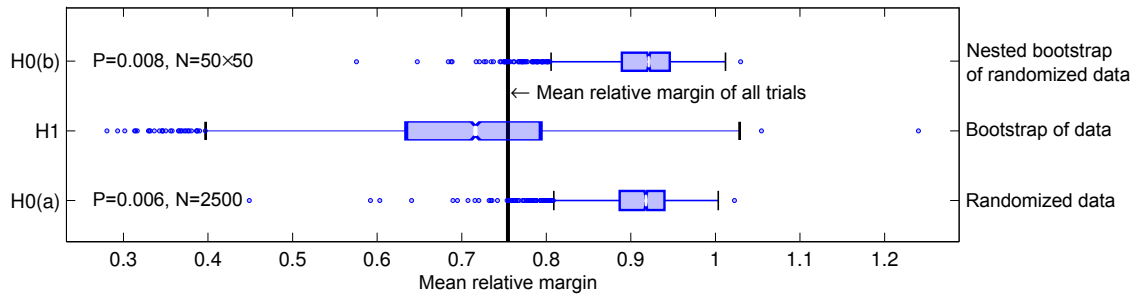

Figure 3.5: Bootstrap results testing for significance of outcome classification. Each of the three Tukey box-plots showed a distribution containing 2500 bootstrap replicates. The H1 plot represents a distribution created by simple bootstrapping – trials re-sampled with replacement. $H_{0(a)}$ is similar, except the we added a (i.i.d uniform) random phase offset to each trial in each replication creating surrogate data. $H_{0(b)}$ consisted of 50 bootstraps, each of which we randomized in phase similarly to $H_{0(a)}$ and then bootstrapped to create 50 samples from each randomization instead of just one as in $H_{0(a)}$. Each Tukey box-plot shows a box for the inter-quartile range, with a narrow neck indicating the 95 percent confidence interval of the median. Wicks go out to the first data point outside the 10-th and 90-th percentiles, with points outside that range marked as dots. In our P-value estimates, we used the mean relative margin of the entire dataset (thick black line; p-values shown in left edge of plot). The results showed that classes C_0 and C_1 were a statistically significant feature of the data.

Individual variation

The classes C_0 and C_1 were divided with 26 trials in C_0 and to 21 trials in C_1, giving a $\chi^2 = 0.53$ with $P = 0.47$. The trials thus fall into classes with probabilities indistinguishable from random.

By using our transformation of the $\bar{\mathrm{C}}$ statistic, we tested the 11 $\bar{\mathrm{C}}$ values obtained from animals with more than one trial against the uniform distribution. The Kolmogorov-Smirnov statistic obtained has a P-value of 0.56. It is thus reasonable to conclude that animals did not express any individual preferences for ϕ_0 values.

We conclude that our classification was not an artifact of individual variation in animal responses, or in other words that no individual experienced the perturbation in any class more often than expected at random.

3.4.3 Class dependent delay in frequency change

Class $\mathsf{C_0}$, the left tripod, did not change phase until 130 ms post onset – nearly three steps worth of delay, while class $\mathsf{C_1}$ responded within slightly more than a step, and incurred a phase lag of 0.25 $radian$ relative to $\mathsf{C_0}$. The residual phases of both classes gradually converged to similar slopes, and thus exhibited similar changes with respect to the initial frequency. On average, the new frequency was lower than the original frequency by 0.4 Hz. The phase separation between the classes remained unchanged 5 steps after onset of perturbation.

We conclude that kinematic evidence for neural feedback appeared in the recovery of cockroaches from lateral perturbation. Kinematic changes appeared at a delay, and the delay was a function of the animal's pose (i.e., $\mathsf{C_0}$ vs $\mathsf{C_1}$) when it was perturbed.

3.5 Discussion

3.5.1 Neural feedback appears at a multi-step delay

Instantaneous estimates of kinematic phase and frequency allowed the testing of neuromechanical control hypotheses that would otherwise have been impossible. The lack of change in kinematic phase early in recovery (fig. 3.4-**A**) can be most parsimoniously explained by mechanical self-stabilization (fig. 3.1-**A**). Between one and three steps later, a change in kinematic phase supports neural feedback to the CPG (fig. 3.1-**C**).

For the first 50 ms from onset of lateral perturbation to well beyond its peak, running cockroaches followed the pre-perturbation feed-forward motion model. Neither the residual phase (thick dark line, fig. 3.4-**A**) nor the running speed (thick dark line, fig. 3.4-**C**) were changed relative to their pre-perturbation ranges. The most likely interpretation of these results is a reliance on mechanical feedback fig. 3.1-**A**. Schmitt and Holmes (2000a,b) found that a horizontal plane mass-spring model that moves forward by bouncing side to side can self-stabilize to lateral perturbations with little or no neural feedback. By using momentum trading, this Lateral Leg Spring (LLS) model of sprawled posture running animals could recovery rapidly in body orientation and rotational velocity (Schmitt et al., 2002). More detailed studies of hexapedal models with various forms of simulated proprioceptive feedback and heading control (Kukillaya and Holmes, 2007; Kukillaya et al., 2009; Kukillaya and Holmes, 2009) affirm that feedforward neural activation patterns can provide recovery from lateral impulses such as the perturbation we applied here.

Experimental perturbations of running arthropods support the notion that the

mechanical system can assist in stabilization provided that the perturbation is not so large that pushes the animal out of its passive stability basin. Jindrich and Full (2002) induced lateral perturbation to running cockroaches using a jet-pack and found that recovery began within 10-15 ms, challenging the fastest reflexes responses (Holtje and Hustert, 2003; Wilson, 1965; Ridgel et al., 2001) and occurring within the time frame where we observed no change in kinematic phase (fig. 3.4-**A**). Sponberg and Full (2008) showed that two important control muscles do not change their activation pattern when animals negotiate rough terrain that contains obstacles up to three times their "hip" height. Spagna et al. (2007) did not find any change in gait for spiders and cockroaches running over a wire mesh with 90% of its contact area removed. This finding could only be explained with a more anchored model that included the legs and their position or pose. Animals took advantage of the distributed mechanical feedback offered by passive contacts along legs driven by a pre-programmed CPG.

After a step, the mean residual phase established a new trend (thick dark line, fig. 3.4-**A**) with its slope corresponding to an average decrease in frequency by 0.4 Hz from the pre-perturbation values of 11.1 ± 0.2 Hz. The frequency change corresponded to an outcome of the form shown in fig. 3.2-**C**, and rejected both purely mechanical feedback (fig. 3.1-**A**) and tracking feedback (fig. 3.1-**B**) in favour of feedback to the CPG (fig. 3.1-**C**).

Neural and mechanical control share the task of recovery from perturbations at intermediate speeds. Cockroaches appear to apply neural control as delayed feedback, acting well after any mechanical self-stabilization. Experimental support from the same species is found in six of the 150 steps analyzed for rough terrain running (Sponberg and Full, 2008). In these few steps, the animal failed to make contact during its normal gait cycle, resulting in very large perturbations that presumably drove the animal out of its passive basin of stability. Despite the lack of stance initiation, the rhythmic activation of control muscles persisted for one step, suggesting a continuation of the feedforward, CPG signal (Sponberg and Full, 2008, see fig. 7B,C). Examination of the the next step showed that neural feedback acted to delay stance initiation. During these very large perturbations, the dorsal/ventral femoral extensors did not use sensory information to adjust within a step, but acted to shift the phase of the CPGs clock-like signal in the subsequent stride. More anchored horizontal plane models of the cockroach that include neural feedback find that "the feedforward CPG-driven system is marginally stable, with a weakly stable mode and a neutral mode, making it act as a low pass filter that yields fairly easily correctable and steerable dynamics." Kukillaya et al. (2009). We suggest that the passive mechanical system is sufficiently stable to recovery from small perturbations, but not so passively stable as to limit neural feedbacks contribution to maneuvers.

3.5.2 Classes of frequency change outcome

The time delays from perturbation to onset of change in frequency fell into two classes (fig. 3.4-**A** blue vs. red). The two classes represented significantly different residual phase outcomes (fig. 3.5). The fact that phase outcomes fall into distinct classes while classical kinematic measures such as velocity (fig. 3.4-**C**) do not, points at the utility of residual phase as a means for detecting kinematic changes and the power of kinematic phase as a succinct representation of animal state and thus a predictor of future outcomes. Understanding phase and its relation to the experimental outcomes on the one hand, and the mapping from phase into animal pose on the other hand, allows one to relate posture, and with it morphology, to perturbation outcome. From a dynamical systems perspective, the success of phase at predicting future outcomes comes with little surprise – any stable nonlinear oscillator (such as our animals) can be modelled to first order as a periodic function of phase using Floquet theory (Floquet, 1883; Guckenheimer and Holmes, 1983), a fact that may make kinematic phase based methods invaluable to future biomechanical studies.

We found that the delay to onset of frequency change differed in the two outcome classes by more than 50 *ms*. (fig. 3.4-**A** C_0 mean vs C_1 mean lines). The shorter of these delays lagged more than 50 *ms* from onset of perturbation, and more than 15 ms from peak perturbation. While 15 ms bound is similar to the 10-15 *ms* lag from impulse to onset of centre of mass recovery reported in Jindrich and Full (2002), in our case the perturbation itself is not as brief and thus could be detected by the animal well before reaching its peak acceleration.

We hypothesize that the difference in delay before frequency change between the two outcome classes is the consequence of differences in passive mechanical stability with respect to the perturbation. As the cart accelerated to the animals' left, animals experienced a virtual force to their right. In C_1 trials, animals were mostly in a left tripod stance with the front left, middle right and hind left legs on the cart (fig. 3.5, red). In C_0 trials, animals were in right stance with the front right, middle left and hind right on the cart (fig. 3.5, blue). As the animal began to be pulled laterally, the claws of the feet on its left side could engage the substrate to exert considerable lateral force. For C_0 trials, only the middle leg claws were available. When these engage the animal also experienced a torque, as the middle leg is typically in front of the centre of mass. For C_1 trials, two sets of claws were available bracketing the centre of mass front and back. This could allow for a larger lateral force and for the forces to be paired to minimize the torque, allowing recovery while better preserving orientation and heading. Thus animals in the trials C_1 could rely on the mechanical feedback pathway (fig. 3.1-**A**) for longer than those in the C_0 trials, correcting their gait two or three steps after

perturbation instead of in the step immediately following perturbation.

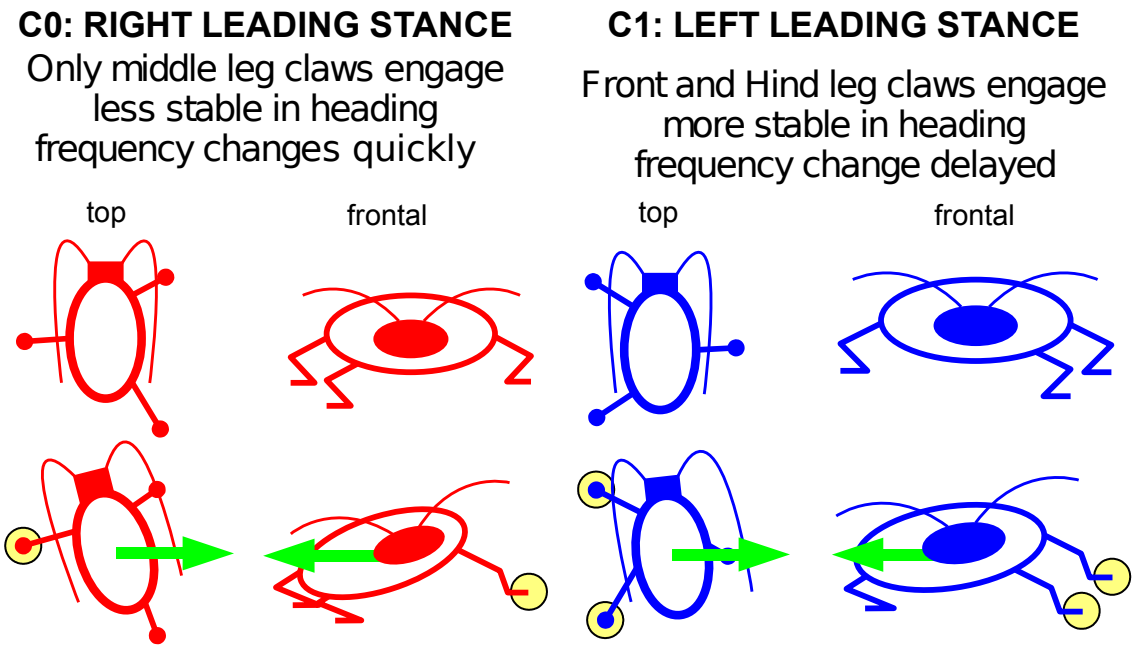

Figure 3.6: The mechanical differences between classes C_0 and C_1. Animals in C_0 trials (left; red) experienced the brunt of the perturbation while in stance on the right tripod. As the cart accelerated to the left, the animals' inertia pulled their bodies to the right (green arrows). In this posture only one foot has claws that can engage to exert a counter-force (circles around middle leg foot). Animals were drawn schematically from top and frontal view with only the stance legs shown. In contrast to C_0, in C_1 trials (right; blue) animals have two legs whose claws can engage, providing more corrective force, and the ability to correct torque independently from force by trading off front and hind leg lateral forces.

Kinematic phase allows the reduction of pose to a univariate time series, so we were able to attribute the difference in perturbation recovery of class C_0 vs. class C_1 trials to a specific animal morphology (fig. 4.5-**)**. While it is commonly assumed that hexpedal designs are the most stable of legged runners because of their ability to maintain a static stability margin throughout the gait cycle or dynamically move the center of mass into the next tripod of support (Ting et al., 1994), our results from lateral perturbations

expose a weakness of the hexapods' alternating tripod gait. As illustrated in fig. 4.5-, the C_0 class (red) is constrained in its ability to exert restorative forces and torques, because only one leg is available on that side of the animal's body. We hypothesize that sprawled morphologies with at least two legs in stance on each side of the body will have a significant advantage in recovering from lateral perturbations.

3.5.3 Dynamical systems bridge bio-inspired simulation and robotics

We found that the delay in appearance of neurally mediated kinematic response in our system was comparable to a step duration. One interpretation of this result is that neural modulation of gait is applied at step intervals rather than as continuous feedback, expressing a limitation of control ability. Recent developments in control theory suggest that replacing high rate periodic feedback (which emulates continuous feedback) with control decisions applied at an opportune moment, can be an effective strategy which also decreases the computational load on the controller (Tabuada, 2007; Mazo et al., 2009). We hypothesize that such approaches are particularly beneficial when applied to self-stabilizing systems such as those that govern cockroach running dynamics, and that the theory of "Self Triggered Control" may prove of value for the study of gait generation in animals.

In addition, new types of biologically inspired controllers may lead to more effective terrain awareness in legged robots (Spenko et al., 2008; Kim et al., 2006; Webb, 2002; Quinn and Ritzmann, 1998; Altendorfer et al., 2001; Bachmann et al., 2009). Kinematic phase-based studies are equally applicable to animals, robots and simulated models. These and other approaches that build on the shared mathematical language of dynamical systems allow for parallel paths of investigation in animal research, robot design and applied mathematics, to the benefit of all three fields.

3.6 Bibliography

M Ackerman. A theoretical study of clusterability and clustering quality. Master's thesis, University of Waterloo, 2007. URL http://www.uwspace.uwaterloo.ca/bitstream/10012/3478/1/thesis.pdf.

A N Ahn and R J Full. A motor and a brake: two leg extensor muscles acting at the same joint manage energy differently in a running insect. *J Exp Biol*, 205(3): 379–389, 2002.

A N Ahn, K Meijer, and R J Full. In situ muscle power differs without varying in vitro mechanical properties in two insect leg muscles innervated by the same motor neuron. *J Exp Biol*, 209(17):3370–3382, SEP 1 2006. ISSN 0022-0949. doi: 10.1242/jeb.02392.

R Altendorfer, N Moore, H Komsuolu, M Buehler, H B Brown, D McMordie, U Saranli, R J Full, and D E Koditschek. Rhex: A biologically inspired hexapod runner. *Autonomous Robots*, 11(3):207–213, Nov 2001. ISSN 1573-7527. doi: 10.1023/A:1012426720699.

R Altendorfer, D E Koditschek, and P Holmes. Stability analysis of legged locomotion models by symmetry-factored return maps. *Int J Rob Res*, 23(10-11):979–999, 2004.

R J Bachmann, F J Boria, R Vaidyanathan, P G Ifju, and R D Quinn. A biologically inspired micro-vehicle capable of aerial and terrestrial locomotion. *Mechanism and Machine Theory*, 44(3):513–526, MAR 2009. ISSN 0094-114X. doi: 10.1016/j.mechmachtheory.2008.08.008.

H Cruse, T Kindermann, M Schumm, J Dean, and J Schmitz. Walknet - a biologically inspired network to control six-legged walking. *Neural Networks*, 11(7-8):1435–1447, 1998.

H. Cruse, V. Durr, and J. Schmitz. Insect walking is based on a decentralized architecture revealing a simple and robust controller. *Philos Trans R Soc Lond , Ser A: Math , Phys Eng Sci*, 365(1850):221–250, January 2007.

F Delcomyn. Neural basis of rhythmic behavior in animals. *Science*, 210(4469):492–498, 1980. doi: 10.1126/science.7423199.

J Duysens, F Clarac, and H Cruse. Load-regulating mechanisms in gait and posture: Comparative aspects. *Physiol Rev*, 80(1):83–133, January 2000. ISSN 0031-9333. URL http://physrev.physiology.org/cgi/content/abstract/80/1/83.

N I Fisher. *Statistical Analysis of Circular Data*. Cambridge University Press, 1993. ISBN 0-521-35018-2.

G Floquet. Sur les équations différentielles linéaires à coefficients périodiques. *Annales Scientifiques de lÉcole Normale Supérieure, Sér*, 2:12, 1883.

R J Full and M S Tu. Mechanics of 6-legged runners. *J Exp Biol*, 148:129–146, JAN 1990. ISSN 0022-0949.

R J Full, R Blickhan, and L H Ting. Leg design in hexapedal runners. *J Exp Biol*, 158:369–390, 1991. ISSN 0022-0949.

R M Ghigliazza, R Altendorfer, P Holmes, and D E Koditschek. A simply stabilized running model. *SIAM Review*, 47(3):519–549, September 2005.

S Grillner. Neurobiological bases of rhythmic motor acts in vertebrates. *Science*, 228: 143–149, 1985.

J Guckenheimer and P Holmes. *Nonlinear Oscillations, Dynamical Systems, and Bifurcations of Vector Fields*. Springer-Verlag, 1983.

M Holtje and R Hustert. Rapid mechano-sensory pathways code leg impact and elicit very rapid reflexes in insects. *J Exp Biol*, 206(16):2715–2724, 2003. ISSN 0022-0949. doi: 10.1242/jeb.00492.

A J Ijspeert. Central pattern generators for locomotion control in animals and robots: A review. *Neural Networks*, 21(4):642–653, MAY 2008. ISSN 0893-6080. doi: 10.1016/j.neunet.2008.03.014.

S Jaric and M L Latash. The equilibrium-point hypothesis is still doing fine. *Hum Movement Sci*, 19(6):933–938, 2000.

D L Jindrich and R J Full. Many-legged maneuverability: Dynamics of turning in hexapods. *J Exp Biol*, 202(12):1603–1623, 1999.

D L Jindrich and R J Full. Dynamic stabilization of rapid hexapedal locomotion. *J Exp Biol*, 205(18):2803–2823, Sep 2002. ISSN 0022-0949.

R E Kalman. A new approach to linear filtering and prediction problems. *Transactions of the ASME - Journal of Basic Engineering*, 82:35–45, 1960.

S Kim, J E Clark, and M R Cutkosky. isprawl: Design and tuning for high-speed autonomous open-loop running. *Int J Robotics Research*, 25(9):903–912, SEP 2006. ISSN 0278-3649. doi: 10.1177/0278364906069150.

R Kram, B Wong, and R J Full. Three-dimensional kinematics and limb kinetic energy of running cockroaches. *J Exp Biol*, 200(13):1919–1929, JUL 1997. ISSN 0022-0949.

T M Kubow and R J Full. The role of the mechanical system in control: a hypothesis of self-stabilization in hexapedal runners. *Philos Trans R Soc Lond , Ser B: Biol Sci*, 354(1385):849–861, MAY 29 1999. ISSN 0962-8436.

R Kukillaya, J Proctor, and P Holmes. Neuromechanical models for insect locomotion: Stability, maneuverability, and proprioceptive feedback. *Chaos*, 19(2), JUN 2009. ISSN 1054-1500. doi: 10.1063/1.3141306.

R P Kukillaya and P Holmes. A model for insect locomotion in the horizontal plane: Feedforward activation of fast muscles, stability, and robustness. *J Theor Biol*, 261 (2):210–226, 2009. doi: 10.1016/j.jtbi.2009.07.036.

R P Kukillaya and P J Holmes. A hexapedal jointed-leg model for insect locomotion in the horizontal plane. *Biol Cybern*, 97(5-6):379–395, DEC 2007. ISSN 0340-1200. doi: 10.1007/s00422-007-0180-2.

M MacKay-Lyons. Central pattern generation of locomotion: A review of the evidence. *Physical Therapy*, 82(1):69–83, January 2002. ISSN 0031-9023. URL http://www.ptjournal.org/cgi/content/abstract/82/1/69.

M Mazo, A Anta, and P Tabuada. Self-triggered control: trading actuation for computation. arXiv.org, 2009. URL http://arxiv.org/abs/0906.3588v1.

J A Noah, L Quimby, S F Frazier, and S N Zill. Walking on a peg leg: extensor muscle activities and sensory feedback after distal leg denervation in cockroaches. *J Comp Physiol , A*, 190:217–231, 2004. ISSN 0340-7594. doi: 10.1007/s00359-003-0488-x.

K G Pearson and D F Collins. reversal of the influence of group ib afferents from plantaris on activity in medial gastrocnemius-muscle during locomotor-activity. *J Neurophysiol*, 70(3):1009–1017, SEP 1993. ISSN 0022-3077.

D N Politis. Computer-intensive methods in statistical analysis. *IEEE Signal Processing Magazine*, 15(1):39–55, 1998a. ISSN 1053-5888. doi: 10.1109/79.647042.

D N Politis. A primer on bootstrap methods in statistics. Technical Report 95-19, Purdue University, Apr 1998b. URL http://www.stat.purdue.edu/research/technical_reports/pdfs/1995/tr95-19.pdf.

A Prochazka, D Gillard, and D J Bennett. Implications of positive feedback in the control of movement. *J Neurophysiol*, 77(6):3237–3251, JUN 1997a. ISSN 0022-3077.

A Prochazka, D Gillard, and D J Bennett. Positive force feedback control of muscles. *J Neurophysiol*, 77(6):3226–3236, JUN 1997b. ISSN 0022-3077.

J Proctor and P J Holmes. Steering by transient destabilization in piecewise-holonomic models of legged locomotion. *Regular and Chaotic Dynamics*, 13(4):267–282, 2008. doi: 10.1134/S1560354708040047.

R D Quinn and R E Ritzmann. Construction of a hexapod robot with cockroach kinematics benefits both robotics and biology. *Connect Sci*, 10(3/4):239 – 254, 1998. ISSN 0954-0091. doi: 10.1080/095400998116422.

H E Rauch, F Tung, and C T Striebel. Maximum likelihood estimates of linear dynamic systems. *AIAA J*, 3(8):1445–, 1965. ISSN 0001-1452.

S Revzen, D E Koditschek, and R J Full. *Progress in Motor Control - A Multidisciplinary Perspective*, chapter Towards Testable Neuromechanical Control Architectures for Running, pages 25–56. Springer Science+Business Media, LLC - NY, 2008. doi: 10.1007/978-0-387-77064-2_3.

A Ridgel, F Frazier, and S N Zill. Dynamic responses of tibial campaniform sensilla studied by substrate displacement in freely moving cockroaches. *J Comp Physiol , A*, 187(5):405–420, 2001. doi: 10.1007/s003590100213.

A L Ridgel and R E Ritzmann. Effects of neck and circumoesophageal connective lesions on posture and locomotion in the cockroach. *J Comp Physiol , A*, 191(6):559 – 573, June 2005.

R E Ritzmann and A Bueschges. Adaptive motor behavior in insects. *Curr Opin Neurobiol*, 17(6):629–636, DEC 2007. ISSN 0959-4388. doi: 10.1016/j.conb.2008.01.001.

M Schilling, H Cruse, and P Arena. Hexapod walking: an expansion to walknet dealing with leg amputations and force oscillations. *Biol Cybern*, 96(3):323–340, MAR 2007. ISSN 0340-1200. doi: 10.1007/s00422-006-0117-1.

J Schmitt and P Holmes. Mechanical models for insect locomotion: active muscles and energy losses. *Biol Cybern*, 89(1):43–55, JUL 2003. ISSN 0340-1200. doi: 10.1007/s00422-003-0404-z.

J Schmitt and P Holmes. Mechanical models for insect locomotion: dynamics and stability in the horizontal plane - i. theory. *Biol Cybern*, 83(6):501–515, December 2000a.

J Schmitt and P Holmes. Mechanical models for insect locomotion: dynamics and stability in the horizontal plane - ii. application. *Biol Cybern*, 83(6):517–527, 2000b.

J Schmitt and P Holmes. Mechanical models for insect locomotion: stability and parameter studies. *Phys D: Nonlinear Phenom*, 156(1-2):139–168, 2001.

J Schmitt, M Garcia, R C Razo, P Holmes, and R J Full. Dynamics and stability of legged locomotion in the horizontal plane: a test case using insects. *Biol Cybern*, 86 (5):343–353, 2002.

A Seyfarth, H Geyer, and H Herr. Swing-leg retraction: a simple control model for stable running. *J Exp Biol*, 206(15):2547–2555, 2003.

J C Spagna, D I Goldman, P-C Lin, D E Koditschek, and R J Full. Distributed mechanical feedback in arthropods and robots simplifies control of rapid running on challenging terrain. *Bioinspiration & Biomimetics*, 2(1):9–18, 2007. ISSN 1748-3182. doi: 10.1088/1748-3182/2/1/002.

M J Spenko, G C Haynes, J A Saunders, M R Cutkosky, A A Rizzi, R J Full, and D E Koditschek. Biologically inspired climbing with a hexapedal robot. *J Field Robot*, 25(4-5):223–242, APR-MAY 2008. ISSN 1556-4959. doi: 10.1002/rob.20238.

S Sponberg and R J Full. Neuromechanical response of musculo-skeletal structures in cockroaches during rapid running on rough terrain. *J Exp Biol*, 211(3):433–446, FEB 1 2008. ISSN 0022-0949. doi: 10.1242/jeb.012385.

P Tabuada. Event-triggered real-time scheduling of stabilizing control tasks. *IEEE Trans Automat Contr*, 52(9):1680–1685, SEP 2007. ISSN 0018-9286. doi: 10.1109/TAC.2007.904277.

L H Ting, R Blickhan, and R J Full. Dynamic and static stability in hexapedal runners. *J Exp Biol*, 197:251–269, DEC 1994. ISSN 0022-0949.

J T Watson and R E Ritzmann. Leg kinematics and muscle activity during treadmill running in the cockroach, blaberus discoidalis: I. slow running. *J Comp Physiol , A*, 182(1):11–22, JAN 1998a. ISSN 0340-7594. doi: 10.1007/s003590050153.

J T Watson and R E Ritzmann. Leg kinematics and muscle activity during treadmill running in the cockroach, blaberus discoidalis: Ii. fast running. *J Comp Physiol , A*, 182(1):23–33, JAN 1998b. ISSN 0340-7594. doi: 10.1007/s003590050154.

J T Watson, R E Ritzmann, and A J Pollack. Control of climbing behavior in the cockroach, blaberus discoidalis. ii. motor activities associated with joint movement. *J Comp Physiol , A*, 188(1):55–69, FEB 2002a. ISSN 0340-7594. doi: 10.1007/s00359-002-0278-x.

J T Watson, R E Ritzmann, S N Zill, and A J Pollack. Control of obstacle climbing in the cockroach, blaberus discoidalis. i. kinematics. *J Comp Physiol , A*, 188(1):39–53, FEB 2002b. ISSN 0340-7594. doi: 10.1007/s00359-002-0277-y.

B Webb. Robots in invertebrate neuroscience. *Nature*, 417(6886):359–363, MAY 16 2002. ISSN 0028-0836.

D M Wilson. Proprioceptive leg reflexes in cockroaches. *J Exp Biol*, 43(3):397–409, 1965. URL http://jeb.biologists.org/cgi/content/abstract/43/3/397.

E P Zehr and R B Stein. What functions do reflexes serve during human locomotion? *Prog Neurobiol*, 58(2):185–205, June 1999. ISSN 0301-0082.

S N Zill, D T Moran, and F G Varela. The exoskeleton and insect proprioception .2. reflex effects of tibial campaniform sensilla in the american cockroach, periplaneta-americana. *J Exp Biol*, 94(Oct):43–55, 1981. ISSN 0022-0949.

S N Zill, J Schmitz, and A Bueschges. Load sensing and control of posture and locomotion. *Arthropod Struct Dev*, 33(3):273 – 286, 2004. ISSN 1467-8039. doi: 10.1016/j.asd.2004.05.005. Arthropod Locomotion Systems: from Biological Materials and Systems to Robotics.

S N Zill, B R Keller, and E R Duke. Sensory signals of unloading in one leg follow stance onset in another leg: transfer of load and emergent coordination in cockroach walking. *J Neurophysiol*, 101(5):2297–2304, May 2009. ISSN 0022-3077. doi: 10.1152/jn.00056.2009.

Chapter 4

Data Driven Floquet Analysis

4.1 Summary

We attempted data driven estimation of a dimensionally reduced dynamical model known as a template by using dynamical systems theory to analyze movement. We chose to model the motions of cockroaches (*Blaberus discoidalis*) in the body frame of reference as a (isolated, periodic) limit cycle and applied a new approach to dimensional reduction using Floquet theory. Floquet theory provides for a change of coordinates approximating motions near the cycle as a time invariant linear system with decaying modes. The modes can be grouped into quickly decaying modes and slowly decaying modes. By comparing the results with a random matrix null model, we determined how many of the slowest modes were attributed to the presence of a lower dimensional, systematic, deterministic model of interest (a template). We investigated the control affordance offered by the template modes using the fact that modes interrelate changes in posture and maneuvers of the center of mass.

We analyzed 34 animals running on a treadmill for 532 strides of foot and body positions. We developed a multiple imputation technique that combined data from multiple trials while controlling for individual variation. Results showed that cockroaches running at preferred speed possess a six dimensional template with each dimension recovering by less than 50% in a stride ($P < 0.05$, 11 animals, 24 trials, 532 strides). The local linear approximation (tangent subspace) to this template was clearly resolved ($P < 0.0001$) allowing us to construct a data-driven model of the local dynamical structure that governs its patterns of recovery from perturbation. Our discoveries lend support to the notion of a template (Full and Koditschek, 1999) and suggest extensions in terms of Floquet structure. We hypothesize that the slowest Floquet mode is not tied to maneuver and that the next three slowest modes provide a unicycle-like template, compatible with spring-mass templates that recover slowly or not at all in heading and speed. Our techniques for data driven Floquet analysis are generally applicable in comparative biomechanics, bio-inspired robotics and even other physical sciences.

4.2 Introduction

Simple quantitative models of motion allow comparison of behaviors across taxa and at vastly different physical scales. Higher dimensional, more detailed models allow testing of hypotheses unique to particular morphologies and physiologies. Full and Koditschek (1999) proposed a hypothesis, termed the Template and Anchor Hypothesis, where a defined relationship between reduced and more representative models

can lead to a greater mechanistic understanding of control. A template is a simple model with a small number of variables and parameters that exhibits the behavior of interest. Finding a template for the motions of a detailed high-dimensional *anchor* – a mathematical model of a specific species' musculoskeletal structure – reveals a low-dimensional subset within its high-dimensional space of possible motions that instantiates a more parsimonious representation of the behavior. Templates are anchored within the high dimensional space by the adoption of a preferred posture for each template state. A putative template motivates questions concerning the mechanism of anchoring that accounts for the anchor's collapse of dimension to this template. Hypotheses regarding the similarity in mechanisms of control of motor tasks (locomotion among them) can be directly verified or refuted across many kinds of organisms and behavioral contexts by using the template as a basis for comparison.

Templates and their anchors have a long history in terrestrial locomotion from sagittal plane inverted pendulum and spring-mass templates (Alexander, 1988, 1990, 1992, 1995; Blickhan, 1989; Cavagna et al., 1977; McGeer, 1990; McMahon and Cheng, 1990) and horizontal plane spring-mass templates (Schmitt and Holmes, 2000a,b; Holmes et al., 2006). These templates have been shown to describe and predict the center of mass motion and ground reaction forces of 2-, 4-, 6- and 8-legged animals during steady-state running (Blickhan and Full, 1993; Farley et al., 1993) and in response to perturbations (Jindrich and Full, 2002; Daley et al., 2006).

In all these cases the template is a model produced by an investigator based on physical intuition for the underlying dynamics. The templates were proposed on the basis of mechanical reasoning and seen to be compatible with the data at hand. They were created as models having a specified low dimension, rather than having the choice of dimension emerge as the outcome of some empirical test.

Most of the prevailing evidence for templates in legged locomotion comes from averaged data, whereby the template derived kinematics and kinetics were shown to match some averaged stride formed by data pooled from an ensemble of strides. The fact that an ensemble average of trajectories matches a deterministic model does not imply that the proposed model has any predictive ability for trajectories in that ensemble. Counter-examples can easily be constructed where the ensemble average bears little relationship to the dynamics governing the trajectories themselves. In the current publication, not only are we aiming to characterize the template numerically, but also to determine the template in a fashion that ensures it represents a causal prediction of future motions based on past states within the individual trajectories.

We offer a method based on Floquet theory (Floquet, 1883; Guckenheimer and Holmes, 1983) for establishing the presence of a template directly from data with no intervening modeling step. The method applies to periodic systems, and may be

used not only with animal behaviors, but also with engineered systems and dynamical systems in general. The method allows dimensions and numerical approximations of putative templates to be computed from data, thus suggesting dimensions and, in settings where structure can be adequately resolved from noise, local dynamical features of reduced models as well. Using Floquet theory provides a more complete representation of the system being investigated than previous work in biomechanics (Hurmuzlu and Basdogan, 1994; Dingwell and Kang, 2007) by virtue of incorporating not merely tests for dimension but also estimates of dynamical structure. Our objective in the current publication is to describe a process starting with data collection, proceeding through identification of the template if one is present, and ending with an analysis of the local perturbational control affordance that this putative empirically derived template provides over state variables of interest – variables such as center of mass coordinates, in the case of locomotion.

4.2.1 Operational definition of a numerical template

From a mathematical perspective, templates may be defined as slow stable invariant manifolds of an animal's dynamics (fig. 4.1). While this is well defined mathematically and conceptually, it is not obvious how to test for and identify such a template. Furthermore, any stable oscillator is expected to have some slow stable manifold corresponding to the perturbations from which it recovers most slowly, thus existence of such (relatively) slow stable structures is tautological.

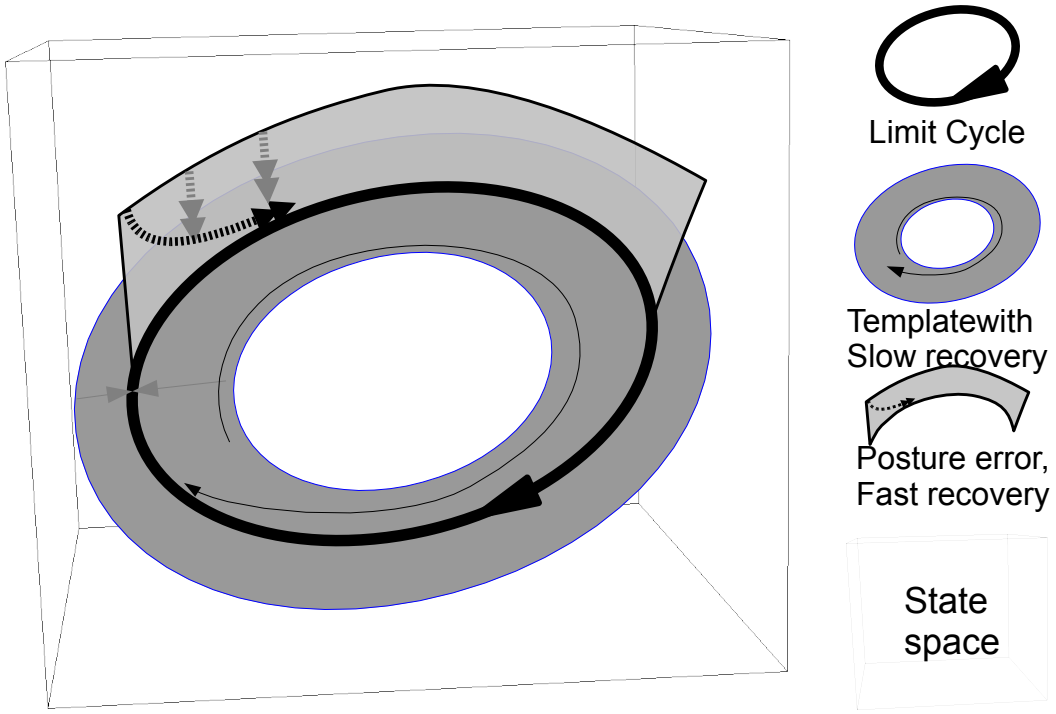

Figure 4.1: Illustrating the dynamics of a periodic behavior governed by a template. The periodic limit cycle (thick dark loop with arrow) represents a kinematic trajectory. The template is shown as a grey oval band representing a family of trajectories and is the target for all perturbed states. Perturbations (shown by a light gray vertical wall perpendicular to the template band) that generate states which are not part of the template are *posture errors* with respect to the behavior, and collapse quickly (double arrows, dashed line) to the template. Perturbations that generate valid template states collapse back to the cycle much more slowly (thin spiral arrow on oval template band).

We define a statistically significant template to be a slow stable manifold which is slower and of lower dimension than could plausibly be generated by an alternative random model of the same dimension. Our characterization is defined with respect to a Poincare section, at which we construct an approximate return map matrix[1]. We split the section into two complementary sub-spaces: a *noise dynamics* sub-space in

[1]The interested reader is directed to Full et al. (2002) for a tutorial exposition of return map analysis and stability for a biology audience.

which the return map dynamics could plausibly be explained by measurement noise or other sources of indeterminism, and its complement, a *significant dynamics* sub-space in which the dynamics cannot be accounted for by this random model. We identify as noise such sub-matrices of the return map as our analysis procedure would construct if it were given trajectories without any causal cycle-to-cycle structure (i.e. random trajectories which cross the section at independently and identically distributed (i.i.d.) Gaussian random points). Numerically, such trajectories give rise to a return map whose eigenvalues are similar to those of a random matrix[2]. We consider a template statistically significant when a splitting procedure that tries to maximize the dimension of the noise dynamics space determines that the significant dynamics space is non-empty and governed by some of the larger (slower) eigenvalues. We then conclude that the template manifold is tangent to the significant dynamics sub-space, and its dynamics may be locally approximated by the corresponding sub-matrix of the return map.

Unlike the templates provided in analytic form, those we hypothesize are not expressed in terms of equations of motion. Instead, they are expressed as an approximation computed numerically, where the first order terms are given by Floquet modes associated with the template expressed as offsets from the limit cycle of the behavior. The starting point for our template models, and indeed the base-point from which we form a local linear approximation of the template manifold, is a data-driven model of the limit cycle characterizing a putative unperturbed behavior. It is for this reason that our method, as described, applies only to motions that are periodic and stable. It is of critical importance for the quality of the subsequent Floquet model to construct an accurate model of this limit cycle and accurately estimate its phase variable.

Concepts from Floquet Theory

Floquet theory provides a canonical, intrinsically determined form for the local dynamics of a stable nonlinear oscillator (Floquet, 1883; Guckenheimer and Holmes, 1983). In its most familiar form it shows that the *Floquet multipliers*, which are the eigenvalues of the linear approximation to the return map, govern the stability of the oscillator under perturbation. Although less well known, Floquet theory also establishes the existence and special properties of the *Floquet frame* – a frame of coordinate axes that is periodic in the phase with its origin on the limit cycle (thick dark line in fig. 4.2). One of the axes of the Floquet frame is always tangent to (i.e., locally lined up with)

[2]We aware of no proofs relating the distributions of noisy trajectories intersecting a Poincare section and the distribution of eigenvalues of the empirically determined return maps thus obtained; our conclusions result from numerical experimentation.

the limit cycle, leaving in a d-dimensional state space d-1 coordinates transverse to the cycle. Each of the *Floquet axes* that comprise the Floquet frame is a periodic vector valued function of phase (see $p_1(\phi)$ and $p_2(\phi)$ in fig. 4.2) which takes as its value at every phase an eigenvector of the return map from that phase to itself (red and blue arrows on both ϕ and θ sections in fig. 4.2). Eigenvalues (Floquet multipliers) are the same at all phases. Each of the Floquet axes threads together eigenvectors at different phases that share the same eigenvalue. Collectively, the Floquet axes ($p_1(\phi)$ and $p_2(\phi)$ in fig. 4.2) comprise the phase-varying Floquet frame that travels around the cycle, defining the directions of decoupled collapse down to the cycle.

We use the term *Floquet mode* to refer to a trajectory that has a continuously phase-varying component along only a single Floquet axis[3]. Because of the role these play in our study, we will refer to these components as *activations* of Floquet modes instead of the traditional mathematical name of *Floquet coordinates*. Expressed in these local coordinate axes, a vector of activations is subject to the constant linear dynamics in the neighborhood of the cycle. Namely, if λ is the eigenvalue associated with a Floquet axis (and thus its mode), T the period and $f(0)$ the initial value of the activation at $t = 0$, then the activation will evolve with the functional form $f(t) = f(0)\lambda^{\frac{t}{T}}$. Thus, the Floquet modes $f(t)$ enjoy a special mathematical role akin to that of eigenvectors in linear dynamics such that for all times t, $f(t)$ satisfies $f(t + T) = \lambda f(t)$.

4.2.2 Analogy of Floquet activations to synergy activations

To best relate our approach to previous advances, we have found it convenient to use the terminology employed in other dimensionally reduced representations of motor control. The notion of "activation" of a synergy (Ting, 2007; Ting and Macpherson, 2005a) refers to the correlated electrical activation of motor units. The activation coordinates of synergies are a reduced dimensional representation of the set of motor unit activations the animal uses, expressed with respect to the basis vectors that show individual synergies. In a similar vein, we used the term activation to describe the representation of animal trajectories with regards to our chosen basis – the basis of Floquet modes[4].

[3]or pair of axes associated with a complex conjugate pair of eigenvalues. Our exposition here we will gloss over details, and treats precisely only the case of distinct positive real Floquet multipliers.

[4]The basis for trajectories starting at some phase ϕ is the collection of Floquet modes scaled so that they have unit magnitudes with respect to the corresponding Floquet axes at phase ϕ.

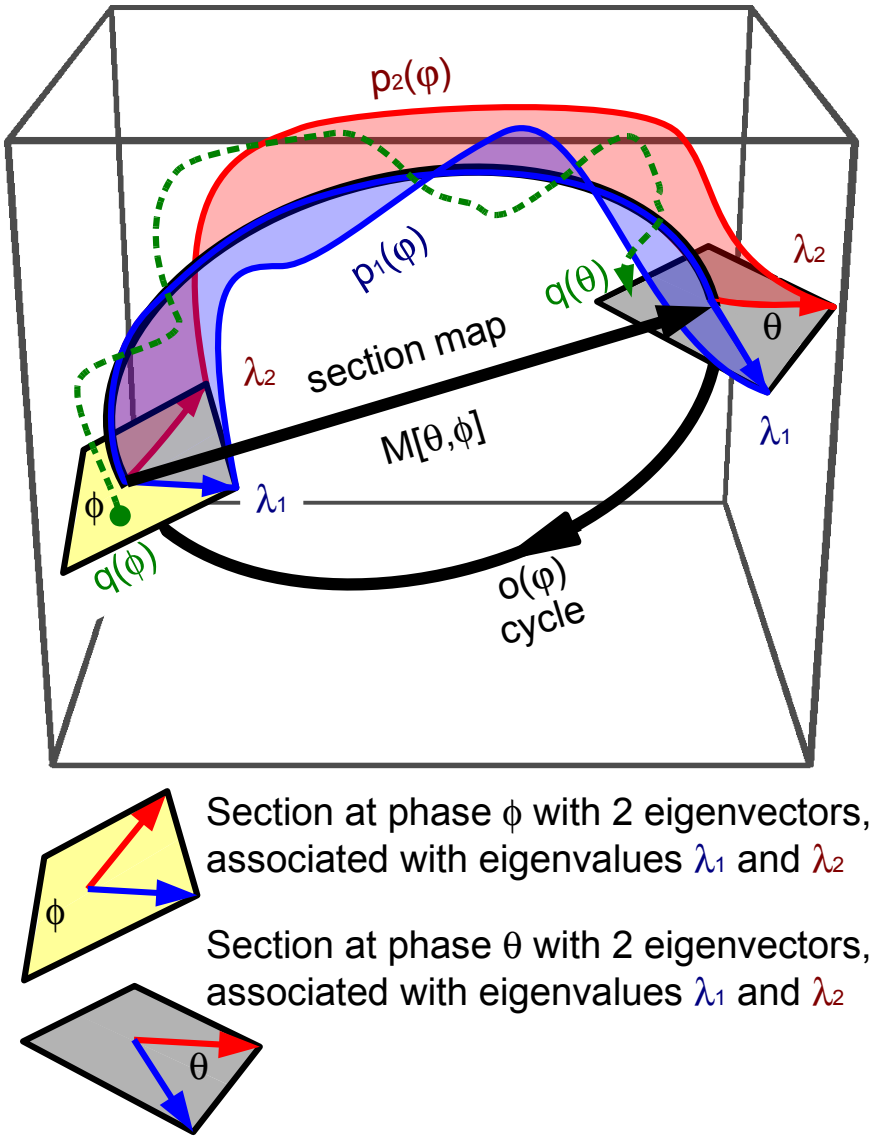

Figure 4.2: Illustration of Floquet structure.

Description of fig. 4.2

Illustration of Floquet structure.

When an animal runs its trajectory describes a periodic cycle in the state space (thick dark looping arrow; corresponding to the same in fig. 4.1). At any phase ϕ in that cycle, if the animal is perturbed in certain directions the perturbation recovery may have a special property similar to that of an eigenvector. For example, on the section representing states with the phase ϕ (yellow square), a perturbation in the direction of the blue arrow (marked with λ_1, representing an eigenvector) will leave the animal's state within the blue surface whose direction tangent to the cycle is swept by the *Floquet axis* $p_1(\cdot)$ associated with λ_1. The perturbed state will return to phase ϕ a cycle later with its distance from the periodic cycle changed by a factor of λ_1 (the eigenvalue, termed a *Floquet multiplier*, of the ϕ return map). A similar property holds for the red arrow, with respect to the red surface and λ_2.

At another phase, for example θ (section represented by gray square), each of the Floquet axes maintains the same eigenvalues (λ_1 for blue; λ_2 for red) but intersects the phase section at a different set of eigenvectors (i.e. the Floquet threads through related eigenvectors at all phases). The phase dependent coordinate frame comprised of all Floquet axes is the *Floquet frame*, and we refer to the state in these coordinates as expressed in terms of *activations*. Each axis defines a different, independent invariant surface tangent to the cycle. An animal recovering from a perturbation and reestablishing its movement on the periodic cycle via a trajectory contained in one of these surfaces has a single non-zero activation and is recovering along a single *Floquet mode*.

The scale of the axis vectors $p_1(\cdot)$, $p_2(\cdot)$, etc. is chosen such that when expressed in activations, a Floquet mode with multiplier λ_1 would have the form $f_1(t) = f_1(0)\lambda_1^{\frac{t}{T}}$. Any trajectory of the (unperturbed) system can be expressed as a sum of Floquet modes, each of which takes this simple exponential form in activations (Floquet coordinates). To find the Floquet axes, we must compute the matrices ($\mathrm{M}[\phi, \theta]$) that map the Floquet frame, whose axes are unit-length eigenvectors of an initial section (ϕ) to the corresponding Floquet frame of unit eigenvectors at a final section (θ). Of particular importance are maps that describe the changes wrought by an entire cycle (the return maps $\mathrm{M}[\phi, \phi + 2\pi]$). We computed the necessary matrices by taking many trajectories of animals (one example being $q(t)$, dashed green arrow), determining their values at the required phases ($q(\phi)$, $q(\theta)$), and computing a linear regression.

Floquet modes by their very definition exhibit decoupled dynamics (i.e., the time derivative of a given mode at each instant is a linear function of only that mode at that instant) and thus provide a natural decomposition of any other motion in terms of a phase-varying, linearly independent basis. By viewing a perturbation as a resetting of the initial conditions and expressing it as a linear combination of activations, Floquet theory predicts the subsequent response as taking the form of a linear combination of the temporally decaying Floquet modes whose coefficients are specified by those of

the initial activation. In particular, the future contribution of every Floquet mode is determined and is independent of the contributions of the others.

No interaction occurs between activations – that is, no activation contributes to a change in state along any other than its own Floquet axis. Because of this independence, Floquet modes afford a decomposition of causal relationships between events that occur at one part of a cycle and those that appear at other phases of the same or in future cycles. Expressed as Floquet mode activations, the periodic nonlinear dynamics become a constant coefficient linear system, similar to that encountered in station keeping tasks. All the power of established methods (Tresch et al., 2006), such as Principal Component Analysis (PCA) (Daffertshofer et al., 2004; Moore, 1981; Ivanenko et al., 2004), Independent Component Analysis (ICA) (Hyvärinen and Oja, 2000) and Nonnegative Matrix Factorization (NMF) (Lee and Seung, 1999; Berry et al., 2007; Ting and Macpherson, 2005b; d'Avella and Bizzi, 2005), which have hitherto been applied to motor control in stationary contexts can be brought to bear on periodic tasks once the data has been represented in terms of its Floquet mode activations.

When compared to methods such as PCA, ICA and NMF in use in biomechanics, whose mathematical properties are compatible with data generated by memoryless transformations, the strength of Floquet theory (which is predicated upon the appearance of attracting periodic cycles and their perturbations) in a dynamical setting becomes evident. Unlike most other methods, Floquet theory hypothesizes, and if not refuted must expose, a dynamical structure intrinsic to the system under analysis. Dimensionality reduction of the system's long-term behavior can then be achieved by truncating the activation vectors and leaving active only the slowest modes to represent the state. The independent evolution of the activations ensures that such a truncation is a valid approximation of the animal's state in the neighborhood of the cycle , in the sense that errors, both relative to the fully activated linearized approximation and also with respect to the actual nonlinear trajectory decay exponentially, at rates easily computable from the Floquet multipliers.

Impact of Floquet modes: an approach to the study of maneuvers

Whenever the animal is perturbed away from the limit cycle, center of mass (COM) velocities differ from their typical, steady state cyclical values. Integrated over all future time, their pattern of recovery back to the steady state in relative body coordinates is associated with an unrecoverable shift in absolute world coordinates of the perturbed animal compared with an unperturbed animal starting at the same phase, position, and heading. Because the appearance and decay of each Floquet mode contributes independently and additively to the motions of the center of mass, the shift induced by

a unit activation of that mode at any given phase can be computed by integrating the center of mass coordinates from the onset of activation to infinity. We refer to this shift as the *impact* of the Floquet mode at that phase[5]. The impact provides a convenient, direct mathematical means to relate modulation of the periodic motion of the body's posture to alteration of its trajectory in the center of mass frame without recourse to any kinematic model. The consequent alteration might be construed as either the non-volitional consequence of an unexpected perturbation or, alternatively, as the animal's ability to maneuver via volitional adjustment of posture or force relative to its nominal steady state periodic behavior.

The validity, and even the very existence of Floquet mode impact as we defined it, deserves some attention. It is natural to assume that the only way an investigator can relate changes of body pose to changes in COM motions is via a mechanical model that reconstructs the forces and torques on the COM and integrates them. Floquet analysis provides an alternative means, predicated upon the persistence in a cycle's neighborhood of the numerically recorded structural "memory" of the actual physical forces and their integrated contributions to mass center position arising from the local dynamical features the analysis reveals. The independence of Floquet mode activations from each other implies causal independence (at least for deterministic systems), which in turn ensures that the COM velocity fluctuations associated with activation along one Floquet axis are causally independent of all other activation coordinates. The impact of a Floquet mode is a correlate of its activation as expressed in terms of COM positions. Determining a mode's impacts summarizes in a computationally explicit manner the linkage between specific, but not explicitly modeled kinematic changes of posture recorded in body-relative coordinates and consequent changes in position (and orientation) of the animal with respect to world coordinates, the absent mechanical model notwithstanding.

By its very definition, impact represents an integrated result. For example, the impact of a mode corresponding to increased forward velocity is an advancement of position. The size of this advancement is the time integral of the (phase dependent) increase in velocity that has a decaying exponential envelope governed by the eigenvalue magnitude. In the case of Floquet modes that decay quickly (compared to a cycle), the impact of the mode may depend strongly on the phase of onset.

For slowly decaying modes, impact can take one of two forms. In the first form, it averages to nearly zero in a cycle and is potentially sensitive to phase of onset

[5]In a formal sense, the impact is an operator taking the standard basis of Floquet mode activations at every phase to the shift it induces in long-term animal state. Linearity of the integration operations ensures that the impact is locally a linear operator that can be represented as a matrix. Details of the computation are given in section 4.7.

of activation. In the second form, it averages to a non-zero value in a cycle, and cannot be sensitive to the phase of onset. To see this, note that even if some modes "orbited around" along the cycle in a very lopsided manner, the fact that their influence persists over long stretches of phase implies that no "lopsided" epoch will fail to be visited during a recovery. In consequence, its local influences on the impacts will be integrated into the eventual final result, even by perturbations starting in phases at which the mode is situated very differently relative to the more typical excursions of that epoch. This insensitivity of the impact of slow Floquet modes to activation time makes them of particular interest as targets of control.The sense in which we propose to explore maneuvers empirically through Floquet analysis complements the approach proposed in Proctor and Holmes (2008). Cast in the language of Floquet analysis, the "steering by transient destabilization" that Proctor and Holmes (2008) proposed is a volitional injection of a perturbation which then proceeds to evolve according to the intrinsic dynamics of the unperturbed system, as governed by the unperturbed system's Floquet structure. Our contribution relative to this hypothesized architecture of maneuvers is twofold. First, theoretically we observe that transient destabilization takes its simplest form when introduced via a single Floquet mode Second, our methods provide the means to experimentally examine actual animals for evidence of a control strategy based on transient destabilization.

4.2.3 Floquet analysis applied to running insects

Terrestrial locomotion in insects offers an exceptional model system for testing hypotheses of data driven templates. Data on the kinematics and kinetics for steady-state running exist (Full et al., 1991; Full and Tu, 1991, 1990; Kram et al., 1997) along with dynamic responses to perturbations (Jindrich and Full, 2002; Kubow and Full, 1999; Spagna et al., 2007; Sponberg and Full, 2008; Ting et al., 1994). The dynamics of center of mass in insects are consistent with the general pattern observed for all legged runners (Blickhan and Full, 1993). Several investigator-created, analytical templates match the measured dynamics. These include sagittal plane spring-mass models (Blickhan and Full, 1993; Full and Tu, 1990), horizontal plane spring-mass models (Schmitt and Holmes, 2000a,b) and unicycle models used to capture tactile navigation dynamics (Cowan et al., 2006; Lee et al., 2008). Horizontal plane templates have been effectively anchored by elaborations of appendages (Seipel et al., 2004; Kukillaya and Holmes, 2007), muscles (Kukillaya et al., 2009; Ghigliazza and Holmes, 2005; Proctor and Holmes, 2008) and sensors (Kukillaya et al., 2009; Lee et al., 2008). Moreover these templates and anchors have been analyzed using dynamical systems approaches (Seipel et al., 2004; Holmes et al., 2006, and references therein). Full et al. (2002)

wrote a tutorial for biologists of the terminology and concepts used in dynamical systems such as limit cycles, return maps, eigenvalues and eigenvectors as they relate to quantifying stability.

Here, we hypothesize that running cockroaches follow a low dimensional template, and report on our tests of this hypothesis with data-driven methods of Floquet analysis we developed for this purpose. To determine if a template can be derived from data, we collected and analyzed kinematic data of animals running – a periodic task in terms of limb motions. Given this ensemble of an approximately periodic time-series of the system's state, we computed phase as accurately as we could. The phase we refer to is an intrinsically defined coordinate of any periodic system, rather than merely a time variable interpolated between some distinguished events (Winfree, 1980; Guckenheimer and Holmes, 1983; Revzen and Guckenheimer, 2008). Using the phase associated with each sample, we averaged the time-series, now taken as a function of that phase (rather than time), to find the limit cycle of the periodic task. Moreover, because we knew the phase, we partitioned the entire set of stride data into *phase sections* – subsets of common phase that geometrically define surfaces transverse to the limit cycle curve at that phase. Using multiple imputation (Efron, 1994; Harel and Zhou, 2007), a statistical technique related to the bootstrap, we estimated a *section return map* (whose linearized approximation we represent as a matrix) and examined it for the statistical signature of a template. Finally, considering in a similar manner the *section maps* between all pairs of phase sections, we extended the eigenvectors of the return maps to compute the Floquet modes and axes.

Here, we propose several immediate applications of the Floquet mode estimation procedure. First, we can verify the presence of a template and identify its dimension. Second, we can integrate Floquet modes activated at various phases to compute their impacts on the center of mass motion. Third, we can examine previously hypothesized template models for steady state level ground running and test to see whether their local linearized structure is compatible with the Floquet multipliers we found and if so then what (local) properties of the posture would be required to produce the Floquet modes that emerge from the empirical analysis. This manuscript present results of the first two and discusses the next step for the third.

4.3 Materials and Methods

To conduct the Floquet analysis, we used kinematic data of cockroaches running on a treadmill. The treadmill data we collected were also used in a previous study examining phase changes in the kinematics of cockroaches traversing a hurdle (Revzen

et al., 2006). In the current analysis, we only used segments of free-running on the treadmill, removed from interaction with the hurdle. To explore whether our results on the treadmill were general, we developed an alternative apparatus allowing animals to run freely in an arena for an extended duration. Our preliminary analysis did not find a difference between the treadmill and arena experimental setups in either leg kinematics or eigenvalue analysis, so we did not pursue a more complete, direct comparison.

4.3.1 Animals

Adult *Blaberus discoidalis* cockroaches were raised in a cage with unlimited food and water and tested at room temperature 25 ± 3 °C (mean,SD).

We used 34 cockroaches of both sexes (mass 3.3 ± 0.34 $gram$; body length 49 ± 2.6 mm) in the treadmill experiment. The dataset consists of 45,132 frames of 500 fps video, each with body position and orientation, and tarsal claw (tip of the foot) position for all six legs. We used three adult cockroaches (mass 3.1 ± 0.12 $gram$; body length 47 ± 0.8 mm) for the arena experiment.

Treadmill data collection and protocol

Details of the methods used to collect treadmill kinematic data are in Revzen (2009) chapter 2. That study examined how the *kinematic phase* (Revzen et al., 2008; Revzen and Guckenheimer, 2008) of cockroach motions responds to hurdle traversal. Each trial consisted of running a cockroach across a 3 mm high hurdle at the animal's preferred running speed. For the Floquet model construction in the present study, we discarded all data proximal to contact with the hurdle. We also included several trials where animals ran on the treadmill without traversing the hurdle.

The animals ran within a plastic enclosure placed on a treadmill with a transparent belt. We manually adjusted treadmill speed to match the animal's preferred running speed in that trial. Speeds ranged uniformly between 17 and $29 cm sec^{-}1$. We recorded video of the animals from below with a high-speed camera (Kodak Ektapro 1000; Eastman Kodak Company, Rochester, NY, USA) and digitized their body and tarsal (i.e. foot) motions in the image (horizontal) plane, along with the front and rear of the body axis.

Prior to splitting the kinematic data into pre- and post-hurdle segments, we selected trials based on two requirements. Animals must not contact the walls of the cage or vertical parts of the hurdle with body, legs or antennae. Animals must not trip by stepping on their own feet, or get a leg caught in the crack between the enclosure and the treadmill belt.

One of the methodological problems in conducting our study was that the matrices we wish to reconstruct can only be derived from a large number of data points – requiring far more data than available in any single trial. This poses special challenges in controlling for trial-to-trial and individual biases, because of the importance of using all available data. Additionally, the Flqouet structure itself expresses the differences in the motions of an animal at different strides, preventing us from constructing averaged strides for a trial or an animal as a means for balancing our experimental design. We address these issues with a *multiple imputation* (Harel and Zhou, 2007; Efron, 1994) technique developed for this purpose. Our method combines multiple imputation and bootstrap, bolstering the low statistical weight of short trials through imputation, and limiting the weight of long trials and data prolific individuals by a randomized sub-sampling bootstrap step. Details of this method are provided in the next sub-section.

The treadmill kinematic data comprised 49 trials collected from 34 adults in an unbalanced experimental design. These trials became 67 segments of uninterrupted running after we split trials where the animal traversed the hurdle into two segments, discarding data one stride before and one and a half strides after contact with hurdle. From hereon, we refer to each such segment as a trial. Based on the trial length distribution, we found the optimal cutoff for number of strides per trial so as to maximize usable data to be 14. Trials with 3 to 14 strides were only used for phase estimator training and limit cycle models, but discarded from the Floquet analysis because they would cause the experimental design to become too unbalanced. The remaining 24 trials had lengths 14 to 36 strides, for a total of 532 strides of data from 11 animals. Each imputation re-sampled trials (with replacement) to a length of 28 strides. The animal providing the most data contributed 5 trials for a total of 149 strides. Five animals provided the least data contributing one trial each for a total of 121 strides combined.

A nonparametric multiple imputation approach

Imputation is a statistical procedure by which stratified data with missing measurements is augmented with /conceptimputed data filling in the missing measurements, typically by constructing a parametric model of each stratum and generating imputed data points at random from this parametric model; each such stratum can be referred to as an *imputed sample* from that stratum. When this procedure is carried out multiple times, taking many alternative random choices of imputed data into account, it is referred to as a multiple imputation method (Harel and Zhou, 2007; Efron, 1994).

The multiple imputation procedure we developed takes a highly unbalanced de-

sign where some trials may be much longer than others, and creates multiple imputed samples with a balanced design to feed into the next steps of our computation. The procedure is a non-parametric extension of existing multiple imputation methods and potentially applicable to a broad range of estimation problems. It generates the samples by discarding very short trials and bootstrap (re-)sampling the remaining trials to the same length. We selected the trial length cutoff for discarding short trials through an optimization procedure. First, we selected a parameter we termed *leverage* – the maximal ratio between the length of the shortest allowable trial and the size of a re-sampled trial. The leverage must clearly be larger than 1, and leverages larger than e (the natural base, about 2.7) imply that short trials are almost certainly duplicated[6]. We selected the leverage to be 2, so as to allow a fairly broad range of trial lengths while at the same time avoiding the near-certain duplication of data points inherent in larger leverages. Armed with the choice of leverage and knowing the length distribution of our trials, we computed the number of strides that would remain usable for each choice of length cutoff, and selected the length that would admit the maximal number of strides into the dataset, while still obeying the leverage limit. We used the imputed samples generated from the admitted trials to estimate section maps, thereby avoiding statistical biases introduced by the differences in trial lengths. Whereas classical imputation methods (Harel and Zhou, 2007; Efron, 1994) use parametric models to fill in the missing measurements, we use the nonparametric method of resampling, thereby using the empirical distribution of the sample itself as our model.

[6]A note on duplication of points: in a standard bootstrap procedure, N data points are re-sampled with replacement. In such a process, about $e^{-1} = 37\%$(e the natural base) of the points will appear more than once in any given bootstrap sample. When creating an $N \times L$ sized bootstrap sample for some leverage L, the expected number of appearances of a data point is L.

4.3.2 Arena design and protocol for control

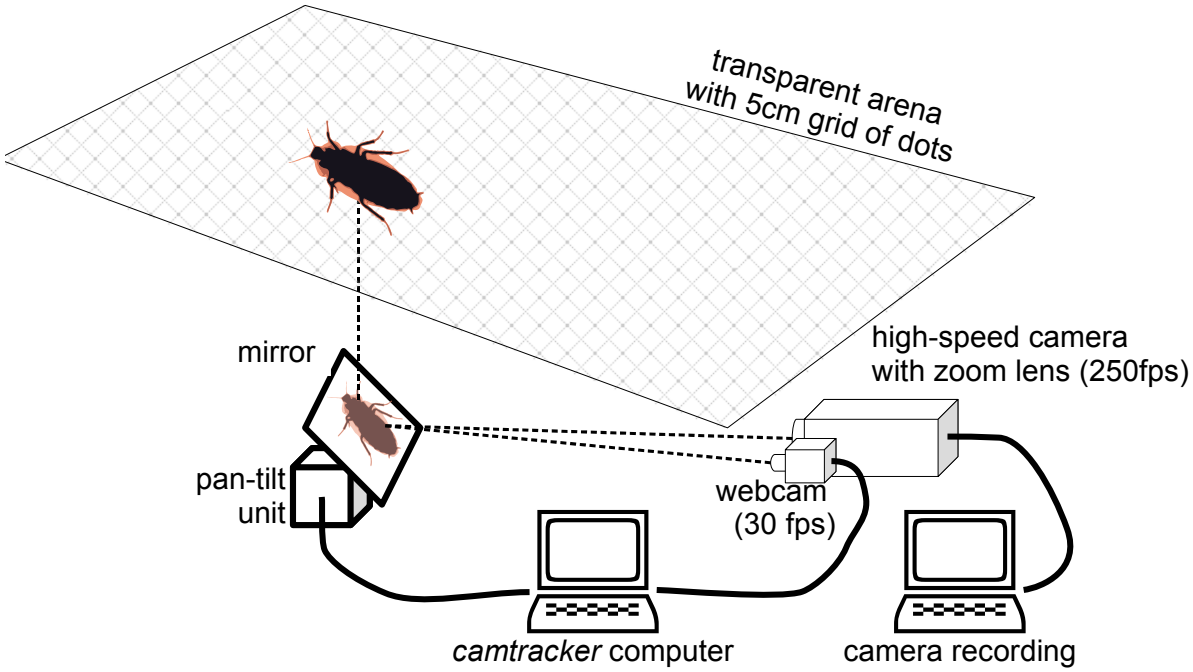

Figure 4.3: Experimental arena design. We used a low resolution, wide-angle webcam to visually servo a mirror that followed the cockroach around the arena by closing a control loop via custom written camtracker software. Simultaneously, we recorded a high resolution, high frame rate video of the animal using a high-speed camera with a zoom lens. We used dots on the arena to recover the mirror motions and correct for perspective errors.

The arena apparatus utilized two cameras working in tandem to solve two separate tasks. We used a low cost FireWire webcam (Unibrain Fire-i; Unibrain, Inc., San Ramon, CA, USA; 640x480 pixels at 30fps) to continuously watch the animal and visually servo a mirror so as to keep the image of the animal in the centre of its field of view. A second camera (AOS X-PRI; AOS Technologies AG, Baden Daettwil, Switzerland; 1280x1024 pixels at 250fps) recorded high-speed video

We used the freely available **OpenCV** library to track visual features indicating the position of the animal in real-time. We then Kalman filtered these positions to

obtain position and velocity in camera image plane coordinates. We converted the position and velocity errors with respect to the centre of the camera's field of view into commands for a pan tilt unit (PTU-46-17.5; Directed Perception, Burlingame, CA, USA) carrying a mirror by multiplying them with a conversion matrix. Our software automatically computed this matrix using a calibration procedure based on letting the camera watch a fixed target while moving the mirror through the pan tilt unit.

The entire real-time video tracking program supporting target tracking, PTU control and real-time transmission of target position over a network is encapsulated in a C program called **camtracker**. Source code is available through the corresponding author's web site. The software (**camtracker**) runs on most modern variants of the Linux operating system.

While the tracker was running, it kept the animal's image close to the centre of the field of view of the webcam. Thus the animal remained within the narrow field of view of the high-speed camera's zoom lens, allowing high-resolution, high-speed video to be collected from animals running freely a distance that is many times their body length (body lengths were 49 ± 2.5 mm (mean,s.d.), ranging from 44 to 55 mm).

By prodding them with a probe, we induced the animals to run on a transparent arena (80 $cm \times 200$ cm) marked with a square grid of points 5 cm apart. We selected the zoom lens viewing angle so that at least three grid steps, i.e. 15 cm, were within the field of view. We developed custom video analysis software (written in **MatLab** version 6.5; The MathWorks, Inc., Natick, MA, USA) to identify the grid coordinates of grid points as they came into view. With the multiple grid points visible in each frame we computed a projective transformation that corrects both perspective and viewing angle errors in the image and converts it to a reference orthographic view. This produced a video that looks as if it was taken by a camera that translates along with the animal, while viewing the arena in the normal direction to its surface.

The naive approach of computing independent projective transformations for every frame of the video turned out to be too sensitive to the appearance of new grid points in the field of view. Such new points always appeared at the boundaries of the image and thus had a large leverage on the estimated transformation causing discontinuities. Instead, we estimated the camera's intrinsic parameters (Heikkila and Silven, 1997) by taking the first middle and last frames of each trial. We then solved for the pan and tilt angles needed to produce the correct projective transformation for every frame.

We discarded trials unless animals ran at least half the length of the arena and did not contact the sides of the arena. We trimmed recordings so that the depth of field limits did not render the images too blurry to analyze. During a recording, tracking would sometimes lag enough to allow the animal to slip outside the field of view of the high-speed camera. We split such recordings into multiple segments, and each was

used as a separate trial. In each such trial the animal was in full view continuously.

4.3.3 Comparing arena and treadmill data

To determine whether the arena and treadmill kinematic data were similar, we selected a contiguous 740 ms segment of video from each treadmill trial and a randomly selected trial from each arena animal. For each segment, we constructed a Fourier series model (order 7; order select based on diminishing return) for the foot position data as a function of phase. We used this model as an exemplar of the motions in that trial when comparing them with other trials. We computed an average model (mean taken in Fourier coefficient domain) of all exemplars of the treadmill data. We then computed the variation of each trial by taking the RMS difference between its exemplar and the average model. The variation of each treadmill animal was taken to be the mean of its variation in all trials, thereby under-estimating the variation among treadmill animals.

Using the distribution of variations in the treadmill data, we assessed the location of the arena animals. All arena animals fell within one standard deviation from the mean of the treadmill animal's data. We conclude that the kinematic data from the arena control was not different from the treadmill data. We also found that the arena trials were not significantly different from one another and therefore selected the arena animal with the most available data to analyze. We found 19 trials meeting our operational definition of a successful run in the arena. We used these trials to construct our phase estimation and limit cycle models. Our multiple imputation algorithm selected a minimal trial length of 19 strides, leaving 7 trials of lengths 19 to 39 strides in the Floquet analysis dataset for a total of 204 strides.

We found no major differences between the primary treadmill data and the preliminary arena data. Given that our main objective was not to compare treadmill versus arena running, we did not find sufficient justification to conduct a more comprehensive comparison at this time.

4.3.4 Estimating the Floquet structure from kinematic data

Because the estimation of the Floquet structure from data is a novel method, it required several new mathematical procedures, and exposed open problems in applied mathematics and statistics. We provide the mathematical details, and a more complete discussion of the statistical issues in the appendices and future publications. For clarity and ease of exposition, our exposition of the mathematics only treats the case of distinct positive real eigenvalues in the range 0 to 1. Correct treatment of complex conjugate and negative eigenvalues is necessary for a working implementation.

In the current publication, we demonstrate the feasibility of using data driven Floquet analysis to directly establish the presence of the low dimensional template embedded within the dynamics of a moving animal, and to obtain a mathematically salient description relating changes in body pose to center of mass maneuvers.

Evaluating the dimension of the template

For analytically defined template models, the dimension of the template is obviously specified by the dimension of the state space used for writing the equations of motion. For example, the classical lateral leg spring (LLS) template (Schmitt and Holmes, 2000a) has a single rigid body whose configuration has 3 DOF and the equations governing this configuration are second order equations which specify the configuration and its time-derivative in terms of higher order terms. Therefore LLS is a 6-dimensional dynamical system, and any collection of measurements we take of an LLS system will fall on a 6-dimensional (but not necessarily flat) surface. For numerically derived templates such as ours, the dimension of the template is inferred from the number of its linearly independent modes. In the absence of a priori theoretical preference for one or another dimension, parsimony dictates that observable structure should be construed as representing all the structure present. Thus to evaluate its dimension, we must identify how many of the slowest (largest) eigenvalues should be attributed to the template and cannot be attributable to noise.

Dynamical systems theory shows that for deterministic systems the eigenvalues computed at all Poincare sections must be the same. However, in our experience, similar to that reported by other biologists (Arellano et al., 2009), numerically computed eigenvalues can vary considerably from one section to another (see section 4.6 for further details). Instead of using the eigenvalues themselves, we chose to use only the eigenvalue magnitudes which correspond to the rate of decay – the time constant of the envelope – associated with each mode. Our numerical investigations consistently suggested that eigenvalue magnitudes (but not complex argument / polar angle) of the larger eigenvalues remain stable despite noise in the data.

To decide which eigenvalues can be ascribed to the presence of a deterministic template, we proceeded to model them as arising from a purely random process parametrized by dimension with the subsequent step of retaining as deterministic only those which could not plausibly fit that model. Specifically, we compared the distribution of the eigenvalues we obtained from imputed samples of experimental data with that of two null hypotheses. The first null hypothesis $H_{0(a)}$ corresponds to random measurements: input-output pairs distributed with a Gaussian distribution on the putative initial and final phase sections (with the Gaussian centered on the intersection

of the section with the limit cycle). Such measurements lead to an eigenvalue distribution seemingly governed by the *Circular Law* (Edelman 1997)(Edelman, 1997), which can be approximated numerically by generating random matrices and computing their eigenvalues (see fig. 4.10 in section 4.6, also [7]).

The second null hypothesis $\mathsf{H}_{0(b)}$ corresponds to breaking the causal relationship which the Floquet analysis aims to recover. We use our phase estimate to segregate data by phase section and compute the eigenvalue distribution of matrices derived from surrogate data (Schreiber and Schmitz, 2000) generated by randomly pairing output data points with input data points. Output data points were selected at random, without replacement, from the final section and paired with input points taken from the initial section in order.

If a template is in fact present, we expect the magnitude of the associated eigenvalues to be larger than those that derived from a circular law eigenvalue distribution expressing the $\mathsf{H}_{0(a)}$ null hypothesis. In addition, we expect those slow eigenvalues to be outside the distribution of eigenvalues one may obtain from randomized surrogate $\mathsf{H}_{0(b)}$ time-series. The latter criterion establishes that these eigenvalues correspond to causal relationships within the data, while the former criterion establishes that the dynamics that these eigenvalues represent are indeed slower and of lower dimension than one would expect to observe in random time-series (noise).

Floquet analysis algorithm

Here, we outline the process of Floquet analysis. Additional details are provided in the appendices and will be defined in future publications.

We estimated phase for every sample in our data and constructed a model of the limit cycle as a function of phase. We then converted the data collected into input-output pairs associated with maps between every possible pair of phase sections (all 210 pairs possible between 20 sections, including return maps from a section to itself). We intersected the trial trajectories with the sections using linear interpolation, and applied linear regression to multiple imputed samples of these intersections to obtain a reliable estimate of the section maps $\mathsf{M}[\cdot,\cdot]$. By using a model selection process, we identified the dimension of the template from eigenvalues and tested for the significance of the sub-spaces tangent to it obtained from their associated eigenvectors, to ensure that posture error directions (see fig. 4.1) could be clearly distinguished from directions

[7] $\mathsf{H}_{0(a)}$ matrices are not stochastic matrices, and therefore their eigenvalues do not fall within the unit disc. In general, these matrices have a scale parameter that decides the radius of the disc containing their eigenvalues. Asymptotically in d for matrices of large dimension d whose entries are distributed as independent standard Gaussians, this disc is of radius $\sqrt{d}$.

tangent to the template – otherwise a local linear approximation of the template dynamics was not well defined. Finally, we used the section maps to recover the Floquet structure of the underlying dynamics and computed the impact of template Floquet modes on the center of mass.

To obtain a reliable estimate of phase from these multivariate time series, we applied the algorithm of Revzen and Guckenheimer (2008) to the six dimensional fore-aft position coordinate data. In preparation for phase estimation, we first detrended the data by subtracting a baseline produced by low pass filtering (Butterworth smoother, cutoff at 4 strides), as the phase estimator requires time series with a stationary mean. The phase estimation algorithm uses phase estimates generated by the Hilbert transform method (Huang et al., 1998) from each leg position, corrects systematic biases and combines them so as to optimize the overall quality of the phase estimate produced measured in terms of expected signal-to-noise ratio and linearity of the phase in time. The algorithm gives all trials equal statistical weight when constructing the phase estimator, irrespective of the trial length. Its output is a time-series of phase for all frames of all trials.

Given a value of phase for each data point, we constructed a periodic model of the state as a function of phase (fig. 4.4-**A,B**) in each trial by fitting a Fourier series (order 11, chosen based on observing diminished returns for further increase) to the data. We constructed a global model of the cycle by averaging corresponding coefficients of each of the Fourier series of all trials. We adapted this global model to each trial by adjusting the mean and variance of each component of the Fourier series.

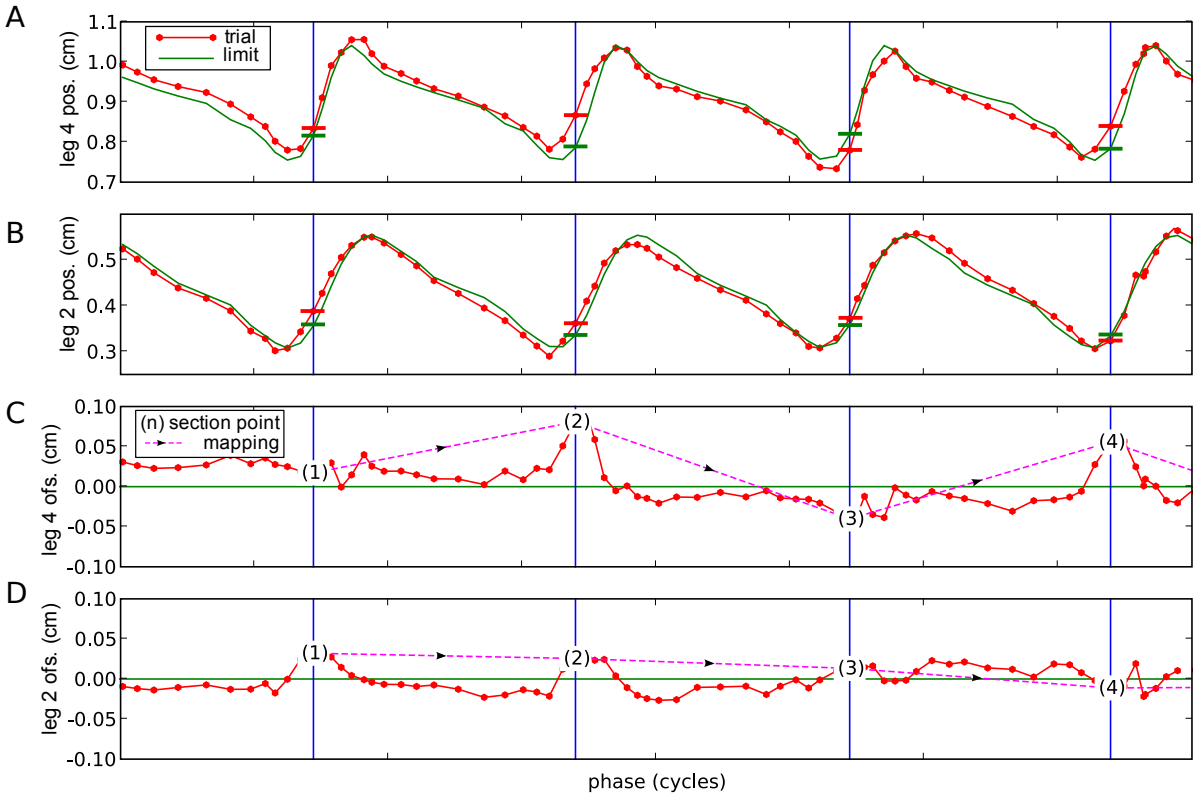

Figure 4.4: From kinematic data to Poincare sections, transition maps and the $\mathsf{M}[\cdot,\cdot]$ matrices.

Description of fig. 4.4

From kinematic data to Poincare sections, Transition Maps and the M$[\cdot,\cdot]$ matrices.

To illustrate our approach, we present kinematic data of fore-aft leg positions for two legs (**A** and **B**; red with dot markers) belonging to the same tripod of one trial as a function of phase. We compared kinematic data from an animal with a Fourier series model (derived from the phase estimates in a manner outlined in the text) of the cycle (**A,B**; green line) evaluated at the same phase. The actual computation used all 27 dimensions of the data (foot positions; foot and COM velocities).

The Floquet structure governs how changes from the limit cycle evolve in time. To fit a linear transformation to such changes from the cycle we used linear regression applied to offsets relative to an origin on the limit cycle at each phase. This origin was taken to be the Fourier model prediction. We computed the offset of the trial from the model at the same phase in consecutive cycles (**A,B**: horizontal red and green marks on blue vertical lines indicating the section phase; **C,D**: red line with dot markers) and constructed a vector from the offset values at each cycle index. The "(1)" labels in the plot denote components of the offset vector in the first crossing of the phase section. The "(2)" labels denote the second crossing, etc.

For the return map computation, we computed a least-squares (**scipy.linalg.lstsq**) regression of all (n+1) vectors against the corresponding (n) vectors; the mapping this matrix approximates takes the numbered crossing points along the dashed magenta arrows. The graphs **C, D** correspond to components of trajectory arrows in fig. 4.5-**C** expressed relative to the orbit position on the section, whereas **A, B** show these same trajectories of fig. 4.5 in absolute coordinates. For other, non-return map section map matrices M$[\cdot,\cdot]$, we computed the sectioning for each section, and we regressed (n) vectors of the second section against the (n) vectors of the first.

There is a fundamental trade-off in selecting how closely a limit cycle model should be adapted to an individual trial. If the cycle were too generic by not taking into account differences in animal body sizes or average pose differences due to a different average speed, the systematic offsets of the individual trial with respect to the limit cycle model might dominate the regression and obscure the stride-to-stride dynamics we hoped to draw out. If the cycle were too specific to a given trial, it might "over-fit" the time series for that trial, and thereby would have reduced the very offsets away from the limit cycle model that we used to conduct our analysis. We tried several alternative model choices, ranging from the least specific global model, through adapted global models, trial specific models and even the section-specific choice of using section data mean as origin. Eigenvalue distributions were similar in all but the first of these. We therefore chose to adapt mean and scale – two parameters – for each of the components of the global Fourier series model. Each 11th order Fourier series model of a component

consisted of 23 parameters – a mean value, and 11 coefficients each for sine and cosine terms.

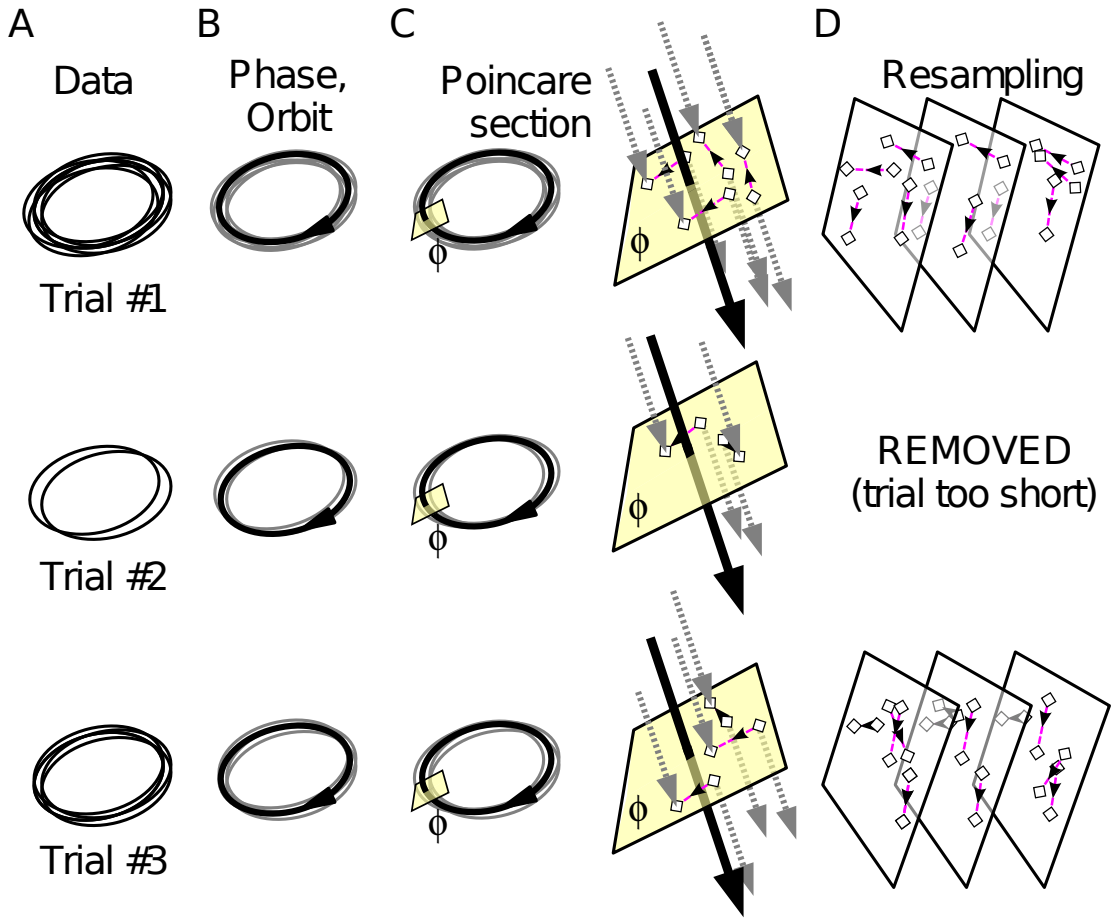

Figure 4.5: Preparing the data for linear regression

Description of fig. 4.5

Preparing the data for linear regression.

We show how data from multiple trials, sectioned as described in fig. 4.4, can be combined into balanced imputed samples. Periodic time-series data from trials (**A**) can vary greatly in length (three examples shown). For each trial, we recovered a phase and computed the Fourier series model of its stable limit cycle (oval with black arrow) in the manner described above (**B**). We then sectioned all trials at the selected phase by computing the intersections of trial time series with the phase section hyperplane at the phase we chose. (**C**, yellow planes) illustrate the section surfaces.

The putative limit cycle itself (thick dark arrow on yellow plane, **C** right) goes through a section arriving and departing in the same point every stride, whereas actual trajectories (thin gray arrows, **C** right), subject as they are to various perturbations that keep them from exact steady state, both leave the section at some point offset from the cycle (arrows below section) and return one stride later to some other point (arrows above section). Each such pair, showing section offset before and after a stride (dashed magenta arrows, corresponding to the same in fig. 4.4), provides one input-output pair for our regression estimate of the return map for that phase.

Some trials have too little data to be useful and must be discarded at this stage (**D**, "removed"). All other trials are used to generate multiple imputed sets of input-output pairs of identical size (4 pairs in figure). Longer trials such as trial #1, with a greater number of strides and thus of crossings through the phase section, provide ample pairs at the selected phase from which the goal number of pairs are randomly selected (with replacement) in each imputation. Shorter trials such as trial #3, having fewer than the goal number of pairs, will have more duplication of points Statistical validity is assessed by constraining what we have termed *leverage*: the ratio of shortest trial length to size of imputed sample.

fig. 4.4 shows how data from a single trial was processed into sections. We computed the difference between the animal's foot trajectory and the adapted cycle model (difference between dotted red "trial" plot and unmarked green "limit cycle" plot fig. 4.4-**A,B** as shown in dotted red "trial" plot of fig. 4.4-**C,D**). Since we required the value of this difference at our chosen phase sections, which were typically not equal to the phase associated with the data points, we linearly interpolated the trajectory from the two samples before and after each phase section to obtain its value on the section hyperplane. Applying this procedure to a trial, we computed the sequence of crossings of the desired phase section (numbered points connected by straight blue lines in fig. 4.4-**C,D**).

The processing of section points is further illustrated in fig. 4.5 which shows how data from multiple trials were combined. The steps of fig. 4.4 correspond to the process in fig. 4.5-**A,B,C** for a single trial: finding a model and sectioning the offset from that

model. Pairs of points with consecutive numbering in fig. 4.4-**C,D** form the input-output pairs, as is indicated by the dashed magenta arrows in fig. 4.4-**C,D** and in fig. 4.5-**C** on the enlarged phase sections. The metrics for our data – trial lengths, imputation sample sizes, etc. are given in section 4.3.1 above.

Use of non-dimensional units

When we computed a least-squares regression of input-output pairs, the computation involved quantities with different physical units – some were positions, some velocities and some angular velocities. If left in these dimensional units, the choice of units would dictate the numbers in the components of the input-output pairs. The least-squares regression treats errors of equal numerical magnitude as equally significant. Thus, if the choice of units remained arbitrary, it would both dictate the metric with respect to which errors are measured and may cause the matrices produced to have poor numeric conditioning.

All the data we used for regression came from residuals with respect to a limit-cycle model. We chose new units of measurement by taking all our trajectories and subtracting the limit-cycle model from each. We grouped the residuals thus obtained into collections partitioned according to their physical units: positions, velocities and time (angular velocity). We used the standard deviation of each collection of numbers as the unit of measurement for that collection. This ensured that all computations use numbers of the order of magnitude of 1, and that at least to the extent that all variables in the regression come from the same position-scale family of probability distributions, errors of equal magnitude in any coordinate correspond to equal likelihood. We refer to these renormalized and dimensionless units as *SD units*.

Multiple imputation used for regressing section maps

The typical stride duration of the animals was 55 samples on the treadmill and 22 in the preliminary arena data. We chose twenty evenly spaced sections of constant phase for examination as Poincare sections (fig. 4.4-**C**) and sectioned the state trajectories at these phases giving input-output pairs for the section mappings $\mathsf{M}[\cdot,\cdot]$. The number 20 was chosen because of our use of linear interpolation to section the trajectories – each section point derived from two adjacent data points. Had we used more than 20 sections, section points in adjacent sections would become similar due to the interpolation mechanism itself having used shared data. We discarded very short trials (shorter than 14 on treadmill and 19 in the arena) and imputed the mapping data from the remaining trials to be a constant size across all trials of each setup (28 on treadmill and

38 in arena). We kept unused input-output pairs for testing the predictive ability of the estimated maps (see section 4.6 for use of these prediction metrics). We combined the imputed samples and performed a linear regression step to estimate a single matrix for the input-output mapping of the combined trials. We repeated this imputation ("bootstrap") step multiple times, obtaining a collection of $\mathsf{M}[\theta, \phi]$ matrices for each pair of section phases θ and ϕ. We performed $N_S = 2187$ $(= 27 \times 27 \times 3)$ imputations for section maps and $N_R = 7290$ $(= 27 \times 27 \times 10)$ imputations for return maps[8].

We then chose a section to use for estimating template dimension. We collected the eigenvalues of the return map matrices of this section (the $\mathsf{M}[\phi + 2\pi, \phi]$ obtained from the regression) and plotted the distribution of their magnitudes. We compared these to the distribution of magnitudes obtained from both null hypotheses to find an estimate of the template dimension. We repeated this step for multiple sections to ensure a consistent result. The section 4.6 contains a more detailed presentation of the eigenvalue distributions we found and their interpretation.

Even when there is statistically significant evidence for a distinct set of "slow" eigenvalues, the associated eigenvectors may be very poorly known. When eigenvalues have *multiplicity* (that is, when there are multiple identical eigenvalues) the associated invariant subspaces have the dimension of the multiple rather than being distinct one dimensional invariant subspaces. When distinct eigenvalues are numerically close in value it may be very hard to distinguish them (and their unique associated one dimensional invariant subspaces characterized by a single eigenvector) from the case of multiplicity. In such situations, significant, multiple eigenvectors with similar eigenvalues may vary randomly from imputation to imputation within a neighborhood of the higher dimensional subspace that they jointly span across all imputations, making it difficult to individually identify them by comparing the outputs of multiple imputed estimates of the return map.

These common instances of apparent multiplicity require the estimation of their jointly spanned subspace of dimension $p > 1$ (this $p = 1$ for simple eigenvectors). The investigation leads to a consideration of the space of all subspaces of dimension p of a real vector space of dimension n (in our case, $n = 27$), which is the so-called *Grassman Manifold* $GR(n, p)$.

As an example, $GR(3, 2)$ – the space of all two dimensional planes in three dimensional space – can have each of its elements (the planes) represented by picking unit normal basis vectors for some x, y coordinates of that plane. This representation is non-

[8]We were estimating a 27×27 matrix. At least $27 \times 27 + 1$ estimates are required to bound a volume in the space of such matrices; we therefore imputed $N \times 27 \times 27$ times with $N > 1$ for each matrix being estimated.

unique just as the choice of directions for x and y is arbitrary. Similar representation of points by p basis vectors is possible for any $GR(n, p)$.

We developed a method analogous to circular statistics for establishing the statistical significance of a collection of subspaces represented by unit normal basis vectors. By looking at the distance in $GR(n, p)$ between an approximate centroid of the collection and the subspaces, we can establish whether subspaces are far from being randomly distributed or are tightly concentrated around some typical subspace. Previous research (Khatri and Mardia, 1977; Jupp and Mardia, 1979) defined parametric non-uniformity tests on $GR(n, p)$ against a multidimensional Von Mises-Fisher or Bingham alternative.

Averaging used to obtain unique map estimates

For each of the $190 = (20 \times 19)/2$ possible pairs of different section phases θ and ϕ, we obtained a single $\mathsf{M}[\theta, \phi]$ matrix by averaging the $N_S = 2187$ matrices produced in the regressions of multiply imputed (bootstrapped) input-output pairs for that choice of sections. Similarly, we averaged the $N_R = 7290$ imputed estimates of each return map. Simple element-by-element averaging may corrupt the geometric structure that distinguishes the slow eigenvalues, their associated eigenvectors, and the resulting invariant subspaces of the underlying dynamics. This would be almost certain to happen whenever the subspaces spanned by putatively slow eigenvectors are not concentrated very near some centroid on $GR(n, p)$ and are therefore not sharply concentrated in the space of all possible subspaces.

Prior to averaging, we tested each collection of matrices to ensure that averaging would not corrupt the results by comparing element-by-element averages of a sub-sample with a geometrically computed average of that sub-sample. Several algorithms could be used for subspace averaging when element-by-element averaging fails (Absil et al., 2004). We adopted a simple approach using a gradient solver (**SciPy.optimize.fmin**) in a local coordinate chart of $GR(n, p)$ at an approximate centroid.

Floquet structure reconstructed from eigenvectors using section maps

By using accurately determined section maps, we propagated eigenvectors of a return map to all phases, thereby providing a numerical description of Floquet modes. We computed the Floquet axes $P(\phi)$ by multiplying these modes with an increasing matrix exponential that canceled the contraction associated with the eigenvalues[9]. The

[9]Negative real eigenvalues in the return map and complex conjugate pairs raise particular difficulties here.

result is the Floquet frame: a periodic matrix of eigenvectors given as a function of phase.

Setting a given activation to unity represents a unit perturbation in the direction of the related Floquet axis at every phase. We computed the impact of this unit perturbation on the centre of mass position by integrating its effect from onset through its exponential decay to time infinity (see section 4.7.2 for details). For a deterministic system, Floquet theory guarantees that this impact on centre of mass motions will act independently and additively with the impact of other activations.

4.4 Results

We first report on the template dimension revealed by the data, then reconstruct its local representation from the data, and finally use that representation to explore the impact – that is, the effective body maneuver – associated with some of its degrees of freedom.

Summarized in brief, we discovered that the dimension of the template in horizontally running cockroaches on a treadmill was six. The direction of phase (whose eigenvalue is 1) and five Floquet modes which decay at a rate of 0.5 or slower per stride. We found the same dimension in a set of control experiments in which animals were allowed to run freely in an arena. We found that the direction of the five dimensional Floquet frame axes was very sharply concentrated in the space of all possible five dimensional directions, allowing directions tangent to and transverse to the template to be clearly distinguished. In fig. 4.1 this corresponds to having found that the surface of the template (dark gray ring) is very flat (has consistent tangent directions) next to the orbit, making the differentiation between template and posture error (light gray surface) directions possible. Having conclusively distinguished the template in terms of both its dimension and the directions tangent to its surface, we proceeded to compute the Floquet axes and the impacts associated with the Floquet modes. The slowest mode in the template, decaying at 0.8 per stride, had little effect on center of mass motion. We offer some speculative comments on its possible "utility" in the Conclusion. All three of the next slowest modes had eigenvalues close to 0.63 (0.66,$0.61+0.06i$,$0.61-0.06i$). Equality in eigenvalue – the case of multiplicity described above – implies that these comprise a single three dimensional subspace which cannot be further decomposed into a span of uniquely selected lower dimensional subspaces and must be treated as a unit by means of the Grassman manifold estimation procedure outlined above. We suggest, via computing mode impacts, that the estimated subspace is associated with changes in fore-aft speed, and with two mechanisms for body heading that differ in the overall

lateral motion they produce. The fifth Floquet mode in the template, with decay rate 0.48 per stride, is again associated with changes in fore-aft speed.

4.4.1 Eigenvalue magnitudes and the dimension of a template

For each imputed return map, we computed eigenvalue magnitudes and sorted them in increasing order, thereby giving every eigenvalue an ordinal number relative to the magnitudes of the other eigenvalues in the same return map estimate. We then plotted (see fig. 4.6) the one-sided $P = 0.05$ confidence interval for each ordinal of eigenvalue magnitude by taking the value of the 95th percentile of the distribution we obtained from multiple imputation. This simple method of confidence interval estimation is often called a "bootstrap confidence interval" (Politis, 1998).

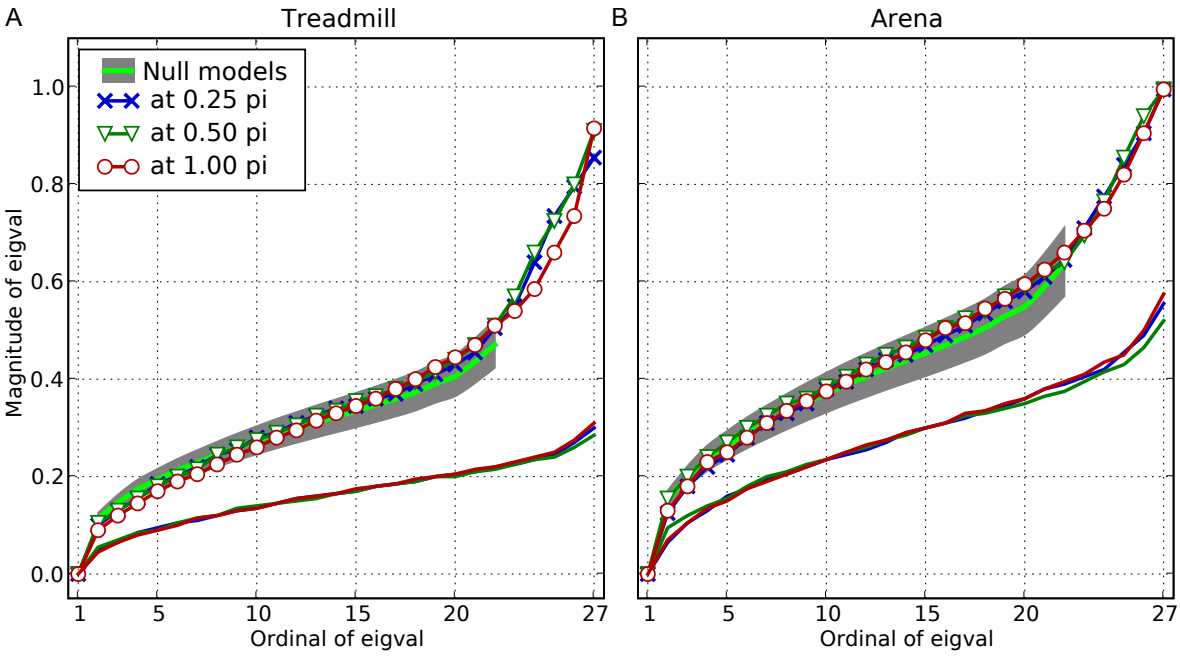

Figure 4.6: Statistics of eigenvalue magnitudes. Abscissa represents eigenvalue ordinal when sorted by magnitude. Ordinate represents eigenvalue magnitude. All colored lines plot magnitudes such that 95% of the eigenvalues with that ordinal are smaller. We conducted analysis at three phase sections $\pi/4$, $\pi/2$, π (represented by line color and marker) for both datasets (Treadmill in **A** and Arena in **B**). Thick gray line shows the $H_{0(a)}$ null hypothesis model that most closely fit to the eigenvalue magnitudes from the experiment. The model was a Circular Law distribution derived numerically from eigenvalues of random matrices of dimension 20. Gray band with green centerline show a one standard deviation range around the null model values (Note: model does not include smallest eigenvalue). Unmarked colored lines show $H_{0(b)}$ surrogate based null hypothesis eigenvalue magnitudes, which were considerably smaller than those from experimental results. The top five eigenvalues are larger than can be accounted for using a $H_{0(a)}$ null model (see also fig. 4.7). Also note that the initial zero eigenvalue is an inevitable feature of our computation – a reflection of the return along the cycle direction (normal to the section) - and does not refute either null hypothesis.

Let us provide an example to facilitate the interpretation Fig. 6. The point at ordinal 20, eigenvalue magnitude 0.6 of the arena data in fig. 4.6-**B** implies that when

sorted by magnitude, 95% of the 20th eigenvalues are smaller than 0.6. This implies, in turn, that at least as many of all eigenvalues smaller than the 20th are also less than 0.6, because in each imputed return map all eigenvalues with ordinals below 20 must have magnitude no larger than that of the 20th eigenvalue. Thus the point at (20,0.6) means it is only in at most 5% of the imputed return maps that we find more than 6 of the 27 return map eigenvalues larger than 0.6. This means that the point at (20,0.6) can be read as "the dimension of a template slower than 0.6 is seven at most with confidence $P < 0.05$". The template dimension implied in this example is seven and not six because six dimensions come from the return map directions we include in the template, and one dimension comes from phase. In the eigenvalue magnitude plots, the subspace associated with phase shows up as a zero eigenvalue, but in the dynamics it has an eigenvalue of exactly 1. The direction of the cycle, which is associated with the phase coordinate, is always part of the template.

Referring to fig. 4.1, when we distinguish the template surface from the posture error surface based on rate of recovery, the more of the dynamics we choose to associate with the template, the faster the fastest recovery rates in the template will be. The graphs in fig. 4.6 directly represent the trade-off between the dimension of a purported template and the fastest rate of recovery allowed for modes in that template, as computed from return maps at the sections $\pi/4$, $\pi/2$ and π.

The null hypothesis $\mathrm{H}_{0(\mathsf{b})}$ tests the effect of breaking down the causal association between return map initial states and final states. Instead of taking the state of an animal in a particular trajectory as an initial state, and mapping it to the state this same animal had a stride later, an $\mathrm{H}_{0(\mathsf{b})}$ surrogate maps that initial state to some state of an animal at the same phase as the original final state. The $\mathrm{H}_{0(\mathsf{b})}$ surrogates break down the causal input-output relationships in the data, but otherwise uses data with the same statistical properties. The change in fig. 4.6 in eigenvalue magnitude between the unmodified (marked colored lines) and $\mathrm{H}_{0(\mathsf{b})}$ surrogate (unmarked colored lines) is considerable – $\mathrm{H}_{0(\mathsf{b})}$ eigenvalue 95th percentiles are at less than 1/2 of the corresponding eigenvalue percentile in the unmodified treadmill data (fig. 4.6-**A**) and similarly at 2/3 of the corresponding eigenvalue percentile in the unmodified arena data (fig. 4.6-**B**). This gives evidence that eigenvalues are strongly tied to the causal relationship between the animals' states in consecutive cycles.

We decided the dimension of the template by solving a model selection problem. First, we found the dimension N of $\mathrm{H}_{0(\mathsf{a})}$ derived eigenvalues which best fits the observed eigenvalue magnitudes. Second, we took $a(k;\phi)$ to be the magnitude of the k-th eigenvalue (skipping the lowest eigenvalue of 0) of the return map at ϕ (one of colored lines in fig. 4.6-**A** or **B**), and $c(k;N)$ to be the magnitude of the k-th eigenvalue in a *Circular Law* distribution for matrices of dimension N. One should not

simply find the least-squares error between $c(k;N)$ and the corresponding $a(k;\phi)$ for two reasons. One, we expect some unknown scale factor $s(N)$ to be necessary, i.e. $s(N)c(k;N) \approx a(k;\phi)$.Two, because $a(k;\phi)$ are sorted, $a(k;\phi)$ is not statistically independent from $a(j;\phi)$ for $j \neq k$.

In our procedure, we first transformed our observations and the models to a form that was independent of the unknown scale[10] and removed the statistical dependence between $a(k;\phi)$ values (bringing them close to being i.i.d). We transformed:

$$a'(k;\phi) = \ln a(k+1;\phi) - \ln a(k;\phi),\ k = 1 \ldots 25 \tag{4.1}$$
$$c'(k;N) = \ln c(k+1;N) - \ln c(k;N),\ k = 1 \ldots N-1 \tag{4.2}$$

thereby making $a'(k;\phi)$ independent of each other[11] and of the unknown scale $s(N)$. We computed $a(k;\phi)$ for all 20 sections, taking the sum of squares error in all:

$$err(N) = \sum_{\phi} \sum_{k=1}^{N-1} \left(a'(k;\phi) - c'(k;N)\right)^2 \tag{4.3}$$

In terms of fig. 4.6, the model selection criterion we used consisted of taking the best $\mathrm{H}_{0(\mathsf{a})}$ model at each order (gray band width green line) and examining the sum squared error between it and the animal data (lines with markers). Typically, such a naive model selection criterion is insufficient because as models are fit to more and more data (increasing N) the error grows, leaving the investigator to decide on some rational means of penalizing models with more free parameters (in our case, $25 - N$ is the number of *free* parameters, because we make no assumptions about the eigenvalues of significant dynamics except for their lower bound). Fortunately, in our case the larger N models fit the data so much better than those with small N that total squared error decreased with the increase in N (see fig. 4.7), only to sharply increase when the noise subspace dimension grew beyond 21. We did not find such an increase in the eigenvalue magnitude distribution of the surrogates (testing the $\mathrm{H}_{0(\mathsf{b})}$ null hypotheses) for which the fitting error continued to decrease until the dimension reached its maximal value[12].

[10] "pivotal" in statistical terms, i.e. independent of those unknown parameters of the probability distribution that we are not interested in.

[11] The statistically astute reader no doubt realizes that the lower and upper bounds $0 < a(k;\phi) < 1$ imply that some dependence still remains among the largest and among the smallest k values. However, this dependence is much weaker than that induced by sorting.

[12] Note that in our model selection process we identify the template with the significant dynamics sub-space, and conflate the template's complement with the noise sub-space.

We therefore conclude that the animal data has a 21 dimensional subspace in which the dynamics are noise-like, and the remaining 6 dimensions , unaccounted for by the null model, must be attributed to the template. Such a separation is not evident in the $H_{0(b)}$ surrogates, implying that the separation is due to the stride-to-stride causal structure in the animal data.

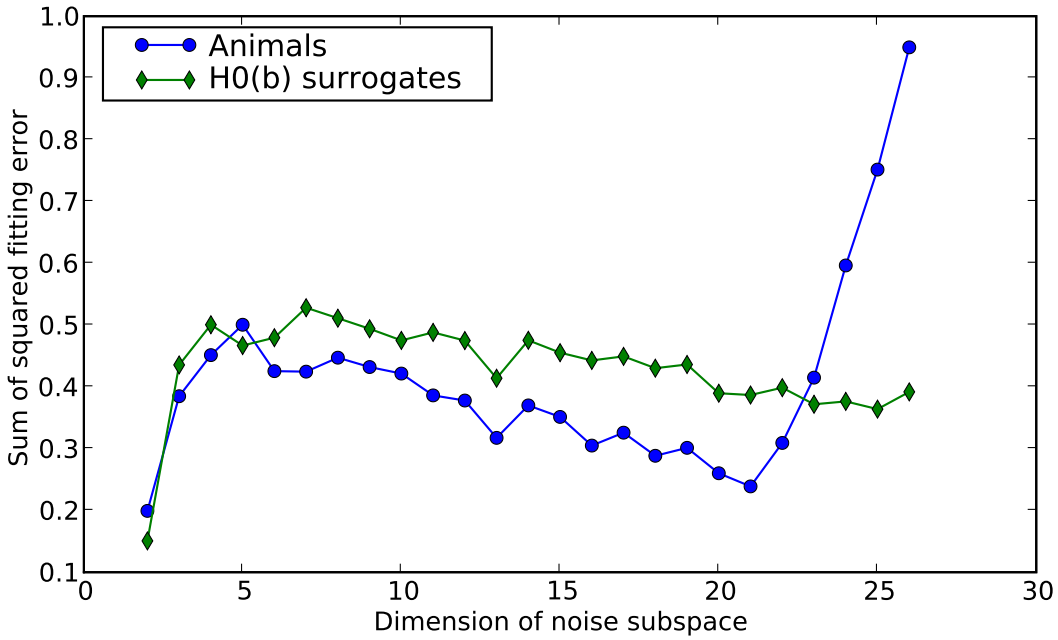

Figure 4.7: Sum of squared differences between random matrix (null hypothesis $H_{0(a)}$) eigenvalue magnitudes and corresponding eigenvalue magnitudes from animal data. We computed the 95th percentile of eigenvalue magnitudes by ordinal (as plots in fig. 4.6), symbolized by $a(k;\phi)$, and converted these sequences of numbers to the form $a'(k;\phi)$ as described in eqn. 4.1. This form is suitable for comparing *Circular Law* distributions $c(k;N)$, which were similarly transformed to $c'(k;N)$ for this purpose. Graphs show the fitting errors $err(N)$ of eqn. 4.3 for animal data (blue line with circle markers) and surrogate data with input-output pairing randomized (as per null hypothesis $H_{0(b)}$; green line with diamond markers). Results show the best fit noise dynamics dimension is 21, implying a template contained in the complementary subspace to the noise has dimension is 6 $(= 27 - 21)$.See section 4.6 for further discussion of eigenvalue distributions.

We concluded that the dimension of the significant dynamics was six, with one dimension tangent to the limit cycle and five dimensions transverse to the cycle and associated with the five largest eigenvalues of the return maps. We have found that the template surface (dark gray ring; fig. 4.1) is six-dimensional. One dimension is along the axis of the ring (tangent to the cycle), and five other linearly independent directions spanning the ring width. The remaining 21 linearly independent directions point outside the template (ring) surface and are thus posture error directions.

From fig. 4.6, we obtained an estimated lower bound on the magnitude of the eigenvalues of the template. Rounding to one decimal place, the largest five eigenvalues are larger than 0.5 in 95% of the imputed return maps. The dimension of the noise subspace in surrogate data (randomizing input-output pairing to test the $\mathsf{H}_{\mathsf{0(b)}}$ alternative) was that of the full space. We therefore concluded that the six-dimensional dynamics we found truly represent a causal effect allowing the animals' state to be predicted stride to stride.

We observed the same excursion towards larger eigenvalues in the five slowest modes of the arena control data fig. 4.6-**B** as we did in the treadmill data fig. 4.6-**A**. We produced the arena data from a single animal which ran freely (7 trials, $n = 204$ strides). The similarity between the eigenvalue magnitude distribution found in a single animal (fig. 4.6-**B**) and that found from data combined from multiple animals (fig. 4.6-**A**) supported the notion that our main results in fig. 4.6-**A** are a consequence of individual animals having such an eigenvalue structure, rather than the observed structure being a computational artifact of inter-animal variability.

All subsequent results reported were computed from treadmill data alone.

4.4.2 Template subspace of the Poincare section

Our analysis of the eigenvalue magnitudes lead us to deduce the presence of a six dimensional template with five of those dimensions being transverse to the cycle. Before proceeding to attempt reconstruction of Floquet modes, we tested whether the template itself is clearly distinguished statistically. In fig. 4.1, we set out to test whether the directions tangent to the template surface are clearly identified, and thus distinguishable from their complement, the directions of the posture error surfaces. It is entirely possible to have obtained template eigenvalues that are significant by our previous tests, but have eigenvectors that are so inconsistent that no partition of space into template and non-template directions would have been statistically justified[13].

[13]For example, every 90° rotation matrix in three dimensions will have an identical set of eigenvalues: 1, i and $-i$. Consider the collection of such matrices whose axes of rotation are uniformly distributed on

The problem of identifying whether a collection of subspaces has a distinguished direction is a multidimensional generalization of directional statistics (Khatri and Mardia, 1977; Jupp and Mardia, 1979). For example, testing whether a collection of animal velocities align along a statistically significant 3D direction is a test of whether a collection of 1D subspaces – the lines parallel to these velocities – have a preferred direction. The subspaces, whose directionality we wished to confirm, were those spanned by the eigenvectors associated with eigenvalues that we attributed to the template. Each imputed return map provided us with five such eigenvectors.

We used a test based on measuring distance between directions of subspaces as points on the Grassman manifold $GR(26, 5)$. The measure of distance we used is the arc-length distance, also known as the geodesic distance (Edelman et al., 1998, section 4.3). First, we found an approximate centroid from our collection of sub-spaces using a method inspired by Eppstein and Wang (2001) and implemented by iteratively selecting for high centrality points by finding the most central point with respect to randomly selected partners. Then, we measured the distances between the approximate centroid and the other subspaces found from our data and compared to distances between the centroid and randomly chosen subspaces. The distances from the centroid in our data subspaces were 1.44 ± 0.26 (mean,SD), whereas the distances to random subspaces were 2.70 ± 0.26 and distances between orthogonal subspaces are 3.51. In 100,000 randomly generated subspaces, the closest we came to the centroid was 2.17, suggesting that the directions of subspaces found in animal data occupy less than the 10^{-5} fraction of the space of all possible 5 dimensional directions in 26 dimensional space. We conclude that template directions are sharply concentrated.

Reconstruction of Floquet modes

We averaged the matrices created by multiple imputation to obtain a unique estimate of the section map between each of the $190 = 20 \times 19/2$ pairs of the 20 phase sections. We then used the eigenvectors of the 10 largest eigenvalues of each return map to generate 10 of the 27 axes of the Floquet frame. The choice of ten eigenvalues was motivated by the observation that as eigenvalues grew smaller, resulting Floquet axes became less and less consistent. We wished to examine all modes of the putative template, and a few modes beyond. The 10th largest eigenvalue was approximately of magnitude 0.4, thus associated with modes that decay by a factor of 2 in less than a

the sphere. Although each matrix has distinct invariant sub-spaces of dimensions 2 and 1 representing the plane of the rotation and its axis, no such splitting makes sense for the the entire collection of matrices, which is a maximally inconsistent outcome for matrices with identical eigenvalues in a three dimensional (as opposed to 27 dimensional) ambient space.

stride.

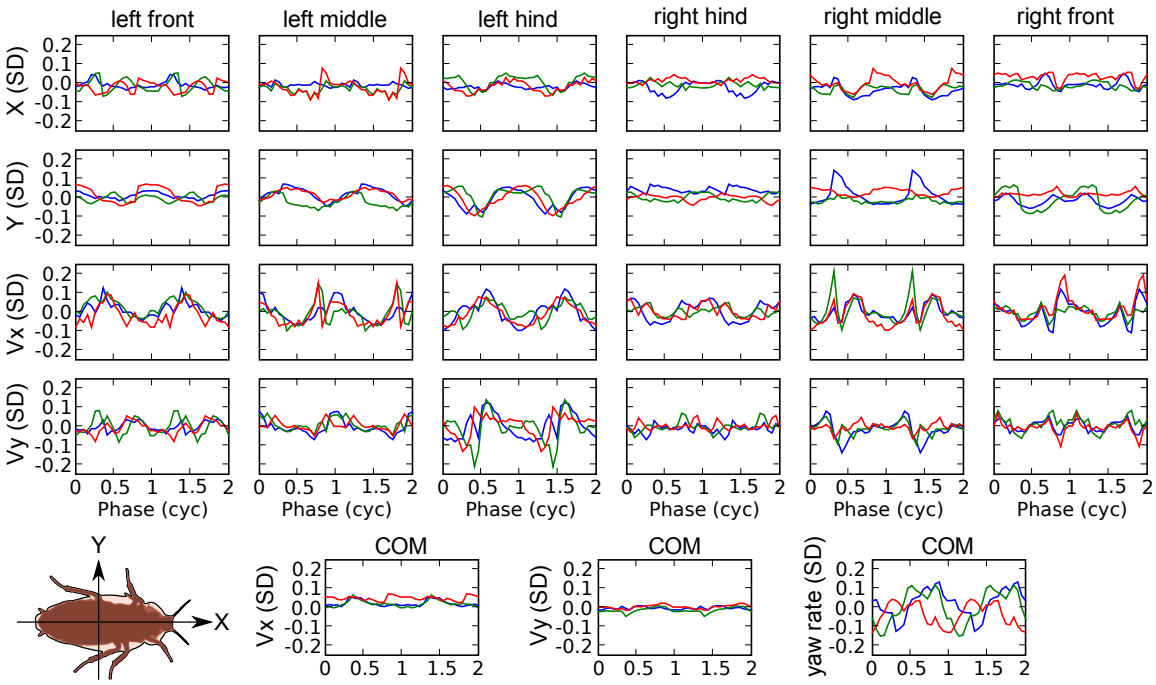

Figure 4.8: Floquet axis associated with the largest eigenvalue as a function of phase

Description of fig. 4.8

Floquet axis associated with the largest eigenvalue as a function of phase.

We plotted two consecutive strides to make the periodic nature of the components of the Floquet axis vector more obvious. The horizontal range of the plots spans 0 to 2 in units of a cycle (stride). Each panel presents the plot of one of the 27 state variables we used. With respect to fig. 4.2 these plots show the breakdown of the vector $p_1(\phi)$ – the axis of the phase-dependent Floquet frame tied to the largest return-map eigenvalue – with one element of the vector plotted against phase in each panel. The panels refer to positions and velocities of all six tarsi, ground velocity of the center of mass, and yaw rate (time derivative of body orientation). Plots of tarsi data are arranged in a grid: columns correspond to legs (label at head of column) and rows are X and Y positions and their velocities V_{x} and V_{y} (axes shown on cockroach schematic). Plots of COM data are individually labeled. The ordinates are in SD units (non-dimensional units; see section 4.3.4 above).

The plots show, for example, that an increase in left-hind leg lateral motion peaking at phase 0.5 cycle is associated with fore-aft velocity changes in the right-front leg at phase 0.9 cycle. different phases. The three different lines in each plot correspond to Floquet axis estimates constructed by starting with return maps at three arbitrarily selected phases: 1.7 (green), 3.6 (blue) and 5.3 (red). If these three estimates were overlapping and smooth (as is the case for noiseless simulation data), we would have near certainty that the Floquet axis was correctly resolved from the data; if they were very dissimilar, we would conclude that the Floquet analysis procedure failed to recover the axis. Our results lie in between these extremes.

We plotted the phase varying physical (kinematic) axis of the Floquet mode associated with the largest (non-unity) eigenvalue, computed from three different starting sections (fig. 4.8). In an ideal noiseless system, the choice of phase section used for starting the construction of the Floquet axes would not matter, and the resulting axis vectors would be smooth functions of phase at all phases for which the system itself is smooth.

The plots in fig. 4.8 demonstrate that neither property holds, even for the axis associated with the largest (non-unity) eigenvalue and is thus expected to be the most robust with respect to measurement noise. The resulting axis changes as a function of starting section (difference between line colors), and is not entirely smooth. We found that Floquet modes with nearby eigenvalues that we computed by starting at different sections were more correlated to each other than to modes with very different eigenvalues, leading us to conclude that the expected self-consistency of the Floquet axis estimation was not lost. Details of the numerical test used are relegated a future publication. We conclude that the Floquet axes we recovered do represent an actual feature of the dynamics of the animal, but their detailed structure should not be

considered reliable.

Impact of template modes on the center of mass

We restricted our analysis of Floquet mode impact to the slowest five modes - those which putatively belong to the template. We computed all five independent modes starting from the same base section. Although the Floquet axes we obtained starting from other sections were differed as functions of phase, we arrived at similar conclusions with regards to the control capabilities the template as a whole provides.

We hypothesized that the slowest Floquet modes make up the "target of control" (Full and Koditschek, 1999), and therefore computed the effects that activating a mode and letting it decay naturally would have on the center of mass motions. fig. 4.8 shows that the Floquet mode it presents is associated with changes to the centre of mass velocities (seen in the last three coordinates). This particular mode is associated with a slight increase in forward velocity that is localized to phases near 0.4 of a cycle. Whenever this Floquet mode is active, the animals are running faster than average for our data, with this speed change being apparent in only that fraction of the cycle in which the COM V_x plot in fig. 4.8 is significantly removed from zero.

The overall impact such a change induces on the center of mass can be computed by integrating the Floquet mode, i.e. by integrating the decaying exponential that represents its effect on the COM (see detail in section 4.7). Because of the increased variability in our estimates of Floquet modes with smaller eigenvalues, we have chosen to compute the impact of each Floquet mode averaged over a quarter cycle centred around four key phases: landing, mid-stance, liftoff, and mid-swing, where these names are taken with respect to the animals' right tripod.

The results are summarized in table 4.5.3. The table shows the integrated impact of each mode, together with the eigenvalue of that mode[14]. To further simplify the interpretation of the table, we have marked magnitudes larger than 1.0 in boldface, and struck out magnitudes smaller than 0.3.

The modes 2, 3, and 4 had very similar eigenvalues. As a consequence, our analysis procedure would have selected a random basis for the three-dimensional space these modes jointly spanned. We, therefore, analyzed the modes together, and searched for a basis for this subspace that would make interpretation easier. Taking the modes in the table to be M_2, M_3 and M_4, we changed coordinates to $Q_1 1 = 0.54M_2 - 0.44M_3$; $Q_2 = 0.96M_2 + 0.79M_3$, and $Q_3 = 1.17M_2 - 0.81M_4$. The impacts of modes Q_1, Q_2

[14]Note that without reconstruction of the Floquet modes as a function of phase, the impact cannot be computed. It is not a consequence of any single eigenvalue or eigenvector, but rather a result of how the Floquet axes project into the COM velocities as a function of phase.

and Q_3 is given in table 4.5.3. The change of coordinates within the three-dimensional space spanned by these Floquet axes allows it to be expressed in terms of a new set of modes Q_1, Q_2 and Q_3 that have a simple interpretation: $Q1$ acts only on the COM fore-aft position and represents a speed change; Q_2 and Q_3 act primarily on heading and represent steering. Q_2 and Q_3 differ in the associated magnitude of lateral motion for a given heading change.

4.5 Discussion

4.5.1 Signature of a Template with six dimensions

Floquet analysis revealed a numerical simple model or template representing the animal's natural dynamics derived from kinematic data, not created by an investigator based on physical intuition. The template had six dimensions or modes. When activated these six modes recovered slowly and are likely to be actively controlled by neural feedback (Full et al., 2002). By contrast, when the other twenty one modes were activated, recovery was rapid. Identification of rapid recovering modes could lead to a better understanding of the mechanical system's response to perturbations, because recovery may rely more on passive, dynamic self-stabilization.

More specifically, our results showed that the eigenvalue magnitude distribution of the return map matrices generated from cockroaches running on a treadmill can be most parsimoniously attributed to a random matrix $\mathrm{H}_{0(\mathsf{a})}$ model for 21 of the 26 smallest eigenvalues of the return map at all sections tested (fig. 4.6; fig. 4.7). In contrast, no higher dimensional random matrix model can extend to fit the final 5 largest eigenvalues (fig. 4.6-**A**). We interpret this excursion towards larger eigenvalues as indicating the presence of a regular, deterministic dynamical structure of state variation and recovery in the steady-running regime. Such a dynamical structure comprised the signature for a template in the kinematic data.

We found a similar excursion in the eigenvalues of a single, typical individual running in an arena (fig. 4.6-**B**). We collected arena kinematics using a vastly different measurement system from that used for the treadmill data. We interpret the presence of a similar signature in the data of an individual animal as indicating that this signature is neither an artifact of any particular aspect of the treadmill measurement apparatus, nor an artifact of the multiple imputation procedure we used to combine the data from multiple treadmill trials. We are left with the conclusion that the template signature we discovered is a feature of the dynamical processes of individual running animals, as a template is expected to be.

The surrogate $H_{0(b)}$ data formed by randomly scrambling the input-output association between pairs of state measurements tagged with the same phase produced an eigenvalue distribution that can in its entirety be most parsimoniously attributed to a random matrix. This contrast with the deterministic structure exhibited by the properly associated input-output pairs increased our confidence that the top 5 eigenvalues should indeed be attributed to the presence of a template revealed by the return map data. We thus conclude that a template of dimension 6 was present in the 27 dimensional dynamics of the tarsi and center of mass. Our conclusion is consistent with the Templates and Anchors Hypotheses proposed by Full and Koditschek (1999), specifically by asserting the existence of 5 independent modes of perturbation transverse to the cycle that persist longer (decay more slowly) than one would expect at random. With confidence of 95 percent, we assert that these modes decayed more slowly than 0.5 per cycle, and as a computational fact, we point out that this decay rate was more than two standard deviations slower than could be produced by a random stochastic process of the kind posited as the $H_{0(a)}$ null hypothesis.

4.5.2 Template direction distinguished from posture error directions

The presence of a clear template signature in the distribution of eigenvalue magnitudes does not in itself guarantee that our data must distinguish the associated directions of slower recovery to the limit cycle, as would be required to reconstruct the template's dynamics near the limit cycle. However, we established that these directions – the collection of candidates for the linearized approximating surface arising from the local recovery patterns associated with the template – are very sharply concentrated, filling up a volume of less than one thousandth of a percent of the total volume in the space of possible directions. For example, on a sphere this would be equivalent to a cone of directions 0.72 degrees wide. We conclude that the template subspace we found in the tangent space over the limit cycle was statistically significant, and that it may therefore be feasible to try and reconstruct the local template dynamics over the associated low dimensional surface. We know not only that the dimension of this template surface is 6 but that, statistically speaking, we can separate the directions tangent to that surface from those that correspond to posture errors (fig. 4.1; thick dark loop with arrow versus the light gray vertical wall perpendicular to the template band).

4.5.3 Slowest Floquet axes found to limited precision

Having discovered the template subspace in a return map is equivalent to finding the red and blue arrows on the ϕ section of fig. 4.2. The plots of fig. 4.8 depict, coordinate-by-coordinate in the physical kinematic coordinate system of tarsi positions and velocities and body orientation and translational velocities, the phase-varying entries of the (first of five) $p_1(\phi)$ Floquet modes. In each plot, the abscissa represents the phase (the fraction of completion along a $o(\phi)$ cycle; plots are two cycles long) at which the vector to $p_1(\cdot)$ is plotted in the normalized SD units (introduced in the methods section). The three distinctly colored curves correspond to p_1 trajectories initiated at three different sections (i.e. computing the chain of $\mathsf{M}[\phi, \theta]$ eigenvectors starting at different initial ϕ values) as may be envisioned geometrically by trying to obtain the blue surface starting with the blue arrow at some section, say θ_1, and comparing it to the surface obtained starting with the arrow at sections θ_1 and θ_3. In this case, the three distinct values of initial phase correspond to: 1.7 (green), 3.6 (blue) and 5.3 (red).

The imperfect correspondence between these three traces of the putative first Floquet axis components suggests that in computing them, we are reaching some limit precluding our further ability to resolve their structure. Numerical experimentation with simulated Floquet systems of comparable dimension suggests that our methodology requires further improvements in dealing with measurement noise. We have already presented successful application of the same algorithm to simulated systems of dimension 4 (Revzen et al., 2009) in which such inconsistencies were not found.

We caution against attempting to draw any conclusions from the shapes of the Floquet axes unless the results are more consistent by at least two metrics. First, Floquet modes of a smooth system are expected to be smooth. Second, Floquet axes should be similar irrespective of the section from which they were constructed. This latter property is associated with the accuracy with which the $\mathsf{M}[\cdot, \cdot]$ matrices do indeed satisfy the expected conjugacy relationships (see section 4.7 for further details). The development of estimation methods that enforce and utilize the required self consistency may be fruitful subject for further mathematical research.

In our results, Floquet axes computed starting from different base sections showed cleart similarity. The process of computing the impact of a Floquet mode averages the effects of that mode over the duration of its decay, and is therefore less sensitive to noise as function of phase than the computation of the Floquet axes themselves. We have also averaged these impacts over quarter-cycles of onset phases, thereby decreasing such sensitivity further. Although the results obtained in table 4.5.3 and table 4.5.3 are suggestive, they do not arise from statistical methods as well established as do the

results establishing template dimension and tangent directions. Further development of data driven Floquet analysis would benefit from a detailed statistical treatment of the question of impact variability and reliability.

Our preliminary development of the methods can no doubt be superseded by more capable means of studying these same datasets. At this time, we know of no theoretical treatment that provides a statement of the fundamental limitations of the Floquet analysis procedures we have used. It is unclear whether the greatest benefits will come from methodological improvements in data collection or from improvements in the analysis procedures themselves.

Table 4.1: Maneuvers induced by the Floquet modes of the template

	Mode#	1	2	3	4	5
	Decay rate	0.78	0.66	0.61	0.61	0.48
fore-aft	Lift	—	1.55	-1.96	2.28	-1.66
	Swing	—	1.50	-1.95	2.16	-1.55
	Land	—	1.61	-1.91	2.30	-1.59
	Stand	—	1.70	-1.91	2.41	-1.67
lateral	Lift	—	—	0.48	-0.74	—
	Swing	—	—	0.47	-0.67	—
	Land	—	—	0.49	-0.80	—
	Stand	—	—	0.51	-0.86	—
heading	Lift	—	0.88	0.88	-0.60	—
	Swing	—	0.72	0.59	-0.57	—
	Land	—	1.03	1.00	-0.59	—
	Stand	0.41	1.18	1.27	-0.64	—

The detectable presence of a template – a deterministic, low dimensional, slow dynamics whose structure emerges above the noise floor – implies the presence of a low dimensional set of slowly decaying Floquet modes. The activations of these modes persist for a relatively long time, and can therefore have potentially large impacts. Because these modes are slow, their impact integrals average the phase dependent effects of the Floquet mode over a long period of time, and are thus rather insensitive to noise in the estimate of the Floquet axes at any given section phase. Nevertheless, the results depend on the onset phase at which the perturbation was induced in a manner that generalizes the way in which the familiar "phase response curve" (Winfree, 1980; Glass and Winfree, 1984) varies with phase. In table 4.5.3 and table 4.5.3 we reported the impacts of the slow modes averaged over biomechanically meaningful quarter cycles.

These impacts should be interpreted with care, as the underlying Floquet axes do not clearly meet some self-consistency checks. We consider the following impact analysis as interpreting a hypothesis of the shape of the Floquet axes, its consequent impacts of various modes and its implications for their role in control, rather than drawing conclusions from conclusively proven estimates of the Floquet axes.

The greatest surprise in our Floquet mode results was that the slowest mode seems unrelated to maneuver, and its impact has little to no discernible magnitude effect on the COM. There is some anecdotal evidence that *Blaberus discoidalis* cockroaches sometimes run in a reared up posture (e.g. when anticipating an obstacle (Watson et al., 2002)), and sometimes run more parallel to the ground. Such a pair of related gaits could account for the existence of a slow Floquet mode that is unrelated to maneuver; this remains a topic for future investigation.

The next three slowest modes must be construed as representative of a multiplicity-3 invariant subspace – that is, the subspace in the tangent space over the limit cycle spanned by those modes is "irreducible" algebraically and introduces impacts that operate at the same timescale. With a change of basis to this sub-space, these three modes achieve the impacts summarized in table 4.5.3.

Table 4.2: Second, third and fourth modes, after coordinate change

	Mode#	Q_1	Q_2	Q_3
fore-aft	Lift	1.70	—	—
	Swing	1.67	—	—
	Land	1.71	—	—
	Stand	1.76	—	—
lateral	Lift	—	0.38	0.60
	Swing	—	0.37	0.54
	Land	—	0.39	0.65
	Stand	—	0.40	0.70
heading	Lift	—	1.54	1.52
	Swing	—	1.16	1.30
	Land	—	1.78	1.68
	Stand	—	2.14	1.90

4.5.4 Template mode impacts suggest a unicycle-style of mobility affordance

Empirical estimates of eigenvalues from trajectories of systems with unit eigenvalues, estimated by least squares regression as we have done, are not expected to have unit magnitude. A contraction of unit eigenvalues into the unit disc (decreasing their magnitude) is an inevitable consequence of trial selection. Any quantity governed by a unit eigenvalue maintains its state indefinitely, and as a consequence evolves as a random walk in a system subjected to noise. For systems whose states are perturbed with Gaussian noise, this implies a growth proportional to $t^0.5$, and is therefore unbounded. In truncating experiments (e.g. by discarding experiments where animals contact the sides of their cages) experimentalists prevent such unbounded growth and inadvertently scale down the magnitudes of unit eigenvalues.

The combined effects of the three Floquet modes 1, 2 and 3 allowed the animals to change speed and heading, producing similar changes in these variables irrespective of the phase of activation. Considering the impacts of these modes as representing an animal's potential affordance via template adjustment over its absolute world-frame state, the resulting perturbed motions resemble the changing fore-aft speed and heading angle characteristic of a unicycle. Such a "unicycle-like" affordance is consistent with the expectations one would derive from the lateral leg spring (LLS) template of horizontal running (Schmitt and Holmes, 2001), which has both velocity and heading associated with unit eigenvalues. Our results support that some of the slowest modes obtained through numerical Floquet analysis (modes 2, 3 and 4) provide the same function as the unit eigenvalue modes of the lateral leg spring template. The change from magnitude 1 eigenvalues in the theoretical model to magnitude 0.66 eigenvalues in our results may be attributed, at least in part, to our choice of methods for eigenvalue estimation.

Characterizing the cockroach's horizontal plane mobility as unicycle, with fore-aft speed and heading control inputs, has already been successful in generating useful biological predictions. Specifically, the requirement for phasic feedback when cockroaches perform a wall following behaviour, in which they run along a wall while dragging an antenna on its surface and use the tactile sense this affords to maintain their distance. Cowan et al. (2006) and Lee et al. (2008) use a unicycle model for cockroach running to derive their predictions.

4.5.5 Phase independence of Floquet mode impact simplifies control

We consider the implication of interpreting the activations of modes 2, 3 and 4 as control inputs for a unicycle. These inputs produce a consistent offset in the centre of mass motions irrespective of the phase of activation. Sponberg et al. (2009) showed that the combined phasic and tonic response from cockroach antennae closely matches the requisite controller output of the wall following controller predicted in Cowan et al. (2006). We propose that the signals from the antennae could be converted directly to a positive or negative activation of the relevant Floquet mode, i.e. that the Floquet modes function as the target of control for wall following, with the proportional-derivative control implemented in the antennae themselves.

More generally, we put forth the hypothesis that control in rapid behaviors takes a particularly simple form. We propose that control requires changes in the activation of only a few Floquet modes, these modes being among the slowest modes, and having impacts indifferent to activation phase. This hypothesis is an experimentally testable elaboration of the statement that "templates are a target of control" from Full and Koditschek (1999).

We further suggest the possibility that templates are a desirable target of control not only because of the simplification inherent in reducing the dimension of the problem. Slower modes associated with the template will often possess the property of having less sensitivity to onset phase in their long-term impact. Thus controlling the dynamics in terms of activation of slow modes may simplify the control by requiring less context, and less neural computation, for production of a predictable outcome.

4.5.6 Future directions for data driven Floquet analysis

A natural language for rhythmic movements

Floquet modes express in local linearized form the stride-to-stride integrated dynamics of the underlying nonlinear musculo-skeletal system on the body's absolute world-frame state. As such, they describe to first order the native toolbox of independent maneuvers that these dynamics offer. By using methods such as we have applied herein, investigators can present a moving animal in terms of the intrinsically defined Floquet mode activations which express the natural dynamics as a locally linear superposition of independent effects.

The hypothesis that similar locomotor templates recur in multiple animal taxa (Dickinson et al., 2000) may be further refined into the statement that animals present

a similar set of useful Floquet modes with large eigenvalues, and that from a dynamical perspective these form the basic channels of mobility affordance through which control is exercised. We propose to explore whether individual Floquet modes persist with little modification across functionally and morphologically related behaviors, or persist across morphologically similar taxa. As animals learn to execute locomotor behaviors with underlying templates, the Floquet modes may form building blocks from which templates are constructed: their causal independence recommends them as natural targets for motor learning.

Active motor control

We would like to encourage the interpretation of the Floquet structure not merely as an alphabet of independent pathways of perturbation recovery. If, through some mechanism outside the dynamics used for reconstructing the Floquet structure (e.g. volitional changes), the activation of a mode is held constant instead of being allowed to decay back to zero at its eigenvalue defined rate, this activated state can be seen to be a new limit cycle, shifted from the original cycle along the Floquet axis of that mode. As a consequence of linearity, the convergence of the remaining modes is unaffected (activations decay independently of each other), except that the limit cycle itself has changed.

Seen in this light, it is mathematically straightforward to interpret persistent activation of Floquet modes as a means of modulating an equilibrium point control trajectory (Jaric and Latash, 2000). The closer the eigenvalue magnitude of the mode is to unity, the smaller the change required to keep the Floquet mode activation from decaying. This suggests that the slow Floquet modes comprising the template prescribe the space of equilibrium point trajectories the animal can adopt with only small changes to its dynamics.

The relationship between the Floquet analysis approach and optimal control theory (Todorov and Jordan, 2002) is far from obvious despite the vast amount of related mathematical tools in both fields. Data driven Floquet analysis allows motions of animals to be re-written as simple, independently decaying activations. Optimal trajectories would remain optimal even when written in terms of Floquet mode activations. The causal independence of Floquet modes requires that individual modes be solutions of the optimal control problem – otherwise the optimal controller would mix the Floquet activations. A study of optimal control along the lines of Nagengast et al. (2009), but applied to a rhythmic task, may reveal whether Floquet modes are indeed optimal with respect to some well-defined cost functional.

Revealing mechanisms of maneuver

The most obvious utility of Floquet analysis is in its ability to relate changes of posture and excursions within the template to changes in center of mass motions at a later part of the same or later cycles. This begs its application to datasets of those animals whose means of control is unclear, in hopes of producing candidate maneuvers. Our experience suggests that long trials and high signal to noise ratios are particularly important for this analysis.

There is no fundamental reason to restrict the data subjected to Floquet analysis to kinematic variables. Our reasons for making this choice were of expedience, considering the difficulty of collecting large volumes of data. If similar methods are applied to data including muscle activation, kinematic and dynamic information, the process may reveal some of the causal relationships between changes in muscle activation and maneuver that have so far been very difficult to substantiate.

Opening new behaviors to investigation

The promise of Floquet analysis for biomechanics is to study control in terms of the natural dynamics of the animal rather than in terms of some theoretically imposed model, however enlightened it may be. It is attractive in that it identifies the interactions between events that occur at one phase and outcomes that occur at another phase, and brings our attention back to the question of how long term outcomes are controlled. It also opens the possibility of identifying not merely the local template dynamics of a given species but, through comparisons of its embedding in varied morphologies, advancing hypotheses concerning the role of postures in anchoring it.

Perhaps the greatest strength and promise of Floquet analysis is that the change of coordinates from native measurement coordinates to the Floquet mode activations converts the problem of control in periodic tasks that stabilize a cycle (such as locomotion) to an equivalent linear fixed point task that stabilizes a point. The point being stabilized is the zero level of Floquet mode activation, i.e. the stable limit cycle itself.

Once the periodic relationships tying together perturbations at different phases have been factored out by data driven Floquet analysis, the linear representation of system dynamics expressed in activations is identical in setting to fixed point tasks such as standing in place. This conversion may allow the same methods that have been used successfully for fixed point tasks (e.g. muscle synergy discovery through non-negative matrix factorization; Ting and Macpherson 2005b) to be applied to locomotion.

Applications outside of functional biomechanics

Another potential application of Floquet analysis is to allow the slowest Floquet modes to be compared across species and through ontogeny. This can even be extended to bio-inspired robots: mimicking modes of a model animal in bio-inspired robots modeled on that animal may improve our ability to reproduce animal-like locomotor performance.

Data driven quantitative analysis of Floquet modes may also find application in the design and tuning of robots unrelated to any bio-inspired motivation by allowing for better empirical understanding of their intrinsic dynamics, and in clinical applications of gait analysis and prosthetic design for similar reasons. It is an approach broadly applicable to oscillating physical systems.

Further improvements to the statistical tools

Significant challenges remain in the development and validation of the mathematical and statistical tools, especially when applied animals whose dynamical state requires high dimensional description. Of particular importance are tools that will allow for a valid inference of section maps based on data taken from multiple trials from multiple individuals. While we have made some progress in developing such tools, many of these steps were validated by simulation and would greatly benefit from careful consideration by expert statisticians

4.6 Appendix: examination of eigenvalue distributions

In this addendum we describe our approach towards interpretation and analysis of eigenvalue distributions obtained through our multiple imputation estimation procedure. We hope to convince the reader that examining the distribution of eigenvalues under the prevailing measurement noise conditions provides deeper and more reliable insight than producing a single estimate of eigenvalues. Our treatment will in many ways mirror the treatment in the remainder of the publication, except that we will discuss eigenvalue distributions on the complex plane instead of eigenvalue magnitude distributions on the non-negative reals.

4.6.1 What eigenvalues tell us about dynamics

The eigenvalues of an iterated map[15], such as the return map in a periodic behavior, govern its stability at fixed points. In general, eigenvalues of a real-valued map can be complex numbers. Eigenvalues which are real numbers may appear alone; eigenvalues which have a non-zero imaginary part always appear in pairs with an equal and opposite imaginary part.

The importance of eigenvalues stems from two properties: they govern the rate of return to equilibrium and they enable a partitioning of the dynamics into linearly independent invariant subspaces. The former property has received much attention in the experimental biomechanics community (Hurmuzlu and Basdogan, 1994; Dingwell and Kang, 2007; Arellano et al., 2009) and is treated in tutorial form in Full et al. (2002). However it is the latter property that is of interest from the perspective of further Floquet analysis.

An animal perturbed in a direction belonging to some invariant subspace will continue to remain in that subspace throughout its return to equilibrium. Any perturbation can be expressed as having components in multiple invariant subspaces; its recovery will appear as if each component evolves separately in time within its own sub-space, oblivious to all others. The rate of recovery within each invariant subspace is given by the magnitude of the eigenvalues associated with that subspace, with the magnitude of the eigenvalue giving the fraction of the perturbation remaining after a cycle. It is for this reason that eigenvalues with different magnitudes are always associated with different invariant subspaces. A corollary of these properties is that if we observe dynamics with multiple eigenvalues, we can always conceive of these as being (to first order approximation) separate processes operating in parallel.

The eigenvectors produces by standard numerical packages are basis vectors for the invariant subspaces of the corresponding eigenvalues. As such, the are not uniquely determined. For single real eigenvalues, the eigenvectors are usually normalized, and thus determined up to sign. For complex conjugate pairs, the eigenvectors produced by different calculations need only span the same 2-dimensional subspace. This indeterminacy in the numerical representation raises many practical difficulties in the implementation of Floquet analysis methods.

[15]Formally speaking, we mean eigenvalues of the Jacobian of the return map, which is a linear approximation to the map near a fixed point.

4.6.2 Eigenvalues and noise

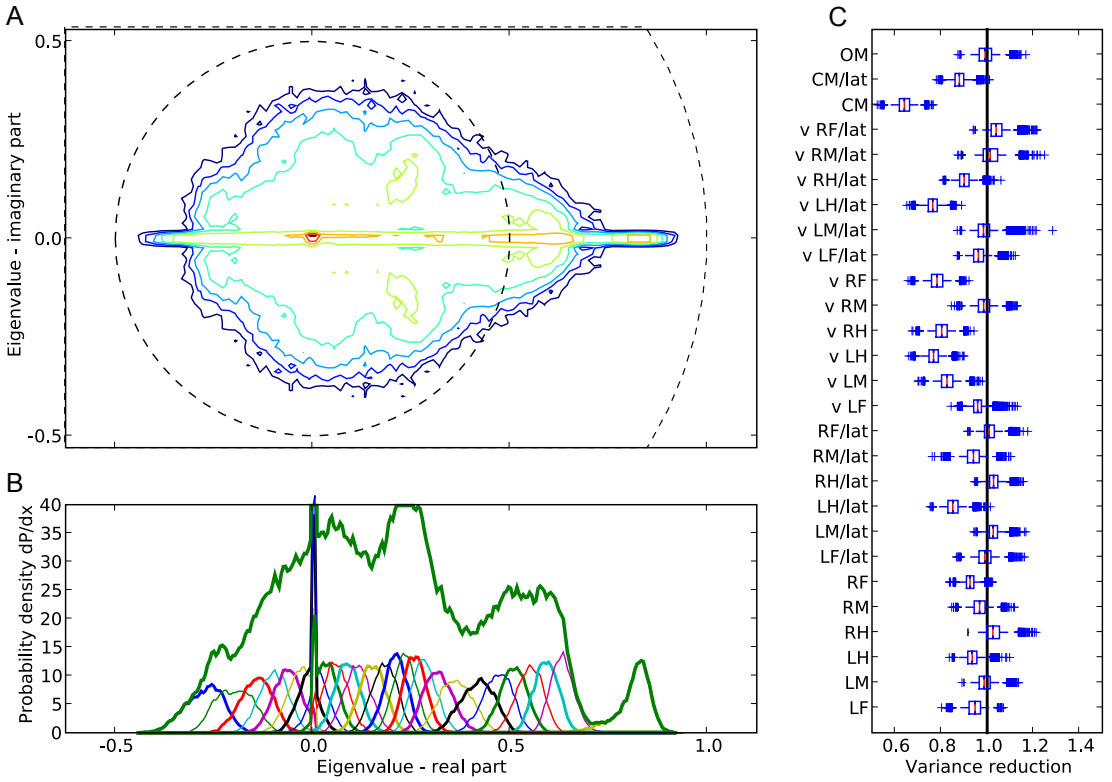

Figure 4.9: Study of return map: eigenvalue distribution on the complex plane **A** shows a distinct lobe on the positive real axis. Distribution on the real axis **C** shows both individual eigenvalues (sorted by real part) and the total density for all eigenvalues. The lobe comprises six or seven eigenvalues, with real parts ranging from 0.4 to 0.9. Tukey box-plots in **B** show the reduction in variance (ratio of variance with prediction to variance with no prediction) that was achieved in each coordinate by using the return map as a predictor. A value of 0 is perfect prediction; a value of 1 means no appreciable improvement. When predicting random data, value is larger than one (prediction does worse than doing guessing a constant).

Little is known about eigenvalue estimates from least squares regression of noisy data. In general, with a source of noise corrupting our measurements we would expect to see some eigenvalues from the noise and some eigenvalues from the system being examined (e.g. compare fig. 4.9-**A** with fig. 4.10). Noise will tend to move eigenvalues around. If an experiment is repeated, one may expect to obtain distributions of eigenvalues surrounding the true values. If eigenvalues are estimated from noisy data, some notion of confidence interval must be entertained to decide when eigenvalues are different enough to provide prima faci evidence for distinct invariant subspaces.

Multiple imputation by bootstrap mechanisms provides a means to produce many re-sampling replications of the return map estimate, and thus allows us to reproduce the distribution of eigenvalues we would expect to obtain from replicated experiments. Our experience with multiple imputation in our system has been that noise is sufficiently large to make it impossible to track "individual" eigenvalues and match them across imputations.

For "pure noise", it seems (by numerical experimentation; we know of no proof of this) that regressing Gaussian noise against itself generates random matrices with Gaussian random entries. The eigenvalues of random matrices whose entries are i.i.d. standard Gaussian follow a known distribution called the Circular Law. In fig. 4.10 we present a contour plot of an approximation to this distribution for the dimension of interest to us. It should be noted that the radius of the disc scales with variance of the Gaussian used for the matrix entries, and with the square root of the dimension of the matrix (Edelman, 1997).

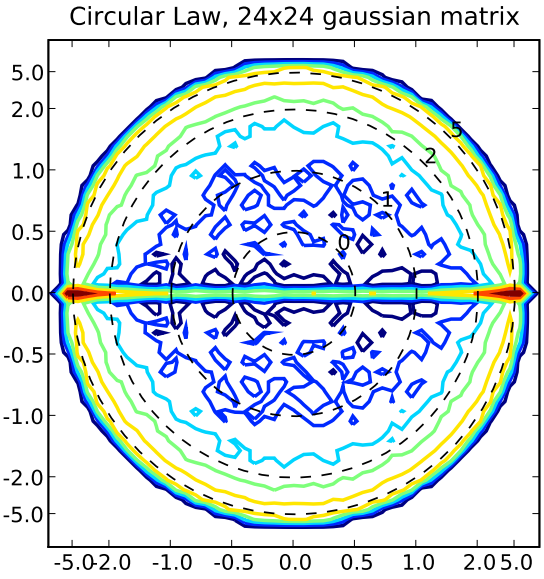

Figure 4.10: Numerically derived distribution of eigenvalues for random 27×27 matrices with independent gaussian entries. The eigenvalues fall in a disc, with an emphasis on the real line. Radius of the disc is near $\sqrt{27}$. This distribution, at various dimensions, is used as our $H_{0(a)}$ null hypothesis when determining the dimension of a template.

4.6.3 Statistically significant return map structures

The distribution obtained in fig. 4.9-**A** can be interpreted as a superposition of a circular law disc of radius near 0.3 on a collection of real positive eigenvalues, with only a few complex conjugate pairs unrelated to the disc.

Such a disc of radius 0.3 in can arise from 27 dimensional matrices with entries whose variance is $0.3/\sqrt{27} = 0.06$, but can also arise from having matrices be random on a small subspace, but with larger variance.

In fig. 4.9-**C** we plotted the distribution of individual eigenvalues, identified by their ordinal when sorted by their real part. For example, the third bell curve from the right gives the distribution of the real part of the eigenvalue with the third largest real part. This curve reveals that the largest eigenvalue is isolated, and is followed in magnitude by a clump of six eigenvalues that still protrude well outside the disc of small eigenvalues. These observations are suggestive of our results in that the largest eigenvalue seemed to play a different role than the remaining template eigenvalues.

A more dynamically meaningful way of matching eigenvalues from different imputed estimates may be of value.

4.6.4 Return map eigenvalues vary with section, contrary to deterministic models

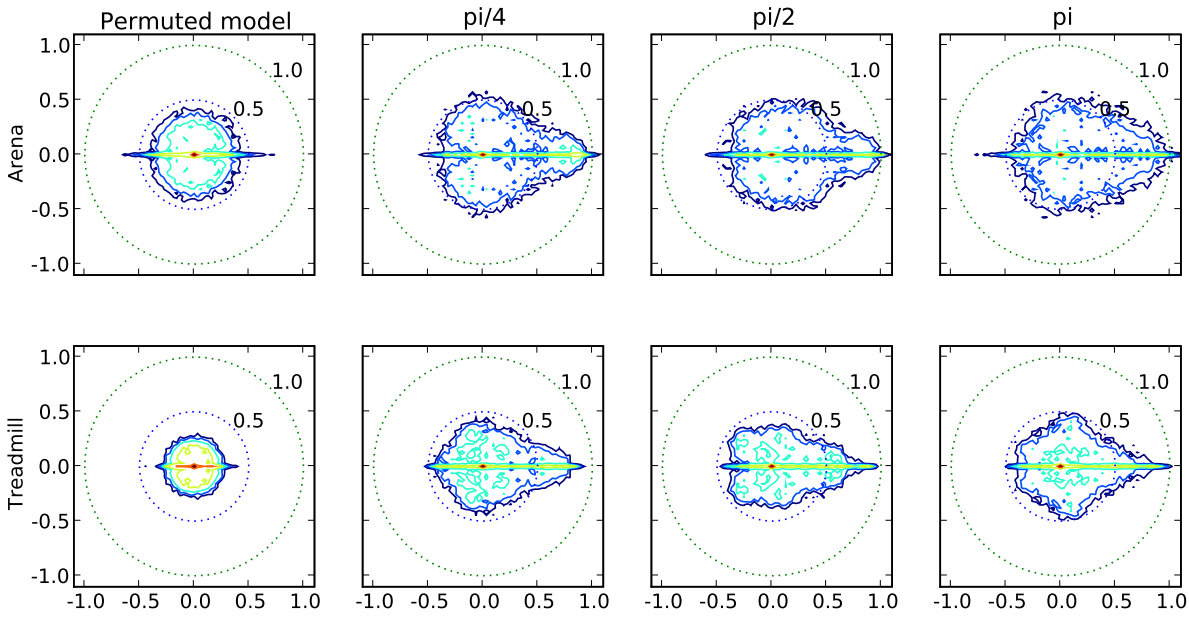

Figure 4.11: Eigenvalue density visualizations for sections at three phases $\pi/4$; $\pi/2$; π in columns 2,3,4 for both datasets (in rows). Leftmost column shows eigenvalues for surrogate based control: outputs of the return map were permuted relative to the inputs prior to regression, eliminating any causal relationship between input and output. While controls seem similar to a Circular Law distribution fig. 4.10, animal data shows distinct structures with large real eigenvalues. Despite these superficial similarities, the eigenvalue distributions at different phases are distinct.

For a deterministic system, the return map eigenvalues must be the same for all Poincare sections. This is immediate obvious from the fact that the section map $\mathsf{M}[\phi, \theta]$ induces a matrix similarity transformation between the return map at ϕ $\mathsf{M}[\phi, \phi + 2\pi]$ and the return map at θ $\mathsf{M}[\theta, \theta + 2\pi]$.

The estimated eigenvalue distribution varies from section to section, mostly in the eigenvalues of intermediate magnitude.

We believe that this variability is due to different errors introduced by noise at different phases. Noise distributions vary greatly with phase. As the Floquet axes vary the angles between them change, implying that the effects of noise are correlated among them to a different degree. This may introduce phase dependent systematic errors in the eigenvalue estimates. This is one of many mechanisms that could contribute to the corruption of eigenvalue estimates from noisy data. The authors would like to encourage further examination of this broadly applicable issue.

Despite the variability seen in fig. 4.11, we observe that the eigenvalue distributions of both arena and treadmill datasets are similar in their general shape. The disc of "noise eigenvalues" is larger in the arena data, which contained only half as many data points as the treadmill data and was generated from an entirely different measurement apparatus. This strengthens our confidence in the interpretation of the disc as being a property of the measurement instrument (such as measurement noise) rather than a property of the animals.

On the left of fig. 4.11 we plot the eigenvalue distribution obtained from $H_{0(b)}$ surrogate data (Schreiber and Schmitz, 2000). The surrogates were created by taking the imputed input-output pairs used for linear regression and permuting the outputs with respect to the inputs. This preserves the statistical distributions of outputs and inputs while breaking the causal relationships constituting the return map. The resulting eigenvalue distributions bear strong resemblance to the Circular Law distribution of fig. 4.10, lending support to the notion that eigenvalues outside these discs are due to having captured some deterministic causal structures of the dynamics.

4.7 Appendix: Mathematical overview

In this addendum we provide an informal mathematical definition of our system model and describe some of the computational steps in greater detail.

4.7.1 Definition of the dynamical system

We assume that the animals' motions are governed by a stochastically perturbed ordinary differential equation, expressible in terms of state evolution with additive noise.

$$x' = F(x) + \nu \tag{4.4}$$
$$\nu \sim N(0, \sigma_\nu) \tag{4.5}$$

The animals perform a periodic locomotor behaviour. This periodic behaviour is assumed to arise from a stable limit cycle $o(\cdot)$ which is a solution of the deterministic part of the ODE.

$$o'(t) = F(o(t)) \tag{4.6}$$
$$o(t + \tau) = o(t) \tag{4.7}$$
$$\|x(t) - o(t)\| \to 0 \tag{4.8}$$

As is true of any periodic system with a stable limit cycle, the limit cycle describing the animals' gait introduces an intrinsic phase coordinate ϕ, with respect to which unperturbed trajectories of the deterministic system evolve at a constant rate.

$$\nabla\varphi \cdot F = \frac{2\pi}{\tau} \tag{4.9}$$
$$x'(\varphi) = \frac{2\pi}{\tau} \tag{4.10}$$
$$o(\varphi + 2\pi) = o(\varphi) \tag{4.11}$$

For deterministic systems satisfying the definitions above, Floquet's Theorem (Floquet, 1883) provides for the existence of a coordinate change that considerably simplifies the representation of the dynamics.

Defining the "perturbation" to be $q(t) = x(t) - o(t)$, Floquet proved there exists a periodic change of coordinates $P(\cdot)$ and a return map matrix e^Λ that satisfy[16]:

$$q(\theta) = P(\theta)\mathrm{e}^{\frac{\theta}{2\pi}\Lambda}P^\dagger(\varphi)q(\varphi) \tag{4.12}$$
$$P(\varphi) = P(\varphi + 2\pi) \tag{4.13}$$

The Floquet modes are solutions ξ_k for q of the form:

$$\xi_k(t) = \mathrm{e}^{\frac{t}{\tau}\lambda_k}p_k(\varphi) \tag{4.14}$$

[16]Because we must work over the real numbers, Lambda can only be brought to real Jordan form. Since there is noise in the system, degenerate Jordan blocks cannot appear, and the matrix is block 2×2 diagonal. We omit details relating to work with non-real eigenvalues.

4.7.2 Impact of a Floquet mode

The equations of motion that govern the animals cannot depend on absolute position and heading, as these arise from the arbitrary choice of a laboratory coordinate frame. Consequently only the derivatives of the centre of mass coordinates appear in our state. When an animal is perturbed from the limit cycle motions, these derivatives may change from their limit cycle values.

Letting Π_{COM} be a projection onto the centre of mass coordinates, and $\xi_k(t)$ denote the linear combination of floquet modes under study, we define its impact to be:

$$\Xi_k(t_0) = \int_{t=t_0}^{\infty} \Pi_{COM}\xi_k(t)\ dt \tag{4.15}$$

4.8 Chapter Glossary

For each term we offer both a technical, mathematical definition of our usage of the term and a non-technical description. The definitions we provide are not general definitions of the terms; they are specific to way each of these technical terms is used in preceding text.

Eigenvalue (of a return map) a value associated with a return map $R[\phi]$ at some phase section ϕ. The number c is an eigenvalue of $R[\phi]$ if there exists an eigenvector vector x such that for the limit cycle $o(\cdot)$: $R[\phi](o(\phi) + x) = o(\phi) + cx$.

Eigenvalues represent rates of decay of perturbations. An eigenvalue of c implies that after a stride only c of the perturbation remains. Eigenvalues don't exists for all perturbations; when they do, those perturbations are said to lie on an eigenvector.

Eigenvector (of a return map) a vector associated with a return map $R[\phi]$ at some phase section ϕ. The vector x is an eigevector of $R[\phi]$ if there exists a vector x for the limit cycle $o(\cdot)$ such that $R[\phi](o(\phi) + x) = o(\phi) + cx$.

Eigenvectors are perturbations for which there exist eigenvalues.

Floquet mode A trajectory $x(\cdot)$ with the property that $x(t+T) - o(t+T) = x(t+T) - o(t) = c(x(t) - o(t))$ for $o(\cdot)$ the limit cycle, T the period and c a scalar (the Floquet multiplier).

Floquet modes are "pure" modes of perturbation recovery, with only one non-zero activation. They are the trajectories of animals who were perturbed along only one eigenvector and then left to recover.

Floquet multiplier an eigenvalue of a return map.

Floquet coordinates: the numbers representing the state of an animal with respect to the Floquet frame associated with its current phase; also the real valued functions of state that return these numbers.

Numbers that represent how far along each Floquet axis the animal's state projects. As the animal's state evolves in time, these numbers follow a simple exponential relationship. Coordinate k will evolve by a factor of $e^(c_k t/T)$ for c_k the k-th Floquet multiplier.

Floquet frame A Floquet frame is a periodic and smooth function of phase, taking phase ϕ into the eigenvectors of the return map at phase ϕ. This creates a coordinate frame with respect to which solutions of the equations of motion take a diagonal form.

Floquet axis a single axis of a Floquet frame; a continuous function mapping phase into eigenvectors. This is the periodic part of a Floquet mode. Each Floquet mode $x(t)$ with Floquet multiplier c can be expressed as $f(tmodT)\exp(ct/T)$

A function of phase showing related eigenvectors at different phases, scaled in a consistent way.

Phase for deterministic dynamical systems– the equivalence class of states that collapse to same point on the limit cycle; also a scalar function of state whose level sets represent these classes, and whose derivative along trajectories is the constant $2\pi/T$. For systems with noise perturbing the state– the phase of the same state assuming noiseless evolution from this time on.

A function of state indicating where on the limit cycle the animal will end up, once it returns to the limit cycle.

Phase section The linear approximation to an isochron near the limit cycle. A domain in a hyperplane that intersects the limit cycle and is normal to the gradient of phase on the limit cycle. Phase is constant to first order on a section.

The hyper-plane of constant phase intersecting the limit cycle at a given phase

Section map a mapping from one phase section to another induced by the trajectories of the system; also the linear approximation thereof, denoted by $\mathsf{M}[\phi, \theta]$, and written with respect to coordinate origins at the limit cycle points $o(\phi)$ and $o(\theta)$ for the domain and co-domain.

The matrix that maps the state of animals starting at phase ϕ to where they end up at phase θ.

Return map a section map from a phase section to itself one cycle later; the return map $R[\phi]$ is equal to the section map $\mathsf{M}[\phi, \phi + 2pi]$. Return maps have equal domain and co-domain, and are therefore amenable to eigenvalue decomposition; we use the term for both the nonlinear map and its linear approximation with respect to an origin placed at the limit cycle point $o(\phi)$.

The matrix that maps where animal starting at phase ϕ end up one cycle later.

Input-Output Pair a pair of points from the same experimentally obtained trajectory, the "input" x on section ϕ and the "output" y on section θ, such that we expect (in a least squares sense): $y = \mathsf{M}[\phi, \theta]x$

The pairs of data points that go into the regression of section maps.

Imputation a statistical procedure for filling in missing measurement with model-derived data so as to provide an appropriately structured sample for the next steps in the analysis. In the context of "multiple imputation" one iteration of imputing missing measurements. We use imputation for balancing out the experimental design for input-output pairs used for section map regression.

Multiple Imputation performing many imputations (see Imputation) using a randomization procedure to not only estimate the statistics of interest, but also the effects of the imputation procedure itself on the results.

The process that balances out samples so that long trials don't have greater leverage on the results than short trials do.

Rhythmic a system is "rhythmic" if the deterministic part of its dynamics is periodic. Since we consider systems whose dynamics are being influenced by external noise sources, they are not periodic in the usual formal sense.

Characteristic cycle the characteristic cycle of a system is the expected value of its state as a function of phase, with respect to the ensemble from which the experimental data is a sample. For deterministic systems, this is the limit cycle.

The average stride when binning state by phase.

Circular Law letting X be a matrix over the reals, of dimension d, with entries being independently and identically distributed gaussian random variables with mean zero and standard deviation sigma. The probability distribution of a randomly chosen eigenvalue of X is a circular law distribution. Trivially, sigma scales all eigenvalues, and therefore one usually refers to the circular law distributions by a dimension and no scale. Scaling by $d^{-frac12}$ and taking the limit of d to infinity, this is a uniform distribution on the unit disc; hence the name.

The probability law governing distribution of eigenvalues for random matrices.

4.9 Bibliography

P A Absil, R Mahony, and R Sepulchre. Riemannian geometry of grassmann manifolds with a view on algorithmic computation. *Acta Applicandae Mathematicae: An International Survey Journal on Applying Mathematics and Mathematical Applications*, 80(2):199–220, 2004. doi: 10.1023/B:ACAP.0000013855.14971.91.

R M Alexander. Why mammals gallop. *Am Zool*, 28(1):237–245, 1988. ISSN 0003-1569.

R M Alexander. Elastic mechanisms in the locomotion of vertebrates. *Neth J Zool*, 40 (1-2):93–105, 1990. ISSN 0028-2960.

R M Alexander. A model of bipedal locomotion on compliant legs. *Philos Trans R Soc Lond , Ser B: Biol Sci*, 338(1284):189–198, OCT 29 1992. ISSN 0962-8436.

R M Alexander. Leg design and jumping technique for humans, other vertebrates and insects. *Philos Trans R Soc Lond , Ser B: Biol Sci*, 347(1321):235–248, FEB 28 1995. ISSN 0962-8436.

C J Arellano, D P O'Connor, C Layne, and M J Kurz. The independent effect of added mass on the stability of the sagittal plane leg kinematics during steady-state human walking. *J Exp Biol*, 212(12):1965–1970, JUN 15 2009. ISSN 0022-0949. doi: 10.1242/jeb.026153.

M W Berry, M Browne, A N Langville, V P Pauca, and R J Plemmons. Algorithms and applications for approximate nonnegative matrix factorization. *Computational Statistics & Data Analysis*, 52(1):155–173, SEP 15 2007. ISSN 0167-9473. doi: 10.1016/j.csda.2006.11.006.

R Blickhan. The spring mass model for running and hopping. *J Biomech*, 22(11-12): 1217–1227, 1989.

R Blickhan and R J Full. Similarity in multilegged locomotion - bouncing like a monopode. *J Comp Physiol , A*, 173(5):509–517, 1993. ISSN 0340-7594.

G A Cavagna, N C Heglund, and C R Taylor. Mechanical work in terrestrial locomotion - 2 basic mechanisms for minimizing energy-expenditure. *Am J Physiol*, 233(5): R243–R261, 1977. ISSN 0002-9513.

NJ Cowan, J Lee, and RJ Full. Task-level control of rapid wall following in the american cockroach. *J Exp Biol*, 209(9):1617–1629, 2006. ISSN 0022-0949. doi: 10.1242/jeb.02166.

A Daffertshofer, C J C Lamoth, O G Meijer, and P J Beek. Pca in studying coordination and variability: a tutorial. *Clin Biomech*, 19(4):415–428, MAY 2004. ISSN 0268-0033. doi: 10.1016/j.clinbiomech.2004.01.005.

M A Daley, J R Usherwood, G Felix, and A A Biewener. Running over rough terrain: guinea fowl maintain dynamic stability despite a large unexpected change in substrate height. *J Exp Biol*, 209(1):171–187, January 2006. ISSN 0022-0949. doi: 10.1242/jeb.01986.

A d'Avella and E Bizzi. Shared and specific muscle synergies in natural motor behaviors. *PNAS*, 102(8):3076–3081, FEB 22 2005. ISSN 0027-8424. doi: 10.1073/pnas.0500199102.

M H Dickinson, C T Farley, R J Full, M A R Koehl, R Kram, and S Lehman. How animals move: an integrative view. *Science*, 288:100–106, 2000.

J B Dingwell and H G Kang. Differences between local and orbital dynamic stability during human walking. *J Biomechanical Engineering*, 129:586, 2007. doi: 10.1115/1.2746383.

A Edelman. The probability that a random real gaussian matrix has k real eigenvalues, related distributions, and the circular law. *J Multivariate Analysis*, 60(2):203–232, FEB 1997. ISSN 0047-259X.

A Edelman, T A Arias, and S T Smith. The geometry of algorithms with orthogonality constraints. *SIAM J Matrix Analysis and Applications*, 20(2):303–353, OCT 20 1998. ISSN 0895-4798.

B Efron. Missing data, imputation, and the bootstrap. *J American Statistical Association*, 89(426):463–475, 1994. ISSN 01621459. URL http://www.jstor.org/stable/2290846.

D Eppstein and J Wang. Fast approximation of centrality. In *SODA '01: Proceedings of the twelfth annual ACM-SIAM symposium on Discrete algorithms*, pages 228–229, Philadelphia, PA, USA, 2001. Society for Industrial and Applied Mathematics. ISBN 0-89871-490-7.

C T Farley, J Glasheen, and T A McMahon. Running springs - speed and animal size. *J Exp Biol*, 185:71–86, DEC 1993. ISSN 0022-0949.

G Floquet. Sur les équations différentielles linéaires à coefficients périodiques. *Annales Scientifiques de lÉcole Normale Supérieure, Sér*, 2:12, 1883.

R J Full and D E Koditschek. Templates and anchors: Neuromechanical hypotheses of legged locomotion on land. *J Exp Biol*, 202(23):3325–3332, 1999.

R J Full and M S Tu. Mechanics of 6-legged runners. *J Exp Biol*, 148:129–146, JAN 1990. ISSN 0022-0949.

R J Full and M S Tu. Mechanics of a rapid running insect - 2-legged, 4-legged and 6-legged locomotion. *J Exp Biol*, 156:215–231, MAR 1991. ISSN 0022-0949.

R J Full, R Blickhan, and L H Ting. Leg design in hexapedal runners. *J Exp Biol*, 158:369–390, 1991. ISSN 0022-0949.

R J Full, T Kubow, J Schmitt, P Holmes, and D Koditschek. Quantifying dynamic stability and maneuverability in legged locomotion. *Integr Comp Biol*, 42(1):149–157, FEB 2002. ISSN 1540-7063.

R M Ghigliazza and P Holmes. Towards a neuromechanical model for insect locomotion: Hybrid dynamical systems. *Regular & Chaotic Dynamics*, 10(2):193–225, 2005. ISSN 1560-3547. doi: 10.1070/RD2005v010n02ABEH000311.

L Glass and A T Winfree. Discontinuities in phase-resetting experiments. *Am J Physiol Regul Integr Comp Physiol*, 246:R251–R258, 1984. PMID: 6696148.

J Guckenheimer and P Holmes. *Nonlinear Oscillations, Dynamical Systems, and Bifurcations of Vector Fields*. Springer-Verlag, 1983.

O Harel and Xiao-Hua Zhou. Multiple imputation: review of theory, implementation and software. *Stat Med*, 26(16):3057–3077, 2007. doi: 10.1002/sim.2787. ON: 1097-0258, PN: 0277-6715.

J Heikkila and O Silven. A four-step camera calibration procedure with implicit image correction. In *Computer Vision and Pattern Recognition, 1997. Proceedings., 1997 IEEE Computer Society Conference on*, pages 1106–1112, Jun 1997. ISBN 0-8186-7822-4. doi: 10.1109/CVPR.1997.609468.

P Holmes, R J Full, D E Koditschek, and J M Guckenheimer. The dynamics of legged locomotion: Models, analyses, and challenges. *SIAM Review*, 48(2):207–304, June 2006. ISSN 0036-1445. doi: 10.1137/S003614450445133.

N E Huang, Z Shen, S R Long, M C Wu, H H Shih, Q Zheng, et al. The empirical mode decomposition and the hilbert spectrum for nonlinear and non-stationary time series analysis. *Proceedings: Mathematical, Physical and Engineering Sciences*, 454(1971): 903–995, 1998. ISSN 13645021. URL http://www.jstor.org/stable/53161.

Y Hurmuzlu and C Basdogan. On the measurement of dynamic stability of human locomotion. *J Biomech Eng Trans ASME*, 116(1):30–36, FEB 1994. ISSN 0148-0731.

A. Hyvärinen and E. Oja. Independent component analysis: algorithms and applications. *Neural Networks*, 13(4-5):411–430, 2000. doi: 10.1016/S0893-6080(00)00026-5.

Y P Ivanenko, R E Poppele, and F Lacquaniti. Five basic muscle activation patterns account for muscle activity during human locomotion. *J Physiol*, 556(1):267–282, 2004. doi: 10.1113/jphysiol.2003.057174.

S Jaric and M L Latash. The equilibrium-point hypothesis is still doing fine. *Hum Movement Sci*, 19(6):933–938, 2000.

D L Jindrich and R J Full. Dynamic stabilization of rapid hexapedal locomotion. *J Exp Biol*, 205(18):2803–2823, Sep 2002. ISSN 0022-0949.

P E Jupp and K V Mardia. Maximum likelihood estimators for the matrix von mises-fisher and bingham distributions. *The Annals of Statistics*, 7(3):599–606, 1979. ISSN 00905364. URL http://www.jstor.org/stable/2958745.

C G Khatri and K V Mardia. The von mises-fisher matrix distribution in orientation statistics. *J Roy Stat Soc, B*, 39(1):95–106, 1977. ISSN 00359246. URL http://www.jstor.org/stable/2984884.

R Kram, B Wong, and R J Full. Three-dimensional kinematics and limb kinetic energy of running cockroaches. *J Exp Biol*, 200(13):1919–1929, JUL 1997. ISSN 0022-0949.

T M Kubow and R J Full. The role of the mechanical system in control: a hypothesis of self-stabilization in hexapedal runners. *Philos Trans R Soc Lond , Ser B: Biol Sci*, 354(1385):849–861, MAY 29 1999. ISSN 0962-8436.

R Kukillaya, J Proctor, and P Holmes. Neuromechanical models for insect locomotion: Stability, maneuverability, and proprioceptive feedback. *Chaos*, 19(2), JUN 2009. ISSN 1054-1500. doi: 10.1063/1.3141306.

R P Kukillaya and P J Holmes. A hexapedal jointed-leg model for insect locomotion in the horizontal plane. *Biol Cybern*, 97(5-6):379–395, DEC 2007. ISSN 0340-1200. doi: 10.1007/s00422-007-0180-2.

D D Lee and H S Seung. Learning the parts of objects by non-negative matrix factorization. *Nature*, 401(6755):788–791, OCT 21 1999. ISSN 0028-0836. doi: 10.1038/44565.

J Lee, S N Sponberg, O Y Loh, A G Lamperski, R J Full, and N J Cowan. Templates and anchors for antenna-based wall following in cockroaches and robots. *IEEE Trans Robotics*, 24(1):130–143, February 2008. ISSN 1552-3098. doi: 10.1109/TRO.2007.913981.

T McGeer. Passive bipedal running. *Proc R Soc Lond , Ser B: Biol Sci*, 240(1297):107–134, MAY 22 1990. ISSN 0962-8452.

T A McMahon and G C Cheng. The mechanics of running - how does stiffness couple with speed. *J Biomech*, 23(Suppl. 1):65–78, 1990. ISSN 0021-9290.

B Moore. Principal component analysis in linear systems: Controllability, observability, and model reduction. *IEEE Trans Automat Contr*, 26(1):17–32, 1981. ISSN 0018-9286. URL http://ieeexplore.ieee.org/xpl/freeabs_all.jsp?arnumber=1102568.

A J Nagengast, D A Braun, and D M Wolpert. Optimal control predicts human performance on objects with internal degrees of freedom. *PLoS Comput Biol*, 5(6):e1000419, 06 2009. doi: 10.1371/journal.pcbi.1000419.

D N Politis. Computer-intensive methods in statistical analysis. *IEEE Signal Processing Magazine*, 15(1):39–55, 1998. ISSN 1053-5888. doi: 10.1109/79.647042.

J Proctor and P J Holmes. Steering by transient destabilization in piecewise-holonomic models of legged locomotion. *Regular and Chaotic Dynamics*, 13(4):267–282, 2008. doi: 10.1134/S1560354708040047.

S Revzen. *Neuromechanical Control Architectures in Arthropod Locomotion*. PhD thesis, Univeristy of California, Berkeley, 2009. in-prep.

S Revzen and J M Guckenheimer. Estimating the phase of synchronized oscillators. *Phys Rev E*, 78(5):051907, November 2008. doi: 10.1103/PhysRevE.78.051907.

S Revzen, D E Koditschek, and R J Full. Testing feedforward control models in rapid running insects using large perturbations (abstract only). *Integr Comp Biol*, 46(suppl 1):e1–162, 2006. doi: 10.1093/icb/icl056.

S Revzen, D E Koditschek, and R J Full. *Progress in Motor Control - A Multidisciplinary Perspective*, chapter Towards Testable Neuromechanical Control Architectures for Running, pages 25–56. Springer Science+Business Media, LLC - NY, 2008. doi: 10.1007/978-0-387-77064-2_3.

S Revzen, J M Guckenheimer, and R J Full. Study of the neuromechanical control of rhythmic behaviors by floquet analysis (abstract only; inp-prep). In *Yearly meeting of the Society for Integrative and Comparative Biology*, 2009.

J Schmitt and P Holmes. Mechanical models for insect locomotion: dynamics and stability in the horizontal plane - i. theory. *Biol Cybern*, 83(6):501–515, December 2000a.

J Schmitt and P Holmes. Mechanical models for insect locomotion: dynamics and stability in the horizontal plane - ii. application. *Biol Cybern*, 83(6):517–527, 2000b.

J Schmitt and P Holmes. Mechanical models for insect locomotion: stability and parameter studies. *Phys D: Nonlinear Phenom*, 156(1-2):139–168, 2001.

T Schreiber and A Schmitz. Surrogate time series. *Phys D: Nonlinear Phenom*, 142(3-4):346–382, 2000. ISSN 0167-2789. doi: http://dx.doi.org/10.1016/S0167-2789(00)00043-9.

J E Seipel, P J Holmes, and R J Full. Dynamics and stability of insect locomotion: a hexapedal model for horizontal plane motions. *Biol Cybern*, 91(2):76–90, AUG 2004. ISSN 0340-1200. doi: 10.1007/s00422-004-0498-y.

J C Spagna, D I Goldman, P-C Lin, D E Koditschek, and R J Full. Distributed mechanical feedback in arthropods and robots simplifies control of rapid running on challenging terrain. *Bioinspiration & Biomimetics*, 2(1):9–18, 2007. ISSN 1748-3182. doi: 10.1088/1748-3182/2/1/002.

S Sponberg and R J Full. Neuromechanical response of musculo-skeletal structures in cockroaches during rapid running on rough terrain. *J Exp Biol*, 211(3):433–446, FEB 1 2008. ISSN 0022-0949. doi: 10.1242/jeb.012385.

S Sponberg, J M Mongeau, J P Miller, and R J Full. Decoding cockroach antennal tactile navigation using naturalistic and white noise stimuli in a control theoretic framework. *Integr Comp Biol*, 49(Suppl. 1):E161, FEB 2009. ISSN 1540-7063.

L H Ting. Computational neuroscience: Theoretical insights into brain function. chapter Dimensional reduction in sensorimotor systems: a framework for understanding muscle coordination of posture, pages 299–321. Elsevier Science Ltd, 2007.

L H Ting and J M Macpherson. A limited set of muscle synergies for force control during a postural task. *J Neurophysiol*, 93(1):609–613, 2005a. ISSN 0022-3077. doi: 10.1152/jn.00681.2004.

L H Ting and J M Macpherson. A limited set of muscle synergies for force control during a postural task. *J Neurophysiol*, 93(1):609–613, JAN 2005b. ISSN 0022-3077. doi: 10.1152/jn.00681.2004.

L H Ting, R Blickhan, and R J Full. Dynamic and static stability in hexapedal runners. *J Exp Biol*, 197:251–269, DEC 1994. ISSN 0022-0949.

E Todorov and M I Jordan. Optimal feedback control as a theory of motor coordination. *Nat Neurosci*, 5(11):1226–1235, 2002. doi: 10.1038/nn963.

M C Tresch, V C K Cheung, and A d'Avella. Matrix factorization algorithms for the identification of muscle synergies: Evaluation on simulated and experimental data sets. *J Neurophysiol*, 95(4):2199–2212, APR 2006. ISSN 0022-3077. doi: 10.1152/jn.00222.2005.

J T Watson, R E Ritzmann, S N Zill, and A J Pollack. Control of obstacle climbing in the cockroach, blaberus discoidalis. i. kinematics. *J Comp Physiol , A*, 188(1): 39–53, FEB 2002. ISSN 0340-7594. doi: 10.1007/s00359-002-0277-y.

A T Winfree. *The Geometry of Biological Time*. Springer-Verlag, New York, 1980.

List of Symbols

$\Delta\Phi_{\mathsf{i}}$ residual phase

$\mathsf{M}[\theta, \phi]$ Linearized section map from phase section ϕ to phase section θ

Φ_{G} global phase

Φ_{K} kinematic phase

Φ_{M} mechanical phase

$\hat{\Phi}_{\mathsf{ext}}$ extrapolated phase model

ϕ_L phase of left leg or tripod

ϕ_R phase of left leg or tripod

H_1 Dynamic Stability One of the "Templates and Anchors" hypotheses

H_2 Collapse of dimensions One of the "Templates and Anchors" hypotheses

H_3 Tunable coordination One of the "Templates and Anchors" hypotheses

$o(\cdot)$ limit cycle for rhythmic motions

$p_1(\phi), p_2(\phi)$ Floquet axes as vector functions of phase ϕ

Q_1, Q_2, Q_3 second to fourth Floquet modes, after a coordinate change

$R[\theta]$ Linearized return map for phase section θ, also equal to $\mathsf{M}[\theta, \theta + 2\pi]$

C_0 one of two classes of lateral perturbation trials, based on phase at perturbation

C_1 one of two classes of lateral perturbation trials, based on phase at perturbation

$H_{0(\phi)}$ Statistical hypothesis that animal classes and ϕ_0 values are uniformly distributed

$H_{0(a)}$ Null hypothesis - random measurements on sections

$H_{0(a)}$ simple surrogates relative margins of simple boostrap of surrogate data

$H_{0(b)}$ Null hypothesis - surrogate data without causal structure

$H_{0(b)}$ bootstrapped surrogates relative margins of nested boostrap of surrogate data

$H_{1(\phi)}$ Statistical hypothesis that animal have preferred trials classes due to a perferred ϕ_0 value

H_1 animal data relative margins of animal data

GR(n,p) Grassman Manifold of p dimensional subspaces of n dimensional space

NCA0 Reflex-cascade architecture or Spring Mass with No Clock

NCA1 Clocked spring mass architecture with only mechanical feedback

NCA2 Clock or Leg Tracker architecture with time invariant tracking error feedback

NCA3 Clock Adapting architecture allowing pattern to be modulated

outcome D phase changes, discrete with respect to perturbation

outcome F frequency changes

outcome N animal / system fails

outcome O orbit changes qualitatively

outcome P phase changes, continuous with respect to perturbation